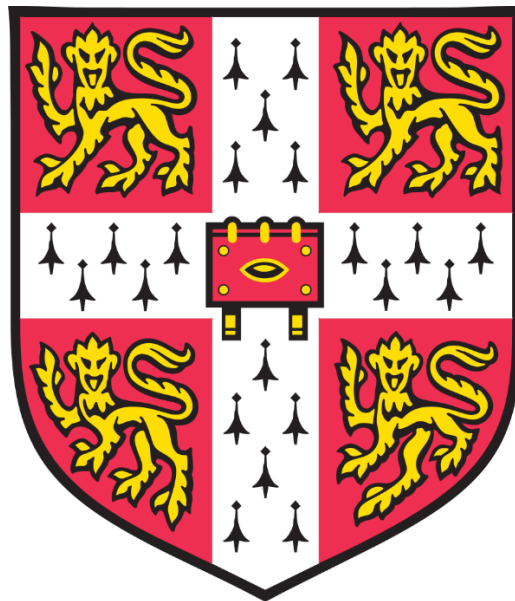


The formation of carbonate minerals in laboratory and environmental settings



Lin Chin Yik
Selwyn College, Cambridge

October 2018

This dissertation is submitted for the degree of Doctor of Philosophy

Declaration

This dissertation is the result of my own work and includes nothing which is the outcome of work done in collaboration except as declared in the Preface and specified in the text. It does not exceed the page limit and is not substantially the same as any work that has been or is being submitted to any university for any degree, diploma or other qualification.

Lin Chin Yik

Abstract

Microbial sulfate reduction, couple to organic matter oxidation or methane oxidation, is one of the key processes driving the formation of sedimentary carbonate minerals. While some work has been done exploring the formation of carbonate minerals via microbial sulfate reduction, less attention has been given to the detailed processes involved in this microbially induced carbonate mineral formation and how the carbonate minerals form may transform and change over time. In this thesis, I investigated the role that microbial sulfate reduction has on the types of calcium carbonate polymorphs precipitated. For this, I grew sulfate-reducing bacteria (*Desulfovibrio bizertensis*) in media with varying Mg/Ca and different types of seeding materials. My results suggest that sulfate-reducing bacteria induce carbonate precipitation and serve as a nucleation for the growing carbonate minerals. In media where the Mg/Ca is greater than 2, a crystalline monohydrocalcite is the primary carbonate mineral produced. In addition, I examine the role of different seeding materials such as calcite and kaolinite have on the generation of alkalinity and microbial growth in the incubation experiments. My results show higher alkalinity production and rates of sulfate reduction in samples with kaolinite seeds. I suggest this is due to the fact that bacteria grow better in the presence of clay minerals that have a higher surface area. In the final chapter of my thesis, I extend my research from the laboratory setting to the field, in the Norfolk saltmarshes. Using an incubation approach of the saltmarsh sediment allows high-resolution monitoring of the evolution of pore fluid chemistry and thus the stability of siderite in conditions that mimic the saltmarsh. My incubation results suggest that the formation of siderite nodule can be very rapid (within weeks) after burial when there is a substantial iron source. My research thus explores the mineralisation of carbonate through microbial processes and how the diversity of carbonate minerals may be explained and examined in the geological record.

Acknowledgements

First and foremost, I would like to thank my supervisor, Dr. Alexandra Turchyn for her brilliant guidance in my PhD. research. This thesis would not be possible without her constant guidance. I am particularly grateful for her patience, trust, encouragement, endless support, and friendly discussions. I enjoyed the time working with Sasha, who provide valuable advice in many aspects, not just academic, but also sharing thoughts and life experiences such as selfless, communications and interaction skills with people. Sasha's supervision has developed me into a person with better confidence in decision making, writing and how to think for myself. Thank you very much for giving me the opportunity to work in this group and sending me to numerous conferences and making me a better writer in academic writing.

I would like to thank Dr. Gilad Antler, Dr. Harold Bradbury, Dr. Tony Dickson, Dr. Zvika Steiner for their constant guidance, countless discussions and advice along my PhD. study. In particular, I would like to thank Dr. Giulio Lampronti for training me on the XRD and SEM and providing with the support and the analysis of mineral quantification. Besides, I would also not forget the discussion, knowledge and guidance on PHREEQC received from Dr. Pieter Bots, special thanks to Pieter. Also, I would like to thank numerous members of the Ocean Biogeochemistry group including Alec Hutchings, Dr. Jo Clegg, Beth O'Connell, Katie Halloran, Florence Chen, Dr. Andrea Erhardt, Dr. Sambuddha Misra for the countless conversations and wonderful time spent in the laboratory.

I am also indebted to Dr. Nicholas Tosca for providing invaluable thoughts and comments in manuscript writing and Dr. Thomas Bennett, and Dr. Shi Chun Li for helping in the BET analysis. My gratitude also goes to my academic friends Dr. Alexander Piotrowski and Professor Nick McCave, and my graduate tutor Professor Nick Butterfield, Dr. Gavin Jarvis, Dr. Anita Faul for their discussions and endless support in my life in Cambridge. Not forgot to mention James Rolfe, Jason Day, Mervyn Greaves, Iris Buisman, Simon Crowhurst, Martin Walker, Christopher Parish, Rob, Vitaliy Turchyn, Alena Giesche, Rui Guo for their help in sample analysis and field survey. Special thanks also go to Professor Nurgul Balci, Dr. Sena Akcer-On, and Bora for their warm hospitality during my sampling trip in Turkey. Also, I would like to acknowledge the Ministry of Education Malaysia for the SLAI (Skim Latihan Akademik IPTA) scholarship and University of Malaya for providing the study leave.

I would like to thank my beloved parents and family for their eternal care, understanding and motivation. Without them, this work would not be possible. Last but not least, I would like to sincerely thank Monica Deng for her love, care, support, patience and trust throughout my PhD. study.

Table of Contents

CHAPTER 1	1
The role of microbial sulfate reduction in the precipitation of calcium carbonates	1
Introduction.....	1
The alkalinity engine and saturation index.....	3
The relation between chemical kinetics and chemical equilibrium.....	8
Authigenic carbonate.....	9
Authigenic carbonate in various environments.....	10
Microbial sulfate reduction.....	10
The Mg/Ca ratio.....	11
Microbial mediation of mineral formation.....	13
Objectives.....	13
Thesis Roadmap.....	14
CHAPTER 2	15
The development of method for incubation experiments in the laboratory	15
2.1 Introduction.....	15
2.2 Analytical methods.....	15
2.2.1 Incubation experiments.....	15
2.2.2 Preparation of medium.....	16
2.2.3 Inoculation of sulfate reducing bacteria.....	19
2.2.4 Aqueous sample analysis.....	19
2.2.5 Solid phase analysis.....	19
2.2.6 Saturation index and DIC calculation.....	20
2.3 Method development.....	20
2.3.1 Incubation Experiment A.....	21
2.3.2 Incubation Experiment B.....	23
2.3.3 Incubation Experiment C.....	25
2.3.4 Incubation Experiment D.....	26
2.3.5 Incubation Experiment E.....	29
2.3.6 Incubation Experiment F.....	33
2.3.7 Incubation Experiment G.....	35
2.4 Conclusions.....	38

CHAPTER 3	39
The role of microbial sulfate reduction in calcium carbonate polymorphs selection	39
3.1 Introduction	39
3.2 Experimental	41
3.2.1 Incubation experiments.....	41
3.2.2 Composition of culture medium and inoculation.....	41
3.2.3 Biotic incubation experiment.....	42
3.2.4 Aqueous sample analysis.....	43
3.2.5 Abiotic precipitation experiment.....	44
3.2.6 Solid phase analysis.....	45
3.2.7 XRD analysis and Rietveld refinements.....	45
3.2.8 Monohydrocalcite transformation experiment.....	51
3.2.9 Saturation index and solution chemistry modelling.....	52
3.3 Results	52
3.3.1 Evolution of aqueous chemistry.....	52
3.3.2 Experiment with kaolinite seeds.....	53
3.3.3 Experiments with calcite seeds.....	56
3.3.4 Results from geochemical modelling.....	58
3.3.5 Results from mineralogical characterization.....	59
3.3.6 Abiotic precipitation experiments.....	60
3.3.7 Microbial evidence in mineral precipitates.....	61
3.3.8 Transformation experiment.....	62
3.4 Discussion	64
3.4.1 The influence of microbial sulfate reduction on calcium carbonate precipitation.....	64
3.4.2 Evolving chemical controls on CaCO ₃ precipitation and polymorph selection.....	68
3.4.3 Influence of seeding material on the formation of calcium carbonate polymorphs.....	73
3.4.4 Synthesis, stability and transformation of MHC.....	75
3.4.5 The role of microbial sulfate reduction in carbonate polymorphism in the natural environment.....	78
3.5 Conclusions and Implications	80

CHAPTER 4	82
The effect of seeding materials on the precipitation of calcium carbonate polymorphs	
4.1 Introduction	82
4.2 Materials and method	82
4.2.1 Analytical methods.....	82
4.3 Results and discussion	82
4.3.1 Experiment H (Clay as seeding material).....	83
4.3.2 Experiment I (Calcite as seeding material).....	83
4.3.3 Experiment J (Calcite and kaolinite seeded experiment).....	86
4.3.4 Experiment L (Calcite and kaolinite seeded experiment).....	91
4.3.5 Evolution of saturation index for various calcium carbonate polymorphs.....	93
4.3.6 Variation of phosphate concentration.....	96
4.3.7 Quantitative element mapping of solid precipitates during early precipitation.....	99
4.4 Conclusions	99
CHAPTER 5	101
The influence of sediment mineralogy on the microbial sulfate-reduction in marine sediments	101
5.1 Introduction	101
5.2 Materials and Method	102
5.2.1 Incubation experiment.....	102
5.2.2 Abiotic experiments.....	103
5.2.3 Aqueous sample analysis.....	103
5.2.4 Solid sample analysis.....	104
5.2.5 Statistical application on OPD database.....	105
5.3 Results	106
5.3.1 Mineral seeds experiments.....	106
5.3.2 Result from abiotic experiment.....	109
5.3.3 Nutrient control experiments.....	109
5.3.4 Results from mineralogical characterization and BET surface area.....	111
5.3.5 Results from statistical analysis.....	111
5.4 Discussion	113
5.4.1 The role of mineral seeds on microbial sulfate-reduction rate.....	113

5.4.2	Surface area or nutrient control?.....	116
5.4.3	The influence of substrate mineralogy on calcium carbonate precipitation.....	117
5.4.4	Insights of substrate driven metabolism into ODP cores.....	118
5.5	Conclusions.....	120
CHAPTER 6		122
The formation of siderite in the laboratory and salt-marsh system		
6.1	Introduction.....	122
6.2	Materials and Method.....	123
6.2.1	Field sampling.....	123
6.2.2	Analysis of concretions.....	124
6.2.3	Pore-fluid analysis.....	125
6.2.4	Incubation experiment with pure Norfolk salt-marsh sediment.....	126
6.2.5	Magnetic susceptibility in the salt-marsh.....	127
6.2.6	Transformation experiment.....	129
6.3	Results and discussion.....	132
6.3.1	Concretion mineralogy and geochemistry.....	132
6.3.2	Pore fluid geochemistry.....	137
6.3.3	Mineral saturation state in the sedimentary pore fluids.....	139
6.3.4	Incubation experiments with Norfolk sediment.....	141
6.3.5	Magnetic susceptibility mapping in the Norfolk salt-marshes.....	148
6.3.6	Transformation experiments.....	150
6.3.7	Proposed formation of siderite concretion in the marsh.....	154
6.4	Conclusions.....	156
CHAPTER 7		158
Conclusions.....		
		158
References.....		
		161
Appendix.....		
		183

List of Figures

Figure 1.1: The structure of MHC viewed down 001. (a) The $P3_121$ subcell structure of Effenberger (1981) showing the disordered carbonate groups, (b) the superstructure $P3_1$ model of Effenberger, and (c) the structure refined in $P3_1$. The principal difference between structures b and c can be seen in the orientations of the carbonate groups about the screw axis at $(1/3, 2/3, z)$ (Figure adopted from Kimura and Koga, 2011).....	2
Figure 1.2: Comparison of the modeled effect of seawater sulfate reduction on calcite saturation index (SI) for different electron donors (After Gallagher et al., 2012) and general organic matter, CH_2O (Meister, 2013).....	7
Figure 1.3: Relative abundance of $CaCO_3$ polymorphs incubated under three experimental seawater of different Mg/Ca ratio (After Ries et al., 2008).....	12
Figure 1.4: Distribution of calcium carbonate polymorph as a function of solution chemistry (Mg/Ca ratio and sulfate concentrations). After Bots et al., (2011).....	12
Figure 2.1: Variables measured in Experiment A where A-T1 and A-T2 have different amount of silica (glass) nucleation seeds. Solid precipitates were observed after 300 hours. Note that a control (blank) sample was not set up in this trial experiment.....	23
Figure 2.2: Concentration of sulfide, magnesium and calcium in Experiment B. Sample B-W and B-G are different samples and only sample B-W was measured for cations. Data for the quiescence sample (in red) were from Experiment A whereas the results on shaker (blue) is from Experiment B. XRD diffractogram of MHC forms from culture medium incubated after two years.....	24
Figure 2.3: Elemental results for Experiment C. $FeSO_4$ was added in sample C-A after autoclaving while before autoclaving for sample C-B. Note that there is no significant difference between sample C-A and C-B.....	26
Figure 2.4: OD1 indicates the OD measured within one minute after sampling while OD5 indicates the OD measured at the fifth minutes after sampling. The results suggest that time does not impact the OD reading. The plot also shows that rpm of 800 – 1200 is the most suitable centrifuge speed for measuring OD of the samples. Note that the data plotted in black are samples being shaken before sampling while data in red are samples being carefully sampled without shaking. At rpm < 800, centrifugation is less effective to separate the suspended seeds and the bacteria cells in the medium. At higher rpm (> 1200), the bacteria cells started to separate from the medium. Therefore, a centrifuge speed between 800 – 1200 rpm is the best speed to measure OD in my samples.....	27

Figure 2.5: Changes in pH, OD600, Ca, Mg and Sr concentration in the sample medium of Experiment D.....	29
Figure 2.6: Variables measured in Experiment E where sample E-T is seawater, sample E-R and E-S are artificial seawater with Mg/Ca ratio of 0 and 1. Saturation indices for each mineral were calculated using PHREEQC. Note that iron was added at 475 hours in samples T1, R1 and S1.....	33
Figure 2.7: Evolution of aqueous chemistry in the samples over time in Experiment F.....	35
Figure 2.8: Experiment G was sampled over a longer period approximately 2000 hours due to slower growth.....	38
Figure 3.1: Thick gelatinous layer was observed immediately after the addition of Na ₂ CO ₃ in abiotic experiment without yeast extract (left). Over time, the gelatinous layer gets thinner and eventually vanished after 24-hour incubation (right). A longer period is required for the thinning process in sample with high Mg/Ca and yeast extract and vice versa.....	45
Figure 3.2: Measured calcite wt % in standard versus calcite wt % as calculated from Rietveld refinement. The linear fit yielded $y = 6 \pm 4 + (0.99 \pm 0.06) x$. $R^2 = 0.99$	47
Figure 3.3: Rietveld refinement experimental (blue), calculated (red) and difference (grey) curves for the control sample. Peak position marks are shown for kaolinite (green) and halite (blue). The pattern was collected on instrument nr.2 - see experimental details in the manuscript. Collections conditions were: 10-70° in 2θ, 0.04° step size, 40 seconds/step. Final R_{wp} and χ^2 are 21.01% and 1.70 respectively.....	47
Figure 3.4: Rietveld refinement experimental (blue), calculated (red) and difference (grey) curves for sample K-4:1. Peak position marks are shown for kaolinite (blue), monohydrocalcite (green) and halite (pink). The pattern was collected on instrument nr.2.....	48
Figure 3.5: Rietveld refinement experimental (blue), calculated (red) and difference (grey) curves for the abiotic with Yeast Extract (stirred). Peak position marks are shown for calcite (blue), kaolinite (green) and halite (pink). The pattern was collected on instrument nr.3.....	49
Figure 3.6: Rietveld refinement experimental (blue), calculated (red) and difference (grey) curves for sample NOYE (stir). Peak position marks are shown for halite (blue), aragonite (green) and kaolinite (pink). The pattern was collected	

on instrument nr.3 - see experimental details.....	47
Figure 3.7: Rietveld refinement experimental (blue), calculated (red) and difference (grey) curves for sample No Yeast Extract (Stirred). Peak position marks are shown for monohydrocalcite (blue), halite (green) and kaolinite (pink). The pattern was collected on instrument nr.3.....	50
Figure 3.8: Rietveld refinement experimental (blue), calculated (red) and difference (grey) curves for sample K-4:4. Peak position marks are shown for calcite (blue), Mg-calcite (green) and halite (pink). The pattern was collected on instrument nr.1	50
Figure 3.9: Aqueous chemistry data for the experiments with kaolinite seeds (a) optical density; (b) SO_4^{2-} ; (c) pH; (d) total alkalinity; (e) Ca^{2+} ; (f) Mg/Ca ratio; (g) ionic activity product for $CaCO_3$; and (h) SI_{MHC} calculated immediately after inoculation until 546 hours. I did not observe any significant change in the killed samples (shown in supporting online material F). Sample code explanation – K = kaolinite seeded; C = calcite seeded; 3:1 = Mg 30 mM: Ca 10 mM; Alt-SW = Atlantic Seawater (Mg/Ca = 5.2) [See Table 5].....	55
Figure 3.10: Aqueous chemistry data for the experiments with calcite seeds (a) optical density; (b) SO_4^{2-} ; (c) pH; (d) total alkalinity; (e) Ca^{2+} ; (f) Mg/Ca ratio; (g) ionic activity product for $CaCO_3$; and (h) SI_{MHC} measured immediately after inoculation until 546 hours. A drop in pH and calcium concentrations in C-Alt-SW is not apparent although precipitation of MHC (measured by XRD and SEM) occurred. Sample code explanation – K = kaolinite seeded; C = calcite seeded; 3:1 = Mg 30 mM: Ca 10 mM; Alt-SW = Atlantic Seawater (Mg/Ca = 5.2) [See Table 3.1].....	56
Figure 3.11: Comparison of experimental and modelled evolution of aqueous chemistry in samples with different seeding materials. A larger discrepancy between experiment and model was observed in samples with kaolinite seeds (a and c) compared to calcite seeds (b and d). An increase in the mismatch between experimental and modelled results is observed with an increasing Mg/Ca. The line labelled 'uncorrected' indicates the initial modelled values without any addition or removal of $NaHCO_3$ from the solution input.....	58
Figure 3.12: Powder X-Ray diffraction patterns collected from selected incubation samples in the three biotic experiments, (a) Mg/Ca=1 (kaolinite); (b) Mg/Ca=1 (calcite); and (c) Mg/Ca=3 and 9 (kaolinite and calcite). Intensity is reported in counts.....	60

Figure 3.13: SEM images (backscattered electron) showing (a) MHC hemisphere with bacteria colony concentrated at the hollow core – sample C-Alt-SW; (b) triplet hemi-spherulitic MHC structure with hollow core – sample C-Alt-SW; (c) dumbbell-shaped structure with protruding well-preserved bacterial cell observed in sample K-4:4; (d) precipitated calcite located adjacent to fossilized bacterial colony – sample K-4:4 with closeup secondary electron (SE) image showing instantaneous calcification of *Desulfovibrio bizertensis* by the nano-sized crystals. All the images showing the morphology and microstructure of carbonate minerals linked to microbial sulfate reduction..... 62

Figure 3.14: SEM images show the morphology of minerals precipitated in the biotic and abiotic experiments. (a) Initial spherulitic MHC from the biotic experiments; and (b) sub-micron aggregated platelets (cauliflower-shaped) MHC from abiotic experiment. The mineralogy of these final products was confirmed using XRD. Image (c) – T-Alt-SW, (d) – T-MQ, (e) – T-Alt-SW-YE, and (f) – T-Alt-SW-PO4 are transformation products of Figure 5a after thermal dehydration at 100°C for 48 hours. I note the distinct morphological alteration of the final products (aragonitic needles, calcite rhomb and bigger hollow core of preserved spherulitic MHC). Mineral composition of these final polymorphs is reported in Table 3.6..... 64

Figure 3.15: SEM images showing the coexistence of amorphous-liked and nano-crystalline minerals in the samples. Nano-sized crystallites growing on the bacterial surfaces and the base which eventually entombed the bacteria. a) AYE(ACC) – abiotic sample with yeast extract added; b) K-4:4; c) K-4:4; and d) C-3:1..... 68

Figure 3.16: The stability field for MHC and calcite. The data points are taken from the point in the experiment where precipitation occurs, although the initial solution chemistry and subsequent solution chemistry evolve. Square symbols indicate calcite is the final polymorph, circle symbols indicate MHC and diamond symbols have mix mineralogy (both MHC and Mg-calcite). Open symbols mark samples with calcite as seeding material while close symbols are kaolinite seeded samples. Experiments from this study are plotted on an abiotic stability field delineated by Blue et al., (2017) – the dot-dash line. The MHC domain in my experiments (dashed line) has shifted left (from aMg^{2+}/aCa^{2+} approximately 8 to 2)..... 70

Figure 3.17: Evolution trajectories of samples with different initial Mg/Ca (selected samples are shown) when carbonate precipitated. Square symbols

indicate calcite is the final polymorph while circle symbols indicate MHC as the major stable product at the end of the incubation experiment. Enlarged symbols with a cross or round shape marked the early nucleation stage. The experiments from this study were plotted on an abiotic stability field delineated Blue et al., (2017). Note the boundary of MHC domain has shifted towards left in the microbial induced studies, suggesting the effect of phosphate in stabilizing the MHC in biotic studies..... 71

Figure 3.18: The precipitation of MHC in wt % (of total solid sample) as a function of Mg/Ca (before precipitation) in experiment with different seeding materials. Error bars represent the estimated standard deviation calculated from Rietveld refinement..... 74

Figure 3.19: Submicron to nano-sized magnesium calcite crystals grow on calcite seeds (a) C-3:1 and; (b) C-2:1. Arrows show two forms of magnesium calcite growing epitaxially on calcite seeds..... 75

Figure 3.20: Cross plot between saturation index and aMg^{2+}/aCa^{2+} indicates that SI_{MHC} higher than 1.0 is required for the formation of MHC at aMg^{2+}/aCa^{2+} greater than 2. The data points are measurements taken before the precipitation of calcium carbonate. Abiotically precipitated calcium carbonate reported in Rodriguez-Blanco et al. (2014) were compared and given in square symbols..... 77

Figure 3.21: SEM elemental mapping (Ca, Mg and P) of MHC. (a) chemical composition of MHC prior to transformation experiment; (b) hemispherulite MHC with higher Mg distribution at the core prior to transformation; (c) cross section of spherulitic MHC (T-Atl-SW-YE); and (d) surface chemical compositions of MHC (T-Atl-SW-YE) after transformation process..... 78

Figure 4.1: Parameters measured in Experiment H- from top to bottom Alkalinity, pH, OD, SO_4^{2-} , Ca^{2+} , Mg^{2+} , and Mg/Ca. (Kaolinite seeding). Phosphate was not measured in series H due to some errors during the analysis and is shown in Figure 4.8..... 88

Figure 4.2: Parameters measured in Experiment I- from top to bottom Alkalinity, pH, OD, sulfides, SO_4^{2-} , Ca^{2+} , Mg^{2+} , and Mg/Ca (Calcite seeding)..... 89

Figure 4.3: (a-b) Epitaxial growth of magnesium calcite on calcite seeds. (c-d) No surface growth was found on kaolinite. Note that Figure 4.3c is sample with mixed seeding materials where epitaxial growth of calcium carbonate can be seen on the calcite seeds but not on kaolinite (middle and scattered around the calcite)..... 90

Figure 4.4: (a-b) Bacterial imprints on calcite. Note that the number of cells is low for a given surface area; (c-d) SE images show that more bacterial cells are found aggregated on kaolinite seeds, forming a colony. This implies that the sulfate-reducing bacteria grow better in kaolinite seeds compared to calcite seeds 91

Figure 4.5: Parameters measured in series J (Kaolinite or calcite seeding) K=kaolinite seeding; C=calcite seeding 93

Figure 4.6: Parameters measured in series L (Kaolinite or calcite seeding) K=kaolinite seeding; C=calcite seeding 95

Figure 4.7a-e: The solution chemistry started mostly undersaturated with respect to different calcium carbonate polymorphs (aragonite, calcite, and vaterite). After 100 hours all calcium carbonate polymorphs were supersaturated. The upper row shows the experiments with kaolinite seeds, while the lower row with calcite seeds 97

Figure 4.8: Drop of phosphate concentration over time in the kaolinite and calcite seeded experiment 98

Figure 4.9: Crossplot of the phosphate reduced versus the rate of change in calcium concentration 98

Figure 4.10: Quantitative elemental mapping of samples showing the phosphorus enriched CaCO₃ phase during the early stage of precipitation. More EDX-spectra of the samples are shown in Appendix A 99

Figure 5.1: The first incubation with varying proportion of CaCO₃ was presented with a color gradient, where the darker color lines indicate a higher proportion of CaCO₃. Open circle symbol is the sample without mineral seeds. Note that the first incubation experiment was conducted in two separate runs. The first run are samples with 100%, 75%, 50%, 25%, 0% CaCO₃ and the seedless sample. The second run includes samples with 100%, 99%, 90%, 80% and 10% CaCO₃. The two experiments were run for slightly different amounts of time, which is why some lines are shorter than others. Incubation experiment results with varying proportion of CaCO₃ to various aqueous chemistry variables, (a) OD600; (b) alkalinity; (c) pH; (d) sulfate; (e) sulfide; (f) calcium; (g) magnesium; and (h) sodium. I did not observe any significant change in the control samples (shown in Appendix C) 108

Figure 5.2: Plots showing the results of (a) pH; and (b) alkalinity in abiotic experiments with varying proportion of carbonate to clay and the total volume of mineral seeds 109

Figure 5.3: Second incubation experiment using different seeding materials to examine the influence on bacterial growth and the evolution of aqueous chemistry (a) OD600; (b) pH; (c) alkalinity; (d) sulfate; (e) phosphate; (f) sulfides; (g) calcium; and (h) magnesium. The results of control samples are given in the Appendix D. The error bars in the figure represents the standard deviation of triplicates. The calcium carbonate minerals formed from the incubation samples are shown in Appendix E..... 110

Figure 5.4: XRD patterns collected from selected biotic incubation samples. Monohydrocalcite (MHC) and Mg-calcite are the main calcium carbonate polymorphs that precipitate from the samples. The proportion of MHC increases as the proportion of calcium carbonate in the original seeding material decreases. A small amount of silicon powder is added to the sample as an internal standard to calibrate the peak position (dotted line). Sub-figure shows the presence of MHC in samples with calcite lower than 80% at a low 2θ value (marked in red)..... 111

Figure 5.5: The relationship between alkalinity and sulfate reduced in incubation samples at 400 hours shows that after correction for the occurrence of carbonate precipitation a majority of the samples sit close to the calculated metabolic stoichiometry of sulfate reduction coupled to formate oxidation (Gallagher et al., 2012): $4\text{CHO}_2^- + \text{SO}_4^{2-} + \text{H}_2\text{O} \rightarrow 4\text{HCO}_3^- + \text{HS}^- + \text{OH}^-$. The red line indicates the calculated stoichiometry without carbonate precipitation while the takes carbonate precipitation into account. Samples marked in blue indicate the actual measured concentrations at 400 hours, whereas samples in orange are corrected for the alkalinity lost due to carbonate precipitation. The correction was made by adding twice the difference in both calcium and magnesium concentration between 0 hours and 400 hours (assuming calcium and magnesium were lost due to carbonate precipitation). Error bars in the plot indicate the measurement errors of the method used..... 115

Figure 5.6: Changes in maximum alkalinity and pH as a function of CaCO₃ in the incubation experiments. The data plotted displays maximum alkalinity and pH recorded over the course of the experiment..... 116

Figure 5.7: Data extracted from ODP database shows that the geochemistry of a majority of sediments are influenced by sulfate reduction. This process is largely influenced by the CaCO₃ content of the substrate. The CaCO₃ (%) is categorized and the data in y-axis were averaged. The bars in the graph represent maximum alkalinity (mEq L⁻¹) while the line with markers indicates the minimum sulfate

concentration (mM). The number of samples considered in the analysis is presented in colours.....	119
Figure 5.8: (a) Cross plot of alkalinity vs. sediment CaCO ₃ (%) with PC1 scores on z-axis; (b) Distribution of ODP cores influenced by PC1.....	120
Figure 6.1: The salt-marshes in North Norfolk is an ideal natural laboratory where siderite concretions are actively forming. The geochemical nature of the ponds can be easily distinguished in the field by examining the presence of sulfides.....	124
Figure 6.2: Two carbonate/siderite concretions (O and N) with diameter ~15 cm were cut into parallel slices for mineralogical and geochemical analysis. For mineralogical analysis, different parts of the concretion (blue circle) were carefully excavated and pulverized prior to analysing by a D8 Bruker X-Ray Diffractometer (XRD). To examine the bulk geochemical composition across the concretions (12mm dotted line box of A-A', B-B' and C-C'), freshly cut samples were scanned by an Avaatech XRF core scanner.....	125
Figure 6.3: Schematic drawing of a grid. The arrows indicate the traverse direction (in zig-zag mode).....	128
Figure 6.4: Elemental distribution along the cross-section of the concretions (a – f), x-axis in centimeters; and cross-plots with titanium normalized (g, h and i) of the studied elements. Note that higher resolution of scanning is done across transect C of concretion O#1.....	135
Figure 6.5: Geochemical data of pore-fluid in the salt-marsh. Note that the red color dots represent iron-rich core while black colored data belongs to sulfidic core. CO ₂ , HCO ₃ ⁻ , CO ₃ ²⁻ , pCO ₂ , DIC were calculated using CO2Calc. Dissolved iron data for sulfidic core were obtained from ICP-OES. C-Alk (carbonate alkalinity) was calculated by subtracting the sulfide concentration from alkalinity data. Ionic strength was manually calculated with a concentration of Ca ²⁺ , Mg ²⁺ , Na ⁺ , K ⁺ and SO ₄ ²⁻ , Cl ⁻ measured in the pore-fluid using the equation $I = \frac{1}{2} \sum m_i \cdot z_i^2$. Dotted lines plotted along the bicarbonate are the alkalinity. The open circle is the measured DIC concentration of different sediment cores from the salt-marsh while the filled circle is my calculation (Warham – Red; and Blakeney - Black). The DIC measurement (open circle) was previously done by Gilad Antler.....	139
Figure 6.6: Saturation states (Ω) of various minerals in the salt-marsh. If $SI < -0.2$, the pore-fluid is undersaturated with respect to that particular mineral. While $SI = -0.2 \leq 0 \leq 0.2$, it means that the pore-fluid is in equilibrium with that mineral.	

<i>If SI > 0.2, this indicates that the pore-fluid is oversaturated with respect to that mineral.....</i>	140
Figure 6.7: <i>Incubation samples using Blakeney sediment samples with formate and acetate as electron donor – (a) alkalinity; (b) pH; (c) iron; and (d) phosphate. Precipitation of siderite is absence in both samples.....</i>	142
Figure 6.8: <i>The second incubation experiment with plots showing (a) alkalinity; (b) pH; (c) iron; (d) sulfate; (e) sulfide; (f) chloride; (g) SO₄²⁻/Cl⁻; (h) calcium; (i) magnesium; (j) Mg/Ca; (k) Fe/Ca; and (l) saturation index of siderite.....</i>	146
Figure 6.9: <i>Powder X-ray diffraction pattern of the incubation samples (a) outer layer of steel ball; and (b) sediments after the incubation. Q = quartz; S = siderite; K = kaolinite; I = illite; C = calcite.....</i>	146
Figure 6.10: <i>Secondary electron images and backscattered electron images of siderite collected from the steel balls. Figures in colour show the elemental distribution for iron, calcium, oxygen, and aluminium from both replicates of the incubation samples.....</i>	147
Figure 6.11: <i>Trigonal siderite found in replicate one of the incubated sediment.....</i>	148
Figure 6.12: <i>SEM images show the presence of framboidal pyrite in the incubation sample (replicate 1).....</i>	148
Figure 6.13: <i>Magnetic susceptibility map (unit in nano-Tesla) in Norfolk saltmarshes. Grid 16 and 29 are situated in Blakeney; Grid 19, 20 and 21 in Warham saltmarsh; and Grid 23, 25, 26 and 28 in Stiffkey. Siderite concretion was buried at the middle (marked by a red star) of the plots in both Grid 16 and 20, 21, 23, 26, and 29. Grid 19 is the same plot as Grid 20 and is surveyed without concretion buried. Same goes to Grid 23 and Grid 25; Grid 26 and Grid 28. Grid 25 and 28 are just background without concretion.....</i>	149
Figure 6.14: <i>Morphology of transformation samples. Spherulitic siderite in sample T11c after heated in modified medium for 48 hours at 100 °C. (a) Aggregates of spherulitic siderite; (b) individual aggregates of spherulitic siderite; (c) rhombohedral siderite; and (d) coating of iron oxide minerals.....</i>	154

List of Tables

Table 1.1: Stabilities of common carbonate minerals under standard pressure and temperature (1 atm, 20 °C) conditions (Adapted from Morse et al., 2007). <i>pK</i> values are thermodynamic $-\log K_{sp}$. <i>pK</i> is the negative logarithmic scale of equilibrium constant and K_{sp} is the equilibrium constant of the solubility product. Crystal system of the carbonate minerals were also reported.....	3
Table 1.2: Balanced redox equation for dissimilatory sulfate reduction of several low molecular weight compounds commonly used by sulfate-reducing bacteria.....	7
Table 2.1: List of chemicals used in making up the medium needed in the incubation experiments.....	17
Table 2.2: List of chemicals used to prepare artificial seawater.....	18
Table 2.3: List of chemicals used and the final concentration in the seawater medium.....	21
Table 3.1: Summary of experiment setup for biotic incubation experiments.....	43
Table 3.2: Instrument and Rietveld refinement details for all samples. R_{wp} shows the quality of the least square refinement after background subtraction. The “Chi squared” or χ^2 is the goodness of fit of the model and data (Toby, 2006).....	50
Table 3.3: Initial and final weight of calcite seeds in control samples.....	57
Table 3.4: Summary of XRD results with Rietveld quantitative analysis of minerals (wt % with estimated standard deviation) for all experiments. Calcite and Magnesium Calcite differ in their concentration of magnesium and have different XRD patterns.....	59
Table 3.5: Summary of final polymorphs obtained from the abiotic precipitation experiment. The initial chemical composition (i.e. the amount of yeast extract) and medium preparation procedures in this experiment are virtually identical to those of the biotic experiments except there is no inoculation. Kaolinite was used as seeding material.....	61
Table 3.6: Mineralogical composition of calcium carbonate polymorphs (in wt %) derived from MHC transformation.....	63
Table 5.1: Selected variables from the ODP cores and their justifications for consideration in the statistical analysis.....	106
Table 5.2: Principal components of various variables relevant to microbial sulfate reduction in the ODP cores. Note that all data was log-normalized before PCA. The missing data were treated with multiple imputation functions before the analysis. Significant PC loadings greater than 0.4 were given in bold.....	112

Table 6.1: Summary of the materials and setup in the first and second incubation experiments.....	127
Table 6.2: Grids surveyed in the salt marsh, GPS locations and information of the grids	129
Table 6.3: Summary of the initial media and mineral seeds used in the transformation experiments. Incubation samples with varying iron concentrations were labelled as medium in the initial and followed by the concentration of iron in millimolar. For example, MQ50 indicate the medium is MQ-water with 50 mM of iron. SW denotes seawater as the medium. MQ100 – SW10 were incubated under anoxic condition to make sure ferrous iron is in its dissolved form. Initial CaCO ₃ with MHC/Calcite indicates that the initial media is incubated with MHC or calcite (marked with a different colour in the table) and a seedless control in separated vials, therefore, one line on the table, or one type of media may represent three samples.....	131
Table 6.4: Weight percentages of phases for concretion samples with relative e.s.d. (in parenthesis). Additional samples collected from the concretions (not shown in Figure 6.2) were homogenized, and analysed in bulk. Abbreviation of the samples are given in the Table’s footnote. Sample O#1 is shaded in grey.....	133
Table 6.5: Selected locations (C1 – C8) of concretion N#2 with interval approximately 1-2 mm were drilled across from the center to the edge of the concretion. The drilled materials were examined for carbon and oxygen isotopic composition in the Godwin Laboratory. W1 is wood materials located at the center of the concretion; C9 was sampled near to the edge of the concretion where the dark and extremely rigid material is.....	137
Table 6.6: Summary of the aqueous chemistry and the initial and final calcium carbonate polymorphs in the transformation experiment. The experiment was carried out in the oven at 100 °C for 48 hours except stated otherwise. T01 – T04 were presented in Chapter 3. Rows with common shaded colour shared a same initial solution chemistry. T32 and T35 are control samples. Sample T40 – T63 were incubated under anoxic condition. Estimated standard deviation, R_{wp} and χ^2 values for Rietveld quantifications are given in Appendix I.....	152

Chapter 1

The role of microbial sulfate reduction in the precipitation of calcium carbonates

1.0 Introduction

Around 42% of all carbon on Earth is locked up in the form of carbonate minerals and rocks, mostly calcium carbonate (Ehrlich, 1996). The formation of carbonate minerals thus plays a significant role in the global carbon cycle. The global carbon cycle refers to the exchange of carbon between the surface and subsurface of Earth, as well as the exchange of carbon among the many different surface reservoirs such as the atmosphere, ocean, and biosphere (Bernier, 2003). Carbon that is at Earth's surface in one of these many different surface reservoirs may leave Earth's surface through burial and lithification of organic carbon and carbonate minerals; this occurs largely in marine sediments (Bernier, 2003; Falkowski et al., 2000).

In the ocean, the most common calcium carbonate minerals are aragonite and calcite, which have the same chemical formula but different mineral structures, making them polymorphs. At Earth-surface conditions, calcite is the more thermodynamically stable form of calcium carbonate (Sekkal and Zaoui, 2013; Millero, 1982). Marine calcite may also contain variable amounts (approximately 10 to 30 mol%) of MgCO_3 in solid solution, known as magnesian calcite or 'high-mag calcite'. The solubilities of some common carbonate minerals are summarized in Table 1.1. Aragonite is both denser and more soluble than calcite. These two phases also differ in their tendency to accept divalent cations other than Ca^{2+} in the mineral phase (Morse et al., 2007). Vaterite ($\mu\text{-CaCO}_3$) is also a calcium carbonate polymorph that is metastable with respect to calcite and aragonite and limited to minor biogenic occurrences; hydrated calcium carbonate phases (e.g. ikaite) are found only in very low temperature, high-pressure environments (Morse et al., 2007); and monohydrocalcite is reported to form in a range of environments (such as saline springs, marine polar systems and lacustrine deposits) but is also believed to be metastable (Ito, 1993; Bird et al., 1991; Dahl and Buchardt, 2006; Stoffers and Fischbeck, 1974; Taylor 1975)

Laboratory synthesis of MHC has been succeeded from artificial seawater or from a mixed solution of calcium chloride and magnesium chloride, where Mg^{2+} ion in the mother solution plays a predominant role for the selective precipitation of MHC in the mother solution. The

crystal structure of MHC (hexagonal system - trigonal) has been determined by single crystal diffraction as $P3_1$ with $a = b = 10.5536 \text{ \AA}$ and $c = 7.5446 \text{ \AA}$ (Effenberger, 1981) (Figure 1.1), which was reexamined by neutron and X-ray diffractions making refinements on the hydrogen bonding structure and orientations of carbonate groups. Two different morphologies of MHC crystalline particles can be found in the literature, one is spherulite and the other is an aggregate of platelets, which indicate the different reaction behaviors during the thermal dehydration of crystalline water (Kimura and Koga, 2011). The detail crystallographic data of calcite, siderite, magnesite and dolomite were reported in Effenberger et al. (1981) and Cygan et al. (2002).

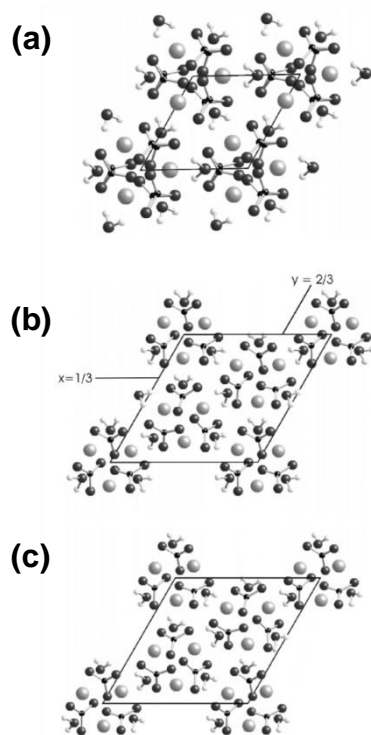


Figure 1.1: The structure of MHC viewed down 001. (a) The $P3_121$ subcell structure of Effenberger (1981) showing the disordered carbonate groups, (b) the superstructure $P3_1$ model of Effenberger, and (c) the structure refined in $P3_1$. The principal difference between structures b and c can be seen in the orientations of the carbonate groups about the screw axis at $(1/3, 2/3, z)$ (Figure adopted from Kimura and Koga, 2011).

Table 1.1: Stabilities of common carbonate minerals under standard pressure and temperature (1 atm, 20 °C) conditions (Adapted from Morse et al., 2007). *pK* values are thermodynamic $-\log K_{sp}$. *pK* is the negative logarithmic scale of equilibrium constant and K_{sp} is the equilibrium constant of the solubility product. Crystal system of the carbonate minerals were also reported.

Phase	Formula	<i>pK</i>	Crystal system
Aragonite	CaCO ₃	8.30	Orthorhombic
Calcite	CaCO ₃	8.48	Trigonal
Magnesite	MgCO ₃	8.04	Trigonal
Siderite	FeCO ₃	10.52	Trigonal
Rhodochrosite	MnCO ₃	10.08	Trigonal
Dolomite	CaMg(CO ₃) ₂	18.15	Trigonal

The majority of carbonate minerals found in marine sediments comes from a wide variety of benthic and pelagic organisms that build their skeletons out of various carbonate minerals (Morse et al., 2007; Tucker and Wright, 1990). Within marine sediments, production of carbonate minerals may occur abiotically, through bacterial iron or manganese reduction, urea hydrolysis, microbial sulfate reduction and anaerobic methane oxidation, as these metabolic processes yield an increase in the pH of the microenvironment and thus favor carbonate mineral precipitation (Soetaert et al., 2007).

There are three different mechanisms involved under the broad term ‘biogenic production of calcium carbonate’. (1) **Biologically controlled mineralization** consists of cellular activities that specifically control the formation of minerals. In this process, organisms control both the nucleation and the growth of minerals. This is common for benthic and pelagic organisms that build their skeletons out of various carbonate minerals (2) **Biologically influenced mineralization**, through which passive mineral precipitation is caused by the presence of cell surface organic matter such as extracellular polymeric substances (EPS) associated with biofilms. This mechanism is common in marine sediments (3) **Biologically induced mineralization** is similar to biologically influenced mineralization, in that it involves chemical modification of an environment by metabolic processes that results in supersaturation and the precipitation of minerals (Anbu et al., 2016; Dupraz et al., 2009).

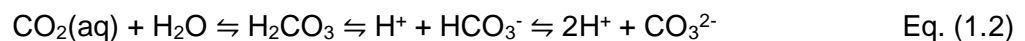
1.1 The alkalinity engine and saturation index

Aqueous solutions do not contain free protons and free electrons, but it is nevertheless possible to define relative proton and electron activities. pH measures the relative tendency of a solution to accept or transfer protons. pH may be defined in terms of hydrogen ion activity.

$$\text{pH} = -\log [\text{H}^+] \quad \text{Eq. (1.1)}$$

Within the ionic medium convention, Eq.1.1 may be used operationally because one can usually measure $-\log [H^+] = -\log \{H^+\}$ rather accurately. An electrode system is calibrated with solutions of known concentrations of strong acid (e.g. $HClO_4$), which are adjusted with an electrolyte to the appropriate ionic strength, the observed potentiometer (pH meter) reading being compared with $[H^+]$. Ionic strength, is the measure of the internionic effect resulting primarily from electrical attraction and repulsions between the various ions (Stumm and Morgan, 1996).

In aqueous environments, carbon dioxide exists in three different inorganic forms: as aqueous carbon dioxide, $CO_2(aq)$ as the bicarbonate ion, HCO_3^- , and as the carbonate ion, CO_3^{2-} . A fourth form, H_2CO_3 (< 0.3%) is very unstable and readily dissociates into HCO_3^- and H^+ . The carbonate species are related by the following chemical equilibria (Eq. 1.1) (Zeebe and Wolf-Gladrow, 2001):



The left arrow is the equilibrium constant for hydrolysis according to Henry's Law (K_H). The middle arrow has a pK_1 of 5.9 and the right arrow has pK_2 of 8.9, at 25 °C, at 1 bar atmospheric pressure and 35 PSU salinity (Zeebe and Wolf-Gladrow, 2001). The quantitative evaluation of the systematic relations that determine equilibrium concentrations (or activities) of a solution constitutes a purely mathematical problem. Any acid-base equilibrium can be described by a system of fundamental equations. The appropriate set of equations comprises the equilibrium constant (or mass law) relationships (which define the acidity constants and the ion product of water) and any two equations describing the constitution of the solution (Stumm and Morgan, 1996).

The sum of the dissolved forms CO_2 , HCO_3^- , and CO_3^{2-} , is called total dissolved inorganic carbon, which is often denoted by DIC or ΣCO_2 :

$$DIC \equiv \Sigma CO_2 = [CO_2] + [HCO_3^-] + [CO_3^{2-}] \quad \text{Eq. (1.3)}$$

The next essential quantity for the description of the carbonate system is the alkalinity, which is closely related to the charge balance. Total DIC refers to the total amount of dissolved carbon, whereas alkalinity keeps track of the charges in the solution. The carbonate alkalinity, CA is defined as:

$$CA = [HCO_3^-] + 2[CO_3^{2-}] \quad \text{Eq. (1.4)}$$

Where carbonate ions, CO_3^{2-} , are counted twice because of its double negative charge. Carbonate alkalinity is a simplification in that it is part of total alkalinity (TA), which given as (Zeebe and Wolf-Gladrow, 2001):

$$\text{TA} = [\text{HCO}_3^-] + 2[\text{CO}_3^{2-}] + [\text{B}(\text{OH})_4^-] + [\text{OH}^-] - [\text{H}^+] + \text{minor components.} \quad \text{Eq. (1.5)}$$

Carbonate mineral precipitation is a function of the concentration of calcium and carbonate ions, which combined define the saturation for calcium carbonate minerals. The concentration of the carbonate ion depends on the total DIC and the alkalinity/pH. Saturation indices are useful to evaluate the equilibrium between various minerals and their aqueous environment. The saturation condition of a mineral in a solution can be expressed by the ratio between *IAP* and *K*, or saturation state Ω – Eq (1.5):

$$\Omega = \text{IAP}/K_{sp} \quad \text{Eq. (1.6)}$$

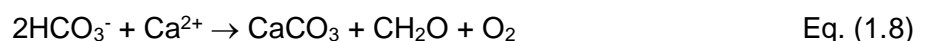
where *IAP* denotes the ion activity product (i.e. $\{\text{Ca}^{2+}\} \times \{\text{CO}_3^{2-}\}$) and K_{sp} , is the solubility product of the corresponding mineral (Stumm and Morgan, 1996). Thus for $\Omega = 1$, there is equilibrium and no propensity to dissolve or precipitate the mineral of interest, $\Omega > 1$ indicates supersaturation and $\Omega < 1$ undersaturation (Appelo and Postma, 2005). The actual $\{\text{CO}_3^{2-}\}$ depends on the carbonate equilibrium presented in Eq (1.1).

When the saturation state (Ω) values are too large to offer a good comparison, the saturation index (SI) become a more useful measure.

$$\text{Saturation index (SI)} = \log \Omega \quad \text{(Eq. 1.7)}$$

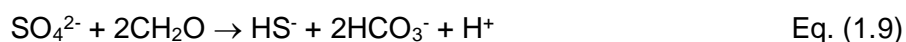
where $\text{SI} > 0.2$ indicates supersaturation, SI between -0.2 to 0.2 indicates equilibrium and $\text{SI} < -0.2$ indicates undersaturation with respect to the mineral of interest.

Various processes at Earth's surface can increase the saturation state of calcium carbonate, promoting carbonate precipitation. For example, photosynthesis involves the removal of CO_2 in solution, thereby, increase the pH, drive the equilibrium in Eq 1.1 to the right, increasing $[\text{CO}_3^{2-}]$ and favour calcium carbonate precipitation. The combined net reaction of photosynthesis and subsequent calcium carbonate precipitation is (Dupraz et al., 2009):



Other metabolisms such as aerobic respiration and methanogenesis increase the dissolved inorganic carbon (DIC) or produce organic acids, which could lead to a decrease in pH and trigger carbonate dissolution (Dupraz et al., 2009). Different microbial metabolisms often interplay within microbial communities. However, it is the net community metabolism that may create conditions favorable to mineral precipitation (or dissolution) (Visscher et al., 1998; Dupraz and Visscher, 2005).

Carbonate precipitation as a result of microbial sulfate reduction has been suggested to occur because sulfate reduction produces dissolved inorganic carbon and increases alkalinity (Berner, 1970; Gallagher et al., 2012; Meister, 2013) (Eq. 1.8):



Due to the production of one mole of H^+ per mole of sulfate reduced, sulfate reduction also lowers pH, which counteracts the increase in carbonate saturation state and therefore acts as an alkalinity sink. Unless the reaction is coupled with pyrite precipitation, the formation of carbonate minerals may be limited if sulfide is accumulating in the system (Sun and Turchyn, 2014; Higgins et al., 2009; Soetaert et al., 2007; Ben-Yaakov, 1973). Models of the pH change during lactate oxidation (not shown in Eq. 1.7) coupled to microbial sulfate reduction have substantiated this decrease in pH (Soetaert et al., 2007), demonstrating that sulfate reduction and methane production are both processes that yield pore fluid with pH~6, which is believed to be too low for carbonate precipitation. On the other hand, anaerobic oxidation of methane (AOM), not discussed here, which is often coupled to sulfate reduction, yields high pore fluid pH around 7.9, which in turns aids in the precipitation of authigenic carbonate minerals due to the increased carbonate ion concentration. Another modeling and culture experiment carried out by Meister (2013) demonstrated that in modern seawater/hypersaline water, sulfate reduction initially lowers the saturation of carbonate minerals due to a rapid drop in pH. As sulfate reduction progresses, the pH begins to stabilize at 6.5 to 7, and carbonate saturation slowly increases as a result of increasing DIC concentration. However, it should be noted that pH alone does not control whether carbonate will precipitate or dissolve. Numerous studies have shown that carbonate can be formed even in low-pH systems (Sanchez-Roman et al., 2014; Fernandez-Remolar et al., 2012).

Several culturing and modeling studies have successfully shown that the specific electron donor, or carbon source, for microbial sulfate reduction influences the change in pH and thus the carbonate saturation index of the medium (Gallagher et al., 2012; Han et al., 2016; Meister

2013; Gallagher et al., 2014). The effect of electron donors on pH and carbonate mineral saturation index are summarized and presented in Table 1.2 and Figure 1.2, respectively:

Table 1.2: Balanced redox equation for dissimilatory sulfate reduction of several low molecular weight compounds commonly used by sulfate-reducing bacteria.

Electron Donor	Summary equation (at seawater pH)	Predicted pH change
Hydrogen	$4\text{H}_2 + \text{SO}_4^{2-} \rightarrow \text{HS}^- + \text{OH}^- + 3\text{H}_2\text{O}$	Increase
Formate	$4\text{CHO}_2^- + \text{SO}_4^{2-} + \text{H}_2\text{O} \rightarrow 4\text{HCO}_3^- + \text{HS}^- + \text{OH}^-$	Increase
Acetate	$\text{C}_2\text{H}_3\text{O}_2^- + \text{SO}_4^{2-} \rightarrow 2\text{HCO}_3^- + \text{HS}^-$	Decrease
Lactate (Complete)	$2\text{C}_3\text{H}_5\text{O}_3^- + 3\text{SO}_4^{2-} \rightarrow 6\text{HCO}_3^- + 3\text{HS}^- + \text{H}^+$	Decrease
Lactate (Incomplete)	$2\text{C}_3\text{H}_5\text{O}_3^- + \text{SO}_4^{2-} \rightarrow 2\text{HCO}_3^- + 2\text{C}_2\text{H}_3\text{O}_2^- + \text{HS}^- + \text{H}^+$	Decrease

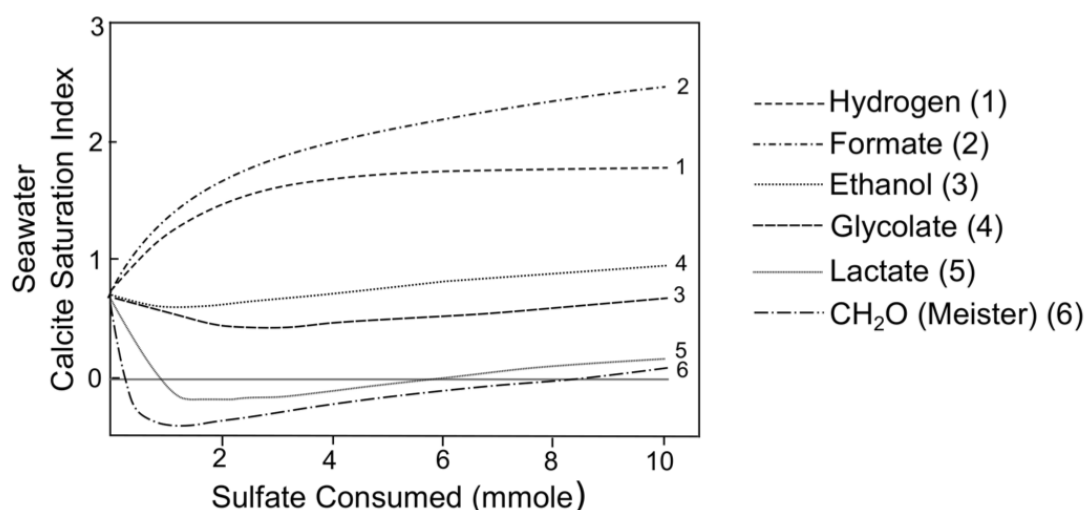


Figure 1.2: Comparison of the modeled effect of seawater sulfate reduction on calcite saturation index (SI) for different electron donors (After Gallagher et al., 2012) and general organic matter, CH_2O (Meister, 2013).

Because of the use of a single electron donor in pure culture and modeling experiments, Meister (2014) argued that many studies might not reflect the actual conditions in the natural environment where there are likely multiple carbon sources and electron donors for microbial sulfate reduction. In fact, he suggested that it is the overall process that affects the pH and saturation index of the solution, which may reflect a complex interplay among many variables. Therefore, care should be taken when one decides which electron donor is used in culture studies.

1.2 The relation between chemical kinetics and chemical equilibrium

The law of chemical equilibrium is derived from the law of mass action. For a reversible chemical reaction (Eq. 1.9): $aA + bB \rightleftharpoons cC + dD$ (Eq. 1.10)

Where a, b, c and d are stoichiometric coefficients in the balanced equation. From the law of mass action, the rate of the forward reaction (Eq. 2.0)

$$r_f = k_1[A]^a[B]^b \quad (\text{Eq. 1.11})$$

where [A] represents the concentration of A and so on. The rate of the backward reaction is (Eq. 1.11)

$$r_b = k_2[C]^c[D]^d \quad (\text{Eq. 1.12})$$

At equilibrium, $r_f = r_b$ (Eq. 1.12), so,

$$\frac{k_1}{k_2} = \frac{[C]^c[D]^d}{[A]^a[B]^b} \quad (\text{Eq. 1.13})$$

Replacing $\frac{k_1}{k_2}$ by K_c (Eq. 1.13),

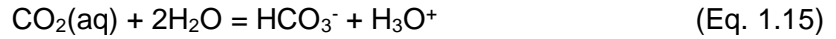
$$K_c = \frac{[C]^c[D]^d}{[A]^a[B]^b} \quad (\text{Eq. 1.14})$$

which is the law of chemical equilibrium. K_c is supposed to be constant, for any concentration of the reactants, at a particular temperature.

Kinetics and thermodynamics are related to each other in ways that can be explained by using chemical reactions. It is important to mention that a chemical reaction has kinetic and thermodynamic aspects. The quantity related to kinetics is the rate constant k ; this constant is associated with the activation energy required for the reaction to proceed, that is, the reactivity of the reactants. The thermodynamic quantity is the energy difference resulting from the free energy (ΔG) given off during a chemical reaction – the stability of the products relative to the reactant. Although kinetics describes the rates of reactions and how fast equilibrium is reached, it gives no information about conditions once the reaction equilibrates. In the same measure, thermodynamics only gives information regarding the equilibrium conditions of products after the reaction takes place, but does not explain the rate of reaction (Ozery, 2014).

The rate constant, k , measures how fast a chemical reaction reaches equilibrium assuming the reactions were supplied with enough activation energy to enable the reaction to proceed in the forward direction – reactants to products. This requirement for input of energy symbolizes the fact that the reactants are unreactive under certain conditions. The reaction must have some sort of energy input before it can proceed; otherwise, the reactants cannot cross the activation energy threshold and convert to products. The reaction is activated by energy supplied to the reactants by different energy sources. The rate of reaction, the rate

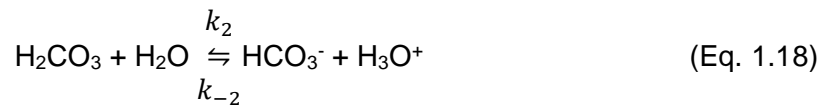
constant, and the kinetic energy required for activation of reaction indicate how fast the reaction reaches equilibrium. The reaction of dissolved carbon dioxide, $\text{CO}_2(\text{aq})$, with water is complex (Eq. 1.14). It is instructive to consider briefly the presently understood mechanism and the rate expression based on it.



An experimentally derived rate expression for this reaction (Eq. 1.15) is

$$R = -\frac{d[\text{CO}_2]}{dt} = (k_{f1} + k_{f2}[\text{OH}^-])[\text{CO}_2] - (k_{b1} + k_{b2}[\text{H}^+])[\text{HCO}_3^-] \quad (\text{Eq. 1.16})$$

A mechanism consistent with the rate expression consists of the concurrent reversible reactions



The first (Eq. 1.16) and third (Eq. 1.18) steps are slow at room temperature, while the second is extremely rapid. The relative importance of the third step to the overall hydration rate increases with increasing pH in the range of natural waters (Stumm and Morgan, 1996).

1.3 Authigenic carbonate

Although most of the ocean floor is bathed in water that is undersaturated with respect to calcium carbonate minerals, authigenic carbonate minerals form within sediments because excess alkalinity is generated through the decomposition of sedimentary organic matter via anaerobic respiration of microbes (Meister et al., 2007; Dela Pierre et al., 2012; Warthmann et al., 2000). Most authigenic carbonate minerals forming in marine sediments are calcite (CaCO_3), aragonite (CaCO_3), dolomite ($\text{CaMg}(\text{CO}_3)_2$), Mg-calcite (MgCO_3), and siderite (FeCO_3); which of these forms largely depends on the chemistry of the pore fluid where the carbonate precipitates (Irwin et al., 1977; Mozley and Burns, 1993).

Authigenic carbonate was recently invoked as the third major global carbon sink in addition to primary marine carbonate minerals and organic carbon (Archer, 2010; Schrag et al., 2013; Zhao, et al., 2016). Sun and Turchyn (2014) modeled marine pore fluid profiles to suggest that this sink might account for 10% of deep ocean carbonate accumulation, or about 3% of the total carbonate mineral sink in the modern, oxic ocean. It has been suggested that

enhanced deposition of authigenic carbonate is likely to be driven by global changes in surface redox conditions, surface saturation state, and/or eustatic sea level (Schrag et al., 2013). However, our understanding of what drives authigenic carbonate precipitation in the modern ocean, marginal marine and lacustrine environments are still far from complete. By understanding the formation of these authigenic carbonate minerals in modern environments, we gain a better understanding of the formation of carbonate minerals in the past.

1.4 *Authigenic carbonate in various environments*

Actively forming authigenic carbonate can be found in wide range of terrestrial environments including soil in arid or semi-arid environments (Eswaran et al, 2000), loessic soils (Kolesar and Curlik, 2015), spring systems (Blank et al., 2009) and lakes (Rosen et al., 1989; Wright, 1999; Balci et al., 2016). Apart from marine authigenic carbonate, the formation of authigenic carbonate in lacustrine and salt-marsh environments has not received much attention. The formation of carbonate minerals in lacustrine and salt-marsh environments may be more varied as these environments receive input from a vast range of reservoirs and have a more varied range of chemistry, therefore, a wider range of carbonate minerals may be stable. The terrestrial carbon cycle involves lithogenous input, atmospheric input, biological input, and hydrological input. In addition, the chemical conditions and some environmental processes such as weathering, evaporation, and leaching may lead to higher concentrations of certain elements such as iron, manganese, and magnesium. This permits a wide spectrum of geochemistry that interacts and controls a wider range of polymorphs of carbonate mineral, for instance, the Mg/Ca ratio, temperature, iron, phosphate and sulfate concentration of the surface and subsurface water.

1.5 *Microbial sulfate reduction*

Many studies have shown that microbes are closely associated with the formation of authigenic carbonate minerals (Warthmann et al., 2000; Disnar et al., 2011). Specifically, sulfate-reducing bacteria play a key role in overcoming kinetic inhibitors to authigenic carbonate formation by raising the pH and alkalinity. The bacterial cell surface can also serve as a nucleation place for carbonate minerals to grow (Wacey et al., 2007; Visscher and Stolz, 2005; van lith, 2001). Van Lith (2001) found that influence of the metabolic rate of different sulfate-reducing bacteria strains might have an indirect influence on the type of authigenic mineral that precipitates. Sulfate-reducing microbial activity leading to carbonate mineralization is also found in stromatolites (Visscher et al., 1998; Visscher et al., 2000; Aloisi, G., 2008; Thompson and Ferris, 1990), marine sediments (Raiswell and Fisher, 2004),

microbial mats (Dupraz et al., 2004; Dupraz et al., 2009) and carbonate concretions (Coleman et al., 1993). Today, some of these microbial structures only form under particular conditions, such as highly alkaline, hypersaline or high-energy settings, but many of these minerals are widespread in the geological record (Meister, 2013; Dupraz et al., 2004). In modern stromatolites and many hypersaline mats, high rates of sulfate reduction were found to occur in the horizons where cyanobacterial photosynthesis peaks (Jorgensen et al., 1983; Baumgartner et al., 2006) and contributed to the lithification of the system (Bosak and Newman, 2003; Reid et al., 2000; Visscher et al., 2000). The formation of stromatolites and the lithification of microbial mats are known to be microbially induced by (1) raising the pH, alkalinity and saturation index; (2) cell material serves as a nucleation site for carbonate to precipitate (Bosak and Newman, 2003). Although many studies seem to support the role of sulfate-reducing bacteria in net mineral precipitation, the contribution of their metabolisms to this specific process in mats is still not understood and is still controversial (Gallagher et al., 2012).

1.6 The Mg/Ca ratio

Among all other driving factors (sulfate concentration, salinity, temperature, $p\text{CO}_2$, pH and alkalinity), aqueous Mg/Ca ratio is thought to have been the major driving force that dictates the types of carbonate polymorph that precipitates from a supersaturated solution (De Choudens-Sanchez and Gonzalez, 2009; Morse et al., 1997; Bots et al., 2011; Reis et al., 2008). For example, Ries et al (2008) has shown the predominance of aragonite over calcite as Mg/Ca increases from 1.5 to 5.2 (Figure 1.3). This is thought to be because with increasing Mg/Ca ratio, more magnesium is able to substitute for calcium in the calcite structure, and thereby affecting the thermodynamic stability of calcite, promoting non-classical nucleation pathways and the formation of polymorphs, particularly aragonite (Davis et al., 2000). This followed on from earlier studies which had shown a higher magnesium to calcium ratio causes aragonite to precipitate instead of calcite at an aqueous Mg/Ca > 1.3 (Morse et al., 1997). An experimental study conducted by Ries et al., (2008) showed that biofilms cultured in modern seawater (Mg/Ca = 5.2) produced both aragonite and high-magnesium calcite, while biofilms cultured in experimental calcite seawater (Mg/Ca = 1.5) precipitated exclusively low magnesium calcite. Abiotic experiments with varying sulfate concentrations and Mg/Ca ratio have also been conducted to study the precipitation of different types of carbonate polymorphs (Bots et al., 2011). In this study, the authors were able to show that an increase in dissolved sulfate concentration decreases the Mg/Ca ratio at which calcite is stabilized and aragonite becomes dominant as depicted in Figure 1.4. In the same study, they also suggested that vaterite – another type of CaCO_3 polymorph, inhibition was attained at aqueous Mg/Ca > 0.2,

owing to the changes in the vaterite structure caused by magnesium incorporation. The formation of vaterite is frequently associated with high sulfate concentration (> 20mM).

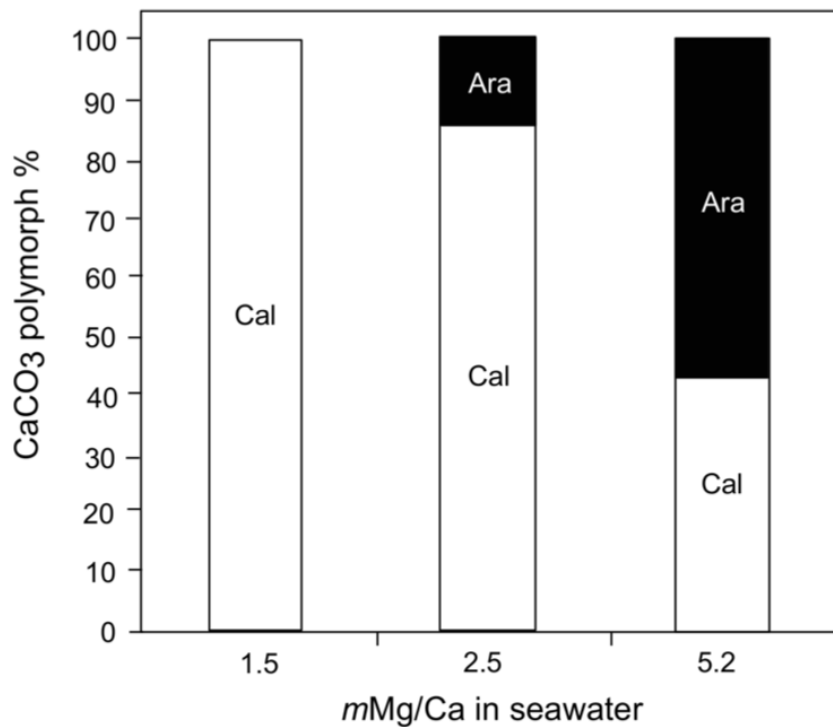


Figure 1.3: Relative abundance of CaCO₃ polymorphs incubated under three experimental seawater of different Mg/Ca ratio (After Ries et al., 2008).

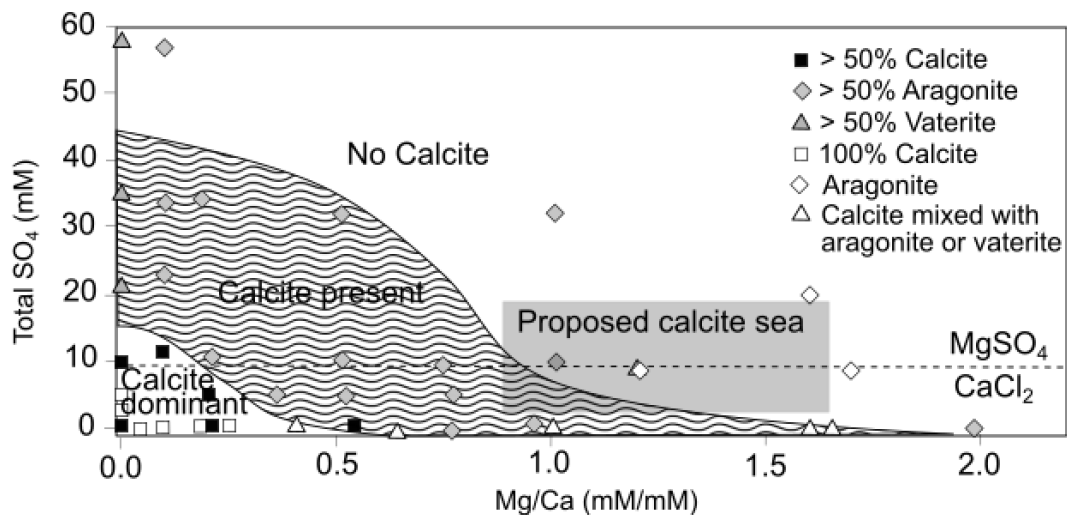


Figure 1.4: Distribution of calcium carbonate polymorph as a function of solution chemistry (Mg/Ca ratio and sulfate concentrations). After Bots et al., (2011).

1.7 *Microbial mediation of mineral formation*

Microbial metabolic activity can directly influence the micro-environment around the cell, leading to a localized oversaturation of a chemical solution. This can induce mineral precipitation by lowering the bulk free energy for homogeneous or heterogeneous nucleation reactions (Hurst, 2016). Due to their small size, microbes have the highest surface-area-to-volume ratio of any group of living organisms and this, together with the presence of charged chemical groups on their cell surface, is responsible for the potent mineral nucleating ability of these cells (Douglas and Beveridge, 1998; Bosak and Newman, 2003.). In addition, microorganisms are able to interact with metal ions in their environment as a consequence of their metabolic activity and the physicochemical properties of their cell surface (Douglas and Beveridge, 1998; van Lith, 2001).

Mineral formation on the microbial cell surface is generally not controlled by the organism; it happens because of the physicochemistry of the cell surface and the chemistry of the cell's environment. Carbonate formation by bacteria involves the ability of the cells to produce an alkaline environment as a result of their physiological activity (Castanier et al., 2000; van Lith, 2001). In addition, some microbes may directly adsorb calcium and magnesium ions or through the production of exopolymeric substances (EPS) due to the negatively charged surface, which in turn complex sulfate or carbonate ions depending on the pH of the solution. When the metabolism drives the pH above 8, carbonate ions complex with the absorbed calcium and magnesium ions leading to the formation of carbonate minerals (Dupraz et al., 2009; Douglas and Beveridge, 1998; van Lith, 2001).

1.8 *Objectives*

This thesis will focus on the use of a novel combination of geochemical and geomicrobiological approaches to explore the mechanisms and factors that drive the formation of authigenic carbonate minerals across a range of environments. With recent advances in analytical geochemistry, the central question is ***what are the surface conditions that contribute to the formation of less common carbonate minerals***. In my thesis, I hope to fill in these gaps through specific studies on the formation of carbonate polymorphs in modern environments. The primary goal of this thesis will be to explore the controls on the precipitation of various polymorphs of carbonate and how they may be limited or accelerated. The main thrust of the project will take three primary objectives:

1. To study the role of sulfate-reducing bacteria on the formation of calcium carbonate polymorphs.
2. To explore the effect of seeding materials (calcite and kaolinite) on the growth rate of sulfate-reducing bacteria and its resulting metabolic products to aqueous chemistry.
3. To investigate the formation of different carbonate polymorphs such as siderite via monohydrocalcite and its possible crystallization pathways in the environment.

1.9 Thesis roadmap

The remaining five chapters of my thesis are comprised of field and laboratory studies, undertaken as part of my Ph.D. In chapter two, I will describe the methods I used to explore the geochemical parameters that influence the precipitation of carbonate polymorphs in pure culture experiments. In Chapter 3, I study the role of sulfate-reducing bacteria on the formation of different calcium carbonate polymorphs; the results presented in Chapter 3 have been published in *Geochimica et Cosmochimica Acta* (Lin et al., 2018). Incubation experiments were set up and a range of experimental variables including Mg/Ca and types of seeding materials will be considered. Chapter 4 stems from Chapter three, and discusses in detail the aqueous chemistry of both biotic and abiotic experiments. This chapter will also explore various types of calcium carbonate polymorphs that can form under various ion pairing (Mg and Ca). Then, using the same incubation techniques developed in the previous chapters, I will explore the effect of seeding materials on the rate of microbial sulfate reduction. The results will be compared with marine core sediments and the observations will be discussed for more global implications. In Chapter six, I will conduct more incubation experiments using environmental samples to examine the formation of siderite. Besides, transformation experiments were set up using monohydrocalcite to explore its possibility as an intermediate mineral/precursor for various calcium carbonate polymorphs including siderite. Then, I will relate the results with the formation of siderite concretions in Norfolk salt-marshes where its geochemical environment has been characterized. Finally, I summarize these results with a theory for what determines the types of authigenic carbonate minerals that form in different natural environments and how it can be used as an analogy to understand and reflect the geochemical conditions in the geological past.

Chapter 2

The development of method for incubation experiments in the laboratory

2.1 Introduction

The vast majority of abiotic studies (free-drift or chemostat) have shown that seawater Mg/Ca has a strong influence on the polymorph of calcium carbonate precipitated (Morse et al., 1997; Muller et al., 1972; Berner, 1975; Stanley and Hardie, 1999). Nevertheless, less focus has been placed on the polymorphs generated when carbonate mineral precipitation is driven by the metabolism of sulfate-reducing bacteria (Ries et al., 2008). Predicting the calcium carbonate polymorph is often difficult using straightforward thermodynamic equilibria, because the mineral is formed as a result of complex reaction kinetics (Morse and Casey, 1988). This chapter reports the method development associated with the incubation of pure cultures of sulfate-reducing bacteria, grown to induce the precipitation of calcium carbonate minerals in the laboratory. This chapter includes the analytical methods, and the results of multiple experimental trials that tested a range of experimental variables such as Mg/Ca ratios, type of headspace gas used in the incubations, seeding materials, and the effect of micro-nutrients on the microbially driven precipitation of calcium carbonate. This chapter lays out the foundation which is developed further in Chapter 3 with the final, publishable, experiments where the ultimate controls on the carbonate polymorph that precipitates during microbially induced carbonate precipitation were determined. The aims of this chapter and Chapter 3 are to investigate the role of variables in the bacterial growth and the types of calcium carbonate polymorphs precipitated. Through a series of initial culture experiments outlined here, I learned the best techniques and established the methods needed to culture sulfate-reducing bacteria in a seawater medium and manipulate the sulfate-reducing bacteria to induce the precipitation of calcium carbonate minerals.

2.2 Analytical methods

2.2.1 Incubation Experiments

Pure culture incubation experiments were set up to explore the role of different initial and evolving geochemical conditions on the formation of different calcium carbonate polymorphs. The incubations were carried out in 125 mL or 100 mL reaction vessels, tightly sealed with a blue butyl rubber stopper under strictly anaerobic conditions. All experiments were performed

at $25 \pm 1^\circ\text{C}$ in a water bath incubator. I designed the incubation experiments with different Mg/Ca ratios, different seeding materials, and different gas compositions to investigate the influence and the controlling factors that determine the precipitation of different calcium carbonate polymorphs. A single bacterial strain was used in all incubation experiments – *Desulfovibrio bizertensis*. The strain was purchased from Leibniz-Institut DSMZ-Deutsche Sammlung von Mikroorganismen und Zellkulturen GmbH (DSMZ) DSM No. 18034. As opposed to the more commonly studied strain (*Desulfovibrio alaskensis* or G20) that was extracted from a soured oil reservoir, *Desulfovibrio bizertensis* was isolated from marine sediment in Tunisia, near Bizerte, hence its name (Haouari et al., 2006; Feio et al., 2004). Therefore, this strain is more representative of bacteria that lives in a marine sediment environment. In addition, this strain can grow rapidly (in two days) and is capable of metabolizing formate while G20, and most *Desulfovibrio sp.* and *Desulfobacter sp.* could not. Formate is used as the sole electron donor in this study as it raises the pH and alkalinity when metabolized by the bacteria, which is essential in precipitating calcium carbonate. The bacteria were initially cultured in the recommended medium given by DSMZ (medium 163) following the special instructions tailored for “Cultivation of Anaerobes”.

2.2.2 Preparation of medium

I modified the recommended media to a seawater media so that it closely mimicked the conditions (pH and salinity etc.) of the ocean. An inoculum was transferred into the media and grown up several times before the experiment began. The recipe for DSMZ medium 163 and seawater medium used in this study are summarized in Table 2.1 below. Artificial seawater was also prepared for samples with different Mg/Ca ratio. The chemicals used in making up the artificial seawater are shown in Table 2.2.

Table 2.1: List of chemicals used in making up the medium needed in the incubation experiments.

Chemicals	DSMZ Medium 163	Seawater medium
Solution A:		
NaCl	25.0 g	
K ₂ HPO ₄	0.5 g	
NH ₄ Cl	1.0 g	
Na ₂ SO ₄	1.0 g	
CaCl ₂ x 2 H ₂ O	0.1 g	
MgSO ₄ x 7 H ₂ O	2.0 g	
Na-DL-lactate	2.0 g	
Na-formate		7.50 g
Yeast extract	1.0 g	2.5 g
Na-resazurin (0.1% w/v)	solution 0.5 mL	0.001 g
Milli-Q water	980.0 mL	
Solution B		
FeSO ₄ x 7 H ₂ O	0.5 g	
Milli-Q water	10.0 mL	
Solution C		
Na-thioglycolate	0.1 g	0.1 g
Ascorbic acid	0.1 g	0.1 g
Milli-Q water	10.0 mL	
Solution D		
Atlantic seawater ¹		1000.0 mL
OR Artificial seawater ²		1000.0 mL

¹ Detailed chemical composition of Atlantic Ocean Standard Seawater is provided in Supplementary Materials.

² Artificial seawater was prepared according to the ASTM method with chemicals summarized in Table 3 below.

Solution A was mixed, boiled then cooled to room temperature while flushing with 100% N₂ gas. Solution B and C were added and the solution adjusted to pH 7.8 with NaOH, and distributed under N₂ gas atmosphere into reaction bottles/serum bottles. The medium was

swirled continuously to keep the unknown grey precipitate suspended. For solution D, Atlantic Ocean Standard seawater purchased from Ocean Scientific International Ltd. (OSIL) was used as the medium.

Artificial seawater was prepared in accordance with the Standard Practice for the Preparation of Substitute Ocean Water – Designation: D1141-98 (Reapproved 2013). Stock solutions of artificial seawater were freshly made from analytical grade (Analar) reagents and diluted to the desired Mg/Ca ratio. To prepare one liter of artificial seawater, 24.53 g of sodium chloride (NaCl) and 4.94 g of anhydrous sodium sulfate (Na₂SO₄) were dissolved in 800 mL of Milli-Q water. Then, 20 mL of stock solution A was added slowly with rigorous stirring followed by the addition of 10 mL of stock solution B. The mixture was topped up to 1 liter with Milli-Q water. The amount of electron donor (formate in this case), reductants (ascorbic acid and Na-thioglycolate), yeast extract and oxygen indicator (resazurin) added were similar to the amount used to prepare Atlantic seawater medium listed in Table 2.1. The seeding materials (such as calcite or kaolinite) were first added into a reaction bottle, crimp sealed and then the medium was flushed with either 100% N₂ gas or 90% N₂/10% CO₂ mixed gas for 40 minutes. Finally, the medium was autoclaved for 15 minutes at 121°C. The pinkish-coloured medium turned clear/colourless after heating.

Table 2.2: List of chemicals used to prepare artificial seawater.

Chemicals	Amount
Stock Solution A	
MgCl ₂ .6H ₂ O	3889.0 g (= 555.6 g/L)
CaCl ₂ (anhydrous)	405.6 g (=57.9 g/L)
SrCl ₂ .6H ₂ O	14.6 g (= 2.1 g/L)
Stock Solution B	
KCl	486.2 g (= 69.5 g/L)
NaHCO ₃	140.7 g (= 20.1 g/L)
KBr	70.4 g (= 10.0 g/L)
H ₃ BO ₃	19.0 g (=2.7 g/L)
NaF	2.1 g (=0.3 g/L)

2.2.3 Inoculation of sulfate-reducing bacteria

After autoclaving, the sample medium was cooled to 25°C in the water bath and prepared for inoculation. Approximately 1.5 mL of inoculum was transferred from the actively-growing culture into each sample medium using a syringe and needle. The vials were then left to incubate at 25°C in a water bath. Control samples were immediately re-autoclaved after inoculation to kill the bacteria, then placed into the water bath with the live pure-culture samples. Note that control samples were not set up in the first three experiments since they were preliminary experiments to test if the bacteria are capable of surviving and growing the conditions in the media.

2.2.4 Aqueous sample analysis

Media was collected from the sample bottle at certain time intervals to monitor the changes in the chemistry of the media and to assess the onset of carbonate precipitation. A needle and syringe were used to extract the fluid. Fluid samples were analyzed for pH, alkalinity, optical density (OD), sulfide concentration, major cations and anions. The analytical methods for these analyses are detailed here. pH was measured using an Orion 3 Star meter with micro-electrode (ORION 8220 BNWP PerpHect ROSS). Alkalinity was titrated using a Metrohm 848 Titrino plus with error of 1%. Optical density, dissolved sulfide and phosphate concentrations were determined spectrophotometrically using a Thermo Scientific AquaMate Plus UV-VIS spectrophotometer. Sulfide concentrations were measured using modified methylene blue method with an error of 2% and with a detection limit of 1 µM (Cline, 1969; Mills et al., 2016). I measured the phosphate concentration at certain time intervals, using molybdivanadophosphoric acid method described in Kitsan and Mellon (1944). The major cations (calcium and magnesium) and anions (sulfate and chloride) were measured using an ion chromatograph (Dionex) Thermo Scientific ICS-5000+ SP. The cation concentrations were analysed with cation column IonPac CS168 and 30 mM methanesulfonic acid (MSA) as eluent. Anion concentrations were analysed using an IonPac AS18 column with 31 mM potassium hydroxide (KOH) as eluent.

2.2.5 Solid phase analysis

Samples were killed immediately after the last sampling point. The remaining aqueous solution was decanted slowly into a 50 mL falcon tube. Then, the samples were centrifuged at 5000 rpm for five minutes. The aqueous samples were then discarded while the solid samples were carefully rinsed twice with Milli-Q water to dissolve any residual salt. Subsequently, the bottles

were filled with Milli-Q water and centrifuged for a second time. The Milli-Q water was then discarded and the solid samples deposited at the bottom of the falcon tube were oven dried at 40°C overnight. Dried samples were then powdered prior to mineralogical analysis by an XRD. The dried samples were prepared by pipetting ~0.40 mL of acetone smear containing the precipitate onto a zero background holder. Samples were then kept in a clean cupboard to allow the acetone to evaporate at room temperature prior to analysis. All the XRD data were collected using Bragg-Brentano geometry on a D8 Bruker diffractometer equipped with primary Gobbel mirrors for parallel Cu K α X-rays and a Vantec position sensitive linear detector. Collection conditions were: 15-70° in 2θ , 0.02 step size, 450 seconds/step, divergence slits 0.6 mm. Rietveld refinements were performed with the software Topas 4.1 (Coelho, 2007). Rietveld quantitative analysis is known to be unreliable for minor phases (<5 wt %). The accuracy is considered to be \pm 1-2% relative for major phases, while the estimated standard deviation (e.s.d.) from the Rietveld calculation has no bearing on the accuracy or otherwise of the quantification itself, it is merely related to the mathematical fit of the model (Madsen and Scarlett 2008). The dried precipitates were further analysed by scanning electron microscopy (QEMSCAN 650F FEI) equipped with an energy dispersive X-ray (EDX) detector to examine the morphology and chemical composition of the precipitates. The solid samples were placed on ultra-smooth carbon tape and sputter-coated with gold (~10nm) before SEM analysis.

2.2.6 Saturation index and DIC calculation

To explore the stability of various calcium carbonate polymorphs in the aqueous solution, the program PHREEQC (Parkhurst and Appelo, 1999) was used to calculate the saturation indices of relevant carbonate minerals such as calcite, aragonite, dolomite, and monohydrocalcite. The *Sit* database was used for the stability constants of the minerals (Grenthe et al., 1997; Parkhurst and Appelo, 2013; Guggenheim and Turgeon, 1955). The Davies equation was used for activity coefficients of ion complexes for high ionic strength samples. Dissolved inorganic carbon (DIC) in any sample can also be calculated when pH and alkalinity are known. The equation for the saturation index was given in Chapter 1.

2.3 Method development

This part of Chapter 2 is presented chronologically, with the sequence of experiments that I did during method development to optimize the method for incubating pure cultures of sulfate-reducing bacteria to understand the controls on the dominant polymorph precipitated. To better understand the role of each variable such as the types of seeding materials, the effect

of stirring, the presence of iron, different Mg/Ca ratios, the amount of yeast extract and the types of gas composition on the behavior of sulfate-reducing bacteria and the solution chemistry, I performed series of preliminary experiments, which I term A – G. Each of these experiments were killed when solid precipitates were observed at the bottom of the vials. The preparation of medium, sampling procedures and analytical methods adopted were identical to the large incubation experiments reported in the previous section.

2.3.1 Incubation Experiment A

The objectives of setting up Experiment A were to: (1) identify the types of calcium carbonate polymorphs that precipitated from seawater via microbial sulfate reduction; (2) to test if the silica beads (Retsch 1 mm diameter) can provide an effective surface area for nucleation of calcium carbonate minerals; and (3) whether the amount of silica beads impacts calcium carbonate mineral precipitation. Sample A-T1 had more silica beads (> 30 beads) and sample A-T2 had less silica beads (10 – 20 beads). A blank control sample was not set up since this was a trial experiment and my primary objective was to determine if the amount of silica beads was able to cause calcium carbonate precipitation. The seawater medium for Experiment A are summarized in Table 2.3 and the results shown in Figure 2.1

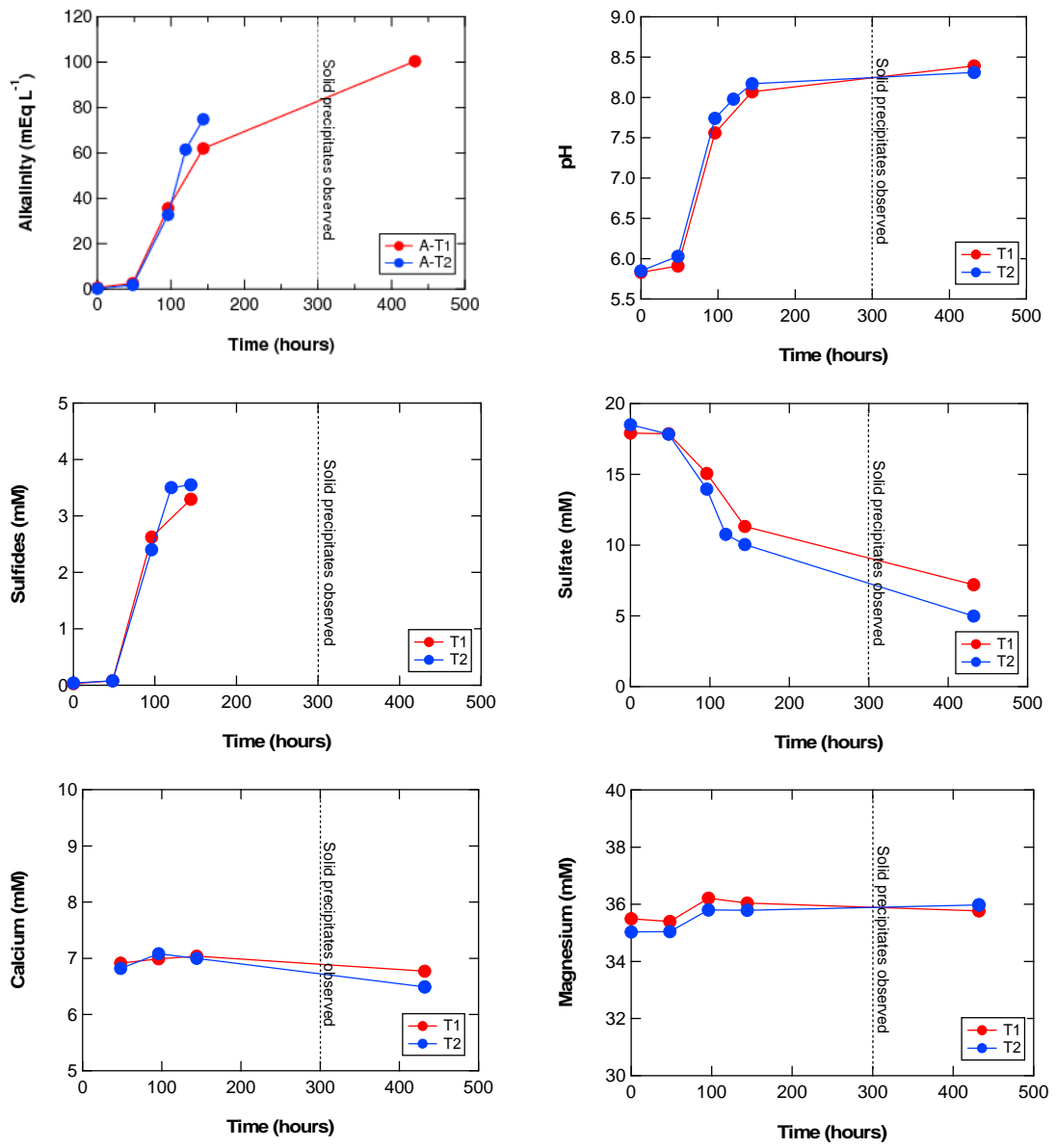
Table 2.3: List of chemicals used and the final concentration in the seawater medium.

Medium composition	Amount	Final concentration
Sodium formate	0.59 g	108.44 mM
Sodium thioglycolate	0.008 g	0.87 mM
Ascorbic acid	0.008 g	0.57 mM
Yeast extract	0.6 % (w/v)	-
Sodium resazurin	0.00008 g	0.4 mM

In this experiment, diluted seawater (approximately 65% seawater) was used and the electron donor was formate. Yeast extract was added to promote bacterial growth (Postgate, 1965; Sorokin, 1966; Mechals and Rittenberg, 1960). The pH, alkalinity and sulfide concentrations show an increase at 50 hours after inoculation and start to plateau after 150 hours. A simultaneous decrease in sulfate concentrations was also seen, further indicating that microbial sulfate reduction had occurred (Figure 2.1). I did not see a drop in pH that would be associated with calcium carbonate precipitation possibly due to the poor sampling resolution. The results show that there is no considerable difference between sample A-T1 and A-T2, suggesting that the amount of glass beads does not affect the solution chemistry and calcium

carbonate precipitation. Despite only a minor drop in calcium concentration, calcium carbonate did precipitate, and I found monohydrocalcite as the final polymorph in the medium.

At the conclusion of experiment A, I had a better sense of how long nucleation of carbonate minerals would take and that the amount of silica beads didn't make much difference. I also familiarized myself with the sampling. This was also my first observation of monohydrocalcite.



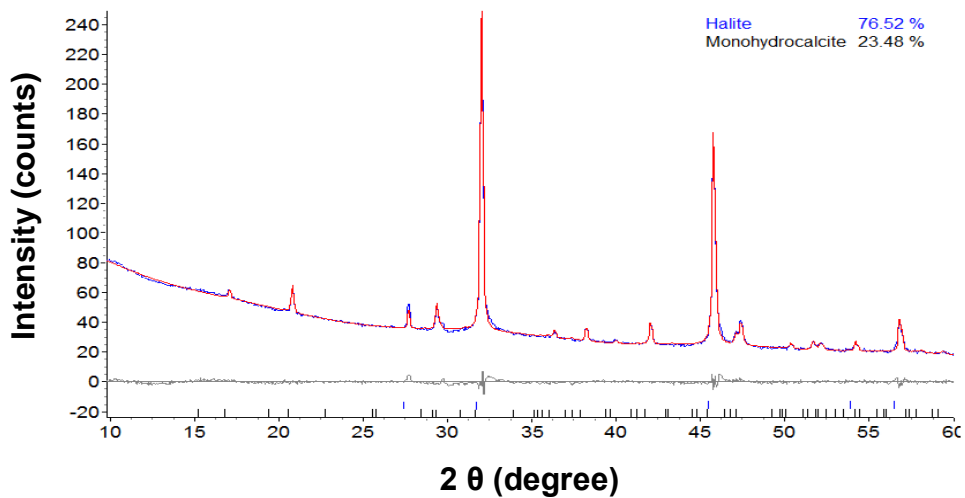
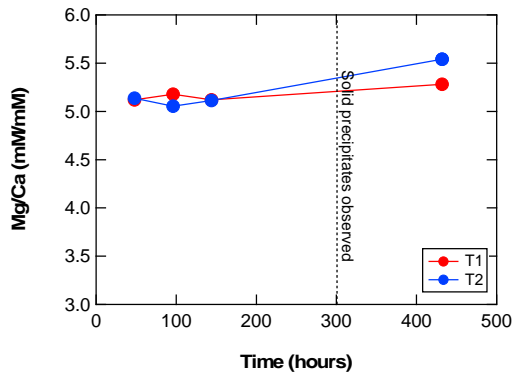


Figure 2.1: Variables measured in Experiment A where A-T1 and A-T2 have different amount of silica (glass) nucleation seeds. Solid precipitates were observed after 300 hours. Note that a control (blank) sample was not set up in this trial experiment.

2.3.2 Incubation Experiment B

In Experiment B, I wanted to test if shaking has an effect on bacteria growth and the rate of calcium carbonate precipitation, and the calcium carbonate polymorphs that precipitate. It has been shown in culture experiments that shaking can affect the growth rate of bacteria by distributing nutrients and oxygen (in this case carbon dioxide and sulfate) in the medium (Henzler and Schedel, 1991; Kaleli and Islam, 1997; McDaniel and Bailey, 1969); whereas stirring narrows the range of Mg/Ca that produces calcite from amorphous calcium carbonate (ACC) in abiotic studies (Blue et al., 2017). Blue et al. (2017) also reported that the formation of calcite with doubled magnesium content (26 mol%) is favored in a solution without stirring. The investigation into the effect of shaking/stirring also allowed me to optimize the method to reduce the time required for carbonate mineral precipitation.

The medium used in this experiment is undiluted seawater and a similar concentration of formate and yeast extract as experiment A were used. Sample vials inoculated with bacteria were wrapped with aluminum foil and placed on an orbital shaker in ambient temperature at 400rpm. The concentration of sulfide, calcium, and magnesium were measured throughout this experiment. An increase in the concentration of sulfide was observed at 60 hours and stabilized after 120 hours at 3.5 mM (Figure 2.2). Precipitation was noted after 400 hours, marked by a decrease in calcium concentration; while magnesium remains constant through the course of the experiment. No significant difference was noted in the concentration of sulfide between Experiment A (no shaker) and B (on the shaker) (Figure 5), suggesting that shaking does not alter bacterial activity and even possibly delayed the time required for calcium carbonate precipitation. Similar to Experiment A, monohydrocalcite is the calcium carbonate polymorph that precipitated from the solution. Anecdotally, I left some monohydrocalcite in culture medium from this experiment over two years at room temperature and found that the monohydrocalcite did not transform into more stable polymorphs (calcite or aragonite).

The conclusion of Experiment B was that shaking was not necessary in my experiments.

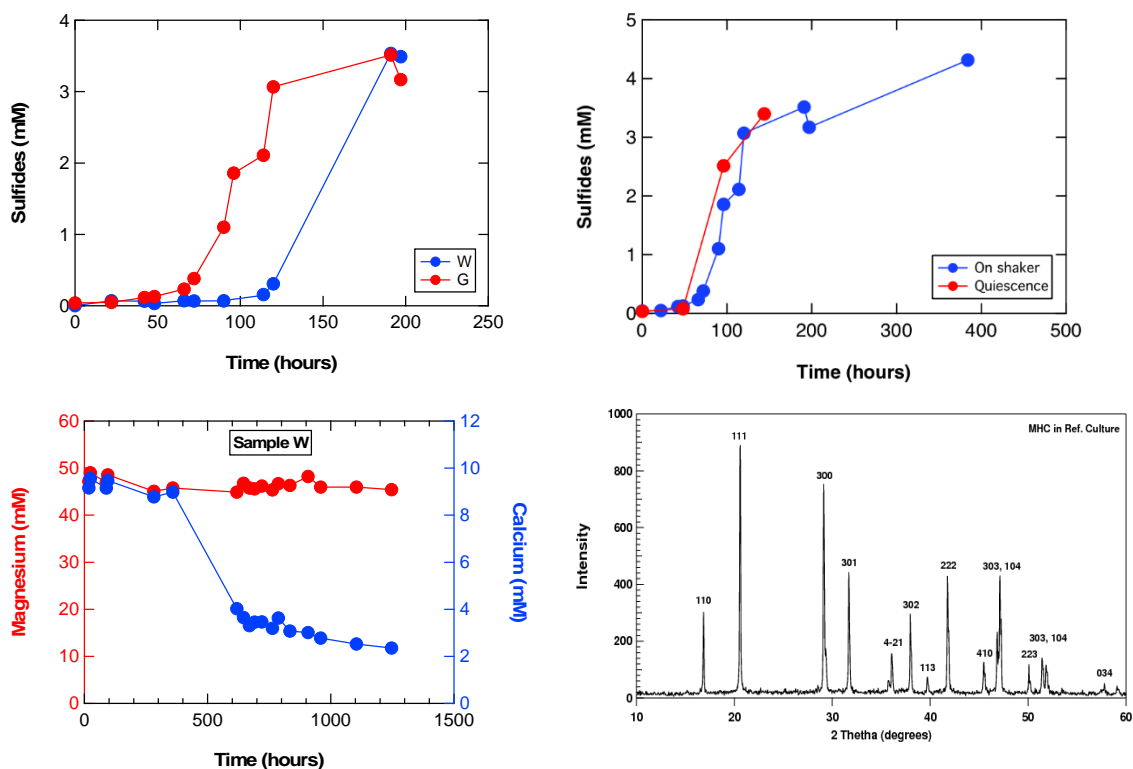


Figure 2.2: Concentration of sulfide, magnesium and calcium in Experiment B. Sample B-W and B-G are different samples and only sample B-W was measured for cations. Data for the

quiescence sample (in red) were from Experiment A whereas the results on shaker (blue) is from Experiment B. XRD diffractogram of MHC forms from culture medium incubated after two years.

2.3.3 Incubation Experiment C

The main goal of Experiment C was to determine the effects of iron on the bacterial growth, and to test the types of carbonate polymorphs that form when iron is in excess in the medium. It is known that iron is an essential micronutrient for *Desulfovibrio sp.* (Postgate 1965; Butlin et al., 1949), however, it is unclear the role of iron in promoting the growth of sulfate-reducing bacteria, beyond scavenging the sulfide released during sulfate-reducing bacterial metabolism, and whether the presence of iron influences the minerals that precipitate. For example, at circum-neutral pH the presence of iron has shown to be detrimental to bacteria growth if the concentration of iron exceeds saturation for iron sulfide (Meier et al., 2012). It has been shown that iron can react rapidly with microbial-released sulfide to produce poorly crystalline iron sulfides, leading to cell surface encrustation and eventually death (Picard et al., 2016; Picard et al., 2018).

Experiment C was prepared as Experiment A except an additional iron source (approximately 2 mM FeSO_4) was added in the initial medium. Sample A denotes the sample with FeSO_4 added after autoclaving whereas in sample B FeSO_4 is added before autoclaving. The concentration of sulfide, iron, cations and total sulfur were measured. Cations (Ca, Fe, K, Li, Mg, Mn, Na, Sr) and total sulfur (S) were measured using an inductively-coupled plasma optical emission spectroscopy (ICP-OES). The results show a decrease in ferrous iron concentrations at 60 hours and a concurrent rise in sulfide concentration in the medium (Figure 2.3). The concentration of cations other than iron remained unchanged over the entire course of the experiment. The lack of a drop in the calcium concentrations suggests there is no precipitation of calcium carbonate minerals throughout the experiment (305 hours). Iron sulfide minerals are the primary minerals that precipitated from the solution as suggested by the drop in iron concentration. It is worth mentioning that the solution turned blackish after two days but the precipitated iron sulfides settled after one week with a thick layer of iron sulfides deposited at the bottom of the experiment vials. However, I think that some bacteria might have survived any entombment by iron sulfide precipitation. This can be shown by a continuous drop in total sulfate and an increase in sulfide after 168 hours when the 2mM of ferrous iron had been depleted. For the rest of the experiments I did, no more iron was added to the culture medium. No carbonate mineral was detected in the samples using XRD.

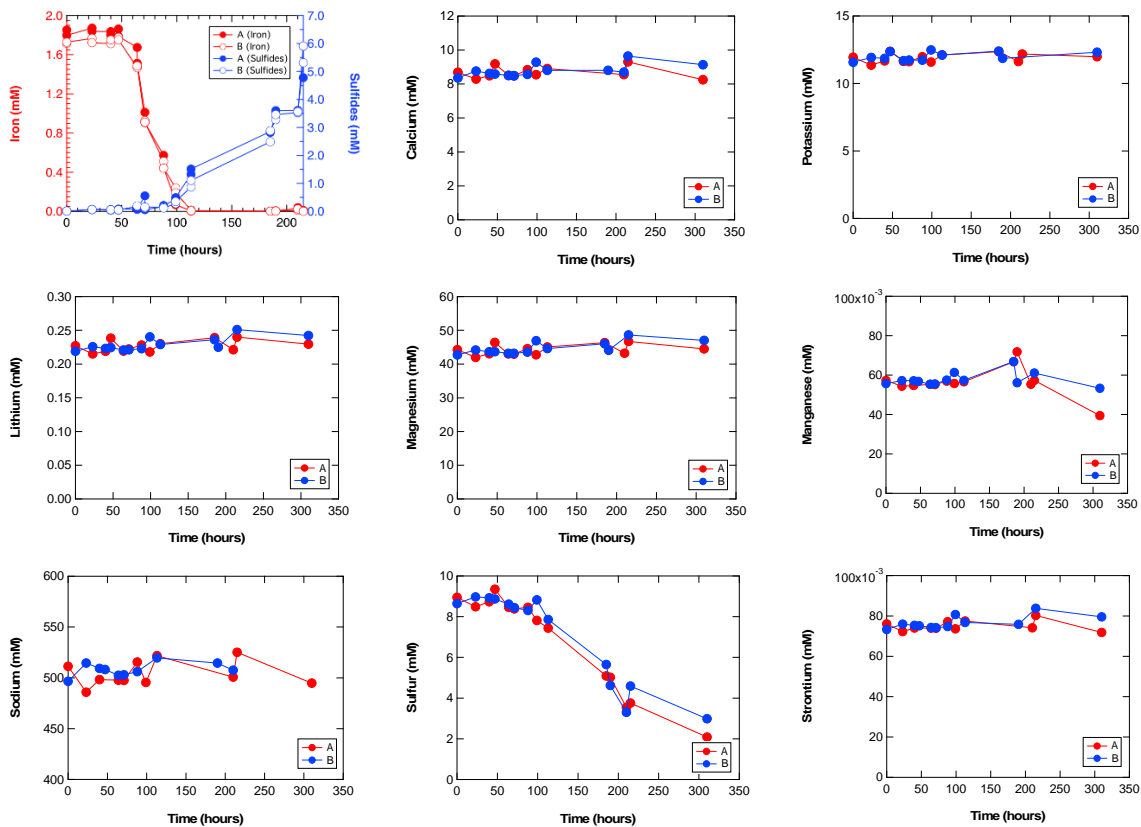


Figure 2.3: Elemental results for Experiment C. $FeSO_4$ was added in sample C-A after autoclaving while before autoclaving for sample C-B. Note that there is no significant difference between sample C-A and C-B.

2.3.4 Incubation Experiment D

The major drawback from the previous experiments is that I did not have an estimate of the microbial growth rate. Therefore, I started experimenting with how to measure OD600, to determine cell density so I can see when the bacteria are in exponential and stationary growth phases and link this to the timing of carbonate precipitation. OD600 refers to analysis of the optical density at wavelength 600nm, which should target cell material, but I had to make sure that this didn't also measure carbonate materials that formed in the medium that might scatter light similar to the cell material. Prior to starting Experiment D, small centrifugation experiments were carried out to investigate the suitable speed to separate the carbonate precipitates from the bacteria cells. I found that 800 – 1200rpm was the best speed to separate the solid minerals and bacteria cells in my samples (Figure 2.4). At centrifugation speed larger than 1200rpm, I start seeing separation of bacteria cells from the medium and a decrease in OD600. Therefore, I used a rpm of 900 as the centrifuge speed to separate the solid from the bacteria cells in all experiments. Samples OD600 were subsequently measured using an AquaMate Plus UV-VIS spectrophotometer at wavelength of 600 nm.

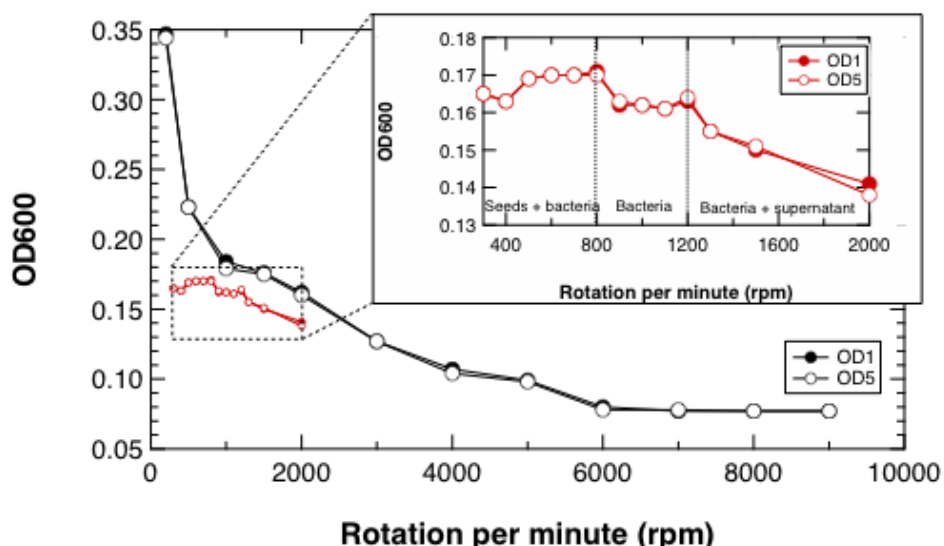
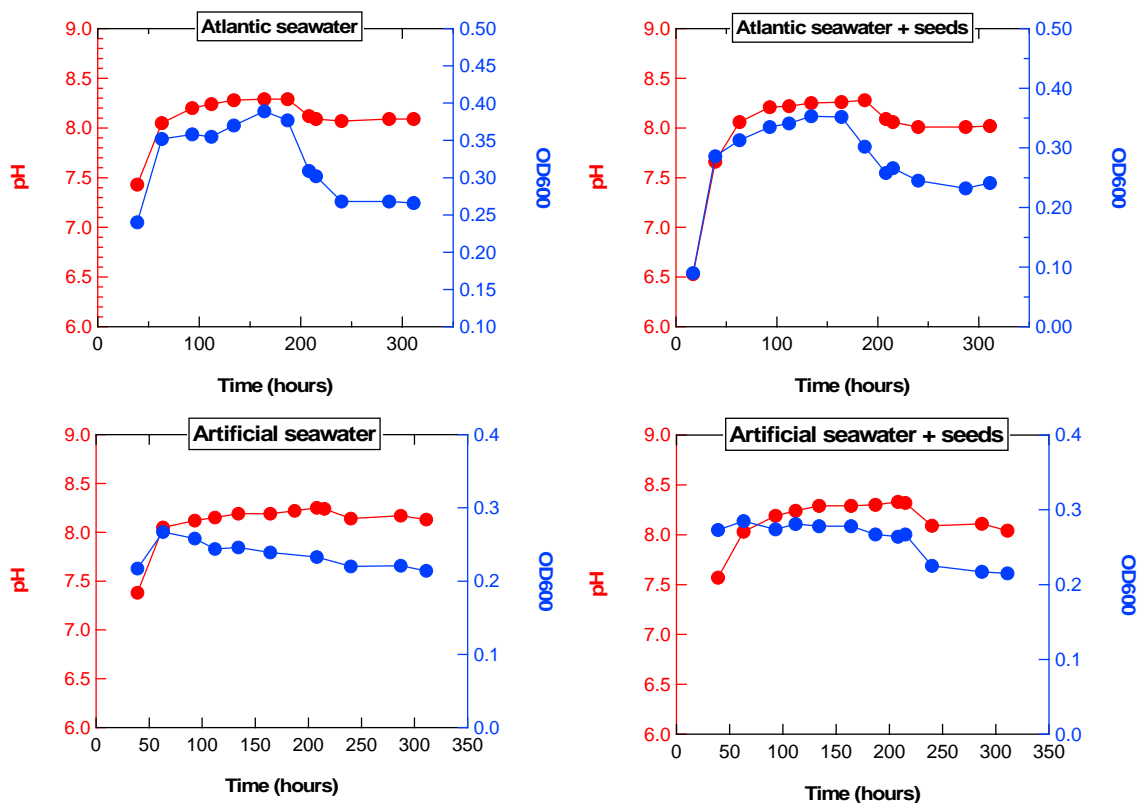


Figure 2.4: OD1 indicates the OD measured within one minute after sampling while OD5 indicates the OD measured at the fifth minutes after sampling. The results suggest that time does not impact the OD reading. The plot also shows that rpm of 800 – 1200 is the most suitable centrifuge speed for measuring OD of the samples. Note that the data plotted in black are samples being shaken before sampling while data in red are samples being carefully sampled without shaking. At rpm < 800, centrifugation is less effective to separate the suspended seeds and the bacteria cells in the medium. At higher rpm (> 1200), the bacteria cells started to separate from the medium. Therefore, a centrifuge speed between 800 – 1200 rpm is the best speed to measure OD in my samples.

Experiment D was set up by using both Atlantic seawater and artificial seawater (artificial seawater was prepared according to the ASTM method as detailed above) with an initial Mg/Ca of 0.1 (Mg = 1.2 mM; Ca = 10.4 mM). Having determined through experiment A that I could grow the bacteria and they would make calcium carbonate on quartz beads, and through experiments B and C that neither stirring nor the supply of iron would help with my objectives, the objectives of experiment D were (1) to study the effect of Mg/Ca ratio on the calcium carbonate polymorphs precipitated, and (2) to test if calcium carbonate seeding helps in the precipitation kinetics and influences the calcium carbonate polymorph made. For this, twenty milligrams of calcite seeds were added to one sample while no seeds were added in another. The media were flushed with 10% CO₂ and 90% N₂ mixed gas and the pH adjusted to 6.2 – 6.5 with 0.1 M NaOH prior to inoculation. pH, OD600 and cations such as calcium, magnesium, and strontium were measured. The pH was measured using a bench top Mettler Toledo pH meter and cations were measured by using an ion chromatography (Dionex) Thermo Scientific ICS-5000+ SP.

The solution pH (both Atlantic and artificial seawater) increased dramatically within 50 hours after inoculation from pH 6 to pH approaching 8. The rise in pH results from microbial sulfate reduction as shown by the concurrent increase in OD600 from approximately 0.10 to 0.30 (Figure 2.5). Both pH and OD600 in most samples (except those in artificial seawater) demonstrated a similar trend, with an initial increase followed by a stabilization period before pH started to drop around 200 hours. A clear log, stationary and death phase of a bacterial growth cycle was observed. The drop in pH is associated with a concurrent decrease in calcium concentration, suggesting the pH drop is associated with the precipitation of calcium carbonate minerals. Magnesium concentrations remain constant throughout the course of the incubation experiment whereas there is a slight drop in strontium concentration. The presence of seeding material slightly reduces the time required for precipitation in the sample in Atlantic seawater. In the sample with artificial seawater, calcite seeds trigger carbonate mineral precipitation at 220 hours, whereas no precipitation is observed in artificial seawater without seeds during the incubation period. The results from this experiment led me to conclude that seeding materials promotes or facilitates calcium carbonate precipitation. Monohydrocalcite is the carbonate mineral that formed in all samples except the sample in artificial seawater as no carbonate mineral precipitation was observed in this sample.



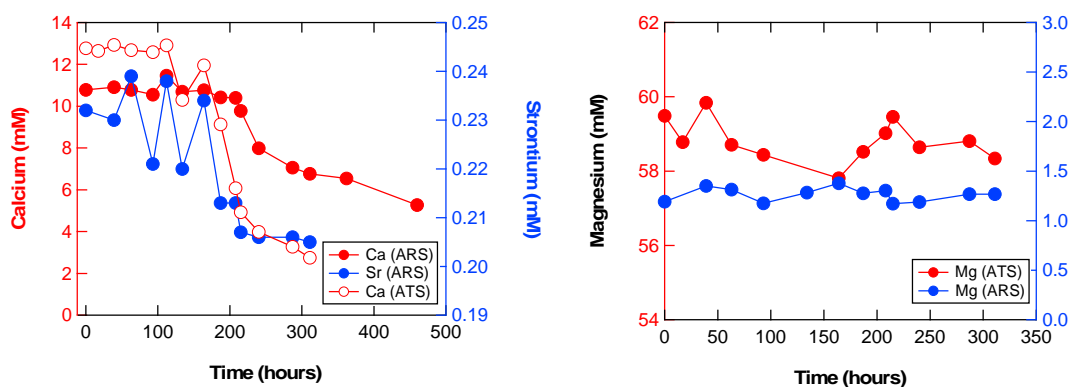


Figure 2.5: Changes in pH, OD600, Ca, Mg and Sr concentration in the sample medium of Experiment D.

2.3.5 Incubation Experiment E

In experiment E, I wanted to investigate if the flushing of different gas composition in the medium may impact the calcium carbonate polymorph that formed. Unlike the previous experiments, where the media were flushed by mixed gas of 90% nitrogen and 10% carbon dioxide, I used pure nitrogen (100%) to flush the initial medium for 60 minutes. This resulted in a higher initial pH (7.9 – 8.0) and lowered medium DIC. Alkalinity was first measured in the samples using the inflection point method (APHA, 1999) and calcite was used as seeding material. Three sets of samples with different Mg/Ca, notably 5.2 (Atlantic seawater), Mg/Ca of 1 with 20 mM of calcium and magnesium (artificial seawater), and Mg/Ca of 0 with 10 mM of calcium and no magnesium (artificial seawater without magnesium), were prepared to study the effect of Mg/Ca on calcium carbonate precipitation at a broader range. Duplicates and control samples were also considered in this series.

During the growth of Experiment E there was a 0.2 drop in pH unit from 7.9 to 7.7 in all samples at 50 hours and an increase to 8.3 around 200 hours (Figure 2.6). Such an initial drop in pH might be due to the dissociation of hydrogen sulfides produced by the bacteria – which is a weak acid and has a pK_a of 7.0 (Soetaert et al., 2007). A smaller drop in pH (0.1 unit) was noted in the control samples, suggesting there could be an abiotic adjustment of pH as well, probably attributed to the formation of amorphous phase minerals at the high pH. After the initial drop (at 50 hours), the pH increases and stabilizes at 8.3 before it experienced a larger drop when carbonate minerals begin to precipitate. It should be noted that an arbitrary amount of $FeCl_2 \cdot 4H_2O$ was added into one of the replicates (E-T1, E-R1, and E-S1) at 475 hours to titrate out the sulfide as I thought that the bacteria growth could be limited by the high concentration of sulfide in the vial (Okabe et al., 1995). Approximately 4 mM and 25 mM of $FeCl_2 \cdot 4H_2O$ were particularly added into sample E-T1, E-R1, and E-S1, respectively. The

ferrous iron reacts instantaneously with dissolved sulfides to form FeS (iron monosulfide) and results in an instantaneous drop in pH (due to the formation of hydrochloric acids from the $\text{FeCl}_2 \cdot \text{H}_2\text{O}$), alkalinity and sulfide concentration. For example, sample E-S1 experienced a decrease in pH from 7.93 to 6.67. Such a major change shifted both the sulfide (Eq. 2.1 and 2.2) and carbonate equilibria (Eq. 2.3) and led to a substantial drop in the alkalinity.



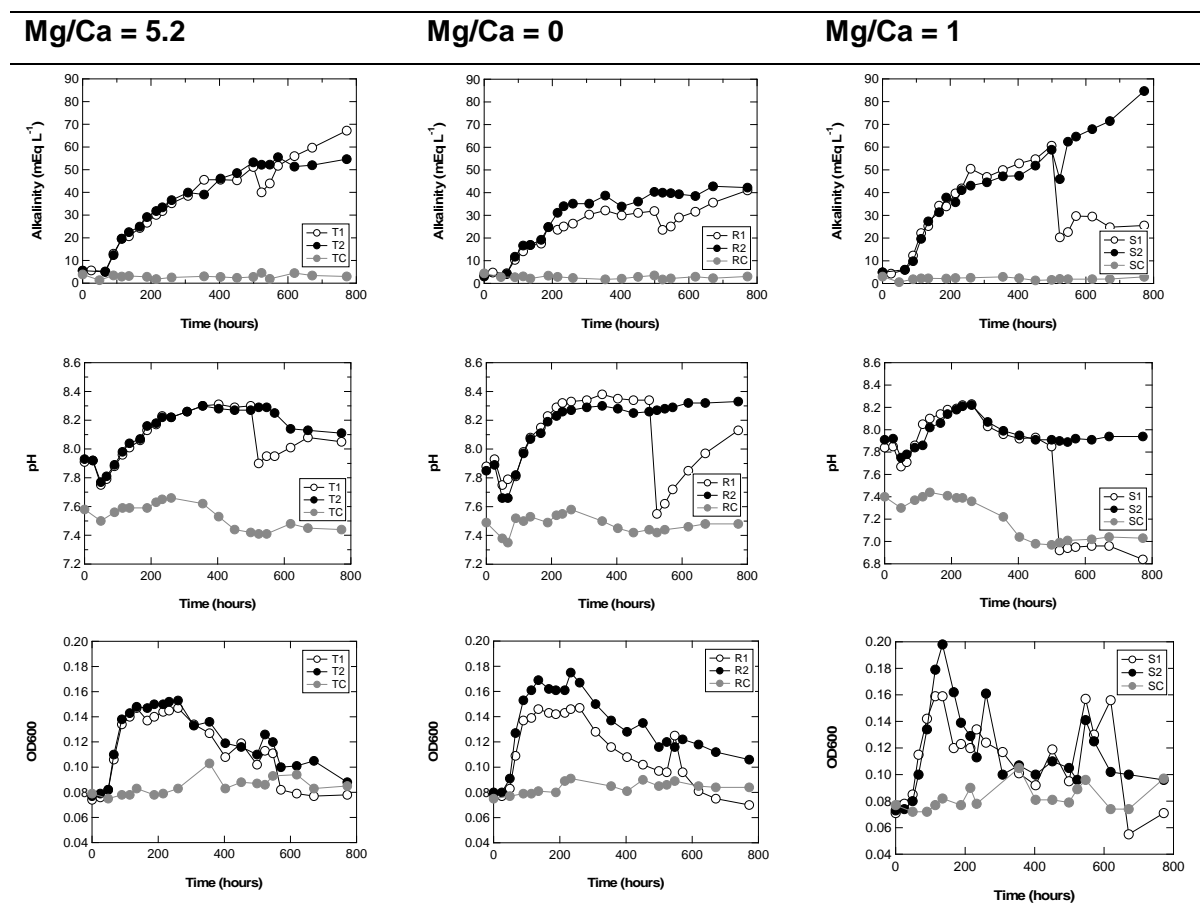
The OD in Experiment E is significantly lower (maximum value is 0.18) and there was a shorter stationary phase compared to the previous experiment. Such a non-ideal growth curve suggests that the bacteria are not growing well in these conditions. Two possible reasons to explain this are: (1) changes in the gas composition used; and (2) the difference in medium Mg/Ca ratio. Ideally, the bacteria should be pre-cultured at least three cycles in the medium of interest prior to starting the main experiment to prevent bacterial culture shock. However, due to limited amount of time and little change in the culture medium chemistry, such a practice was not adopted for this experiment. This could potentially impact bacterial growth rate and thus the precipitation kinetics but should not change the thermodynamics or impact carbonate polymorphism.

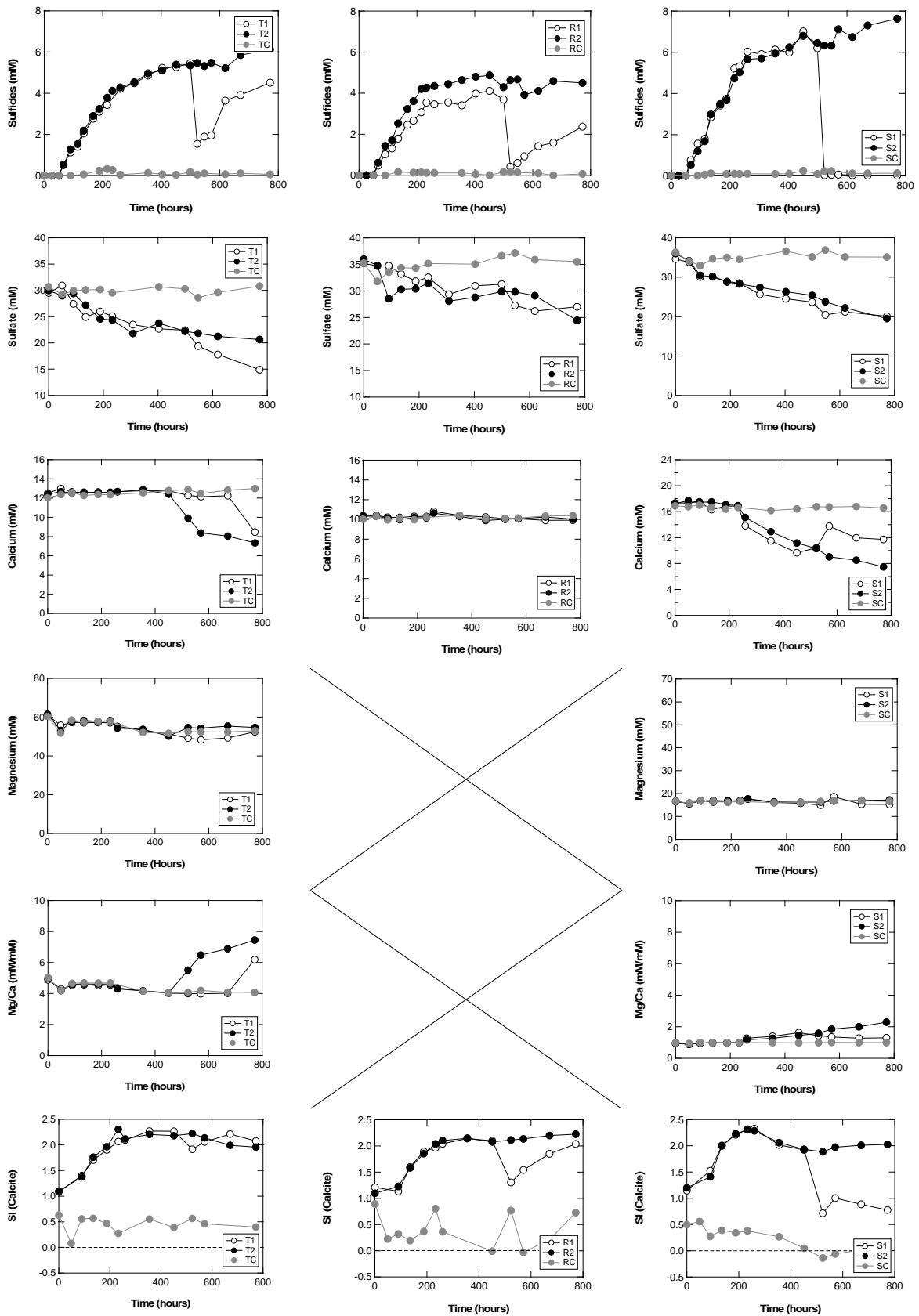
Most anaerobes including *Desulfovibrio sp.* require exogeneous carbon dioxide for biosynthesis of cell material (Killam et al., 2003; Reilly, 1980; Rockwell, 1923; Postgate 1965; Sorokin, 1966). This could explain the impaired bacterial growth in Experiment E. Calcium carbonate precipitation happens two-fold earlier in sample E-S compared to sample E-T. Although there is lack of magnesium (which is an inhibitor for calcite formation) in sample E-R, carbonate mineral precipitation is not observed. This is partly because the bacterial growth may be retarded by the absence of magnesium ions. It has recently been reported that magnesium is also essential in stimulating the growth and activity of sulfate-reducing bacteria (Cao et al., 2009). Exceptionally high magnesium concentrations can also be detrimental to bacterial growth: such effect will be discussed in detail in Chapter 3 in Experiment J.

The difference in bacteria growth rate is also reflected in the cell-specific sulfate reduction rate. The cell-specific sulfate reduction rate (csSRR) is defined as the amount of sulfate reduced per cell per unit time (Eq. 2.4): (Zaarur et al., 2017):

$$\text{csSRR} = K/Y \quad \text{Eq.(2.4)}$$

where K is the specific growth rate, calculated based on the slope on the plot between $\ln(\text{cells})$ vs. time and Y is calculated based on the slope on the plot between cells vs. sulfate reduced (Sim et al. 2011; Antler et al., 2017). The cell-specific sulfate reduction rate in sample E-T, E-R, and E-S are 7.60, 7.33, and 9.70 $\mu\text{mol cell}^{-1} \text{day}^{-1}$, respectively. The saturation index of each calcium carbonate polymorph was calculated using PHREEQC. Despite the SI calculation indicating supersaturation ($SI > 1$) with respect to monohydrocalcite, calcite and aragonite in all biotic samples, monohydrocalcite is the only calcium carbonate minerals that precipitated in sample E-T and E-S2 ($SI_{\text{MHC}} > 1.4$). In fact, there is no solid precipitate in sample E-R, probably due to kinetic hindrance at an SI_{MHC} lower than 1.4. Nanocrystalline hydroxyapatite was found in control sample E-RC likely due to the absence of magnesium; magnesium is a recognized inhibitor for hydroxyapatite (Yang et al., 2011). It should be noted that the source of phosphate in the medium is derived from yeast extract. Later, phosphate measurements indicated that the medium phosphate concentration ranges from 600 – 900 μM . Therefore, formation of minor amount of amorphous calcium phosphate is expected at this high starting pH but such trace amount of amorphous material is not clearly reflected in the XRD spectra.





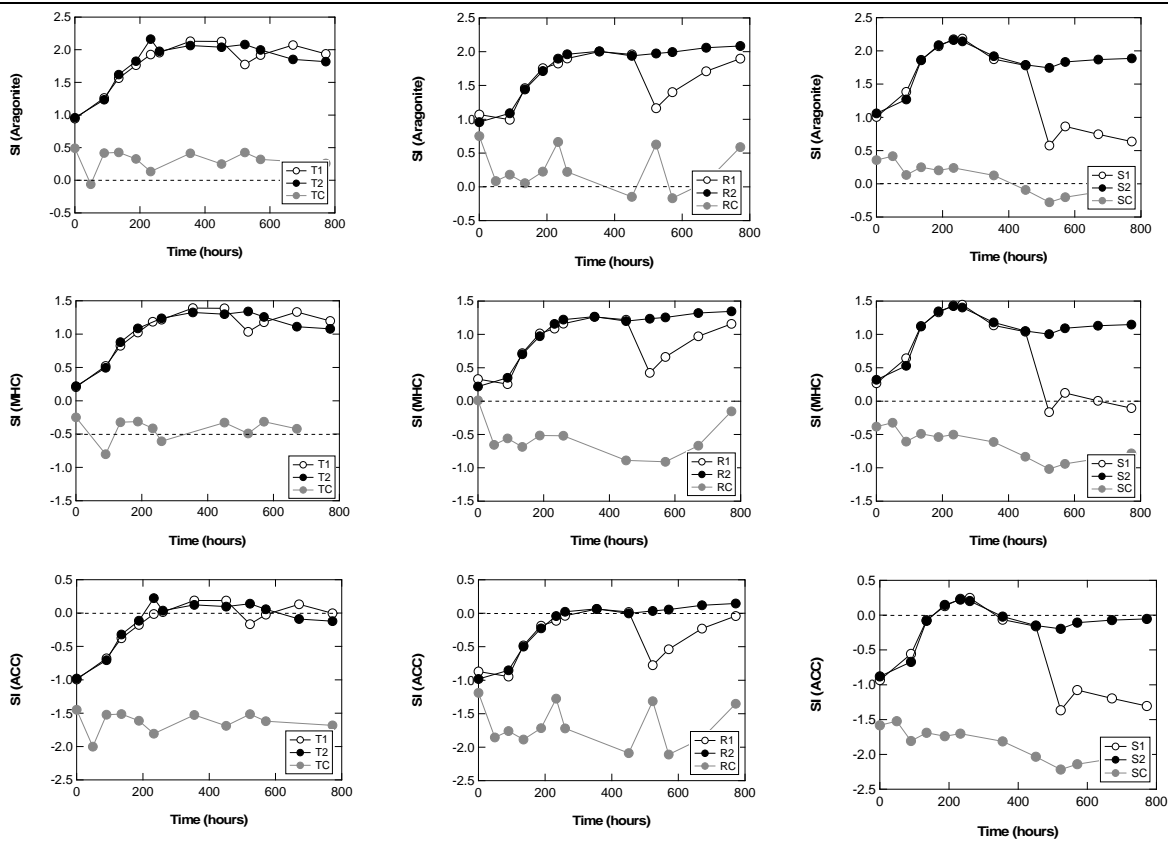
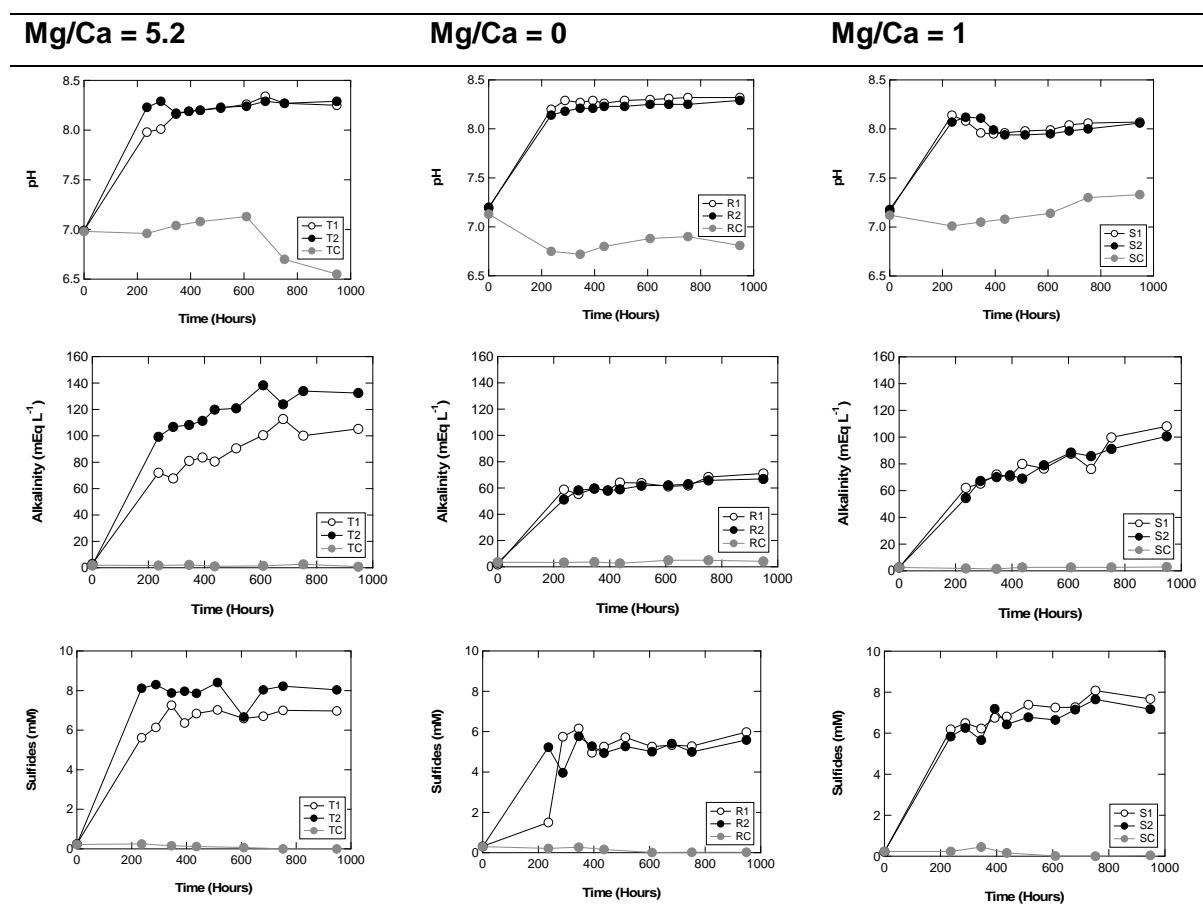


Figure 2.6: Variables measured in Experiment E where sample E-T is seawater, sample E-R, and E-S are artificial seawater with Mg/Ca ratio of 0 and 1. Saturation indices for each mineral were calculated using PHREEQC. Note that iron was added at 475 hours in samples T1, R1, and S1.

2.3.6 Incubation Experiment F

Previous studies have reported that when authigenic minerals are precipitating, they will precipitate with similar mineralogy as the seeding material (Reddy and Nancollas, 1971; Lioliou et al., 2007; Rodriguez-Navarro et al., 2012; Fernandez-Martinez et al., 2013; Donnet et al., 2005). Experiment F was conducted to study the effect of a different seeding material (kaolinite) on the calcium carbonate polymorph. Kaolinite was chosen as the seeding material simply because kaolinite is ubiquitous and known as one of the most abundant clay minerals in the marine environment. In addition, kaolinite has a distinct chemical composition and mineralogy compared to calcite. It has a larger surface area to volume ratio and a negative surface charge which may influence the precipitation kinetics of authigenic minerals. The medium chemistry used in this experiment is identical to the medium in Experiment E – where three sets of medium with different Mg/Ca were used, namely, Atlantic seawater (F-T), artificial seawater without magnesium (F-R) and; artificial seawater with Mg/Ca of 1 (F-S). Pure N₂ was used to flush the medium but at a shorter period – 40 minutes. 15 mg of kaolinite was used.

The initial pH was around 7 and increased to 8 – 8.5 after approximately 200 hours (Figure 2.7). No sample was collected after the first sampling until 200 hours as I was away. Alkalinity increased dramatically over the first 200 hours and started to gradually stabilize. The OD was rather low, suggesting the collapse of the bacteria – an exceptionally early death phase. Because no samples were collected during the bacterial exponential phase, I was unable to calculate the cell-specific sulfate reduction rate for this experiment. The magnesium concentrations in sample F-T and F-S remain constant over time. A decrease in calcium concentration is observed in sample F-T2, F-S1, and F-S2, although F-T2 showed a slower drop in the calcium concentrations and therefore likely a slower carbonate mineral precipitation rate. Such a slower precipitation rate might be due to the higher Mg/Ca ratio and salinity in sample F-T compared to sample F-S, as magnesium can inhibit the formation of calcium carbonate polymorphs. Another reason could be due to the solution chemistry where the rate of alkalinity production is lower in sample F-T compared to sample F-S. This could significantly affect the saturation state of the carbonate mineral and hence the precipitation kinetics. Monohydrocalcite was found in the seawater sample (sample F-T). Magnesium calcite precipitated in sample with Mg/Ca of 1 (sample S).



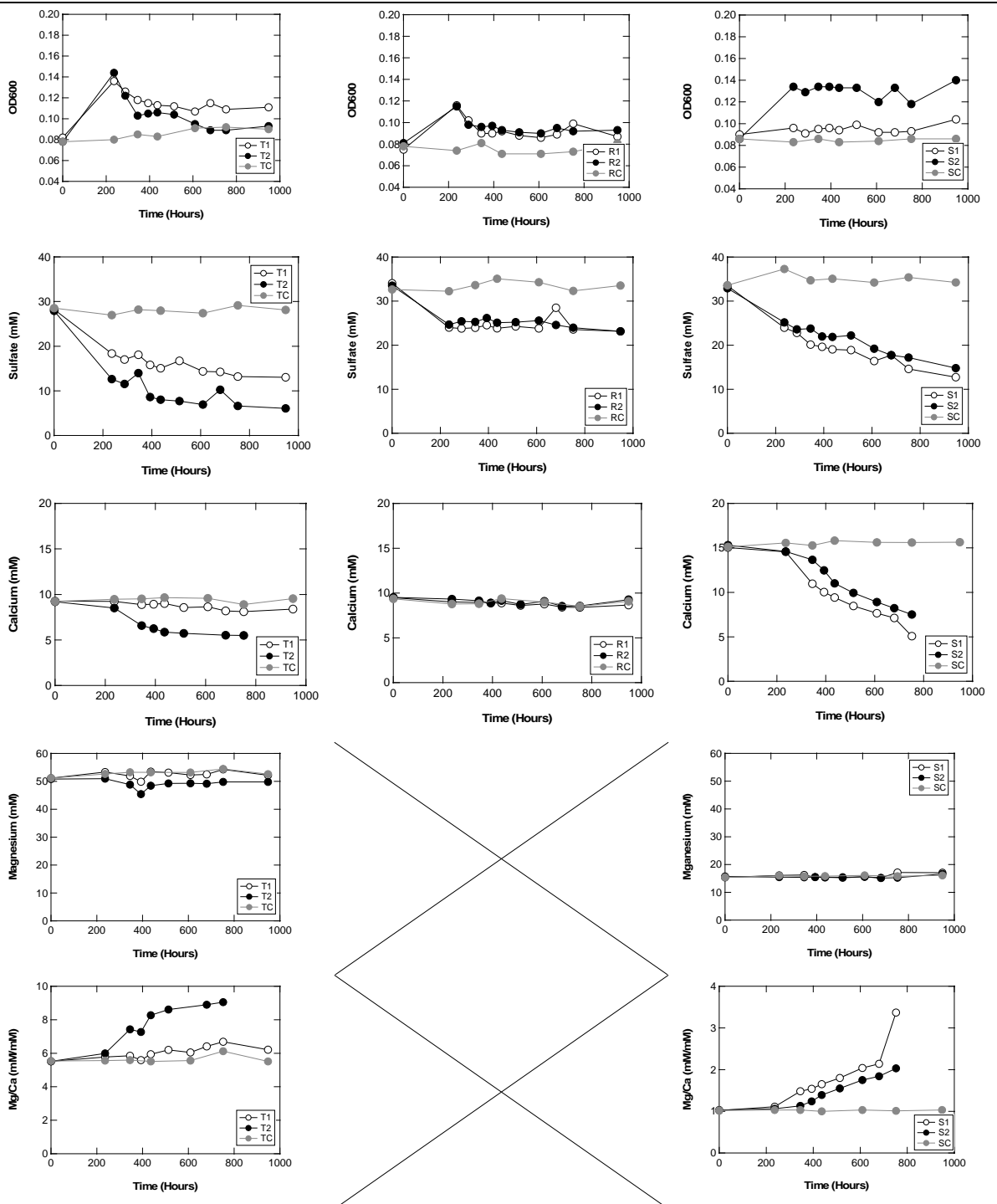


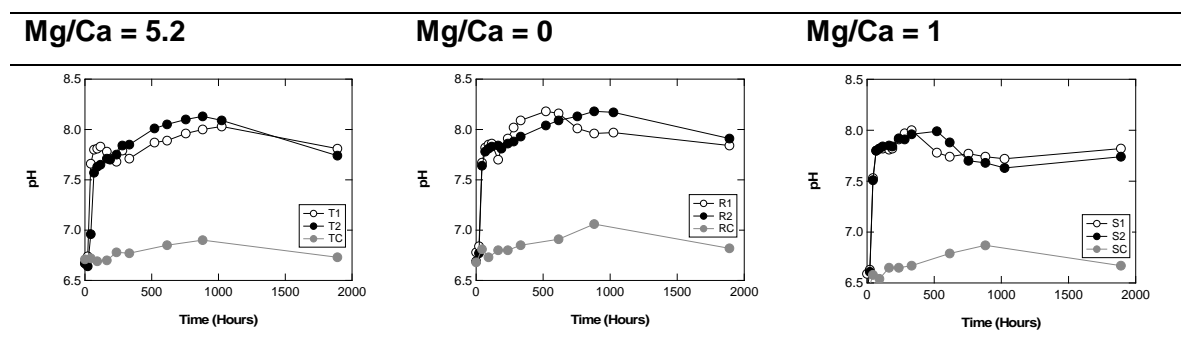
Figure 2.7: Evolution of aqueous chemistry in the samples over time in Experiment F.

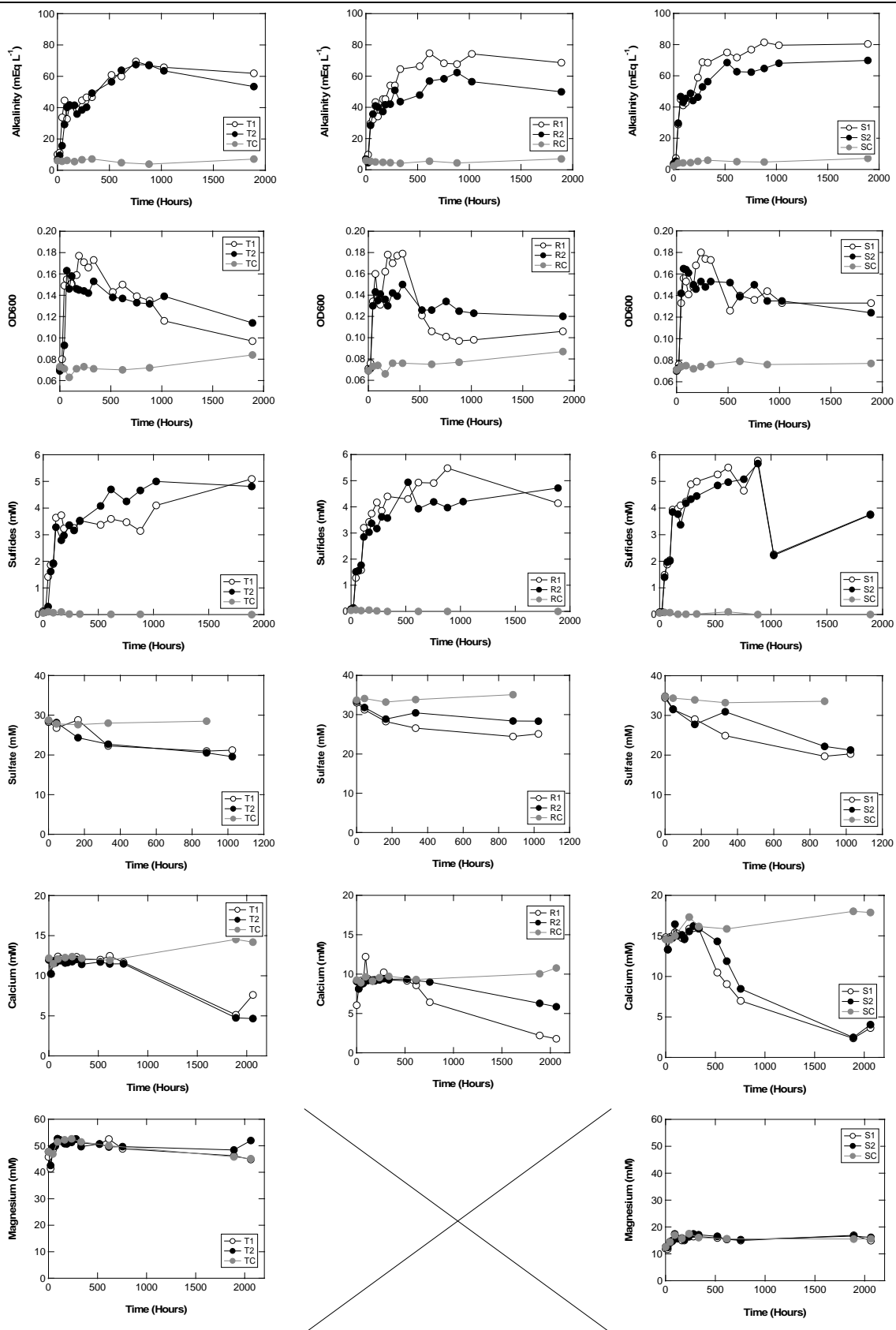
2.3.7 Incubation Experiment G

In experiment E and F, I learned that *Desulfovibrio* sp. requires minor amount of dissolved carbon dioxide in the initial medium for better growth, since in these experiments with N₂ gas the bacteria didn't grow as well. As a result, Experiment G was designed to mimic/repeat Experiment D where the gas used for flushing and filling the headspace is mixed gas of 90%

N₂ and 10% CO₂. 20 mg of calcite was used as seeding material. A similar Mg/Ca range was used in the experiment as in experiment D, namely Mg/Ca = 5.2; Mg/Ca = 0; and Mg/Ca = 1 plus a control. Since it is difficult to know the exact chemical composition of yeast extract as its composition may vary from batch to batch, I decided that it was better to reduce the quantity to a minimum to avoid any extra unknowns in the medium (Grant and Pramer, 1962; Potman et al., 1994). Therefore, I reduced the amount of yeast extract by 70% v/v in the medium.

The pH in Experiment G started at 6.7 and increased to a maximum around 8.2. Early carbonate mineral precipitation was found in sample G-S and G-R1 at 500 hours (Figure 2.8). However, the amount of time for the precipitation doubled compared to the previous experiment. I suspect this could be due to the lowered amount of yeast extract added in the medium as the bacteria may grow slower with less yeast extract, from which they acquire nutrients as well as harness energy. The lower growth rate is seen in the lower alkalinity compared to the previous experiments and a lower cell-specific sulfate reduction rate of 5.05, 3.92 and 5.59 pmol cell⁻¹ day⁻¹ for sample G-T, G-R, and G-S, respectively. The bacterial growth improved significantly after I changed back to N₂/CO₂ mixed gas, where the OD was sustained at a higher value for a longer period. Carbonate mineral precipitation was noted in all samples and marked by a drop in calcium concentration and pH. A longer induction time was seen in sample G-T due to the higher Mg/Ca and salinity (Trask, 1936). There is a slight increasing trend in magnesium concentration in all samples, which I suspect it might be due error during dilution. The Mg/Ca ratio increased as precipitation occurs, however, the reason for the drop in Mg/Ca in the last sample of sample G-T1 and G-S is uncertain. It could be either due to dissolution of the precipitated MHC and calcite and/or sorption of magnesium ions on the carbonate mineral. Monohydrocalcite was precipitated in the seawater samples whereas calcite is found in sample G-R and magnesium calcite is the mineral precipitated in sample G-S.





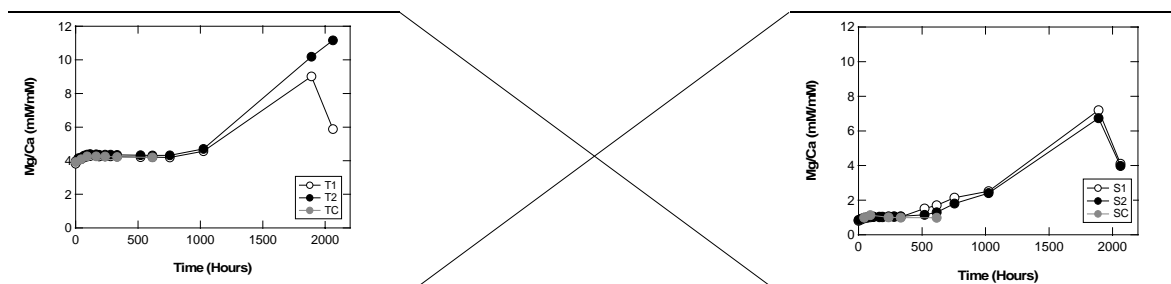


Figure 2.8: Experiment G was sampled over a longer period approximately 2000 hours due to slower growth.

2.4 Conclusions

The method development of the incubation experiments yields interesting insight into the role of sulfate-reducing bacteria on the precipitation of calcium carbonate under different geochemical conditions. The results show that the *Desulfovibrio bizertensis* is able to metabolise formate and this leads to an increase in pH and alkalinity of the medium. The time required for carbonate precipitation depends on the growth rate of the bacteria, where faster growth rate lead to faster precipitation of calcium carbonate, as suggested by the rate of decrease in calcium concentrations in the medium. There are several key factors that influence the bacterial growth rate including the Mg/Ca ratio of the medium, type of gas used and the presence of iron. Shaking, however, does not seem to significantly improve bacterial growth rate. Through these incubation experiments, the limiting factor for *Desulfovibrio bizertensis* under a medium close to seawater salinity was explored. Addition of dissolved iron at the beginning of the culture is detrimental to sulfate-reducing bacteria as the formation of iron-monosulfides likely entomb the bacteria. However, the bacteria are able to re-grow when a concentration of $\text{Fe} < \text{H}_2\text{S}$ is added during stationary phase. In addition, the bacteria show a higher growth rate in medium with Mg/Ca ratio of 1 compared to 5.2 and 0. In fact, carbonate mineral precipitation is often absent in a medium without magnesium. The medium without magnesium has a relatively low pH, low alkalinity, low concentration of sulfide and low sulfate reduction rate, suggesting that magnesium is essential for bacteria growth. Equilibration of 10% carbon dioxide gas with the medium also enhances bacterial growth and promotes a prolonged stationary phase. Monohydrocalcite and magnesium calcite are the precipitated calcium carbonate minerals. None of these experiments produced aragonite despite the high Mg/Ca in the media. The variables that drive the formation of monohydrocalcite remains unclear and will be explored in Chapter 3. Despite Mg/Ca playing a major role in its formation, I suspect that there is another variable that plays a role in the stabilization of monohydrocalcite. This is because monohydrocalcite is known to be unstable and readily transform into other calcium carbonate polymorphs such as calcite and aragonite.

Chapter 3

The role of microbial sulfate reduction in calcium carbonate polymorphs selection

3.1 Introduction

Microbial sulfate reduction, coupled either to organic matter oxidation or anaerobic methane oxidation, is one of the key microbial reactions driving sedimentary carbonate formation in marine sediments, intertidal marshes, and hypersaline lakes (Berner et al., 1970; Pye et al., 1990; Coleman et al., 1993; Visscher et al., 2000; Warthmann et al., 2000; Raiswell and Fisher, 2004; Baumgartner et al., 2009; Gallagher et al., 2012; Meister, 2013). Microbial sulfate reduction, particularly followed by precipitation of sedimentary pyrite, raises pH and increases alkalinity, while the negatively charged bacterial cell surface can serve as a nucleation surface for carbonate/mineral growth (Dong et al., 2000; van Lith, 2001; Bosak and Newman, 2005; Visscher and Stolz, 2005; Aloisi et al., 2006; Wacey et al., 2007; Zhu and Dittrich, 2016; Picard et al., 2018). The production of exopolymeric substances (EPS) around the bacterial cells also aids the nucleation and subsequent precipitation of calcium carbonate (Kawaguchi and Decho, 2002; Braissant et al., 2007; Dupraz et al., 2009; Obst et al., 2009; Tourney and Ngwenya, 2009; Balci et al., 2018). Despite work on the process of microbially-induced carbonate mineral precipitation, our understanding of how microbial sulfate reduction influences calcium carbonate mineralization and the formation of various calcium carbonate polymorphs remains limited. The vast majority of studies exploring the formation of different calcium carbonate polymorphs have focused on abiotic precipitation experiments, despite the fact that the majority of natural calcium carbonate mineral precipitation is biologically controlled.

The earliest studies on the nucleation, crystallization, and transformation of various calcium carbonate polymorphs focused largely on the precipitation of aragonite versus calcite and the role of magnesium ions and Mg/Ca ratio of the solution (Katz, 1973; Berner, 1975; Burton, 1993; Ries et al., 2008; Smeets et al., 2015). It was initially shown that the precipitation of aragonite is favoured in a high ionic strength solution with high Mg/Ca ratio ($Mg/Ca > 1$), while calcite is favoured in solutions with a lower Mg/Ca ratio ($Mg/Ca < 1$). The important role of magnesium in promoting different calcium carbonate polymorphs derives from the fact that magnesium possesses greater hydration energy and therefore promotes the formation of hydrous carbonate phases (Christ and Hostetle, 1970; Lippman, 1973; Ries et al., 2008; de Choudens-Sanchez and Gonzalez, 2009; Politi et al., 2009; Tommaso and de Leeuw, 2010;

Hopkinson et al., 2012; Nishiyama et al., 2013; Blue et al., 2017). The greater ability of magnesium ions (relative to calcium) to attract more water molecules (hydration energy) is because magnesium ions have a greater charge to ionic radius ratio, hence, possess a stronger interaction with the dipole in water molecule. In addition, there is an energetic barrier imposed by magnesium substitution for calcium in the calcite lattice, which may, in part, kinetically inhibit the formation of Mg-rich calcium carbonate minerals promoting polymorphism (Elstnerova et al., 2010; Xu et al., 2013).

Most inorganic precipitation studies have also shown that if the initial calcium carbonate precipitate is metastable (e.g. amorphous calcium carbonate or monohydrocalcite (MHC)), it will transform to calcite or aragonite over time via the Ostwald step rule (the Ostwald step rule states that it is not the most stable but the least stable polymorph that crystallises first) and/or other non-classical nucleation pathways (Munemoto and Fukushi, 2008; Bots et al., 2012; Liu et al., 2013; Rodriguez-Blanco et al., 2014; De Yoreo et al., 2015). However, the transformation mechanisms of amorphous calcium carbonate or MHC in natural environments are still poorly understood (Stoffers and Fischbeck, 1974; Dahl and Buchardt, 2006; Nishiyama et al., 2013; Ihli et al., 2014; Munemoto et al., 2014; Wolf et al., 2015; Meic et al., 2017). To constrain the behavior of these transient intermediate polymorphs, laboratory studies have been performed under both dry and wet conditions (Marschner, 1969; Hull and Turnbull, 1973; Kamiya et al., 1977; Dejehet et al., 1999; Liu et al., 2013). MHC reportedly transforms to aragonite in a heated atmosphere (Brooks et al., 1950; Kamiya et al., 1977), to calcite in a magnesium-free medium (Taylor, 1975) and to aragonite in media with $Mg^{2+}/(Ca^{2+} + Mg^{2+})$ greater than 20 mol% (Munemoto and Fukushi, 2008). Although these inorganic and abiotic studies have highlighted several variables that can influence calcium carbonate mineralisation and polymorphism, microbial systems involve a number of interconnected processes that may affect carbonate mineralization in unanticipated ways. This may obscure the influence of specific metabolic processes on calcium carbonate formation in sediments, and the attendant biogeochemical consequences.

Understanding the dominant calcium carbonate polymorph produced through microbially-induced carbonate mineral precipitation is inherently more difficult because microbial metabolic by-products and solution chemistry evolve over time. Within sedimentary pore fluids, for example, the concentrations of various elements that may promote or inhibit carbonate precipitation or play a role in the type of polymorph precipitated, may change with depth and/or time. For example, dissolved phosphate concentrations, which have been shown to influence carbonate polymorphism, can range from 0 – 600 μ M in sediment pore waters (Delaney, 1998; Burdige, 1991; Sasaki et al., 2001; Faul et al., 2005; Kraal et al., 2012; Sinkko

et al., 2013; Stockmann et al., 2018). An unanswered question is whether during microbially-induced carbonate mineral formation there is a difference in the calcium carbonate polymorphs produced, relative to those found in the well-studied abiotic experiments. If so, what are the master variables that influence the stability field of the precipitating carbonate polymorph?

In this chapter, I will explore how microbial sulfate reduction influences calcium carbonate polymorphism using pure cultures of sulfate-reducing bacteria under varying Mg/Ca and with different seeding materials. Many of the lead-up experiments which were done in preparation for the experiments in this Chapter, or the microbial method development, were explained in Chapter 2. I also investigate the transformation of the microbially induced calcium carbonate polymorphs to more stable polymorphs under a range of geochemical conditions. Finally, I will propose a stability field for calcium carbonate polymorphs obtained from the experiments and suggest the master variables that control the formation of microbially-induced calcium carbonate polymorphs.

3.2 Experimental

Most of the analytical techniques were described in the method development chapter (2). Here only the experimental techniques specific to the experiments in this chapter are described. For the full set of analytical processes please refer to Chapter 2.

3.2.1 *Incubation experiments*

A pure culture of the sulfate-reducing bacteria *Desulfovibrio bizertensis* (single bacteria strain) was used in all incubation experiments. The strain was purchased from Leibniz-Institut DSMZ-Deutsche Sammlung von Mikroorganismen und Zellkulturen GmbH (DSMZ) DSM No. 18034. This strain was originally isolated from marine sediments in the Mediterranean Sea near Bizerte, Tunisia (Haouari et al., 2006). My incubations were carried out in either 125 mL or 100 mL reaction vessels, tightly sealed with a blue butyl rubber stopper under strictly anoxic conditions. All experiments were performed at $25 \pm 1^\circ\text{C}$ in a water bath incubator. The incubation experiments were performed with different Mg/Ca (0:1, 1:1; 2:1, 3:1, 4:1 5.2:1; 9:1) including Atlantic seawater and artificial seawater and different seeding materials (kaolinite and calcite – see below).

3.2.2 *Composition of culture medium and inoculation*

The bacteria were initially cultured in Medium 163 as recommended by DSMZ (in Table 2.1, Chapter 2). An inoculum of the bacteria at stationary phase was transferred into the modified media and grown three times before the experiment began. Artificial seawater was prepared using the Standard Practice for the Preparation of Substitute Ocean Water – Designation: D1141-98 (Reapproved 2013). Stock solutions of artificial seawater were freshly made from analytical grade (Analar) reagents and diluted to the desired Mg/Ca ratio. The seawater solution was heated to approximately 80 °C for two hours to degas O₂. Then, the solution was allowed to cool and the above chemicals were added except yeast extract. Formate (7.5 g L⁻¹ or 110 mM HCOO-Na) was used as the sole electron donor in this study. Approximately 0.01% w/v of reductants (ascorbic acid and Na-thioglycolate), 4.0% w/v yeast extract and 1 mg L⁻¹ resazurin (oxygen indicator) were added into both the Atlantic seawater and artificial seawater medium. About 80 mL of the solution was then decanted into smaller incubation vials with 0.3 g of seeding materials (such as calcite or kaolinite), crimp sealed and flushed with 90% N₂/10% CO₂ gas for 30 minutes. Finally, the medium was autoclaved for 15 minutes at 121°C. The sample medium was subsequently cooled to 25°C in the water bath before being inoculated. Yeast extract solution was added to the medium using a syringe filter (0.2 µm) before inoculation. Control samples were immediately re-autoclaved after inoculation to kill the bacteria, then placed into the water bath.

3.2.3 *Biotic incubation experiment*

Three sets of incubation experiments were undertaken with varying Mg/Ca and seeding materials (Table 3.1). Approximately 0.3 g of seeding material was used. Biotic incubation experiments were performed without stirring (see Chapter 2 for the results of stirred and unstirred experiments). Experiments were sampled every few days until carbonate minerals precipitated – which was identified during the incubation based on a coincident decrease in pH and calcium concentration.

Table 3.1: Summary of experiment setup for biotic incubation experiments.

Experiment	Mg ²⁺ (mM)	Ca ²⁺ (mM)	Mg/Ca	Seeds
K-0:1	0	10	0	Kaolinite
C-0:1	0	10	0	Calcite
K-0:2	0	20	0	Kaolinite
C-0:2	0	20	0	Calcite
K-1:1	10	10	1	Kaolinite
C-1:1	10	10	1	Calcite
K-2:2	20	20	1	Kaolinite
C-2:2	20	20	1	Calcite
K-3:3	30	30	1	Kaolinite
C-3:3	30	30	1	Calcite
K-4:4	40	40	1	Kaolinite
C-4:4	40	40	1	Calcite
K-2:1	20	10	2	Kaolinite
C-2:1	20	10	2	Calcite
K-3:1	30	10	3	Kaolinite
C-3:1	30	10	3	Calcite
K-4:1	40	10	4	Kaolinite
C-4:1	40	10	4	Calcite
K-Atl-SW	52	10	5.2	Kaolinite
C-Atl-SW	52	10	5.2	Calcite
K-9:1	90	10	9	Kaolinite
C-9:1	90	10	9	Calcite

3.2.4 Aqueous sample analysis

Media was collected from the sample bottle over the course of the experiments using a sterilized needle and syringe and without shaking the vials. Samples were filtered using a 0.2 µm filter and analyzed for alkalinity, sulfide concentration, major cations (calcium, magnesium, sodium, and potassium) and anions (sulfate and chloride). The pH was measured at 25°C on the NBS scale using an Orion 3 Star meter with ROSS micro-electrode (ORION 8220 BNWP PerpHect ROSS – platinum wire as a reference in iodine/potassium iodide solution, ROSS internal filling solution is 3M KCl). Samples for alkalinity, anions, and cations were filtered through a 0.2 µm syringe filter. Alkalinity was titrated potentiometrically with 0.1 M of HCl using a Metrohm 848 Titrino plus with an error of 2.5%. The HCl used for titrations was standardized

with certified reference material (CRM) 2.2298 mEq L⁻¹. The CRM batch #157 used was provided by A.G. Dickson of Scripps Institution of Oceanography (Dickson et al., 2003).

An unfiltered sample was centrifuged at 900 rpm to separate any suspended solid in the solution before measurement for Optical density (OD) at 600 nm spectrum in an AquaMate Plus UV-VIS spectrophotometer. Phosphate concentrations were measured on the spectrophotometer using the molybdivanadophosphoric acid method (at 380 nm) described in Kitson and Mellon (1944).

As mentioned in Chapter 2, major cations and anions were diluted 20 times before being measured using ion chromatography on a Dionex ICS-5000+ SP. The cation concentrations were obtained with column IonPac CS168 and methanesulfonic acid (MSA 30mM) as the eluent. The anions were passed through an anion column IonPac AS18 with 31mM of potassium hydroxide (KOH) as eluent. Calibration standards were prepared by dilution of OSIL Atlantic Seawater standard into 2%, 5% and 10% solution for all batches of analyses.

3.2.5 *Abiotic precipitation experiment*

Abiotic experiments were conducted by slowly adding 2 mL of 0.5 M Na₂CO₃ (or 40 mEq L⁻¹ as CaCO₃) to 50 mL of seawater and artificial media over an hour at an average rate of 30 μL min⁻¹: (1) with and without yeast extract added; (2) stirred and non-stirred; and (3) with or without inorganic phosphate (K₂HPO₄) added. An equivalent concentration of inorganic phosphate – 600 – 800 μM (similar to the phosphate concentration in the yeast extract) was used in these abiotic experiments. Non-stirred samples were incubated at 25°C while stirred samples were stirred with a magnetic stirrer for 24 hours at laboratory temperatures of 21 ± 2°C. Samples were then centrifuged at 5000 rpm for 5 minutes, rinsed twice with Milli-Q water, re-centrifuged, before oven dried at 60°C overnight. These abiotic experiments replicate the results of countless previous studies (Kamiya et al., 1977; Dejehet et al., 1999; Bots et al., 2012; Nishiyama et al., 2013; Rodriguez-Blanco et al., 2014; Blue et al., 2017).

The addition of a Na₂CO₃ into non-stirred samples increases the pH of the solution to 8.5 – 9.0, but lower (6.5 – 7.5) in the solution with yeast extract. After the addition of the carbonate salt, the experiments were allowed to equilibrate for 48 hours at room temperature. The formation of a highly gelatinous layer at the bottom of the incubation vial was observed upon mixing of Na₂CO₃ with the medium. The gelatinous layer grows thinner over time and completely vanishes within 48 hours (see photo in Figure 3.1 below). Samples with higher magnesium concentration and with yeast extract/inorganic phosphate had the gelatinous layer

stay for longer in the vial. This gelatinous layer was sampled, processed, and measured in the XRD and SEM and is primarily composed of hydrated amorphous calcium carbonate (Kamiya et al., 1977, Bewernitz et al., 2012, Rodriguez-Blanco et al., 2014, De Yoreo et al., 2015, and Kimura and Koga, 2011).



Figure 3.1: Thick gelatinous layer was observed immediately after the addition of Na_2CO_3 in the abiotic experiment without yeast extract (left). Over time, the gelatinous layer gets thinner and eventually vanished after 24-hour incubation (right). A longer period is required for the thinning process in the sample with high Mg/Ca and yeast extract and vice versa.

3.2.6 Solid phase analysis

Please refer the analytical procedure for solid sample analysis in Chapter 2.

3.2.7 XRD analysis and Rietveld refinements

This section provides more details on the XRD analysis and Rietveld refinements than was presented in Chapter 2. Powder X-ray diffraction data were collected on the following instruments.

Instrument nr 1 - a D8-ADVANCE Bruker diffractometer operating in Bragg-Brentano geometry at 40x40 kVxmA, equipped with a Göbel mirror for parallel primary beam and a Vantec linear position sensitive detector, using $\text{Cu K}\alpha$ radiation. Collections conditions were: 10-60° in 2θ , 0.04° step size, 0.5 seconds/step, divergence slits 0.6 mm.

Instrument nr 2 - a D8-ADVANCE Bruker diffractometer operating in Bragg Brentano geometry at 40x40 kVxmA, equipped with a primary Ge monochromator for $\text{Cu K}\alpha_1$ and a Sol-X solid state detector. Collections conditions were: 10-60° in 2θ , 0.04° step size, 10 seconds/step, divergence slits 0.2 mm, receiving slit 0.2 mm, sample spinning.

Instrument nr 3 - a D5000 Bruker diffractometer operating in Bragg-Brentano geometry at 30x20 kVxmA, using Cu K α radiation. Collections conditions were: 10-60° in 2θ , 0.04° step size, 4 seconds/step, divergence slits 0.6 mm, receiving slit 0.2 mm, sample spinning. Detailed information of samples used in different instruments is given in Table 3.2.

Rietveld refinements were performed with TOPAS Academic V6 software (Cohelo, 2007). The instrumental parameters were refined on LaB6 NIST standard 660b for each instrument. Kaolinite crystal structure retrieved from the Inorganic Crystal Structure Database, ICSD (Allman and Hinek, 2007) (reference code: 63192) was first refined on a control sample from experiments with kaolinite seeds and no calcium carbonate precipitation, using a stacking faults model with 22 layers as shown in the Topas Academic V6 Technical Reference. The refined model was used for all the quantitative Rietveld analysis containing kaolinite.

Rietveld quantitative analysis is known to be unreliable for minor phases (<5 wt %). The accuracy is considered to be \pm 1-2% relative for major phases, while the e.s.d. from the Rietveld calculation has no bearing on the accuracy or otherwise of the quantification itself, is merely related to the mathematical fit of the model (Madsen and Scarlett, 2008). The figures are considered even less accurate when the phases involved show significant differences in microabsorption and crystallinity, as is the case with kaolinite and the calcium carbonates relevant to this work (Madsen and Scarlett, 2008). In order to estimate the accuracy of the quantification, Rietveld refinements were performed on six calcite and kaolinite standards. The Rietveld quantification results on these standards and linear fit are shown in Figure 3.2. It is, therefore, safe to consider an error of up to \pm 10 wt% absolute in samples containing kaolinite and calcium carbonates.

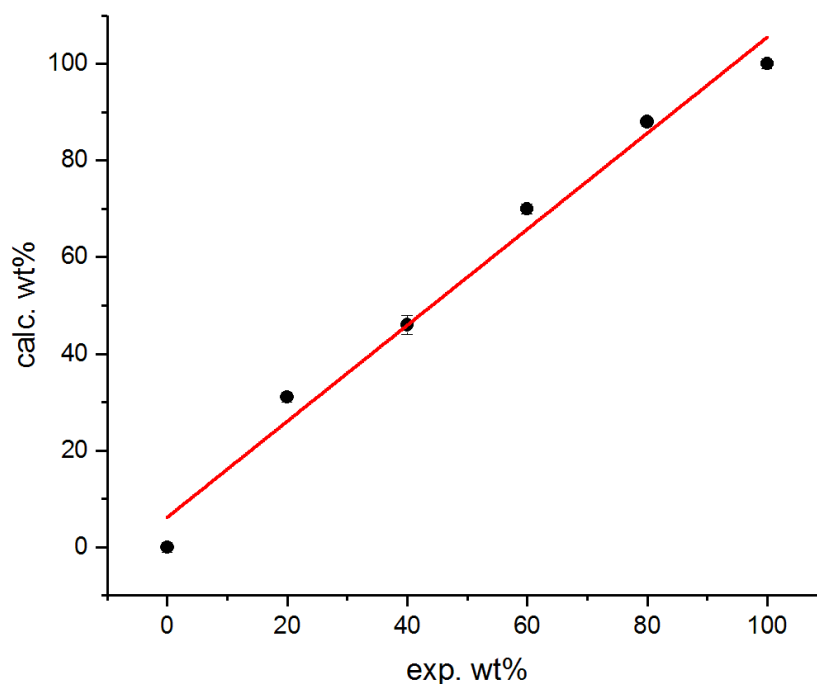


Figure 3.2: Measured calcite wt % in standard versus calcite wt % as calculated from Rietveld refinement. The linear fit yielded $y = 6 \pm 4 + (0.99 \pm 0.06) x$. $R^2 = 0.99$.

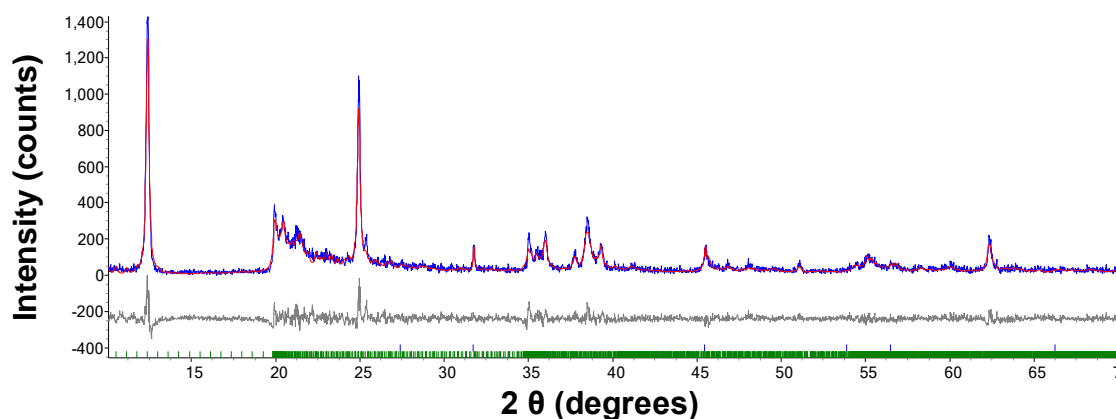


Figure 3.3: Rietveld refinement experimental (blue), calculated (red) and difference (grey) curves for the control sample. Peak position marks are shown for kaolinite (green) and halite (blue). The pattern was collected on instrument nr.2 - see experimental details in the manuscript. Collections conditions were: $10-70^\circ$ in 2θ , 0.04° step size, 40 seconds/step. Final R_{wp} and χ^2 are 21.01% and 1.70 respectively.

Crystal structures for calcite (ICSD reference code: 40109), aragonite (15198), monohydrocalcite (160811) and halite (52233) were retrieved from the ICSD. A Chebyshev function with eight parameters was used to model the background. A Lorentzian peak shape with a single parameter relative to crystal size was convoluted with the Pseudo-Voigt function as refined on the LaB6 NIST standard for each crystal phase. Refined parameters include

scale factor and unit cell parameters. The March-Dollase model for preferred orientation was applied on the (1 0 4) crystal plane of calcite and on the (0 0 1) plane of kaolinite. Figure 3.3 and 3.4 show an example of datasets collected on instrument nr.2.

Figure 3.5, 3.6, 3.7, and 3.8 show a typical refinement on datasets collected on instrument nr.3 and instrument nr.1 respectively. Table 3.2 reports data collection and Rietveld refinement details for all samples. Two different calcite structures were refined for those samples that contain high crystallinity calcite seeds and low crystallinity Mg-rich calcite precipitate - see Figure 3.8 for an example.

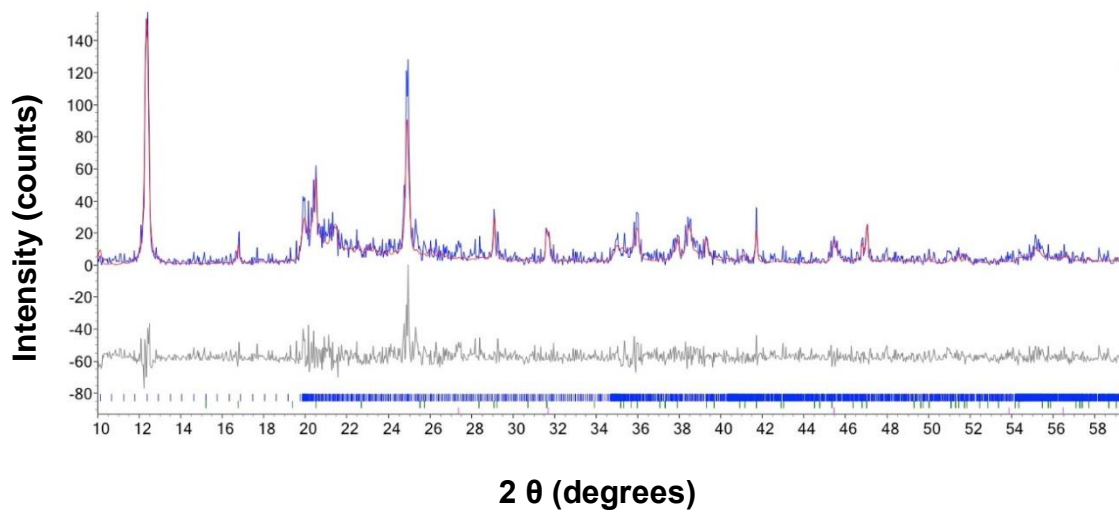


Figure 3.4: Rietveld refinement experimental (blue), calculated (red) and difference (grey) curves for sample K-4:1. Peak position marks are shown for kaolinite (blue), monohydrocalcite (green) and halite (pink). The pattern was collected on instrument nr.2.

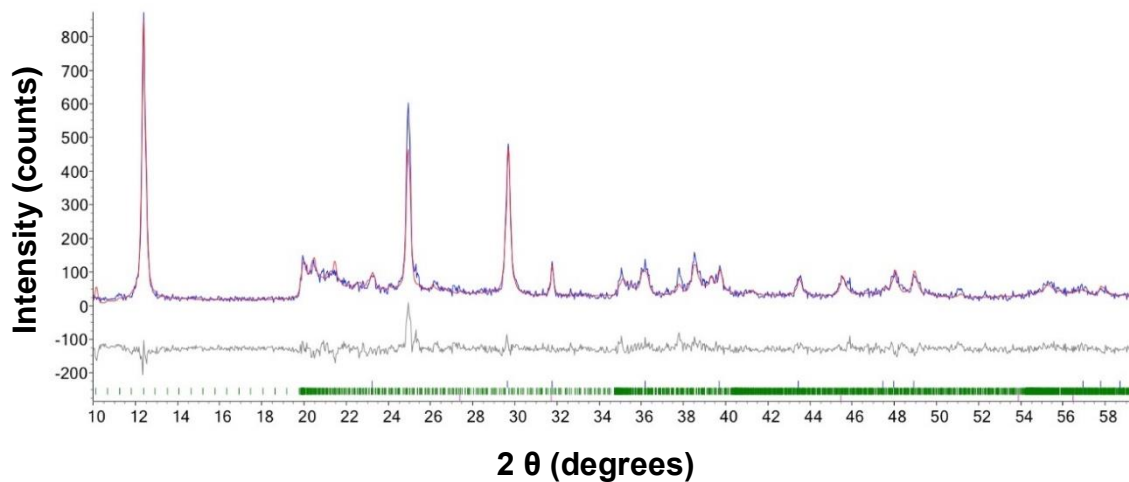


Figure 3.5: Rietveld refinement experimental (blue), calculated (red) and difference (grey) curves for the abiotic with Yeast Extract (stirred). Peak position marks are shown for calcite (blue), kaolinite (green) and halite (pink). The pattern was collected on instrument nr.3.

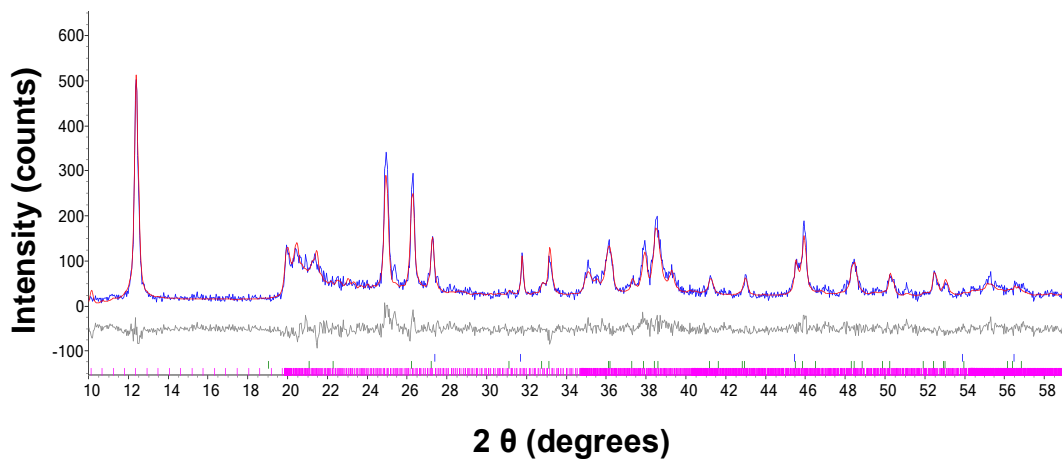


Figure 3.6: Rietveld refinement experimental (blue), calculated (red) and difference (grey) curves for sample NOYE (stir). Peak position marks are shown for halite (blue), aragonite (green) and kaolinite (pink). The pattern was collected on instrument nr.3 - see experimental details.

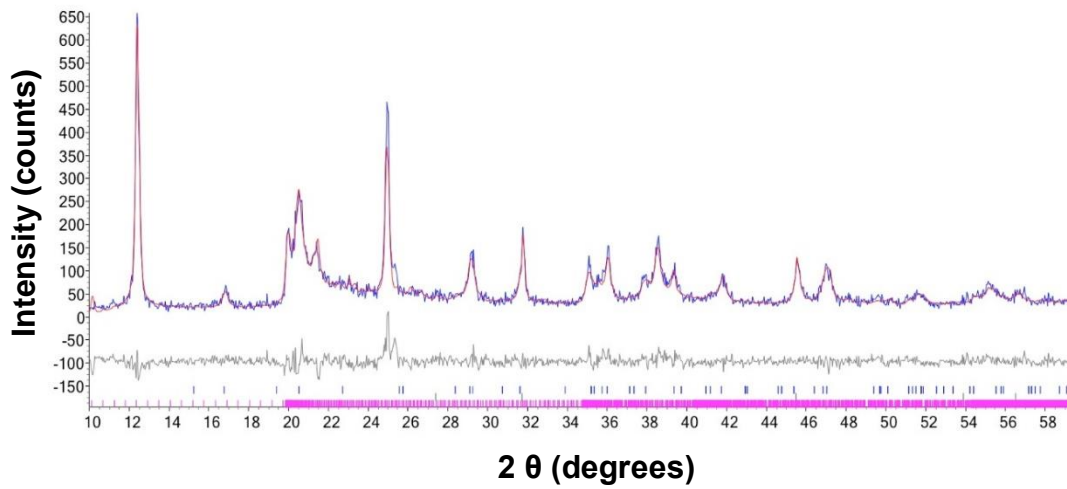


Figure 3.7: Rietveld refinement experimental (blue), calculated (red) and difference (grey) curves for sample No Yeast Extract (Stirred). Peak position marks are shown for monhydrocalcite (blue), halite (green) and kaolinite (pink). The pattern was collected on instrument nr.3.

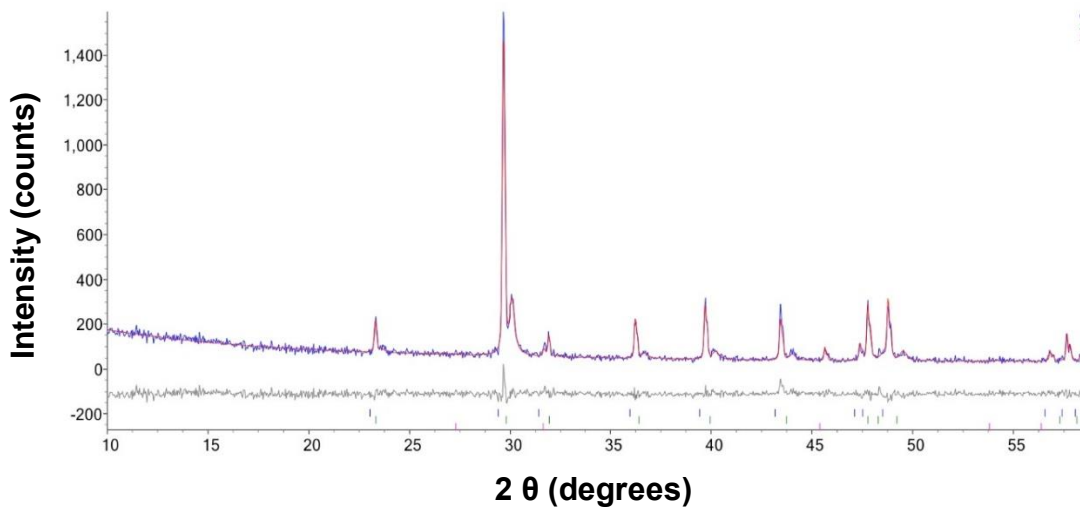


Figure 3.8: Rietveld refinement experimental (blue), calculated (red) and difference (grey) curves for sample K-4:4. Peak position marks are shown for calcite (blue), Mg-calcite (green) and halite (pink). The pattern was collected on instrument nr.1.

Table 3.2: Instrument and Rietveld refinement details for all samples. R_{wp} shows the quality of the least square refinement after background subtraction. The “Chi squared” or χ^2 is the goodness of fit of the model and data (Toby, 2006).

Sample name	Instrument	R_{wp}	χ^2
K-0:1	1	11.61	1.48
C-0:1	1	12.73	1.17
K-0:2	1	10.93	1.30
C-0:2	1	11.76	1.11
K-1:1	1	9.85	1.32
C-1:1	1	12.22	1.16
K-2:1	2	47.80	1.39
C-2:1	2	61.50	1.35
K-3:1	2	44.53	1.18
C-3:1	3	23.33	1.17
K-4:1	2	44.45	1.25
C-4:1	2	50.52	1.13
K-Atl-SW	2	45.35	1.13
C-Atl-SW	2	23.86	1.28
K-9:1	3	18.65	1.42
C-9:1	2	59.41	1.51
K-2:2	1	10.71	1.35
C-2:2	2	49.41	0.82
K-3:3	1	11.06	1.42
C-3:3	1	12.82	1.10
K-4:4	1	11.55	1.42
C-4:4	1	14.91	1.23
With Yeast Extract (Stirred) Atl. SW	3	15.96	1.21
With Yeast Extract (Unstirred) Atl. SW	2	52.99	1.98
No Yeast Extract (Unstirred) Atl. SW	3	17.81	1.41
No Yeast Extract (Stirred) Atl. SW	3	18.43	1.36
With Yeast Extract (Unstirred) Mg/Ca =1	3	17.98	1.38
With Yeast Extract (Stirred) Mg/Ca =1	3	17.90	1.35
No Yeast Extract (Unstirred) Mg/Ca =1	2	17.78	1.43
No Yeast Extract (Stirred) Mg/Ca =1	2	17.97	1.25
T-Alt-SW	3	19.99	1.22
T-MQ	3	21.87	1.24
T-Alt-SW-YE	3	20.02	1.24
T-Alt-SW-PO4	3	18.76	1.17
APO4SW (nostir)	3	27.53	1.46
APO4SW (stir)	3	24.60	1.34
APO41 (nostir)	3	25.98	1.34
APO41 (stir)	3	30.28	1.24

3.2.8 *Monohydrocalcite transformation experiment*

To investigate the transformation and stability of monohydrocalcite initially formed in some experiments, I subjected the mineral to elevated temperatures in an aqueous solution. These experiments were designed to investigate what will be the final calcium carbonate polymorph, hypothesizing MHC will transform to more stable phases over time but which stable phases may depend on the geochemical conditions. I recognize that in doing the transformation experiments at elevated temperatures that I have changed the experimental conditions from the lower temperatures of the initial biotic experiments. Approximately 0.02 g of MHC was heated under different media in sealed bottles at 100°C for 48 hours (Munemoto and Fukushi,

2008; Liu et al., 2013). Two milliliters of the following media were used: (1) Atlantic seawater; (2) Milli-Q water; (3) Atlantic seawater with 4.0% w/v yeast extract added; and (4) Atlantic seawater with 750 μM inorganic phosphate (K_2HPO_4 – Molar mass: 174.2 g mol^{-1}). After heating, the media and the solid samples were separated by centrifugation at 4000 rpm for five minutes. The media was decanted and the remaining solids were rinsed with Milli-Q water and dried before analysis by XRD and scanning electron microscope as above.

3.2.9 Saturation index and solution chemistry modelling

PHREEQC (Parkhurst and Appelo, 1999) was used to evaluate the evolution of geochemistry during the experiments. The SIT database (*sit.dat*) was used to model the evolution of the aqueous geochemistry and to calculate the evolution of the saturation indices of the media with respect to relevant calcium carbonate polymorphs (i.e. calcite, vaterite, amorphous calcium carbonate (ACC) and monohydrocalcite (MHC)). The *sit.dat* uses the specific ion interaction theory to calculate activity coefficients to calculate saturation state in the media throughout the experiment (Brönsted, 1922; Guggenheim and Turgeon, 1955). The measured concentrations of sulfate and calcium were used to predict the evolution of the solution pH and alkalinity of the media at each sampling point. For these predictions, I assumed that the decrease in the sulfate concentration was due to microbial sulfate reduction (Gallagher et al. 2012) and that the decrease in calcium concentrations was due to the precipitation of calcium carbonate. The modelled results for the pH and alkalinity were compared to the measured pH and alkalinity titrations to inform on the validity of the model described above. In the case of a large discrepancy between the modelled and measured alkalinity and pH, the alkalinity was adjusted in the model through the addition of NaHCO_3 to approximate the (de)sorption of carbonate ions from the kaolinite or calcite surfaces, and the pH was adjusted by the release of $\text{CO}_2(\text{g})$ to approximate (partial) equilibration with a low CO_2 headspace. The final results of the model were used to calculate the ion activity product (IAP: $\log a_{\text{Ca}^{2+}} a_{\text{CO}_3^{2-}}$) to determine the saturation state with respect to ACC, which is $\log (\text{IAP}/K_{sp})$ or $\log \Omega$ ($\log K_{sp} = -6.40$; Brecevic and Nielsen, 1989), monohydrocalcite ($\log K_{sp} = -7.60$; Hull and Turnbull, 1973), vaterite ($\log K_{sp} = -7.90$; Plummer and Busenberg, 1982), aragonite ($\log K_{sp} = -8.33$; Plummer and Busenberg, 1982) and calcite ($\log K_{sp} = -8.48$; Plummer and Busenberg, 1982).

3.3 Results

3.3.1 Evolution of aqueous chemistry

The results are separated by the seeding material used in each experiment (kaolinite seeds versus calcite seeds). Here I will present the primary results for each of the experiments, including the saturation state of MHC over the experiments. In Chapter 4 I will delve into the results further and discuss the control samples, and the full range of saturation indices calculation for more calcium carbonate polymorphs.

3.3.2 *Experiments with kaolinite seeds*

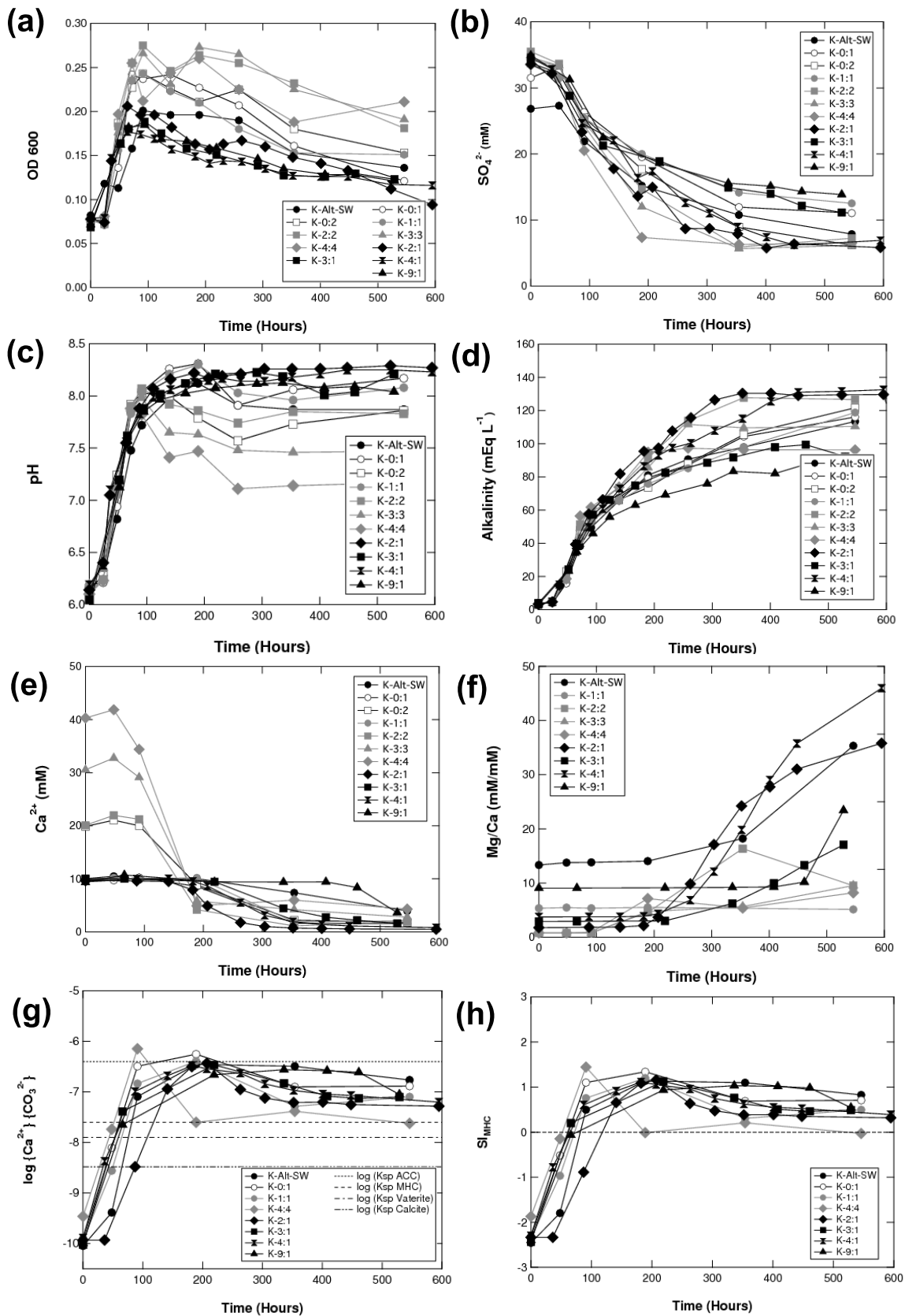


Figure 3.9: Aqueous chemistry data for the experiments with kaolinite seeds (a) optical density; (b) SO_4^{2-} ; (c) pH; (d) total alkalinity; (e) Ca^{2+} ; (f) Mg/Ca ratio; (g) ionic activity product for $CaCO_3$; and (h) SI_{MHC} calculated immediately after inoculation until 546 hours. I did not

observe any significant change in the killed samples (shown in supporting online material F). Sample code explanation – K = kaolinite seeded; C = calcite seeded; 3:1 = Mg 30 mM: Ca 10 mM; Alt-SW = Atlantic Seawater (Mg/Ca = 5.2) [See Table 5].

Significant bacterial growth was observed in all incubated samples over the first 100 hours after which the bacteria reach stationary growth phase (OD 600~0.15 – 0.25) (Figure 3.9a). The pH in all incubated samples increases to ~8 as microbial sulfate reduction progresses (Figure 3.9b and c). After 100 hours, carbonate mineral precipitation is observed in K-2:2, K-3:3 and K-4:4 (with Mg/Ca of 1 and magnesium and calcium concentrations at 20, 30 and 40 mM, respectively). Experiments K-0:1 and K-1:1, with lower calcium concentrations, reach a higher pH before carbonate mineral precipitation starts around 200 hours. A greater magnitude of pH drop (approximately 1 pH unit) is evident in K-4:4 compared to the other vials. Delayed precipitation of calcium carbonate is observed in seawater samples (K-Alt-SW). All experiments began with total alkalinity of approximately $4.0 \pm 0.5 \text{ mEq L}^{-1}$, which then increases to greater than 100 mEq L^{-1} . The alkalinity for experiments K-2:2 and K-4:4 plateaus earlier (200 and 250 hours) relative to the other experiments (Figure 3.9d). The rate of calcium carbonate precipitation, as indicated by the decrease in the calcium concentration, increases with increasing initial calcium concentration (Figure 3.9e). Sulfate concentrations decrease over time, although they are never fully depleted. The rate of sulfate depletion slows as carbonate minerals begin to precipitate. I observe a dramatic increase in the Mg/Ca ratio over time (Figure 3.9f). Samples with initial calcium concentration greater than 20 mM experienced a sharp increase in the saturation index or $\log \Omega$ (saturation state) for all carbonate polymorphs at 100 hours. I observe that nearly double the amount of time is required for samples with 10 mM calcium to reach their highest ionic activity product (IAP) and precipitation starts to slow down or stop when IAP starts to drop (Figure 3.9g and h).

3.3.3 Experiments with calcite seeds

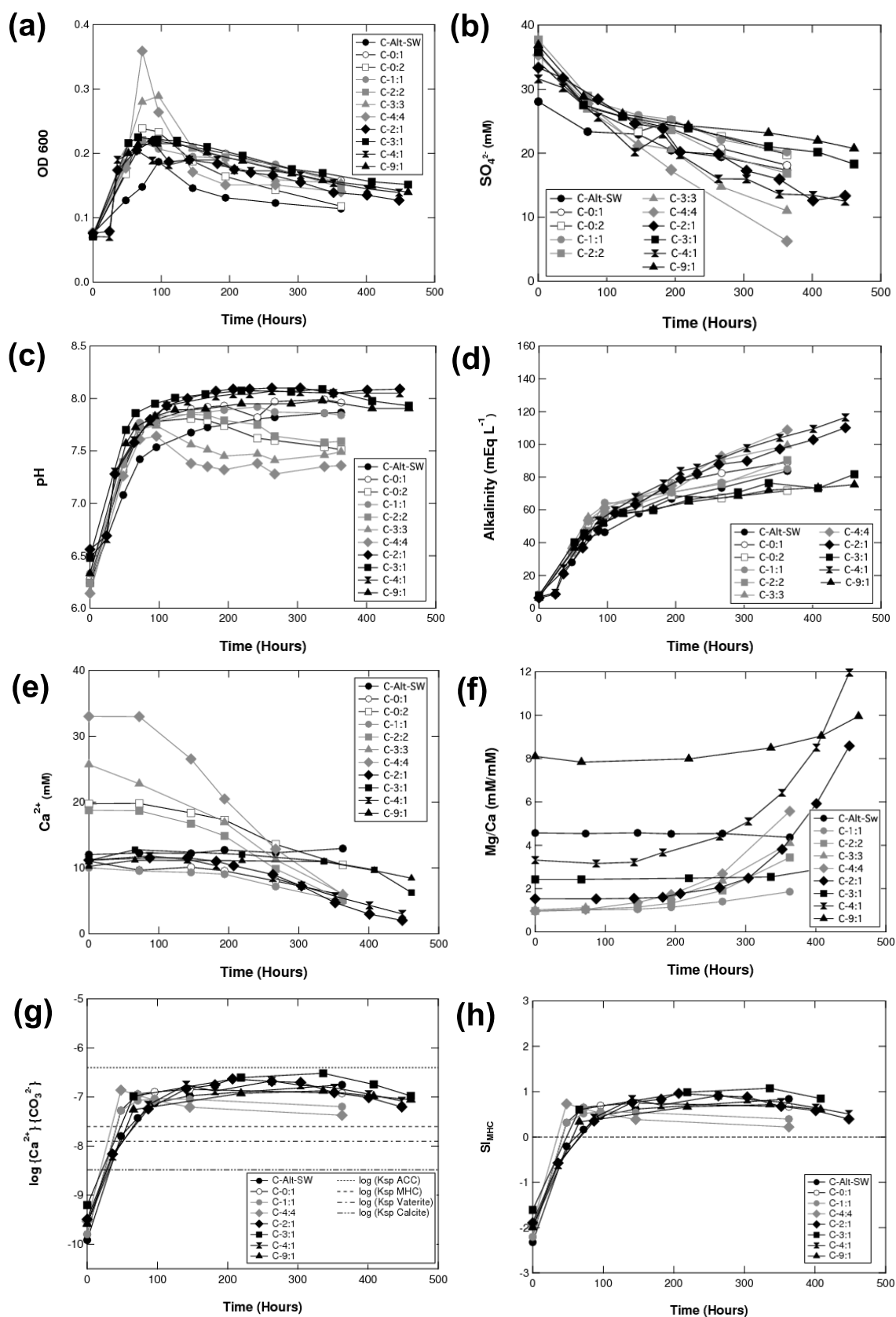


Figure 3.10: Aqueous chemistry data for the experiments with calcite seeds (a) optical density; (b) SO_4^{2-} ; (c) pH; (d) total alkalinity; (e) Ca^{2+} ; (f) Mg/Ca ratio; (g) ionic activity product for

CaCO_3 ; and (h) SI_{MHC} measured immediately after inoculation until 546 hours. A drop in pH and calcium concentrations in C-Alt-SW is not apparent although precipitation of MHC (measured by XRD and SEM) occurred. Sample code explanation – K = kaolinite seeded; C = calcite seeded; 3:1 = Mg 30 mM: Ca 10 mM; Alt-SW = Atlantic Seawater (Mg/Ca = 5.2) [See Table 3.1].

In the calcite-seeded experiment, I observe a sharp rise in OD 600 and pH linked to microbial sulfate reduction within the first 100 hours (Figure 3.10a, b and c), which stabilizes and then gradually drops in the samples with Mg/Ca of 1 at higher absolute magnesium and calcium concentrations (C-3:3 and C-4:4). Although the experiment starts at a lower pH of 6.2 – 6.5, the calcite seeds survive the first 50 hours of undersaturation (gravimetric data showing no loss of calcite seeds is presented in Table 3.3). Total alkalinity increases to maximum values of 110 mEq L^{-1} , compared to the experiments with kaolinite seeds in which alkalinity increases to a maximum of 130 mEq L^{-1} . I observe a decrease in calcium and sulfate concentration (Figure 3.10b and e), although at a lower rate than in the experiments with kaolinite seeds, and an increase in the Mg/Ca (Figure 3.10f). The K_{sp} for ACC in the experiment with calcite seeds is not reached (Figure 3.10g). The saturation index for the various calcium carbonate polymorphs (MHC, calcite, and aragonite) is lower than the saturation index with kaolinite seeds (Figure 3.10h and 3.9h) (SI_{calcite} , $SI_{\text{aragonite}}$, and SI_{vaterite} , are reported in detailed in the next chapter).

Table 3.3: Initial and final weight of calcite seeds in control samples.

Sample name	Initial weight (g)	Final weight (g)	Weight percent lost (%)
MAC (Alt-SW)	0.300	0.277	7.67
NAC (Alt-SW)	0.300	0.287	4.33

3.3.4 Results from geochemical modelling

PHREEQC was used both to calculate the saturation index for various carbonate polymorphs (Figures 3.9h and 3.10h) as well as to model the evolution of alkalinity over the experiment. In the alkalinity model, I note a greater discrepancy between the experimental and the modelled alkalinity in the experiments with kaolinite as seeding material (Figure 3.11a and c) than those with calcite as seeding material (Figure 3.11b and d). Despite the mismatch in some of the calcite seeding samples (Figure 3.11d), I was able to model most of the samples with good agreement between the measured and modelled alkalinity.

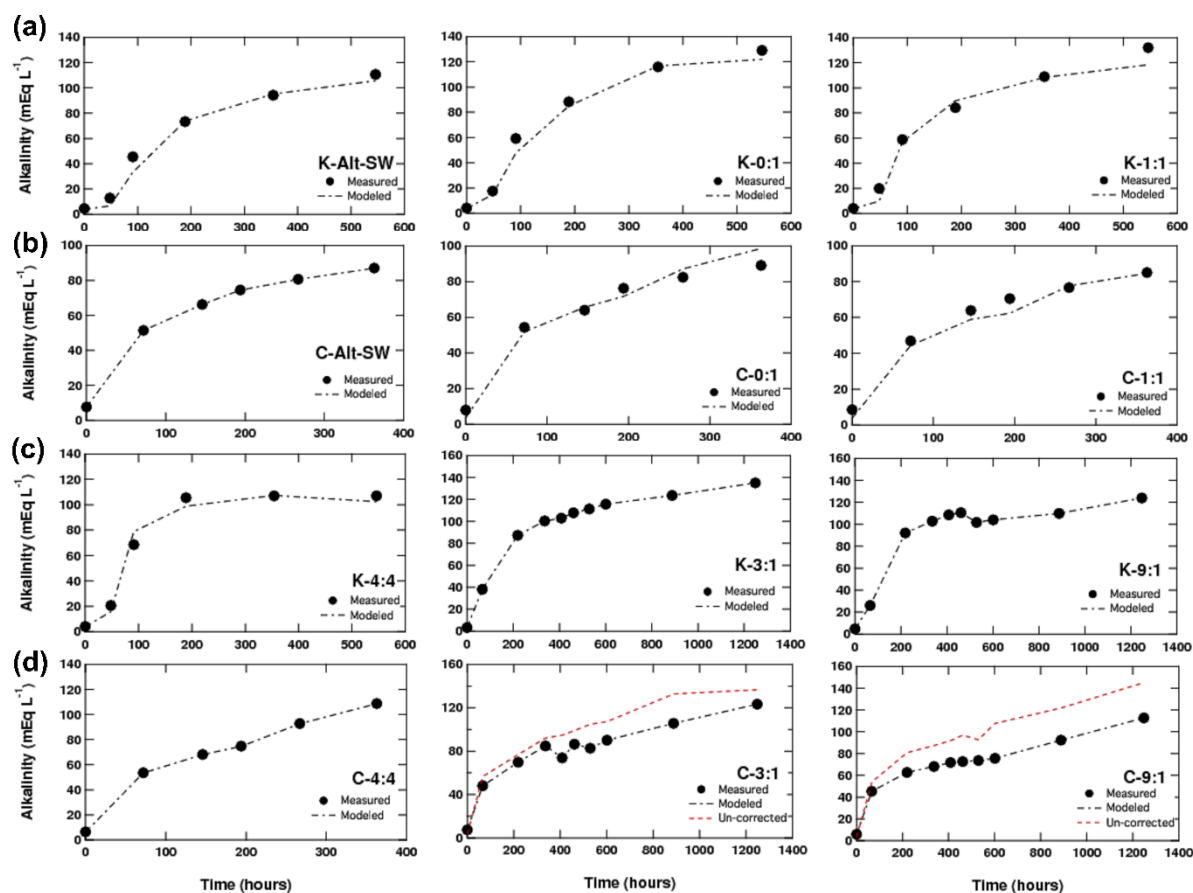


Figure 3.11: Comparison of experimental and modelled evolution of aqueous chemistry in samples with different seeding materials. A larger discrepancy between experiment and model was observed in samples with kaolinite seeds (b and d) compared to calcite seeds (a and c). An increase in the mismatch between experimental and modelled results is observed with an increasing Mg/Ca. The line labelled 'uncorrected' indicates the initial modelled values without any addition or removal of NaHCO_3 from the solution input.

3.3.5 Results from mineralogical characterization

Table 3.4: Summary of XRD results with Rietveld quantitative analysis of minerals (wt % with estimated standard deviation) for all experiments. Calcite and Magnesium Calcite differ in their concentration of magnesium and have different XRD patterns.

Experiment – Mg:Ca	Mg/Ca	Kaolinite (wt %)	Calcite (wt %)	Mg-calcite (wt %)	Monohydrocalcite (wt %)
K-0:1	0	87.4 ± 0.4	12.6 ± 0.4	-	-
C-0:1	0	-	100.0 ± 2.6	-	-
K-0:2	0	72.7 ± 2.9	27.3 ± 1.3	-	-
C-0:2	0	-	100.0 ± 2.0	-	-
K-1:1	1	86.7 ± 3.4	12.7 ± 1.3	-	-
C-1:1	1	-	87.2 ± 2.2	12.6 ± 1.1	-
K-2:2	1	84.6 ± 1.8	-	15.4 ± 0.7	-
C-2:2	1	-	85.2 ± 1.7	14.8 ± 1.7	-
K-3:3	1	80.5 ± 1.6	-	19.6 ± 0.7	-
C-3:3	1	-	55.6 ± 2.4	44.3 ± 2.2	-
K-4:4	1	66.1 ± 1.6	-	33.8 ± 1.0	-
C-4:4	1	-	44.6 ± 2.7	55.5 ± 3.0	-
K-2:1	2	92.4 ± 1.4	-	2.6 ± 1.2	5.0 ± 0.8
C-2:1	2	-	88.9 ± 2.2	11.1 ± 2.2	-
K-3:1	3	90.3 ± 1.2	-	-	9.7 ± 1.0
C-3:1*	3	-	76.0 ± 2.0	21.0 ± 1.6	3.0 ± 0.6
K-4:1	4	85.5 ± 1.0	-	-	14.5 ± 1.0
C-4:1	4	-	93.4 ± 0.7	-	6.6 ± 0.7
K-Atl-SW	5.2	87.5 ± 1.0	-	-	12.5 ± 1.0
C-Atl-SW	5.2	-	87.7 ± 2.3	4.0 ± 0.8	8.2 ± 0.5
K-9:1	9	87.6 ± 0.9	-	-	9.5 ± 0.8
C-9:1	9	-	86.1 ± 1.1	-	13.9 ± 1.0

* Average of two samples.

Characterization of the solid samples using XRD showed that two calcium carbonate polymorphs precipitated from all experiments: MHC and calcite (Table 3.4). My experiments suggest that all solutions with Mg/Ca ratio of greater than 3 dominantly yield MHC, whereas the media with an initial Mg/Ca of 1 or less produces calcite (Table 3.4). The diffraction patterns for MHC and calcite align closely with the crystallographic information for $Mg_{0.1}Ca_{0.9}CO_3$ (Althoff, 1977) (Figure 3.12). The calcite peak becomes broader and shifts

towards higher 2θ over time and with increasing magnesium concentration in the medium (Figure 3.12b). This peak shift and broadening suggest the incorporation of magnesium into the lattice of calcite, decreasing the size of the unit cell and the crystal domains (Lenders et al., 2012; Nielsen et al., 2016; Blue et al., 2017).

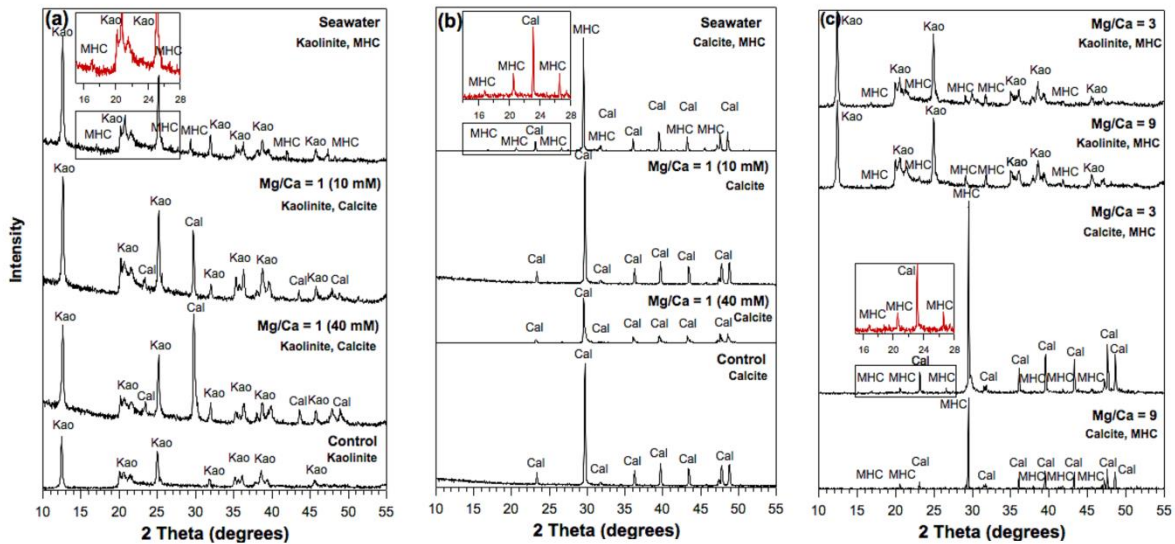


Figure 3.12: Powder X-Ray diffraction patterns collected from selected incubation samples in the three biotic experiments, (a) $Mg/Ca=1$ (kaolinite); (b) $Mg/Ca=1$ (calcite); and (c) $Mg/Ca=3$ and 9 (kaolinite and calcite). Intensity is reported in counts.

3.3.6 Abiotic precipitation experiments

In abiotic experiments, regardless of whether the samples were stirred or not, samples with high Mg/Ca , without yeast extract and inorganic phosphate favour aragonite whereas samples with Mg/Ca of 1 favour calcite (Table 3.5). Close to three weeks were required for calcite to precipitate in the seawater sample with yeast extract and inorganic phosphate, much longer than in the biotic experiments (~8 days). Similar to previous experiments, in stirred conditions, I find more MHC over a larger range of Mg/Ca . Examination under the scanning electron microscope reveals a different morphology of MHC precipitated from the abiotic and biotic experiment. Large spherulitic MHC (~20 – 40 μm) formed in the biotic experiment compared to the small platelets shaped MHC (~2.5 – 5.0 μm) from the stirred, abiotic experiment.

Table 3.5: Summary of final polymorphs obtained from the abiotic precipitation experiment. The initial chemical composition (i.e. the amount of yeast extract) and medium preparation procedures in this experiment are virtually identical to those of the biotic experiments except there is no inoculation. Kaolinite was used as seeding material.

Experiment	Kaolinite (wt %)	Calcite (wt %)	Aragonite (wt %)	Monohydrocalcite (wt %)
Atlantic Seawater (Mg/Ca = 5.2)				
No Yeast Extract (Unstirred)	82.5 ± 0.8	4.0 ± 0.8	13.5 ± 0.8	-
No Yeast Extract (Stirred)	66.5 ± 0.7	-	33.6 ± 0.7	-
*With Yeast Extract (Unstirred)	93.5 ± 1.9	6.5 ± 1.9	-	-
With Yeast Extract (Stirred)	76.0 ± 0.8	-	-	24.1 ± 0.8
PO ₄ ³⁻ Added (Unstirred)	96.7 ± 0.9	-	-	3.3 ± 0.9
PO ₄ ³⁻ Added (Stirred)	85.1 ± 0.9	-	-	14.9 ± 0.8
Artificial Seawater (Mg/Ca = 1)				
No Yeast Extract (Unstirred)	83.8 ± 0.6	16.3 ± 0.5	-	-
No Yeast Extract (Stirred)	25.2 ± 0.8	74.7 ± 0.8	-	-
With Yeast Extract (Unstirred)	92.8 ± 0.7	7.1 ± 0.7	-	-
With Yeast Extract (Stirred)	79.3 ± 0.8	-	-	20.7 ± 0.8
PO ₄ ³⁻ Added (Unstirred)	98.3 ± 1.5	1.5 ± 1.5	-	-
PO ₄ ³⁻ Added (Stirred)	83.3 ± 1.2	7.3 ± 0.9	-	9.4 ± 0.9

*Approximately 4 – 5 mL of Na₂CO₃ was added to speed up precipitation process. Calcite was detected after three weeks. MHC is not found in un-stirred samples (both Mg/Ca =5.2, 1) indicate stirring helps in mixing the solution and thus, favouring the formation of metastable polymorphs.

3.3.7 Microbial evidence in mineral precipitates

In the SEM images, I observe spherulitic MHC with a hollow core where clumps of well-preserved bacterial cells are located (Figure 3.13a and b). Duplet or triplets of spherulitic MHC are also common (Figure 3.13b). In addition to the spherical MHC found, a dumbbell-shaped structure with microbial imprints was also identified in my experiments (Figure 3.13c). Figure 3.13d shows the jagged calcite structure (bottom right) precipitate adjacent to the calcified bacteria colony (upper left). Note the distinct texture of both structures where the calcite is micrometer in size with unique triangular ends while the bacterial cells are calcified by sub-micron to nano-meter scale crystals.

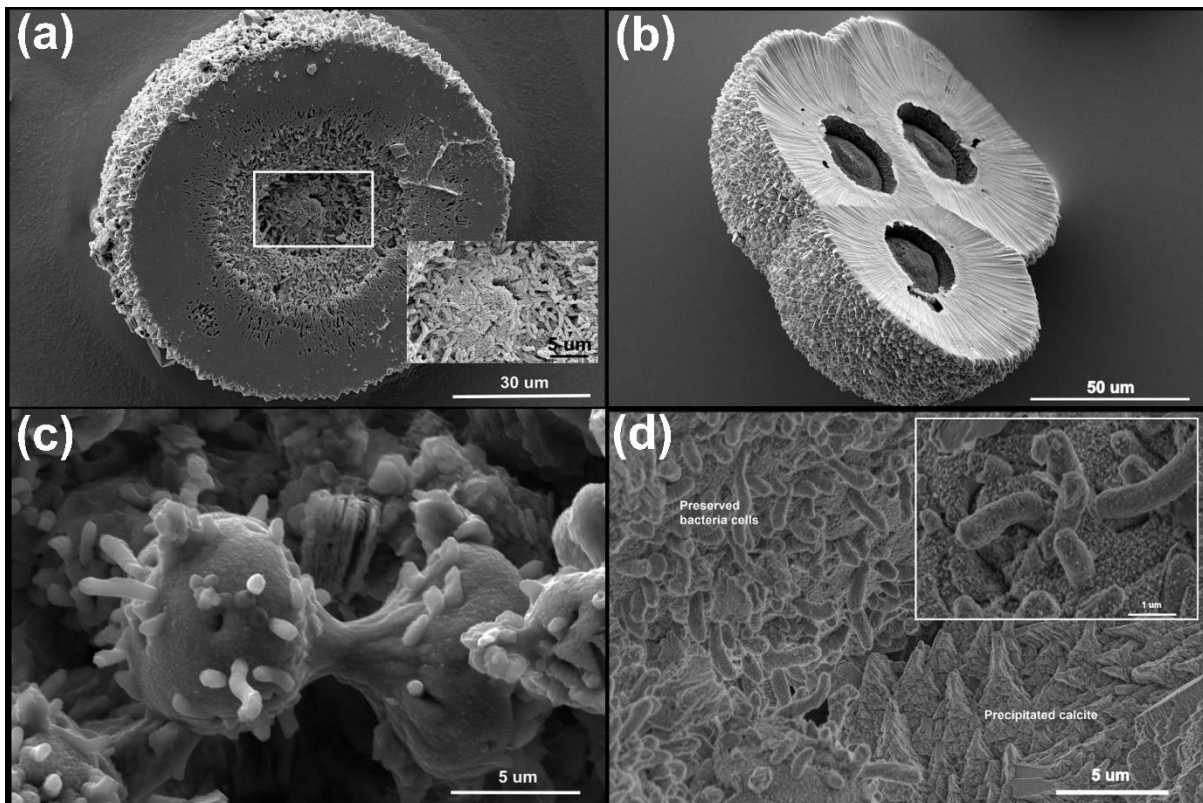


Figure 3.13: SEM images (backscattered electron) showing (a) MHC hemisphere with bacteria colony concentrated at the hollow core – sample C-Alt-SW; (b) triplet hemi-spherulitic MHC structure with hollow core – sample C-Alt-SW; (c) dumbbell-shaped structure with protruding well-preserved bacterial cell observed in sample K-4:4; (d) precipitated calcite located adjacent to fossilized bacterial colony – sample K-4:4 with closeup secondary electron (SE) image showing instantaneous calcification of *Desulfovibrio bizertensis* by the nano-sized crystals. All the images showing the morphology and microstructure of carbonate minerals linked to microbial sulfate reduction.

3.3.8 Transformation experiment

Four different media combinations were tested to examine which stable calcium carbonate polymorphs form from the MHC produced during my experiments (Table 3.6). For this, pure, spherulitic MHC is used (with diameter range between 20 – 40 μm) which had been previously precipitated from an unseeded incubation (Figure 3.14a). Here, I also show abiotically precipitated MHC for comparison (Figure 3.14b). There is a distinct size and morphological difference between the biotic and abiotically precipitated MHC (Figure 3.14a and b). In pure seawater, this MHC transforms into both calcite and aragonite (Table 3.6). In this case, the dehydration of MHC changes its spherulitic structure to elongated needle-like calcite and aragonite crystals (Figure 3.14c). Incubation of MHC with pure Milli-Q water transforms the

MHC into calcite (Figure 3.14d). In contrast, when the transformation happens in seawater with yeast extract or inorganic phosphate, a considerable amount of MHC is retained and not transformed into a more stable calcium carbonate polymorph (sample T-Alt-SW-YE - 79.5 ± 1.5 %, sample T-Alt-SW-PO4 - 26.2 ± 1.7 %) (Figure 3.14e and f).

Table 3.6: Mineralogical composition of calcium carbonate polymorphs (in wt %) derived from MHC transformation.

Medium	MHC	Calcite	Mg-Calcite	Aragonite
T-Atl-SW (Seawater only)	-	77.1 ± 3.9	-	22.9 ± 3.9
T-MQ (MQ-water only)	-	100.0 ± 0	-	-
T-Atl-SW-YE (Seawater + yeast extract)	79.5 ± 1.5	15.5 ± 1.2	5.1 ± 1.2	-
T-Atl-SW-PO4 (Seawater + K_2HPO_4)	26.2 ± 1.7	52.3 ± 3.1	-	17.2 ± 1.3

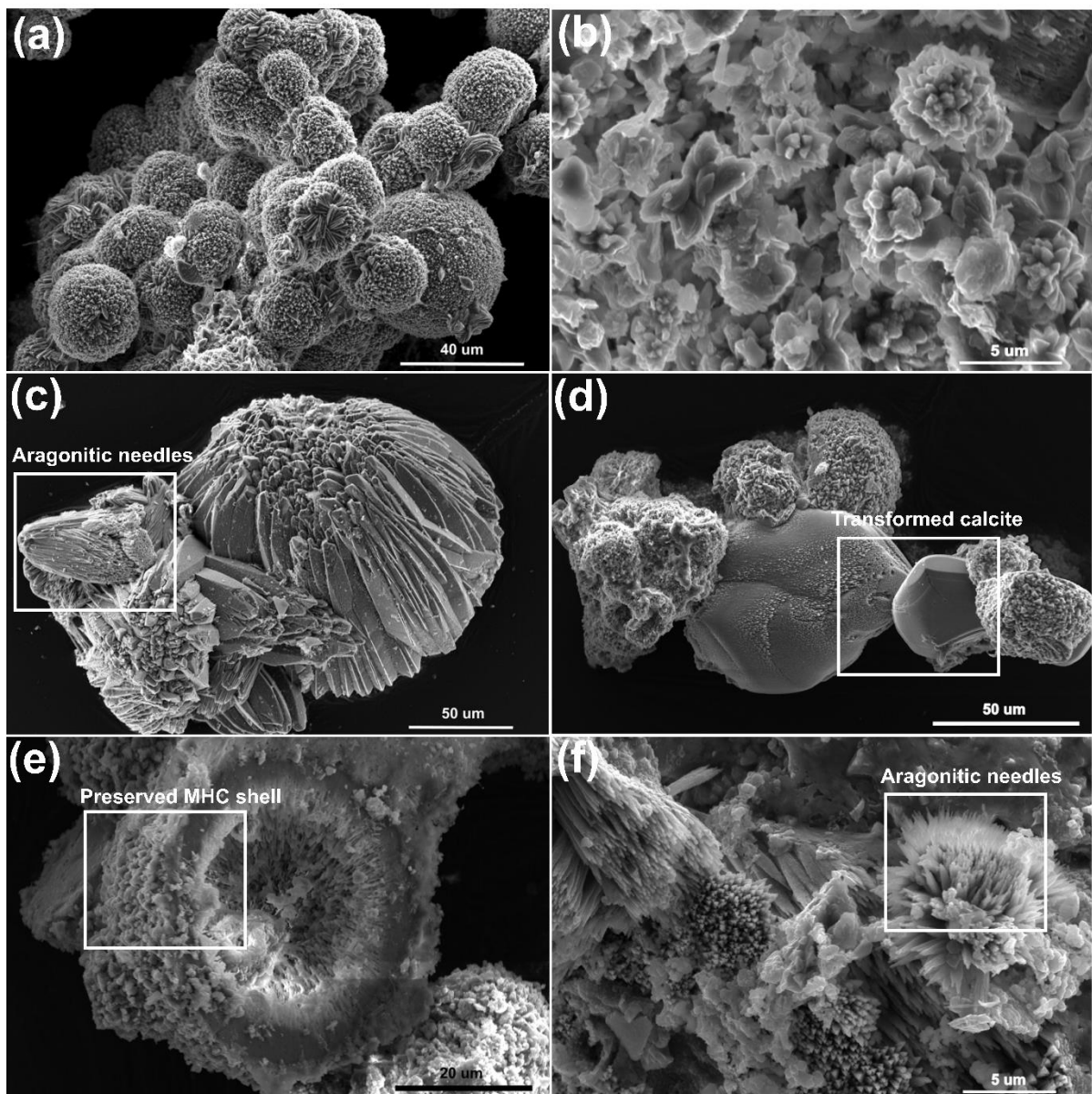


Figure 3.14: SEM images show the morphology of minerals precipitated in the biotic and abiotic experiments. (a) Initial spherulitic MHC from the biotic experiments; and (b) sub-micron aggregated platelets (cauliflower-shaped) MHC from abiotic experiment. The mineralogy of these final products was confirmed using XRD. Image (c) – T-Alt-SW, (d) – T-MQ, (e) – T-Alt-SW-YE, and (f) – T-Alt-SW-PO4 are transformation products of Figure 5a after thermal dehydration at 100°C for 48 hours. I note the distinct morphological alteration of the final products (aragonitic needles, calcite rhomb and bigger hollow core of preserved spherulitic MHC). Mineral composition of these final polymorphs is reported in Table 3.6.

3.4 Discussion

My results indicate that microbial sulfate reduction triggers the precipitation of calcite and MHC. Which of these may dominate appears to depend on the Mg/Ca ratio at the time of mineral nucleation; MHC forms from solutions with Mg/Ca greater than 3, while calcite forms from solution where the Mg/Ca ratio is 1 or less. The media is initially undersaturated with respect to all carbonate minerals, but within 100 hours the media is super saturated and precipitation of calcium carbonate occurs. The rate of precipitation depends on the calcium concentration in the media, and seems to be independent of the mineral seeding material used, and is independent of the Mg/Ca ratio.

The discussion is divided into five parts. First, I discuss the influence of microbial sulfate reduction on the evolving solution chemistry driving carbonate mineral precipitation. Then I discuss the primary controls on the formation of MHC and calcite in these experiments. Next, I demonstrate the effect of seeding materials on the solution chemistry and also the calcium carbonate polymorphs precipitated. In the penultimate section of the discussion, I show the controls on the transformation of MHC to more stable polymorphs. Finally, I explore the implications of my results on sedimentary carbonate precipitation in the natural environment.

3.4.1 The influence of microbial sulfate reduction on calcium carbonate precipitation

My experimental results show that microbial sulfate reduction strongly influences solution chemistry and thus, affects carbonate mineral precipitation in three ways. First, each experiment is accompanied by a significant increase in total alkalinity and pH as microbial sulfate reduction (using formate as electron donor) proceeds (Figures 3.9d, 3.10d) through the overall reaction (Gallagher, 2012):



This relationship suggests an increase of one mole of dissolved inorganic carbon (DIC) as well as an increase of 1.5 moles of total alkalinity per mole of organic carbon (formate) oxidized (Soetaert et al. 2007). This increase in alkalinity leads to dramatic increases in the carbonate mineral saturation state. For example, within the first 100 hours of experiments with kaolinite seeds, I see a 10 to 15-fold increase in alkalinity, which translates to calcite saturation index of $\sim 1 - 2$ (SI_{Calcite}). The increase in pH is mainly driven by the production of hydroxide (OH^-) ions during the metabolism of formate. After carbonate mineral growth begins, the continued increase in pH and DIC from the growth of the sulfate-reducing bacteria is matched by a decrease or stabilization of the pH and DIC concentration due to calcium carbonate precipitation.

This increase in alkalinity from microbial sulfate reduction coupled to formate oxidation was closely replicated with PHREEQC modeling for the experiments with the kaolinite seeds, but there was more of a mismatch with the calcite seeds (Figure 3.11). This suggests that there is a sink for alkalinity in the experiments with calcite seeds that does not exist with the kaolinite seeds. One possibility is the secretion of exopolymeric substances (EPS) by the sulfate-reducing bacteria, which can complex cations across a wide range of solution pH (Braissant et al., 2007; Dupraz et al., 2009; Baker et al., 2010). Qualitatively, we noticed that there was more 'white fluff', often anecdotally attributed to EPS, in the experiments with the calcite seeds than with the kaolinite seeds. EPS was not included in the PHREEQC model, nor was the concentration or type of EPS analysed during the experiment. It is unclear why the sulfate-reducing bacteria might make more EPS in the experiments with calcite seeds, although this was observed in three separate experimental runs and thus the result seems reproducible. Another possibility is that the adsorption onto and desorption from the mineral seeds' surfaces, and the exchange of CO_2 with the headspace might account for the alkalinity difference in the model. Despite the mismatch in some of the calcite seeding samples, I was able to model most of the samples with good agreement between the measured and modelled alkalinity (Figure 3.11).

Although Soetaert et al. (2007) suggested that microbial sulfate reduction alone may not lead to carbonate mineral precipitation because the solution pH is poised too low (the equivalence midpoint is pH 6.7), recent modelling and culture experiments support the notion that microbial sulfate reduction may lead to carbonate mineral precipitation. For example, Meister et al. (2013) demonstrated that while microbial sulfate reduction initially lowers pH and thus initially lowers the carbonate saturation state, it slowly increases as sulfate reduction continues due to increasing dissolved inorganic carbon concentration while pH stabilizes. The Meister et al.

(2013) results are in agreement with my observations – that the chemical evolution of closed (or diffusionally controlled) systems is strongly dependent on the amount of organic carbon respired, and therefore dissolved inorganic carbon generated, in addition to other variables such as pH and buffering capacity.

Second, aside from increases in dissolved inorganic carbon and carbonate saturation state, the concentration of inhibitors of carbonate mineral precipitation, such as sulfate and magnesium, changes over the course of my experiments (Walter and Burton, 1986; Burton and Walter, 1989; Grases and March, 1990; Lin and Singer, 2005). Although sulfate has long been understood to inhibit calcite precipitation (Busenberg and Plummer, 1985; Walter, 1986; Bots et al., 2011), especially in the presence of elevated concentrations of aqueous magnesium (Bots et al., 2011; Nielsen et al., 2016; Dobberschutz et al., 2018), my results show that calcium carbonate mineral nucleation occurs as sulfate is being depleted, but while there is still substantial aqueous sulfate in solution. Furthermore, the Mg/Ca ratio in the solution increases over the course of the experiments. Because the Mg/Ca ratio is recognized as a fundamental control on calcium carbonate polymorphism, changes in this parameter should influence the final carbonate mineral products.

Solution data from my experiments show that microbial sulfate reduction alters the chemical state of the experiments with respect to calcium carbonate mineral stability. The sulfate-reducing bacteria, through their metabolism, produce an extremely high saturation state for all calcium carbonate polymorphs, which triggers nucleation in the presence of multiple inhibitors to nucleation and growth. The SEM images (Figure 3.13) of the carbonate minerals precipitated suggest that the sulfate-reducing bacteria create a highly supersaturated micro-environment driving carbonate precipitation. I suspect that the negatively charged cell surface of the sulfate-reducing bacteria initially attracts dissolved divalent cations such as calcium and magnesium (Qiu et al., 2017). During carbonate precipitation, outward growth of crystals from a substrate eventually introduces geometrical competition where crystals growing normal to the substrate dominate over other orientations; this typically results in outward radiating crystal fabrics which may sometimes adopt a spherical structure if they are grown on a rounded or spherical substrate (i.e., aggregate of bacterial cells) (Dickson, 1993). Analogous observations of fossilized bacterial clump in the core of spherulitic carbonates have also been reported from field samples in Chafetz et al., (2018).

It is interesting to note that the spherulitic structure of carbonate minerals is not unique to microbial sulfate reduction. Rather, variables such as Mg/Ca ratio (between 2 to 8), salinity, nucleation surfaces, and rates of mineral precipitation collectively control the habit and

structural form of the carbonate precipitated (Tracy et al., 1998; Sanchez-Navas et al., 2009; Nyiro-Kosa et al., 2018). Spherulitic growth is also a common product resulting from crystallization of amorphous calcium carbonate (ACC). Spherulitic growth requires a large crystallization driving force, such as a solution with sustained supersaturation from initial formation and subsequent continuous dissolution of ACC, resulting in the aggregation and growth of spherical nanoscale mineral particles (Granasy et al., 2005; Han et al., 2017a; Rodriguez-Blanco et al., 2017). Some field sedimentary characteristics of dolomite also reflect spherulitic growth processes, suggesting that the deposition and crystallization process may have involved the transformation of an amorphous precursor, and thus high supersaturation states (Hood et al., 2011). The hollow core structure of the spherulitic MHC with calcified microbial textures in my experiments are not visible in the carbonate precipitation products during abiotic precipitation experiments (Bots et al., 2012; Rodriguez-Blanco et al., 2014), hence, could serve as unique signature of microbially-mediated precipitation. However, the transformation experiments suggest that such a structure and the associated microbial texture are difficult to preserve when stable carbonate polymorphs are formed and thus could be vulnerable to post-burial processes during early diagenesis.

I suspect the carbonate mineral products must have initially transformed from an amorphous phase (e.g. ACC) prior to crystallization into calcite or MHC. The amorphous phase is often found present together with some other crystalline sample with Bragg peaks on the XRD pattern. Visual examination under SEM also indicates that both amorphous and crystalline solid phases coexist during the early stage of the precipitation (Figure 3.15). Furthermore, as I discuss below, saturation state and calcium carbonate mineralogy provide additional evidence for the role of an amorphous calcium carbonate precursor. Depending on the Mg/Ca ratio of the surrounding fluid, the ACC and calcite may incorporate different amounts of water into the structure due to the difference in hydration energy between the magnesium and calcium ions (Christ and Hostetle, 1970; Gonzalez, 2009; Tommaso and de Leeuw, 2010; Hopkinson et al., 2012; de Choudens-Sanchez and Xu et al., 2013; Nishiyama et al., 2013; Sun et al., 2015). Such a difference in hydration energy has also been shown to affect the transformation into crystalline calcium carbonate polymorphs and induce the transformation of ACC to MHC rather than calcite (Rodriguez-Blanco et al., 2014). The structure of calcite precipitated in the experiments with lower Mg/Ca forms rhombohedral shapes with triangular terminations (Figure 3.13d).

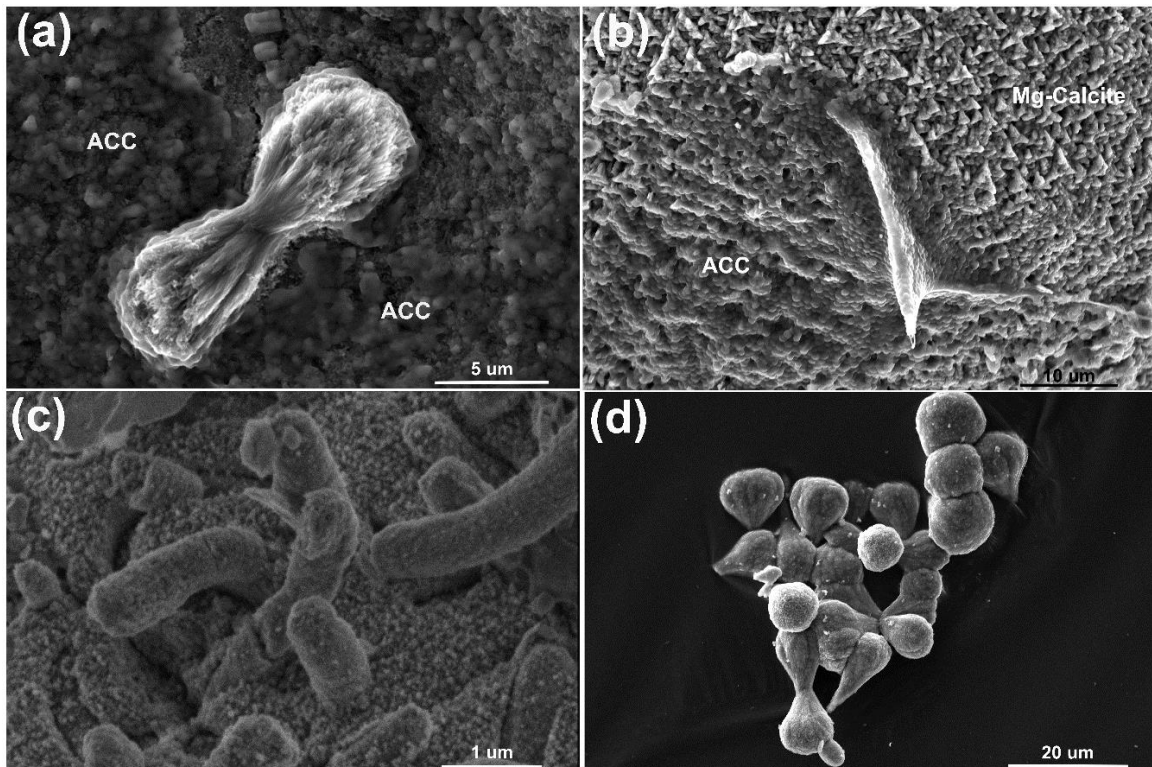


Figure 3.15: SEM images showing the coexistence of amorphous-like and nano-crystalline minerals in the samples. Nano-sized crystallites growing on the bacterial surfaces and the base which eventually entombed the bacteria. a) AYE(ACC) – abiotic sample with yeast extract added; b) K-4:4; c) K-4:4; and d) C-3:1.

3.4.2 Evolving chemical controls on CaCO_3 precipitation and polymorph selection

The chemical evolution discussed above establishes a framework for interpreting the mineral products formed in my experiments, and for predicting the calcium carbonate mineral phases that may be associated with microbial sulfate reduction more broadly in the natural environment. An unexpected observation from my experiments is the dominance of MHC in the biomineralization products, a relatively rare calcium carbonate polymorph in natural systems. Previous work suggests that at Mg/Ca ratios of greater than ~ 2 , aragonite nucleation dominates calcium carbonate mineral precipitation, and therefore the carbonate mineral products precipitated from modern seawater (Katz, 1973; Berner, 1975; Burton, 1993; Ries et al., 2008; Bots et al., 2011). However, aragonite is conspicuously absent in all of my experiments (and, indeed, in nearly all microbially induced carbonate precipitation experiments), despite initial Mg/Ca ratios that ranged from 0 – 9 (Table 3.5). This hints at a strong inhibition of aragonite nucleation in my experiments, remembering that aragonite has a higher energy barrier to nucleation compared to other polymorphs such as MHC, which I suspect results from elevated phosphate concentrations (note that the full phosphate

concentrations and their interpretation are included in Chapter 4). Previous studies have shown that a phosphate concentration of greater than 10 μM inhibits the formation of aragonite, and even phosphate concentrations as low as 5 μM can alter the kinetics of aragonite precipitation (Walter, 1986; Oomori et al., 1988; Burton and Walter, 1990; Yagi and Fukushi, 2011; Tadier et al., 2017). The phosphate concentration in my experiments ranged between 600 – 800 μM , which is on the higher range of that measured in anoxic sediments (Sasaki et al., 2001; Hyacinthe and Van Cappellen, 2004; Sinkko et al., 2013; Egger et al., 2015; Kipp and Stueken, 2017). I suspect that the high range of phosphate concentrations in my experiments inhibits the formation of aragonite. In an experiment with lowered phosphate concentration the bacterial growth was severely impacted and struvite ($\text{NH}_4\text{MgPO}_4 \cdot 6\text{H}_2\text{O}$) was the only precipitate (not shown in the thesis). In the MHC transformation experiments, the role of phosphate in the inhibition of aragonite is also shown as none of the experiments with added phosphate produced aragonite, in spite of high Mg/Ca; I also observed this in abiotic experiments. Phosphate adsorbs rapidly and irreversibly on high energy sites (kink, step, edge, and hole) of mineral surfaces, which drives the inhibitory effects on carbonate mineral growth and dissolution rates (Berner and Morse, 1974).

One possible consequence of the presence of phosphate in my experiments is that the saturation state for various calcium carbonate polymorphs increases well beyond typical range needed for aragonite or calcite nucleation from seawater (Morse and He, 1993). In my experiments, I do not observe calcium carbonate nucleation until the ionic activity product is close to that required for initial ACC precipitation (see dashed lines in Figures 3.9g and 3.10g). These solution data hint that, in the absence of aragonite and calcite nucleation, ACC is the solubility-limiting phase in my experiments, providing a reactive and transient precursor to the formation of more stable crystalline calcium carbonate mineral phases.

In addition to the exceptionally high saturation states needed for carbonate mineral precipitation, the likely initial formation of ACC in my experiments provides a simple mechanism to explain observed carbonate polymorphism. Previous studies have shown that once formed, ACC transforms into several carbonate polymorphs depending on the Mg/Ca, pH, and concentration of DIC (Loste et al., 2003; Kimura and Koga, 2011, Nishiyama et al., 2013; Rodriguez-Blanco et al., 2014; Blue et al., 2017). In particular, at high Mg/Ca (above 8, depending weakly on pH and concentration of dissolved inorganic carbon) ACC has been shown to transform to MHC.

My results suggest that microbial induced ACC transforms to MHC at much lower Mg/Ca than previously shown in these abiotic experiments (Rodriguez-Blanco et al., 2014; Blue et al.,

2017). My results, for the timepoint of precipitation, are superimposed on the stability fields for MHC initially proposed by Blue et al. (2017) (Figure 3.16). I show that dominant carbonate mineral polymorph is determined by the solution chemistry at the time of carbonate mineral nucleation, and although the solution chemistry then evolves into other stability fields (Figure 3.17), the initially precipitated polymorph continues to grow. My experiments suggest a shift in the calcite-MHC boundary to a $a\text{Mg}^{2+}/a\text{Ca}^{2+}$ of 2. However, the abiotic experiment in Blue et al. (2017) did not have phosphate, which I already suspect has influenced carbonate mineralization pathways. Therefore, the apparent stability field suggested by this study may be partly due to the role of phosphate.

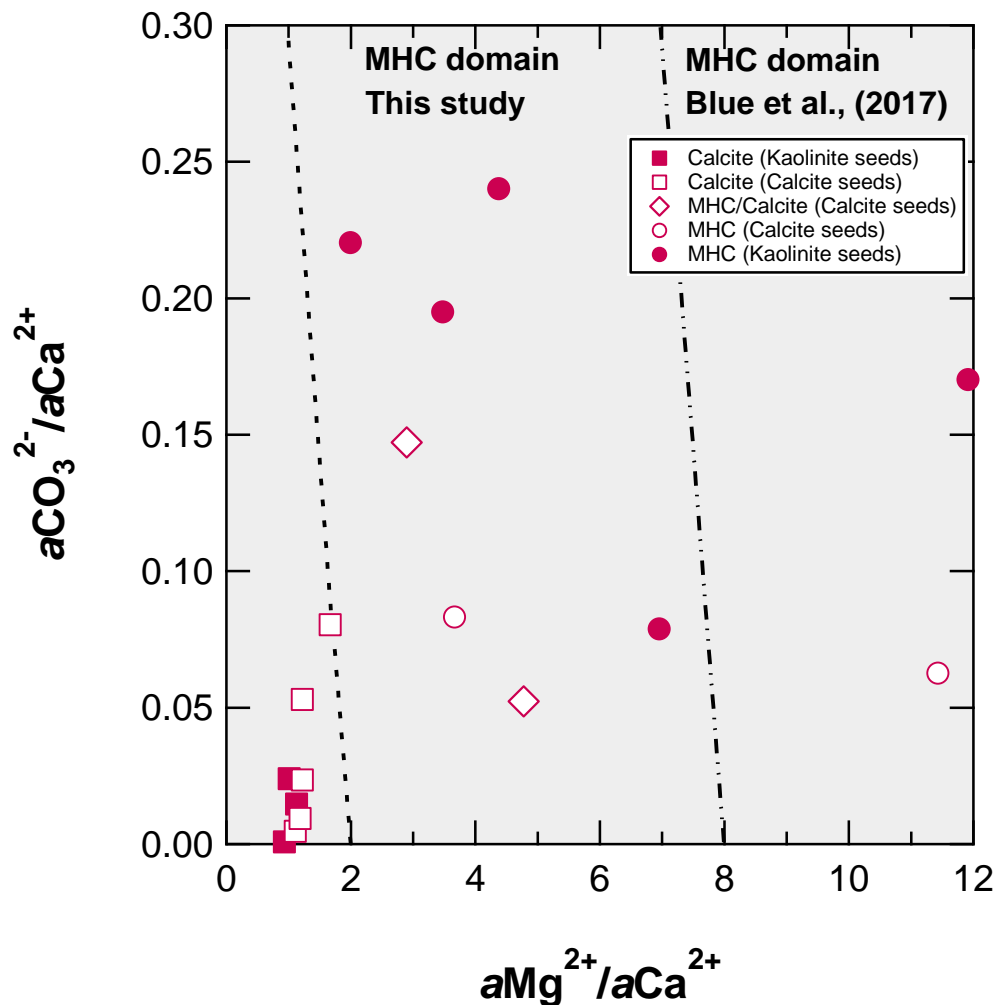


Figure 3.16: The stability field for MHC and calcite. The data points are taken from the point in the experiment where precipitation occurs, although the initial solution chemistry and subsequent solution chemistry evolve. Square symbols indicate calcite is the final polymorph, circle symbols indicate MHC and diamond symbols have mix mineralogy (both MHC and Mg-calcite). Open symbols mark samples with calcite as seeding material while close symbols are kaolinite seeded samples. Experiments from this study are plotted on an abiotic stability field

delineated by Blue et al., (2017) – the dot-dash line. The MHC domain in my experiments (dashed line) has shifted left (from aMg^{2+}/aCa^{2+} approximately 8 to 2).

These experimental results suggest that the experiments where MHC precipitates (higher Mg/Ca ratios) have a longer delay prior to initial mineral precipitation, and a lower pH drop compared to the experiments that precipitate calcite. This may be due to the incorporation of magnesium in the initial ACC, which has been suggested to stabilize ACC and increase the time required for transformation (Lin et al., 2015; Purgstaller et al., 2017). In addition, magnesium incorporation likely decreases the effective solubility of both the ACC and MHC polymorphs, although this is not quantitatively understood at present (Fukushi et al., 2017; Purgstaller et al., 2017).

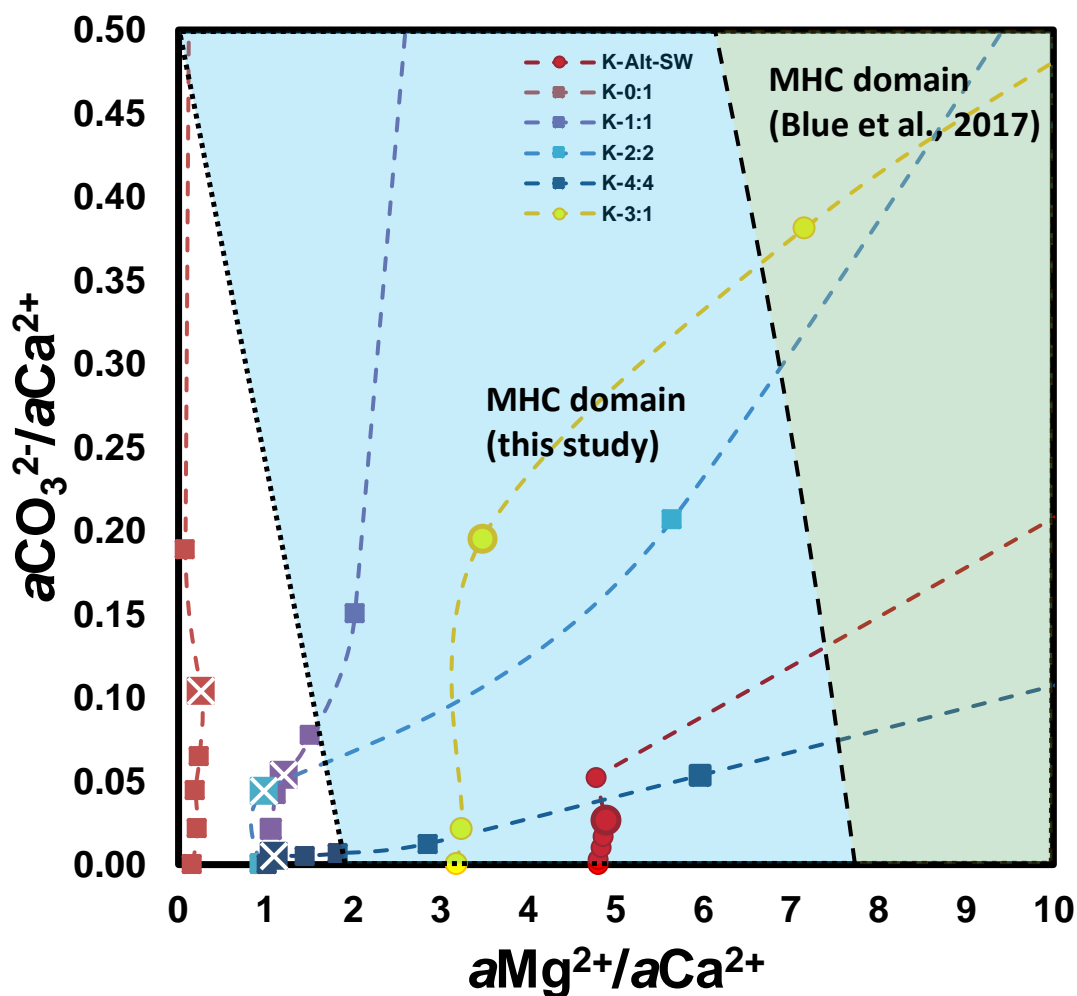


Figure 3.17: Evolution trajectories of samples with different initial Mg/Ca (selected samples are shown) when carbonate precipitated. Square symbols indicate calcite is the final polymorph while circle symbols indicate MHC as the major stable product at the end of the incubation experiment. Enlarged symbols with a cross or round shape marked the early nucleation stage. The experiments from this study were plotted on an abiotic stability field

delineated Blue et al., (2017). Note the boundary of MHC domain has shifted towards left in the microbial induced studies, suggesting the effect of phosphate in stabilizing the MHC in biotic studies.

The evolution of solution chemistry and the formation of different calcium carbonate polymorphs here are comparable to other experiments involving carbonate mineral precipitation and microbial populations conducted by Balci et al. (2016) and Han et al. (2017). Both studies investigated the role of halophilic bacteria in the precipitation of carbonate minerals. Dypingite, hydromagnesite, aragonite, MHC, huntite, and struvite were the primary carbonate minerals that precipitated from a hypersaline solution (Balci et al., 2016; Arias et al., 2017) whereas Han et al., (2017) found MHC, calcite and Mg-rich calcite in varying sodium chloride solutions (3 – 20% w/v) cultured with *Chromohalobacter israelensis*. In contrast to culture experiments reported by Rivadaneira et al., (1998; 2010), my culture samples with high (Mg/Ca = 3) did not precipitate any aragonite. This is probably due to the fact that Rivadaneira et al., (1998; 2010) incubated their samples at a higher temperature (32°C) and liquid-limited environment (a glass coverslip) – however, the presence of water molecules (or activity of water) is the key for hydrated phase MHC to form.

In addition to promoting non-traditional calcium carbonate mineralisation pathways, high phosphate concentrations might also explain the exceptional stability of MHC in my incubation and transformation experiments. In a phosphate-free solution, any MHC I formed through microbial induction should have transformed into a more stable carbonate polymorph over time, even at room temperature. However, the precipitated MHC in my experiments did not transform after sitting in the lab two years with the old media, suggesting the inhibition of MHC transformation (shown in Chapter 2). Furthermore, the mass basis sorption capacity of MHC is significantly higher than those of aragonite and calcite, which may explain the greater impact of phosphate in stabilizing MHC (Yagi and Fukushi, 2011; Fukushi et al., 2011). It is also possible that the formation of stable calcite/calcium phosphate around the outer shell of the growing crystal shields the inner MHC from transforming by protecting the interior of the spherulitic MHC from exposure to the medium. Besides the role of phosphate in MHC stabilization, previous studies have also suggested the possible role of organic acids such as carboxylic acids and EPS in stabilizing precipitated minerals, where it is thought that the EPS could adsorb or to be entrained within the mineral and significantly reduce its reactivity (Omoike and Chorover, 2006; Steiner et al., 2010; Gallagher et al., 2013).

3.4.3 Influence of seeding material on the formation of calcium carbonate polymorphs

Microbially-induced carbonate mineral precipitation and polymorphism also appears to depend on the mineral seeds that are present. Overall, MHC tends to predominantly form from experiments with kaolinite seeds compared to those with calcite seeds (Table 3.5 and Figure 3.18). In addition, MHC forms at slightly lower Mg/Ca ratios in the experiments with kaolinite seeds compared to calcite seeds. I suspect that the delayed and muted precipitation of MHC in calcite-seeded experiments results from an initial overgrowth of a higher-magnesium calcite phase on the calcite seeds. Growth of calcite on calcite seeds require less supersaturation for nucleation and growth to initiate, thereby lowering the induction time and pH for nucleation to happen. A similar observation has been reported in Lioliou et al. (2007) showing that the types of seeding materials can impact precipitation kinetics. SEM images illustrate an epitaxial growth relationship between the original calcite seeds and precipitated calcite, which ranges from submicron to nano-sized (Figure 3.19). A similar observation was also reported in Rodriguez-Navarro et al. (2012) where they found that there is an overruling factor of substrate types on the mineralogy of calcium carbonate precipitated. In these experiments, where calcite overgrowth forms, MHC is never observed, and conversely, where there is no calcite overgrowth, MHC precipitates. There are two exceptions to this: the C-3:1 and C-Alt-SW experiments generate products of mixed mineralogy which could result from multiple precipitation events over the course of the experiment as the Mg/Ca ratio is evolving. No apparent drops in pH or alkalinity were observed in the samples with overgrowth on calcite seeds, suggesting the buffering effects from the calcite seeds impedes high pH values (particularly $\text{CO}_3^{2-}/\text{Ca}^{2+}$) in the system, and therefore, MHC is not favoured. Such a difference in precipitation kinetics in experiments with different seeding materials is illustrated in the change of calcium concentration. Nearly all experiments with calcite seeds (except the experiments where I get mixed mineralogy in the final solid products) showed a gradual decrease of calcium concentration while the calcium concentrations drop rapidly in experiments where kaolinite is used. Particularly in the calcite-seeded experiment, I note a trivial drop in calcium concentration prior to the main precipitation event, suggesting slight removal of calcium during the nucleation process (or epitaxial growth on calcite seeds) before main mineral precipitation follows. Homogeneous precipitation is more likely to occur in the kaolinite-seeded experiments where there is less buffering capacity in the supersaturated solution. Such a sample is often characterized by a sharp drop in pH and calcium concentration (e.g. K-9:1).

Intriguingly, these results suggest that MHC is only present at Mg/Ca ratio of 3 in the calcite-seeded experiments; while MHC is dominant at Mg/Ca ratio of 2 in the kaolinite-seeded

experiments (Figure 3.18). Calcite seeds show an increase in the amount of MHC precipitated as the Mg/Ca ratio increases, whereas the amount of MHC precipitated peaks at Mg/Ca = 4 and drop at Mg/Ca > 4 in experiments with kaolinite seeds. I also note that there is less consistency in the carbonate mineral polymorphs precipitated between replicates of calcite-seeded experiments. Such ambiguity is not observed in the kaolinite seeded experiment, where the boundary of calcite/MHC domain is more clearly defined at a Mg/Ca ratio of 2.

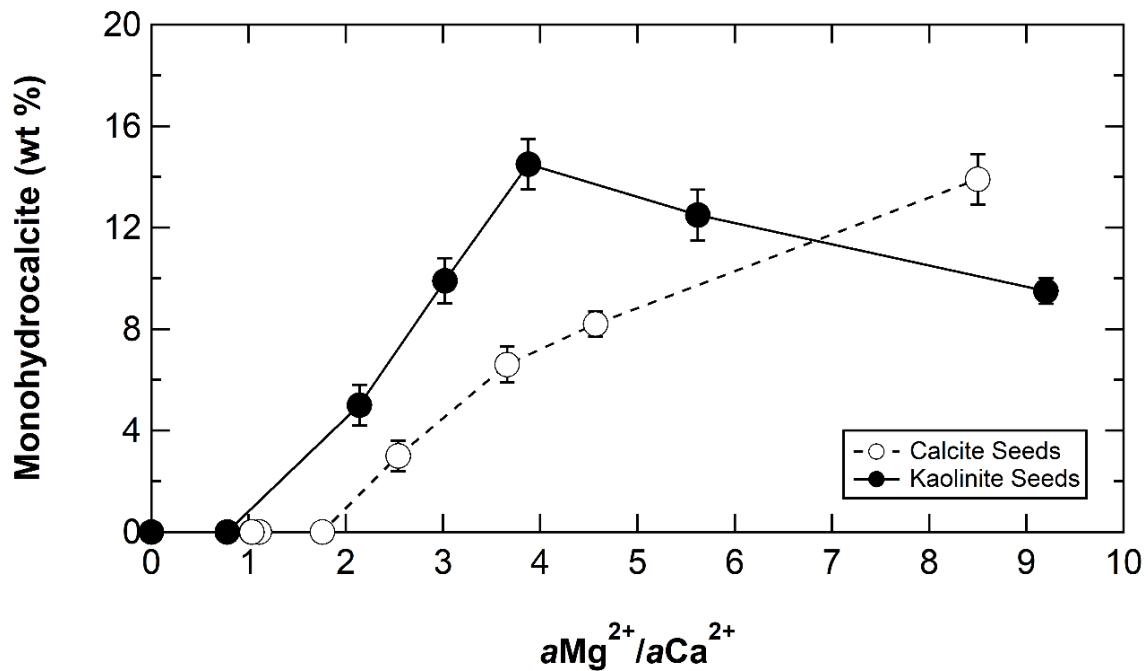


Figure 3.18: The precipitation of MHC in wt % (of total solid sample) as a function of Mg/Ca (before precipitation) in experiment with different seeding materials. Error bars represent the estimated standard deviation calculated from Rietveld refinement.

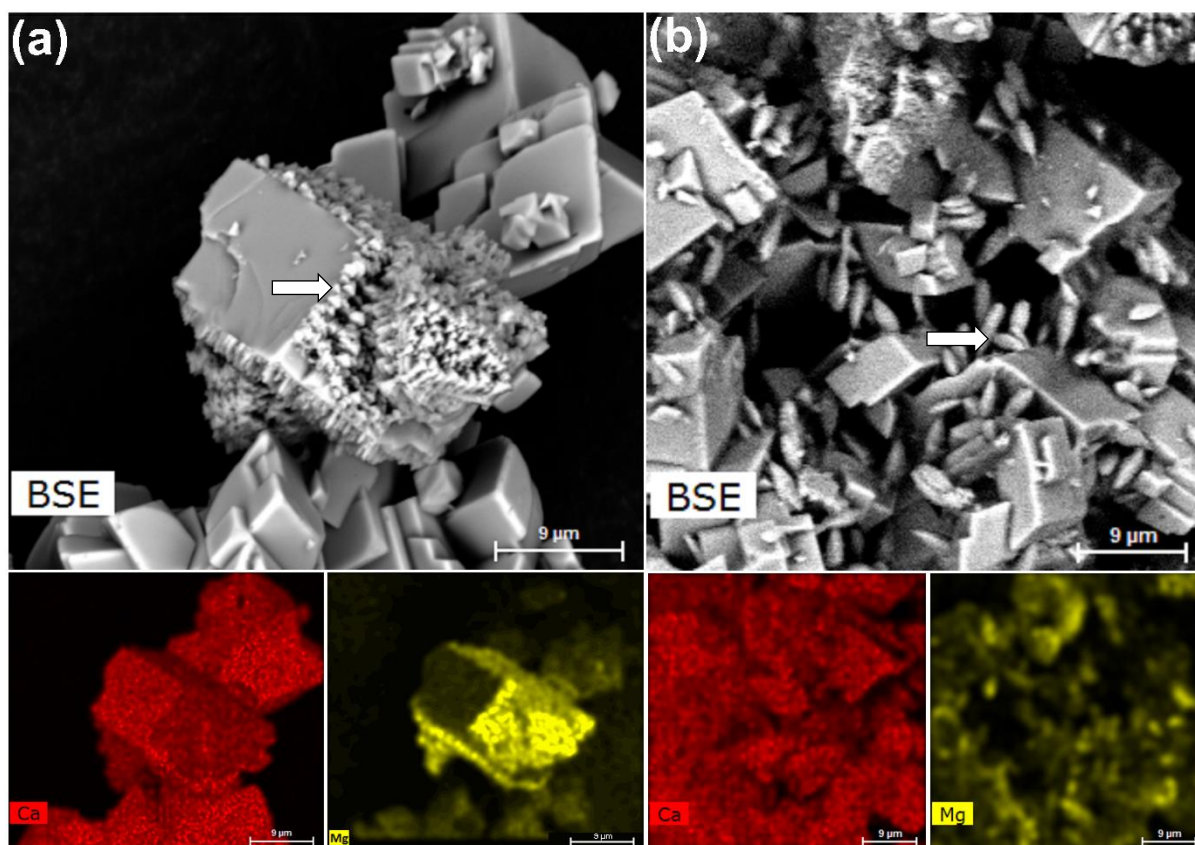


Figure 3.19: Submicron to nano-sized magnesium calcite crystals grow on calcite seeds (a) C-3:1 and; (b) C-2:1. Arrows show two forms of magnesium calcite growing epitaxially on calcite seeds.

3.4.4 Synthesis, stability and transformation of MHC

The earliest studies of MHC formation suggest that three conditions had to be met for MHC to form: (1) the Mg/Ca ratio must be high; (2) the water temperature should be $< 40\text{ }^{\circ}\text{C}$; (3) The water should be oversaturated with respect to calcite, aragonite, and MHC, while preventing oversaturation with respect to hydroxy- and fluorapatite (Stoffers and Fischbeck, 1974; Oomori et al., 1988). My results are consistent with these geochemical conditions. Regardless of the seeding material used, I found that SI_{MHC} has to be greater than one for MHC to form (Figure 3.20). Mixed mineralogy of MHC and calcite (often higher in MHC) is particularly observed at a lower Mg/Ca ratio (between 2 to 4), whereas I found that only MHC precipitates as the Mg/Ca increases. My results also agree with findings reported by Rodriguez-Blanco et al. (2014) in a series of abiotic experiments where MHC is absent at Mg/Ca lower than two although the solution is highly supersaturated with respect to MHC ($SI_{\text{MHC}} = 2$). However, in their experiments, MHC precipitated when the solution SI_{MHC} approached 2.5 or higher, suggesting that the supersaturated solution alters the precipitation kinetics to favor the formation of MHC.

Such a highly saturated condition, however, rarely occurs in biotic studies or in the natural environment.

Contrary to previous work that suggests that it is magnesium that stabilizes MHC, I suggest that phosphate plays a larger role based on abiotic experiments and electron backscatter mapping of my samples (Figure 3.21a and b) (Dejehet et al., 1999). These images indicate that the outer shell of MHC before (Figure 3.21a and b) and after (Figure 3.21c and d) the mineralogical transformation is relatively low in magnesium but enriched with phosphorus (Figure 3.21a, b, c, and d). One possible explanation for the stabilization of MHC during the transformation experiment (both T-Alt-SW-YE and T-Alt-SW-PO₄) could be the common ion effect, where the solubility of MHC with phosphate absorbed on it decreases. Higher magnesium concentrations were found in the inner shell, suggesting the inner shell is initially composed of more Mg-rich carbonate phases (Figure 3.21b and c). I suspect that the inner shell could be unstable, nano-crystalline, less dense and associated with the bacterial colony that formed early in the nucleation stage. The EDS images thus imply the important role of magnesium in MHC nucleation, while phosphate is linked to MHC stabilization. During the transformation process, this unstable phase is susceptible to dehydration and deformation via nano-voids or cracks in the MHC, leaving a hollow chamber behind. Comparable features have been previously observed in studies involving other calcium carbonate polymorphs (Suzuki et al., 2006; Chen et al., 2009). Through the transformation experiment, I observe that the phosphate-rich outer layer of MHC is more stable compared to the inner core (Figure 3.21c), although the exact mechanism of how phosphate stabilizes MHC requires further investigation.

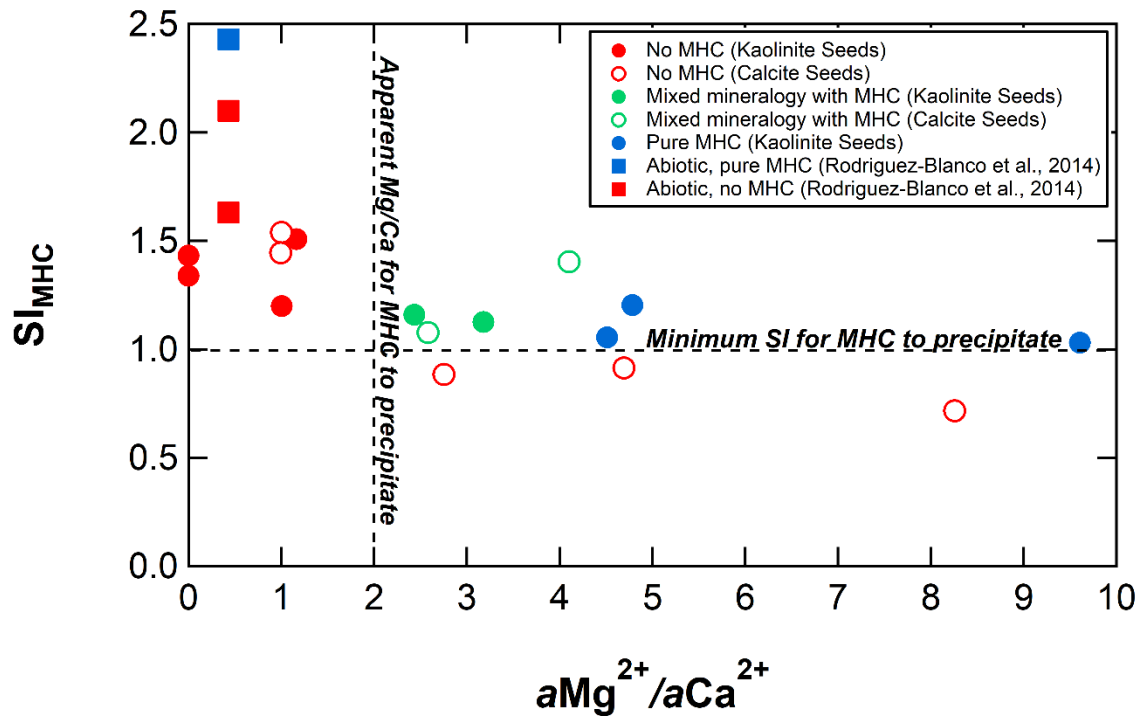


Figure 3.20: Cross plot between saturation index and aMg^{2+}/aCa^{2+} indicates that SI_{MHC} higher than 1.0 is required for the formation of MHC at aMg^{2+}/aCa^{2+} greater than 2. The data points are measurements taken before the precipitation of calcium carbonate. Abiotically precipitated calcium carbonate reported in Rodriguez-Blanco et al. (2014) were compared and given in square symbols.

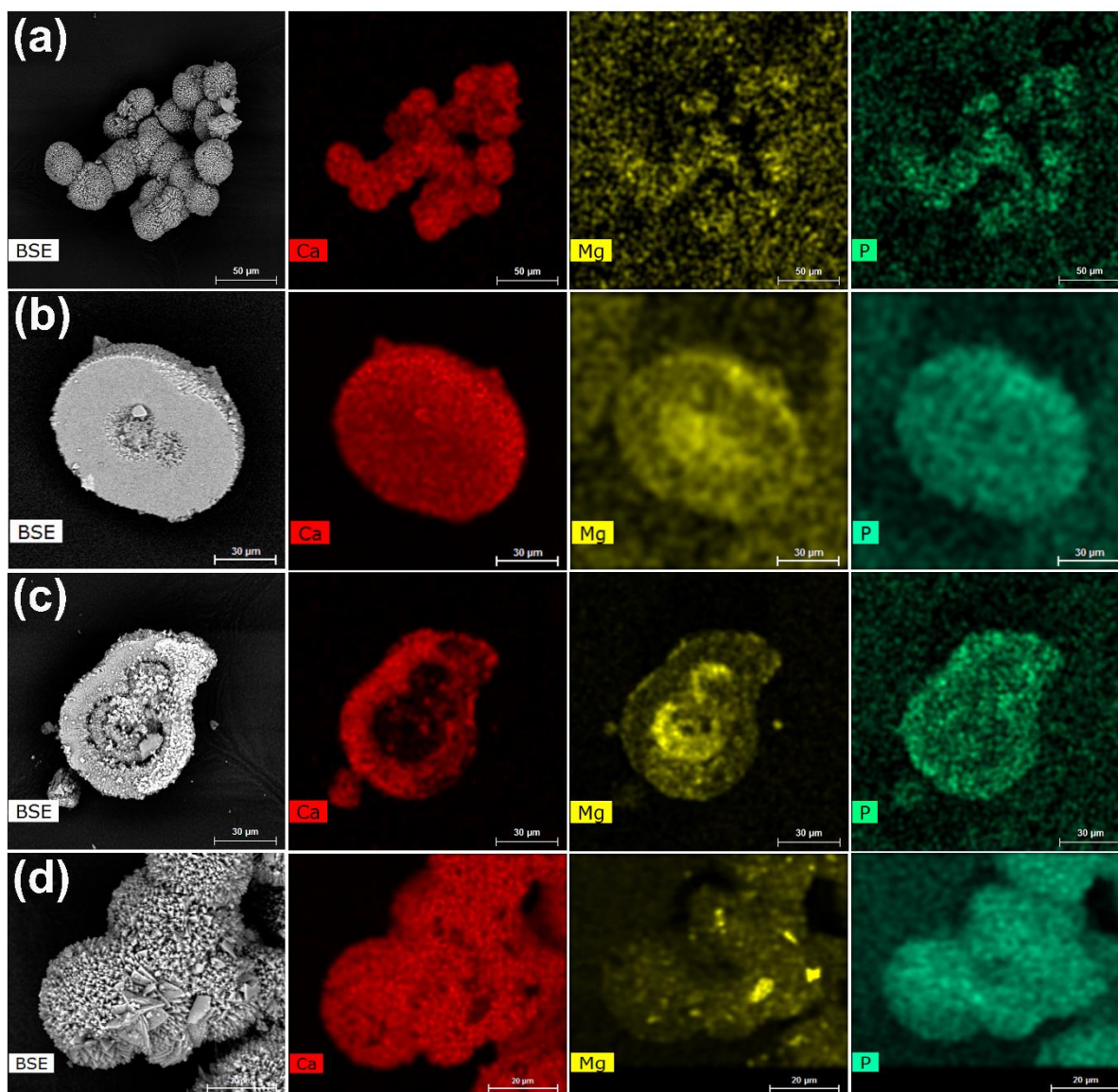


Figure 3.21: SEM elemental mapping (Ca, Mg and P) of MHC. (a) chemical composition of MHC prior to transformation experiment; (b) hemispherulite MHC with higher Mg distribution at the core prior to transformation; (c) cross section of spherulitic MHC (T-Atl-SW-YE); and (d) surface chemical compositions of MHC (T-Atl-SW-YE) after transformation process.

3.4.5 The role of microbial sulfate reduction in carbonate polymorphism in the natural environment

Even if MHC forms under the three conditions above in the natural environment, MHC should readily dehydrate and transform into more stable calcium carbonate polymorphs with time. Therefore, I suggest a fourth condition has to be met to find MHC in the natural environment: (4) phosphate and magnesium must be in solution, which I have shown helps stabilize MHC. This is largely true in anoxic marine sediments which have high magnesium from seawater

and high phosphate from the combined effects of organic carbon oxidation and the liberation of adsorbed phosphate from iron-oxide reduction (Hyacinthe and Van Cappellen, 2004). To understand the presence of MHC in natural sediments, I must also constrain the transformation of MHC to stable calcium carbonate polymorphs at low temperatures; in this regard, the laboratory temperatures are warmer than most marine sedimentary conditions.

In the natural environment, MHC can be formed as a transitional diagenetic phase in the recrystallization process of metastable ikaite to final calcite (Dahl and Buchardt, 2006). The formation of these minerals is often associated with microbial activity, organic materials and the presence of algal mats such as in the sediment of Lake Kivu (Central Africa) (Stoffers and Fischbeck, 1974). Authigenic MHC typically has been found in lacustrine environments, but it also occurs in caves, as weathering products, and fjords (Dahl and Buchardt, 2006). These MHCs are reported to vary in morphology (spherulitic or euhedral) and chemical compositions (variations in magnesium content). For example, several studies have reported the occurrence of spherulitic crystal aggregates in fluid characterized by high organic material and the presence of microorganisms such as microbes and algae (Stoffers and Fischbeck, 1974; Taylor 1975; Teller and Last, 1990; Dahl and Buchardt, 2006). I found close resemblance of some of these naturally-occurring spherulitic MHC with the MHC precipitated in my experiments. This suggests an extended period of supersaturation with respect to MHC in the solution. Nearly all the aqueous phase sample where MHC is forming shared similar geochemical conditions with what I proposed in this study – low temperature, high pH, high alkalinity, high molar Mg/Ca ratios (> 3), and elevated PO_4^{3-} concentration ($> 10 \mu\text{M}$).

My results suggest strongly that microbial sulfate reduction drives calcium carbonate precipitation and will influence the carbonate polymorph of the precipitated sedimentary carbonate. If I apply my laboratory experiments to the natural environment, I anticipate sulfate will have a lesser inhibitory effect on sedimentary carbonate formation relative to dissolved phosphate and magnesium. This is partially due to the nucleation effect of the sulfate-reducing bacteria, which may counter the inhibition effect of dissolved aqueous sulfate. Nevertheless, I sum the influence of the various variables influencing calcium carbonate polymorphism via microbial sulfate reduction under a closed system as follow: $\text{Mg/Ca} \gg \text{PO}_4^{3-} \gg \text{SO}_4^{2-}$. Although I have demonstrated that microbial sulfate reduction can be directly linked to the formation of MHC and other different calcium carbonate polymorphs, whether microbial sulfate reduction in the environment directly involves in the precipitation of MHC is still unclear. It should be noted that the pore-fluid where these microbes thrive in marine sediment is often characterized by the prerequisite geochemical conditions for MHC to form, such as high alkalinity and the presence of nutrients such as phosphate. The formation of single mineralogy

cements can be rare in natural sedimentary systems. Even using pure cultures under controlled conditions, I found mixed mineralogy in some samples (as in sample C-3:1 and C-Alt-SW) that may be due to the unknown growth behavior of the microbes – where the sulfate-reducing bacteria re-grew after the first precipitation event (please refer to growth curve and pH data in Chapter 4). The re-growth further increases the alkalinity and led to a second supersaturation but at a much higher Mg/Ca ratio, causing a precipitation of a different calcium carbonate polymorph than the initial precipitation. In closed or semi-closed marine sediment, it is very likely that the growth cycle of microbes might change over time as a function of food source availability, leading to multiple precipitation events and mixed mineralogy of the precipitated minerals.

3.4 Conclusions and Implications

In conclusion, microbial sulfate reduction is capable of driving precipitation of calcium carbonate polymorphs via metabolic activity that changes the solution chemistry. Bacterial cells can act as effective nucleation surfaces for calcium carbonate polymorphs to grow. The cellular materials are often a better substrate compared to calcite and kaolinite seeds, which likely results from the combined effects of surface energetics and local perturbations to solution chemistry proximal to actively metabolising cells. This also implies that heterogenous precipitation is a dominant precipitation pathway in sediments that host sulfate-reducing bacteria. Under a closed and active system, calcium carbonate polymorph selection depends on the solution chemistry at the time of nucleation, even though the solution chemistry might then evolve. Several variables influence calcium carbonate polymorphism via microbial sulfate reduction under a closed system: $Mg/Ca \gg PO_4^{3-} \gg SO_4^{2-}$ and the type of seeding materials. The growth of magnesium calcite is promoted in experiments with calcite seeds which, in turn, influences the apparent stability domain between calcite and MHC in the presence of calcite and kaolinite seeds. My biotically-mediated spherulitic MHC comprises a unique hollow cavity with calcified microbial textures. This texture is absent in abiotic experiments, and thus could be useful to interpret biotic sedimentary signatures of precipitated minerals in the environment. Nevertheless, my transformation experiment suggests that such a microbial texture/signature is vulnerable to early diagenetic processes in the environment. Results from biotic, abiotic and transformation experiments showed that phosphate stabilizes MHC, while retarding the formation of aragonite and calcite at $Mg/Ca > 2$. I also found that phosphate concentrations have a lesser effect on which polymorph initially precipitates. In the presence of high phosphate concentrations, MHC formed instead of aragonite because phosphate ions inhibit the nucleation of aragonite. Therefore, I suggest that caution should be taken when interpreting the types of calcium carbonate polymorphs formed in biotic studies that use yeast

extract or any additives that have phosphorus content. Similar claim applies to environmental samples where metastable MHC is particularly prone to diagenetic processes. Thus, care should be taken while interpreting environmental samples as any transformation processes of MHC can have a detrimental effect on paleo proxy such as isotopic signature or Mg/Ca in the sedimentary carbonates. In the next chapter, I will explore these results further.

Chapter 4

The effect of seeding materials on the precipitation of calcium carbonate polymorphs

4.1 Introduction

In the previous chapter, I demonstrated the role of sulfate-reducing bacteria in the precipitation of calcium carbonate and showed that type of polymorphs that form is determined by the solution chemistry at the time of precipitation. I found that Mg/Ca is the variable that strongly influences the polymorph of calcium carbonate. A minor shift in the domain of Mg/Ca changes the stability of calcium carbonate minerals from calcite to monohydrocalcite. Phosphate must be present in the solution at higher concentrations ($> 100 \mu\text{M}$), and it has been shown that surface adsorption of phosphate stabilizes monohydrocalcite. Through a series of incubation experiments, I also found that the types of seeding materials also may impact calcium carbonate polymorphism, but this is not straightforward and will be studied in detail in Chapter 5.

Despite the work in Chapter 2 and 3, further work to confirm my conclusions was needed, including a more detailed analysis of the work that went into Chapter 3. In this chapter, I will show, and discuss, in detail how the evolving solution chemistry determines what types of calcium carbonate polymorph forms. I will first show the raw aqueous chemistry data, identify the mineral stability using the saturation index, and then investigate how different mineral seeds might affect calcium carbonate polymorphism. In addition, I will show the changes in phosphate concentration in the medium and its role in the bacterial growth and mineral stabilization. Finally, with the help of SEM-EDS, I will discuss at which stage the phosphate is incorporated into the calcium carbonate minerals.

4.2 Materials and method

4.2.1 Analytical methods

Incubation experiments with varying Mg/Ca and seeding materials were conducted using the method described in Chapter 2 and Chapter 3. Similar analytical methods were also used to measure the chemical variables. Control samples were autoclaved at 121°C for 15 minutes immediately after inoculation. Saturation indices of different calcium carbonate polymorphs were calculated using PHREEQC with SIT database. The precipitates were collected at the

end of the experiments, rinsed and oven dried at 50 °C. Then, the solid samples were attached on a stub and carbon coated before elemental mapped with an SEM coupled with EDS.

4.3 Results and discussion

4.3.1 Experiment H (Clay as seeding material)

Experiment H was the first large experiment that I conducted, with the goal of investigating the impact of varying Mg/Ca on the calcium carbonate polymorphs precipitated in the presence of kaolinite as seeding material, the main results from this experiment were presented in Chapter 3. The reason I included seeding material as an additional variable is because I wanted to mimic the real conditions in anoxic marine sediment as closely as possible. In the natural environment, materials for nucleation of authigenic minerals are ubiquitous. In fact, homogeneous (unnucleated) precipitation of minerals is rare. My experimental setup is non-ideal in resembling the real condition but it provides an insight of what could be the most plausible process inducing carbonate precipitation in anoxic marine sediments, or in oxygen-minimum zones, or in estuaries of large river systems where natural or anthropogenic derived nutrient input is significant. Coastal upwelling processes supply nutrient-rich and oxygen depleted water part of the coast off Northwest Africa, Southern Africa, California and Oregon, Peru and Chile and Somali and Oman (Cury et al., 2000; Curtis Roegner et al., 2011; Takahashi et al., 2009; Harrison et al., 2016). Deoxygenation of part of the water column could also happen due to natural oceanography and topographic factors, for example, the Dead Sea, Baltic Sea, and some fjords. A similar condition is also found in lacustrine environments although the deoxygenation event occurs mainly due to seasonal stratification especially during summer where water mixing is poor. In all of these environments, anoxic microbial communities may stimulate the precipitation of carbonate minerals on clay or carbonate seeds.

Kaolinite was chosen as the seeding materials as broadly representative of clay in the environment. Figure 4.1 shows the results of all samples including all duplicates and controls conducted in Experiment H. The samples' name used was initially different from what reported in Chapter 3, where K-Atl-SW was sample A; K-0:1 = sample B; K-0:2 = sample C; K-1:1 = sample D; K-2:2 = sample E; K-3:3 = sample F and; K-4:4 = sample G, respectively. The naming pattern for samples in the subsequent experiments is the same, where A is always the starting code for the first sample set. The results were outlined in the previous chapter. Control samples remain unchanged over the course of the experiment except in sample K-0:1 (Mg/Ca = 0; Mg = 0 mM, Ca = 10 mM). For an unknown reason, this particular control sample

was contaminated by bacteria after 200 hours. The sample was re-autoclaved and sampling continued. As a result, a hump in alkalinity, pH, and OD was noticeable in 200 hours.

A concurrent drop in pH and calcium concentration was noted at 200 hours when the pH approached 8.0, suggesting the precipitation of calcium carbonate when saturation was reached. Mineral saturation happens (in this case calcium carbonate) when the ionic activity product (IAP) of calcium carbonate increases as a result of an increase in the activity of carbonate ions $[\text{CO}_3^{2-}]$ in the medium. When the IAP values exceeded the constant of the solubility product, calcium carbonate should precipitate. However, supersaturation of a given mineral does not often cause precipitation as kinetic factors need to be taken into account. The kinetic factors will be discussed later in this chapter. Magnesium concentration in the samples and control samples remained unchanged over the course of the experiment (although the Mg/Ca ratio changed dramatically as discussed in Chapter 3), reflecting the conservative behavior of magnesium in the system.

It is also worth mentioning that the time for the increased alkalinity to reach a plateau depends on the higher absolute magnesium and calcium concentration in the medium (Figure 4.1). This is especially evident in sample K-2:2, K-3:3, and K-4:4, where the alkalinity of K-2:2 reaches a plateau at 350 hours, K-3:3 at 250 hours and K-4:4 at 200 hours, respectively. Analogous trends can be observed in sulfate concentration, where the decrease in sulfate stops almost in tandem with the plateau (levelling off) in alkalinity in these samples. The bacteria did not consume all of the available sulfate in the system (approximately 71 – 84 % of sulfate removed) suggest that sulfate is not the growth limiting factor. Using sample K-2:2 as an example, a mass balance calculation (Eq. 4.1) of total alkalinity in the system shows that the measured alkalinity equals the predicted, or calculated, alkalinity if all the electron donor has been consumed.

Calculated alkalinity = [Formate] + $[\text{HS}^- \text{ produced}] + [\text{OH}^- \text{ produced}] - [\text{CO}_3^{2-} \text{ removed}]$ (Eq. 4.1)

If electron donor is the growth-limiting factor,
 $[\text{Calculated alkalinity}] - [\text{measured alkalinity}] \leq 0$

Using K-2:2 as an example (the sample with the most alkalinity produced and followed by a plateau in alkalinity), where:

Calculated alkalinity if all the electron donor has been oxidized = $108.44 + (28 \times 2) - 40 = 124.44$ mEq L⁻¹

Measured alkalinity at time 350 hours = 127.65 ± 3.2 mEq L⁻¹

Therefore,

[Calculated alkalinity] – [measured alkalinity] ≤ 0

The slight surplus in the measured alkalinity could be due to analytical measurement errors and the additional bacterial metabolisms of additives such as the yeast extract in the medium. This implies that the electron donor likely limits the growth of the bacteria in sample K-2:2. It is also worth mentioning that sulfide toxicity could also play a role in limiting the bacterial growth (McCartney and Oleszkiewicz, 1991).

In sample K:3-3 and K-4:4, the electron donor is not the growth limiting factor for the sulfate-reducing bacteria because the total alkalinity measured is less than 124.44 mEq L⁻¹ yet the same amount of electron donor was added. Therefore, something else must be responsible for explaining the plateau in alkalinity. One possible reason is because of the substantial death of bacteria in the medium. This could be due to the significant drop in sulfate reduction rate to almost zero at 200 hours (the same time when the alkalinity plateaus). Entombment of cells seems to be the most logical reason to explain the sudden death of the bacteria in the medium. Two calcium carbonate precipitation events (reflected by a drop in pH) were observed at 100 hours and 200 hours in sample K-3:3 and K-4:4. Although the second drop in pH at 200 hours in sample K-3:3 was less critical than the first precipitation event, the impact was lethal to the bacterial community. This can be shown by a concurrent drop in OD (0.03 – 0.05), suggesting the removal of cells from the water column due to cell entombment. A greater drop in pH was observed in sample K-4:4, where the pH experienced a stepwise drop from 7.9 to 7.2. This corresponds to a greater drop in OD. Nevertheless, it should be noted that the first precipitation event does not kill the entire bacterial community. A post-precipitation re-growth of bacteria was noted after 100 hours, where the OD experienced a sharp increase to a cell density approaching the one before the first carbonate mineral precipitation. The re-growth of bacteria causes further consumption of sulfate and production of alkalinity. The production of alkalinity subsequently contributed to further supersaturation of calcium carbonate minerals and led to second precipitation. In this closed system, where bacterial metabolism is still active, the precipitation of calcium carbonate will continue until the calcium ions are depleted to a level where the IAP is in equilibrium with solubility product of the mineral.

The alkalinity does not reach a plateau in samples K-Atl-SW, K-0:1, K-0:2 and K-1:1 at the time the samples were killed. This is possibly due to the fact that the bacteria were growing at a much slower rate in these samples because of the lower salinity and lack of micronutrients particularly magnesium (or calcium) for growth (Cao et al., 2009; Silver, 2018). A balance between both ions is vital for cell growth. Another reason could be that these samples have a lower absolute calcium concentration, hence, a higher $a\text{CO}_3^{2-}$ for the solution is required to reach calcium carbonate supersaturation. As a result, by the time the saturation state of the solution exceeded the solubility product for calcium carbonate, the bacteria community has entered the dead phase of a typical cell cycle without experiencing large-scale cell entombment. The death of the bacteria not only impacts the production of alkalinity but also increases the kinetic barrier for precipitation as there are less actively metabolizing cells to serve as an effective nucleation point for calcium carbonate to form. I use the term effective nucleation point because sulfate-reducing bacteria produce alkalinity in addition to serving as a nucleation point. This is in comparison to other mineral seeds, which merely serve as surface nucleation point for calcium carbonate to grow. In short, the rate that calcium carbonate reaches supersaturation and precipitation is a function of the overall bacterial growth (or viability) and the concentration of calcium in the medium. Both of these parameters (IAP and the availability of effective nucleation point) contribute to mineral precipitation and need to be considered when predicting a precipitation threshold.

4.3.2 *Experiment I (Calcite as seeding material)*

Experiment H was followed by Experiment I with a similar experimental setup, except I changed the seeding material from kaolinite to calcite. Experiment I was set up to investigate the influence of calcite seeds on the calcium carbonate polymorphs precipitated, thinking that calcite has distinct mineralogy and surface area compared to kaolinite. Figure 4.2 shows the result of all samples including duplicates and controls conducted in Experiment I. The results show similar trends as Experiment H, and were presented in Chapter 3. Variables in the control samples remain constant over time. The concentration of calcium in all samples except C-Atl-SW decreases over time, suggesting the precipitation of calcium carbonate from these samples. Similar to Experiment H, the samples with a higher absolute concentration of magnesium and calcium (C-2:2, C-3:3, and C-4:4) reached slightly higher alkalinity at the end of the experiment compared to the samples with lower magnesium and calcium concentration such as C-Atl-SW, C-0:1, C-0:2 and C-1:1. No plateau is observed in the alkalinity in any of the samples during the course of the experiment. However, it should be noted that the Experiment I has a shorter overall incubation period (363 hours) compared to Experiment H (killed at 546 hours).

In comparison with the results from Experiment H, the alkalinity and pH measured in Experiment I show slightly lower values. Unlike in the previous experiment, the samples' pH in Experiment I stay below 8 and remained stable after the exponential phase while the alkalinity barely exceeds 100 mEq L⁻¹. This will be discussed and explored in detail in Chapter 5. However, briefly here, I suspect that the lower pH and alkalinity could be explained by two factors: (1) a slower sulfate reduction rate/ bacterial growth rate and; (2) the seeding effect from the calcite seeds. First, the reduced sulfate reduction rate is evident in Experiment I relative to Experiment H. One possible reason for a difference in sulfate reduction rate between the two seeding materials used could be due to the mineral surface area. Second, because the kinetic barrier for mineral growth is usually lower in material that has identical mineralogy, therefore, calcite is expected to serve as a better seed for calcite mineral nucleation compared to kaolinite. When the kinetic barrier is lowered, the precipitation of calcium carbonate is favored. Hence, the presence of calcite seeds promotes epitaxial growth of calcium carbonate on calcite seeds and as a result poised the medium at a lower pH. Epitaxial growth of calcium carbonate was not observed in samples with pure kaolinite seeds. The epitaxial growth of calcium carbonate on calcite seeds is clearly shown under SEM images (Figures 4.3).

OD in the samples of Experiment I, on the other hand, is similar to the OD in Experiment H, hovering around 0.20 - 0.25 at 100 hours. Higher OD was seen in sample C-3:3 and C-4:4, hinting that more bacteria are suspended in the medium instead of growing on the calcite seeds (Figure 4.4). The other important observation is that the OD experienced a faster drop in Experiment I compared to Experiment H. The reason for the rapid drop in bacteria density in all samples is unclear. As a result of the lower bacterial survival rate, less than half of the sulfate is reduced in sample C-Atl-SW, C-0:1, C-0:2 and C-1:1. In contrast, the bacteria seem to fare better in sample C-2:2, C-3:3 and C-4:4.

The lower bacterial growth also impacts the precipitation of calcium carbonate. The rate of decrease in calcium concentration linked to calcium carbonate precipitation is relatively slower in most of the samples (C-Atl-SW, C-0:1, C-0:2 and C-1:1) in Experiment I. Magnesium concentration remains constant over the course of the experiment and hence we see an increase in Mg/Ca at the time of calcium carbonate precipitation.

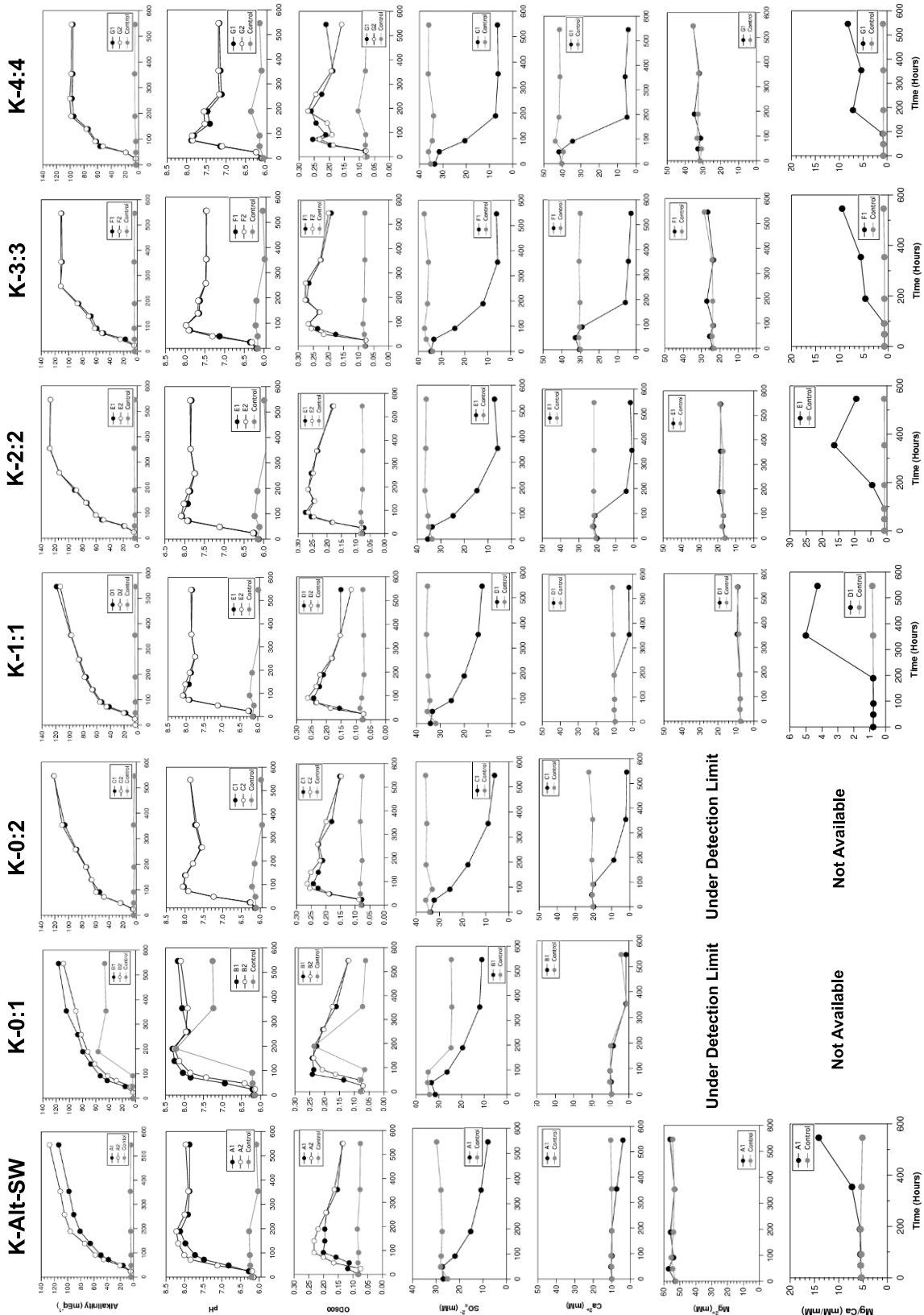


Figure 4.1: Parameters measured in Experiment H- from top to bottom Alkalinity, pH, OD, SO_4^{2-} , Ca^{2+} , Mg^{2+} , and Mg/Ca. (Kaolinite seeding). Phosphate was not measured in series H due to some errors during the analysis and is shown in Figure 4.8.

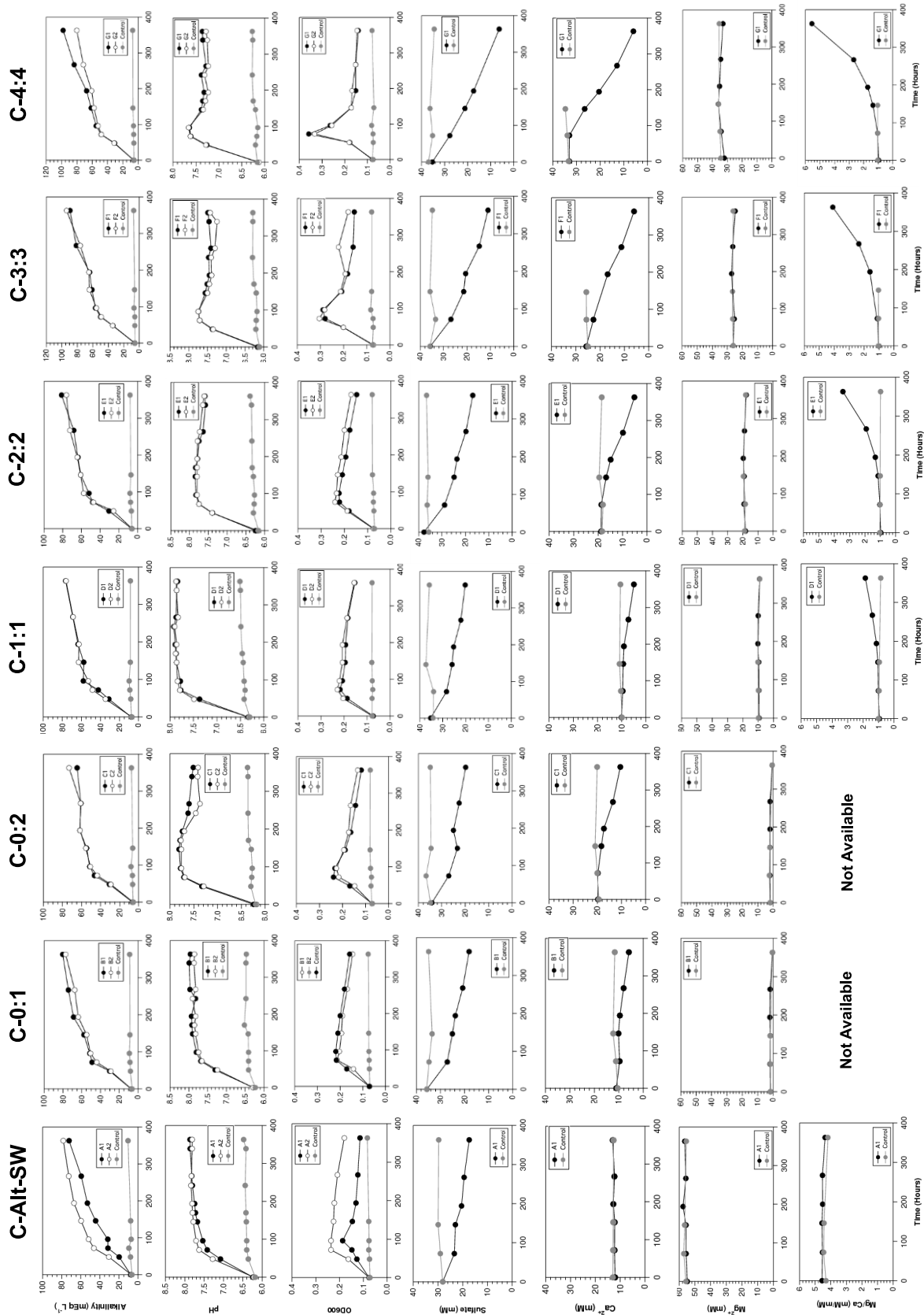


Figure 4.2: Parameters measured in Experiment I- from top to bottom Alkalinity, pH, OD, sulfides, SO₄²⁻, Ca²⁺, Mg²⁺, and Mg/Ca (Calcite seeding).

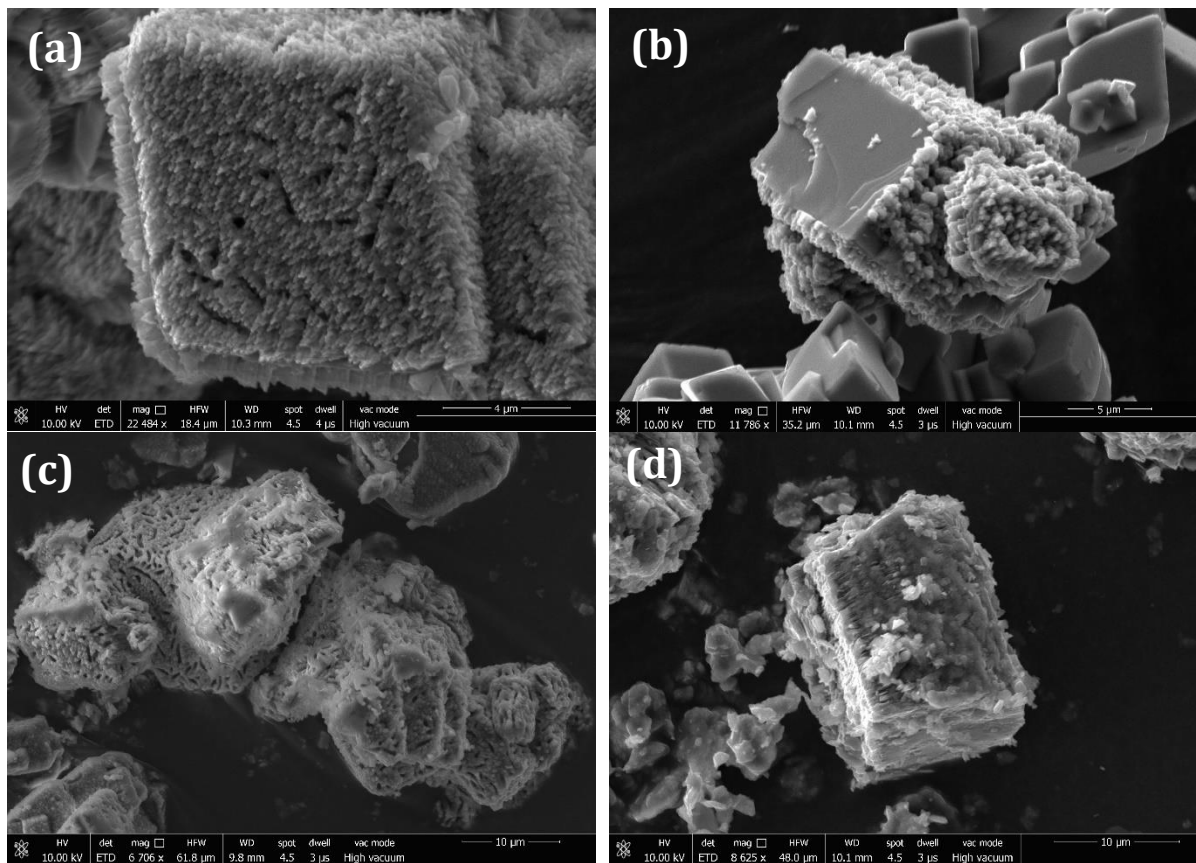


Figure 4.3: (a-b) Epitaxial growth of magnesium calcite on calcite seeds. (c-d) No surface growth was found on kaolinite. Note that Figure 4.3c is sample with mixed seeding materials where epitaxial growth of calcium carbonate can be seen on the calcite seeds but not on kaolinite (middle and scattered around the calcite).

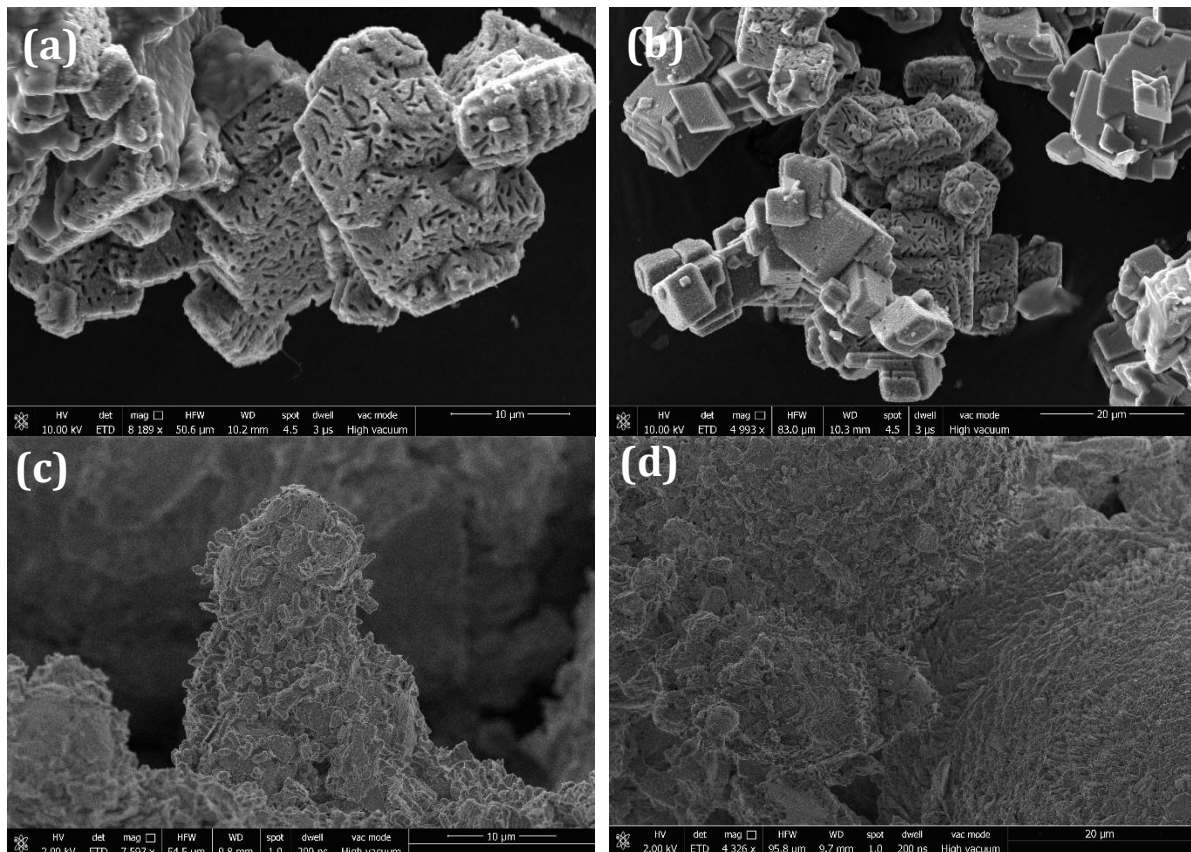


Figure 4.4: (a-b) Bacterial imprints on calcite. Note that the number of cells is low for a given surface area; (c-d) SE images show that more bacterial cells are found aggregated on kaolinite seeds, forming a colony. This implies that the sulfate-reducing bacteria grow better in kaolinite seeds compared to calcite seeds.

4.3.3 Experiment J (Calcite and kaolinite seeded experiment)

In experiment J, I set up a series of growth experiments with kaolinite and calcite seeds incubated separately under Mg/Ca of 3 and 9, respectively (Figure 4.5). Experiment J was incubated longer than the previous experiment (1248 hours or 52 days) as the bacteria growth is much slower in the high Mg/Ca ratio medium. Control samples remain constant over the course of the experiment. Bacterial contamination occurred in the control sample for C-3:1 and K-9:1 at approximately 200 hours. I immediately re-autoclaved the samples to kill the bacteria. I suspect the bacterial contamination originates from the re-used blue butyl rubber stopper, where autoclaving does not seem to effectively sterilize the rubber stopper.

Microbial sulfate reduction increases the alkalinity above 100 mEq L^{-1} and the pH ranging from 8.0 – 8.2. The sharp drop in pH at 380 hours in sample K-3:1 and C-3:1 marks the precipitation of calcium carbonate, accompanied by a drop in calcium concentration. The simultaneous run of kaolinite and calcite experiments clearly demonstrates the OD difference between both

types of seeding materials, where the OD of C-3:1 and C-9:1 is higher than K-3:1 and C-9:1, respectively. This is consistent with the previous notion that calcite seeds do not provide an ideal surface for bacterial to grow. Rather, more bacteria remain suspended in the medium, which resulted in a higher measured OD compared to kaolinite seeds under same solution chemistry. Nevertheless, the higher OD in the solution does not translate into higher sulfate reduction rate. Instead, the calcite seeded samples have a slower sulfate reduction rate compared to kaolinite seeded samples. The slower sulfate reduction rate is particularly obvious during the stationary and death phase (from 94 – 188 hours).

Slightly delayed precipitation of calcium carbonate occurs in sample K-9:1 and C-9:1 at 400 hours, possibly due to the high concentration of magnesium that is an inhibitor to calcium carbonate precipitation. All the samples in Experiment J produced monohydrocalcite. The magnesium concentration remains constant over time, suggesting that magnesium is not incorporated during the formation of monohydrocalcite. Overall, Experiment J strongly suggests that kaolinite helps promote the bacterial sulfate reduction rate; this will be explored further in Chapter 5.

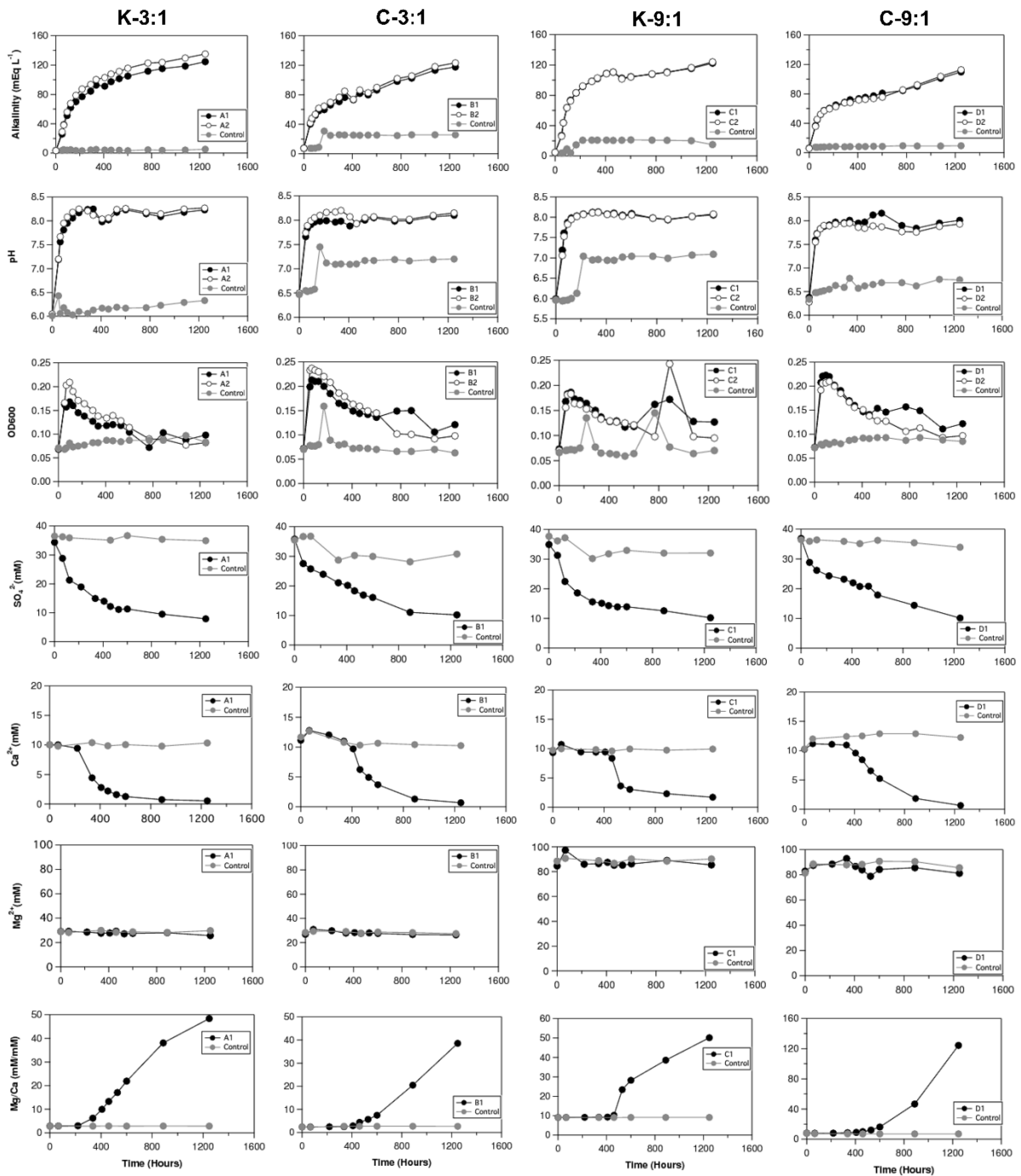


Figure 4.5: Parameters measured in series J (Kaolinite or calcite seeding) K=kaolinite seeding; C=calcite seeding.

4.3.4 Experiment L (Calcite and kaolinite seeded experiment)

In Experiment L, I examined the type of calcium carbonate polymorphs that formed in Mg/Ca of 2 and 4 under both kaolinite and calcite seeded condition. This experiment was run for 881 hours. The overall results closely resemble those in Experiment J, with two conspicuous differences. One is the presence of a plateau in the alkalinity in all samples and second is the

precipitation rate of calcium carbonate in the samples (Figure 4.6). For alkalinity, kaolinite seeded samples plateau earlier than calcite seeded samples. The 40% less time required to reach a plateau in the kaolinite-seeded samples corresponds to the rate of sulfate reduction, and possibly the buffering effect that arises from calcite seeds. A higher sulfate reduction rate in K-2:1 and K-4:1 compared to C-2:1 and C-4:1 also suggests the sulfate-reducing bacteria grow better in a kaolinite environment. The total alkalinity being higher than 124 mEq L^{-1} suggests that the electron donor is the growth limiting factor. The higher sulfate reduction rate in the kaolinite seeded samples also influences the calcium carbonate precipitation rate. Higher sulfate reduction rates increase the solution alkalinity and pH faster. This in turn led to the supersaturation of the solution with respect to calcium carbonate and subsequently precipitation takes place faster in kaolinite seeded samples. In calcite-seeded sample, slower bacterial metabolism/growth is partly responsible for the slower calcium carbonate precipitation rate, which is evident by the more gradual drop in the sulfate and calcium concentration. Similar to the previous experiments, the magnesium concentration remains constant over time.

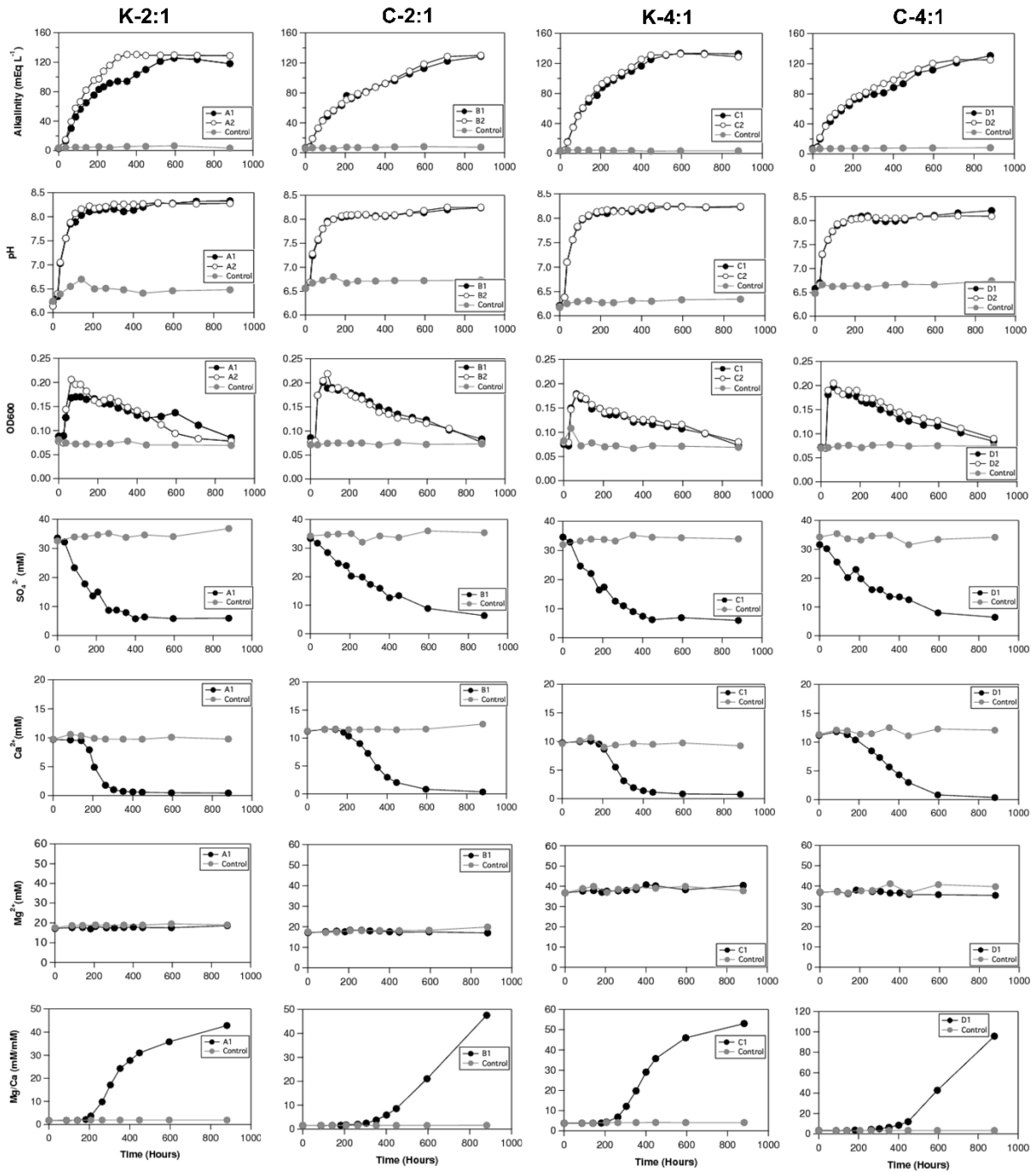


Figure 4.6: Parameters measured in series L (Kaolinite or calcite seeding) K=kaolinite seeding; C=calcite seeding.

4.3.5 Evolution of saturation index for various calcium carbonate polymorphs

In the previous chapter, I presented the saturation index for monohydrocalcite. Here I show the change in the saturation index for aragonite, calcite, and vaterite over the course of all the experiments. Samples with the whole range of Mg/Ca (0 – 9) were selected, where Figure 4.7a – c are kaolinite-seeded experiments (Experiments H, J, L) while, Figure 4.7d – f are calcite-seeded experiments (Experiments I, J, L). In the kaolinite seeded experiments, a dramatic increase in the saturation indices for all calcium carbonate polymorphs is noted over the first 100 hours as a result of the simultaneous increase in pH and DIC in the media. All samples reach supersaturation (with $SI > 0.5$) with respect to aragonite, calcite, and vaterite after 100 hours but precipitation only occurs at 200 hours except K-4:4. Calcium carbonate precipitation is marked by a drop in the SI as calcium and carbonate ions are removed from the solution. It is worth noting that samples with a higher Mg/Ca ratio take a longer time to precipitate, suggesting an inhibition effect of magnesium ions to the formation of calcium carbonates. Although the media are supersaturated with respect to aragonite, calcite, and vaterite, none of these calcium carbonate polymorphs precipitate from solution except sample with a Mg/Ca < 2 . Instead, metastable monohydrocalcite precipitates from the supersaturated media. Such an error in the prediction of thermodynamics can be explained by a kinetic factor such as the presence of inhibitors (magnesium and phosphate ions) in the media. In this case, monohydrocalcite is the kinetically-favoured polymorph when the solution has elevated Mg/Ca and phosphate concentrations.

Overall, the SI is slightly higher in the experiments with kaolinite seeds than the calcite seeds, owing to the difference in bacterial growth/activity and effective seeding from calcite as earlier mentioned. The saturation index in calcite seeded samples has a more constant SI after the media reaches supersaturation ($SI > 0.5$) with respect to aragonite, calcite, and vaterite. The SI for calcite is higher than aragonite and vaterite because the solubility product for calcite is the lowest among the three, followed by aragonite and vaterite. Vaterite is unstable under normal temperature and pressure. It is reported to be stable at solution in the absence of magnesium and high sulfate concentrations (> 20 mM) (Bots et al., 2011). The formation of vaterite is usually transient and often found as an intermediate mineral. It is readily transformed into aragonite and calcite and hence is rarely found in the geological record.

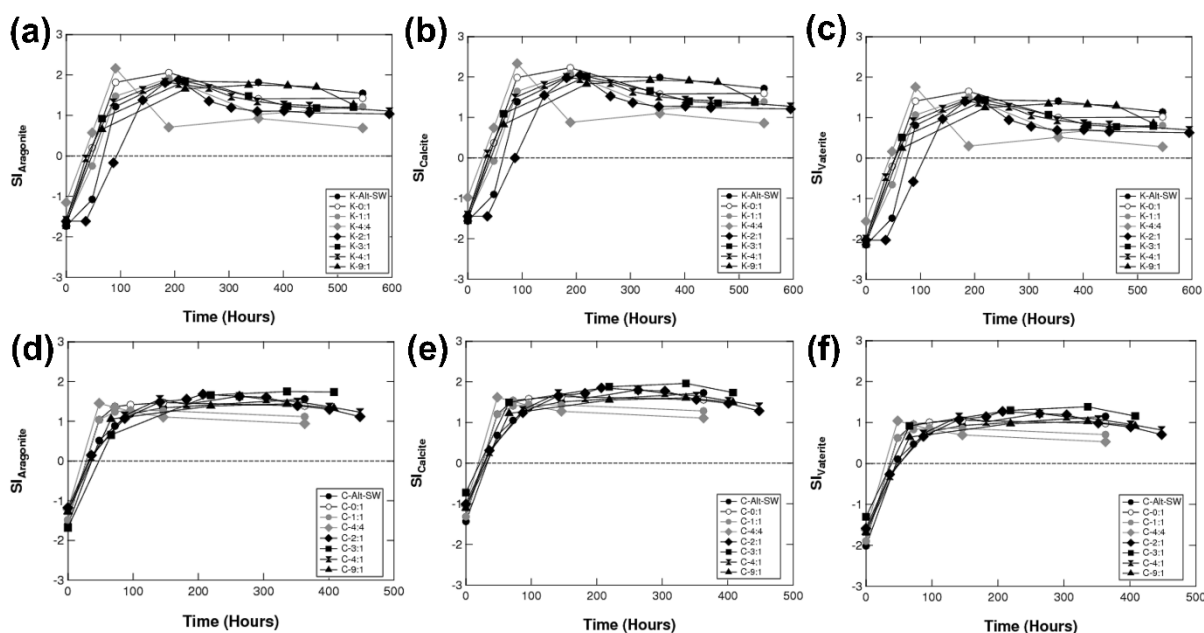


Figure 4.7a-e: The solution chemistry started mostly undersaturated with respect to different calcium carbonate polymorphs (aragonite, calcite, and vaterite). After 100 hours all calcium carbonate polymorphs were supersaturated. The upper row shows the experiments with kaolinite seeds, while the lower row with calcite seeds.

4.3.6 Variation of phosphate concentration

Figure 4.8 shows the variation of phosphate concentration in the all experiments except for Experiment H. Phosphate concentration was not measured in the initial kaolinite experiment because of errors during sample pre-treatment. In general, the phosphate concentrations drop as much as 200 μM from 800 μM to 600 μM over the course of experiment. The decrease in phosphate concentration is possibly due to bacterial consumption for biosynthesis of phospholipids. Precipitation of calcium carbonate also incorporates a small amount of phosphate on mineral surfaces (Berner and Morse, 1974; Rodriguez et al., 2008). This is evident by a more substantial 400 μM drop in phosphate concentration in samples with more calcium carbonate precipitated (C-2:2, C-3:3 and C-4:4) (Figure 4.9). A recent study published by Kawano and Miyashita (2017) also showed that phosphate demonstrated a 4 – 6 times higher adsorption affinity compared to sulfate on surface of calcium carbonate minerals. Therefore, measurement of phosphate concentration in the samples allows me to explore the role of phosphate in stabilization of monohydrocalcite and aragonite inhibition.

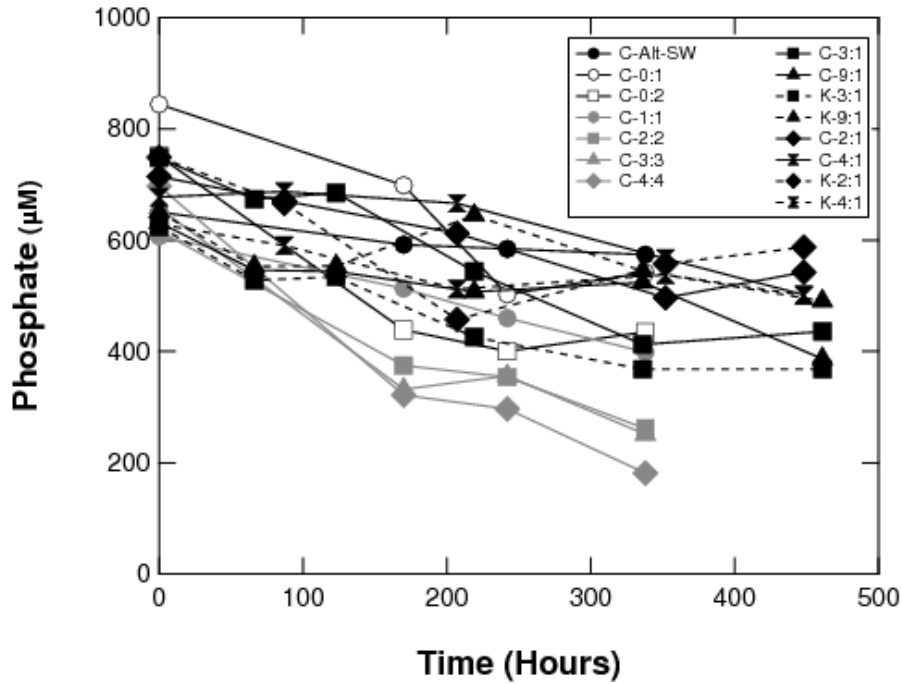


Figure 4.8: Drop of phosphate concentration over time in the kaolinite and calcite seeded experiment.

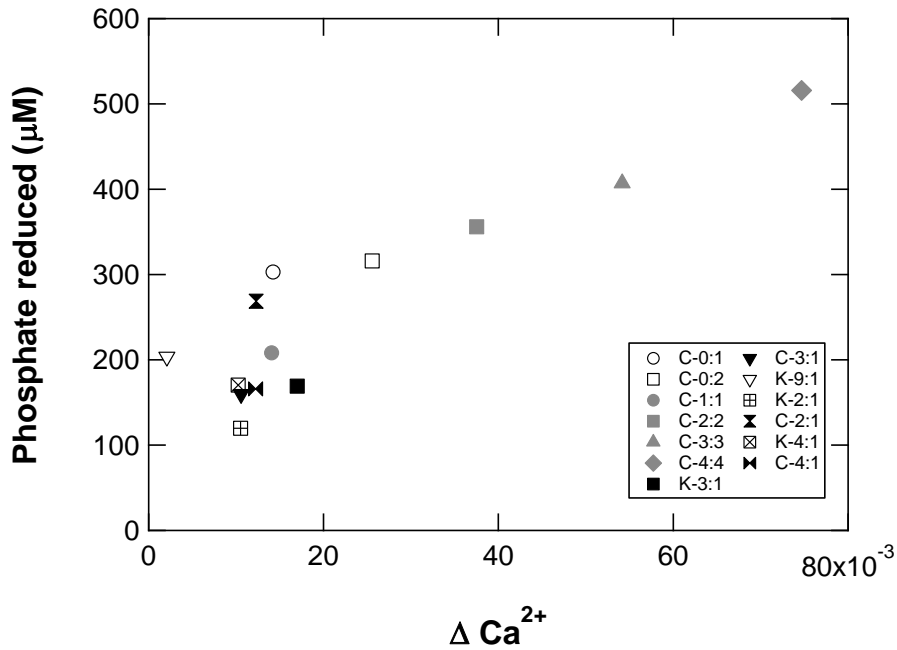


Figure 4.9: Crossplot of the phosphate reduced versus the rate of change in calcium concentration.

4.3.7 Quantitative elemental mapping of solid precipitates during early precipitation

Incorporation of the phosphate ion in the carbonate crystal structure was reported by Rodriguez et al. (2008). In their experiments, they showed that a substantial amount (82-100%) of phosphate can be coprecipitated with calcite linked to microbial sulfate reduction. The simultaneous drop of phosphate and aqueous calcium concentrations in my experiments suggest that phosphate might coprecipitate with CaCO_3 , which is shown in the SEM elemental mapping images in Figure 4.10. The phosphorus enriched phase in calcium carbonate has also been reported by Rivadeneyra et al. (2010) particularly as amorphous Ca-phosphate precursors despite an anhydrous phase CaCO_3 . This amorphous Ca-phosphate is found coated on bacterial surfaces at the early stage of their incubation experiment before the growth of aragonite when pH of the solution increased. Whether both the spherulitic nature and enriched phosphate content of the precipitated calcium carbonates that formed throughout the geological record could be linked to microbial sulfate reduction remain uncertain.

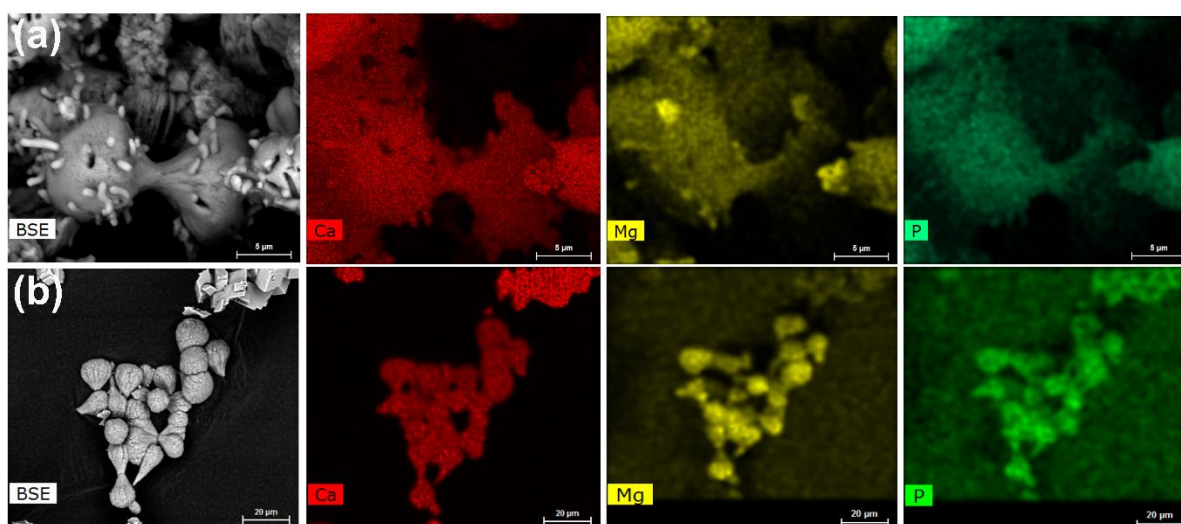


Figure 4.10: Quantitative elemental mapping of samples showing the phosphorus enriched CaCO_3 phase during the early stage of precipitation. More EDX-spectra of the samples are shown in Appendix A.

4.4 Conclusions

In conclusion, in-depth interpretation of the main experiments in Chapter 3 has allowed me to identify the effect of seeding material on the microbial growth. However, such claims were considered anecdotal, and thus, warranted further investigation (Chapter 4). Another interesting finding from this chapter is that kaolinite is a better substrate for sulfate-reducing bacteria to grow compared to calcite. I also found that the plateau in alkalinity is due to the

depletion of electron donors in the system. Although the saturation index is generally a useful tool to predict calcium carbonate precipitation, kinetic factors should also be considered. In particular, kinetic inhibitors such as magnesium and phosphate often play a key role in calcium carbonate polymorphism. Therefore, understanding the concentration of these inhibitors in a calcium carbonate precipitating system is crucial.

Chapter 5

The influence of sediment mineralogy on the microbial sulfate-reduction in marine sediments

5.1 Introduction

Microbial sulfate reduction is ubiquitous in anoxic marine sediments and is one of the major processes that influence the global carbon cycle. This is due to microbial sulfate reduction being responsible for the majority of the sedimentary anaerobic oxidation of organic carbon (Jorgensen, 1982). It has been suggested that relatively small changes in global microbial sulfate reduction may impact total oceanic alkalinity, and consequently, the partitioning of CO₂ between the atmosphere and ocean (D'Hondt et al., 2002). Bowles et al. (2014) estimated that 11.3 Tmol (10¹² mol) of sulfate is reduced microbially each year, although this is likely an underestimate (Egger et al., 2018). Decades of research into microbial metabolism has generated a basic understanding of the drivers of the rate of microbial sulfate reduction in marine sediments, including the availability of nutrients, sediment pH, temperature, sedimentation rate and presence of suitable electron donors and acceptors (Canfield, 1991; Frank et al., 2015; Westrich and Berner, 1984; Westrich and Berner, 1988; Elsgaard et al., 1994; Pallud and Van Capellen, 2006; Sagemann et al., 2009). However, the influence of the type of marine sediment on the metabolic activity of sulfate-reducing bacteria remains unknown.

Marine sediments contain a wide range of detrital and authigenic minerals, but are often broadly divided into two types: carbonate-rich and clay-rich, often reported as the percent of carbonate in the sediment, with the assumption that the remaining sediment is mostly comprised of a range of clay minerals. The distinct physical and chemical characteristics between clay and carbonate minerals creates different sediment characteristics and impacts the sediment porosity, permeability, and therefore the redox geochemistry and the microbial communities present (Ulrich et al. 1998; Fredrickson et al., 1997; Whitman et al., 1998; Heberling et al., 2010; Magnabosco et al., 2018;). Clay minerals, in particular, have been shown to stimulate bacterial growth through a larger surface area-to-volume ratio and a net negative charge which helps neutralize cations from the surrounding solution, promoting surface adhesion and clumping of bacteria (Mueller, 2015; Grim, 1953). Bacterial growth can, in turn, alter the physicochemical characteristics of the sediment through mineral dissolution,

precipitation, refinement and transformation, and reduction/uptake of trace elements. Specifically, bacteria can influence the surface charge of minerals, the cation exchange capacity (CEC), Brunauer-Emmett-Teller (BET) surface, swelling and the rheological properties of clay minerals via the secretion of exopolymeric substances (Mueller, 2015). Although these properties have been linked broadly to general microbial activity, studies specifically involving sulfate-reducing bacteria are more limited; this is striking given the global importance of microbial sulfate reduction in modern marine sediments. My study examines the role of sediment mineralogy (specifically kaolinite versus calcite) in changing the activity of sulfate-reducing bacteria in pure culture. In addition, I have compiled and analyzed sedimentary porewater data from the global ODP/IODP database (shortened to ODP database for the rest of this thesis) to extrapolate my findings to the natural environment. I finish by discussing the effect of mineral substrate on the calcium carbonate polymorph that precipitates.

5.2 Materials and Method

5.2.1 Incubation experiments

The setup of the medium used in this incubation experiment is similar to previous experiments which are based on the recommendation from DSMZ (Lin et al., 2018). I use the sulfate-reducing bacteria *Desulfovibrio bizertensis* grown in 100 mL reaction vessels, tightly sealed with a blue butyl rubber stopper under strictly anoxic conditions. OSIL Atlantic seawater was used to make up the medium and all experiments were performed at $25 \pm 1^\circ\text{C}$ in a water bath incubator.

Two sets of incubation experiments were conducted. The first one aimed to investigate the role of different proportions of seeding materials on bacterial growth. A total of 0.3 g of seeding materials were used and various proportion of the seeds (kaolinite and calcite) were tested: where the proportion of carbonate was 100% (n=2), 99%, 90%, 80%, 75%, 50%, 25%, 10%, 0% and a seedless control experiment. The experiment was run in triplicate and samples taken periodically for pH, alkalinity, concentrations of sulfate, calcium and sulfide, optical density (OD), and phosphate. All control samples were immediately re-autoclaved after inoculation to kill the bacteria, then placed into the water bath and sampled alongside the growing incubations.

The second experiment was conducted to distinguish whether it is the surface area or nutrients that play a key role in influencing bacterial growth. Calcite, original kaolinite, and cleaned

kaolinite were used as seeding materials in this second experiment. Four sets of media were prepared and 0.3 g of kaolinite (from two different sources), 'cleaned kaolinite' and reagent grade calcite seeds (Sigma-Aldrich, ACS reagent, $\geq 99.0\%$, powder – Lot #MKBP1684V, CAS: 471-34-1) were added. Two different types of kaolinite were used, one is the original kaolinite standard for X-ray diffraction used in the initial experiment (mined at Oneal Pit, Macon, Georgia, USA) and the other kaolinite (reagent-grade – Lot #BCBP9408V, CAS: 1332-59-7) was purchased from Sigma-Aldrich. Both the original kaolinite standard and the Sigma-Aldrich reagent-grade kaolinite were also cleaned to determine the potential contamination of nutrients that may be derived from the kaolinite. The cleaning procedure of the kaolinite was designed to remove any organic matter or trace metals, without altering the surface area of the sample. The kaolinite was soaked in 0.5 M NaCl in a falcon tube and sonicated for 20 minutes to disaggregate the clay. Next, the solution was removed and replaced with 5 M H₂O₂ and left overnight on an orbital shaker at 150 rpm. The samples were left to settle and the H₂O₂ solution was decanted, and replaced by 0.5 M NaCl for cation exchange to take place within the clays. The samples were subsequently placed under shaking condition for 18 hours. Finally, the samples were repeatedly rinsed with MQ-water and centrifuged three times prior to being dried in the oven at 50°C.

5.2.2 *Abiotic experiments*

To study the abiotic effect of different seeding materials on changes in solution alkalinity, experiments involving the addition of bicarbonate (HCO₃⁻) were carried in room temperature conditions. The initial solution chemistry of the medium for these experiments was identical to the biotic experiments. Two different volumes of seeding materials were used, 0.3 g and 3.0 g to make sure that the amount of seeding materials did not affect the precipitation kinetics of the solution. The kaolinite to calcite ratio was tested at 100%, 50%, and 0% in separate experiment (therefore six total experiments were run). One mole of sodium bicarbonate (NaHCO₃) was added to artificially raise the alkalinity and pH of the medium (80 mL) to an alkalinity equivalent to the biotic experiment (approximately 140 mEq L⁻¹). The rate of NaHCO₃ addition was 1.25 mL h⁻¹, and the pH and alkalinity were immediately measured after each addition.

5.2.3 *Aqueous sample analysis*

Aqueous samples for all experiments were collected using a sterilized needle and syringe and without shaking the vials to prevent the re-suspension of seeding materials that may affect the OD reading. Samples were filtered using a 0.2 µm filter and analyzed for alkalinity, sulfide

concentration, major cations (calcium, magnesium, sodium, and potassium) and anions (sulfate and chloride). pH was measured at 25°C on the NBS scale using an Orion 3 Star meter with ROSS micro-electrode (ORION 8220 BNWP PerpHect ROSS – platinum wire as a reference in iodine/potassium iodide solution, ROSS internal filling solution is 3M KCl). Alkalinity was titrated potentiometrically with 0.1 M of HCl using a Metrohm 848 Titrino plus with an error of 2.5%. The HCl used for titrations was standardized with certified reference material (CRM) 2.2298 mEq L⁻¹. The CRM batch #157 used was provided by A.G. Dickson of Scripps Institution of Oceanography (Dickson et al., 2003).

An unfiltered sample was centrifuged at 900 rpm to separate any suspended solid in the solution before measurement for OD at 600 nm wavelength in an AquaMate Plus UV-VIS spectrophotometer. Aqueous sulfide was fixed with 0.05 M zinc acetate and spectrophotometrically measured using methylene blue method at a wavelength of 670 nm. Phosphate concentrations were measured on the spectrophotometer using the molybdivanadophosphoric acid method (at 380 nm) described in Kitson and Mellon (1944). Major cations and anions were diluted 20 times before measured using ion chromatography on a Dionex ICS-5000⁺ SP. The cation measurements were run with column IonPac CS16 and methanesulfonic acid (MSA 30mM) as the eluent. The anions were passed through an anion column IonPac AS18 with 31mM of potassium hydroxide (KOH) as eluent. Calibration standards were prepared by dilution of OSIL Atlantic Seawater standard into 2%, 5% and 10% solution for all batch of analyses.

5.2.4 Solid sample analysis

The mineral seeds used in this study were analysed for BET surface area. BET surface area of the seeds was analysed by Micromeritics (ASAP 2020) surface area and porosity analyser. The samples were degassed at 200 °C for 2 hours prior to analysis. The experiments were killed immediately after the final sampling. The sample (both solid and aqueous parts of the experiments) were decanted into a 50 mL falcon tube which was centrifuged at 5000 rpm for five minutes. Then, the solution was discarded. The remaining solid samples were carefully rinsed twice with MQ-water and oven dried at 40 °C overnight. Dried samples were powdered prior to mineralogical analysis through X-Ray Diffraction (XRD). The dried samples were prepared by pipetting ~0.40 mL of an acetone smear containing the precipitate onto a zero-background holder. Samples were then kept in a clean cupboard while the acetone evaporated.

Powder X-ray diffraction was collected from Bruker diffractometers and Rietveld refinements were performed with the software Topas 4.1 (Coelho, 2007). The accuracy is considered to be $\pm 1\text{-}2\%$ for major phases, while the estimated standard deviation from the Rietveld calculation has no bearing on the accuracy or otherwise of the quantification itself, being merely related to the mathematical fit of the model (Madsen and Scarlett 2008).

5.2.5 *Statistical applications on ODP database*

Multivariate statistical analysis was applied on selected variables measured in ODP/IODP cores (a total of 839 sites) to study if my hypothesis generated from the laboratory could be applied to natural marine sediments (Data can be freely obtained from this site: <http://iodp.tamu.edu/janusweb/chemistry/chemiw.shtml> for ODP cores and <http://web.iodp.tamu.edu/LORE/> for IODP cores). Detailed ODP data used in the analysis is given in Appendix B. I did not include the DSDP core as many sites did not have interstitial chemistry and most of the measurements were done in low resolution. The statistical test was computed by using the Statistical Package for Social Sciences (SPSS) for Windows v. 25.0. The variables included in the analysis were: (1) maximum alkalinity; (2) depth of maximum alkalinity; (3) average sediment percent carbonate; (4) average percent organic carbon; (5) gradient of alkalinity; (6) calcium concentrations at maximum alkalinity; (7) sulfate concentrations at maximum alkalinity; and (8) minimum sulfate concentration. The justification of these variables is given in Table 5.1. All data was standardized (log-transformed) before being subjected to principal component analysis. The factors with eigenvalues greater than 1 were extracted and the maximum number of iterations for convergence was set to 25. The extracted factors were then rotated using the orthogonal varimax method. Analysis revealed the Kaiser-Meyer-Olkin measure of sampling adequacy was 0.617, suggesting that the pattern of correlation was relatively compact and thereby yielded distinct and reliable factors. All variables analyzed has a communality of higher than 0.6, indicating the adequate participation of these variables in the factors.

Table 5.1: Selected variables from the ODP cores and their justifications for consideration in the statistical analysis.

Variables	Description and justifications
Maximum alkalinity	The maximum concentration of alkalinity – higher alkalinity often indicates positive microbial sulfate reduction
Maximum alkalinity depth	Depth at which the maximum alkalinity occurs – to test if microbial sulfate reduction is depth driven
*Average sediment CaCO ₃	The percentage of CaCO ₃ in the sediment – to examine the relationship between microbial sulfate reduction and substrate type
Average organic carbon	Percentage of organic carbon in the sediment – to examine if the organic carbon content in sediment is linked to microbial sulfate reduction
Gradient of alkalinity	A higher gradient indicates a greater change in alkalinity over a fixed depth – higher alkalinity gradient suggests a higher rate of sulfate reduction
Ca ²⁺ at maximum alkalinity	The concentration of calcium at maximum alkalinity – a drop in calcium at maximum alkalinity suggests the precipitation of calcium carbonate is microbially induced instead of abiotic precipitation
SO ₄ ²⁻ at maximum alkalinity	Sulfate concentration at maximum alkalinity – primary signature for microbial sulfate reduction
Minimum SO ₄ ²⁻	Lowest sulfate concentration in the core – an indication for the magnitude of microbial sulfate reduction.

* Assumption was made to divide sediments into carbonate and non-carbonate. Non-carbonate sediment is presumed to be clay/silicate dominated.

5.3 Results

Two incubation experiments and one abiotic experiment are presented. All killed controls and SEM images of the solid samples are presented in the Appendix C.

5.3.1 Mineral seeds experiments

Significant bacterial growth is observed in all samples over the first 75 hours with OD 600 ~ 0.15 – 0.25, reaching a stationary phase approximately 100 hours after inoculation (Figure 1a). Bacterial growth is not detected in control samples (see Appendix D). The pH increases

from 6.0 to 8.3 as microbial sulfate reduction progresses. Samples with 0.3 g of calcite seeds reach higher pH before the pH stabilizes, whereas the pH in samples with 3 g of calcite seeds requires a longer time to reach pH stabilization (Figure 5.1c). A clear difference among different experiments is the increase in alkalinity (Figure 5.1b). In general, the incubation reaches higher maximum alkalinity in experiments with low amounts of calcite compared to samples with high amounts of calcite. The experiments with kaolinite seeds stabilized at alkalinity of 140 mEq L⁻¹ when all the electron donors were consumed. However, in the samples with calcite seeds only 55 – 60% of the maximum alkalinity was attained. As a result of microbial sulfate reduction, the sulfate concentrations drop during the course of incubation whereas concentration of aqueous sulfide increases (Figure 5.1d, e). The conversion of sulfate to sulfide is nearly 1:1. Only half of the sulfate was consumed by the sulfate-reducing bacteria in the sample with 100% calcite and seedless samples. Samples with a lower proportion of calcite have a greater rate of sulfate reduction and the sulfate concentration was completely depleted within 200 – 400 hours. In contrast, the sulfate reduction rate is slower in samples with a higher proportion of calcite and the sulfate was not depleted at the end of the experiment. An identical trend was noted in calcium concentration, where carbonate precipitation was observed with a decrease in calcium concentration in experiments that have < 99% CaCO₃. Samples with no clay minerals (including the seedless sample) do not have carbonate precipitation over the course of the incubation experiment, as reflected by an absence of change in calcium concentrations (Figure 5.1f). Magnesium and sodium concentrations remain constant over the course of the experiments (Figure 5.1 g,h).

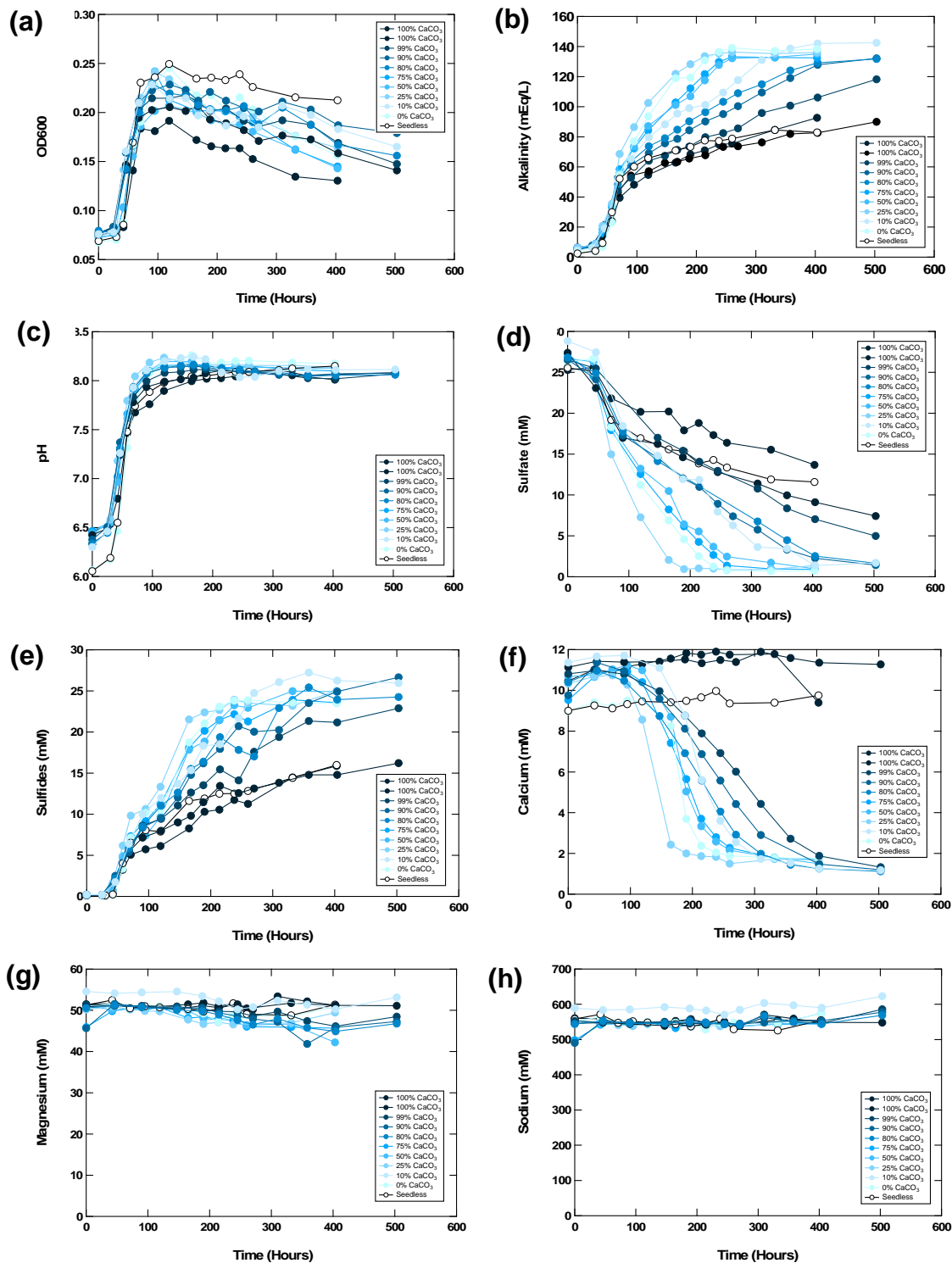


Figure 5.1: The first incubation with varying proportion of CaCO_3 was presented with a color gradient, where the darker color lines indicate a higher proportion of CaCO_3 . Open circle symbol is the sample without mineral seeds. Note that the first incubation experiment was conducted in two separate runs. The first run are samples with 100%, 75%, 50%, 25%, 0% CaCO_3 and the seedless sample. The second run includes samples with 100%, 99%, 90%, 80% and 10% CaCO_3 . The two experiments were run for slightly different amounts of time, which is why some lines are shorter than others. Incubation experiment results with varying

proportion of CaCO_3 to various aqueous chemistry variables, (a) OD600; (b) alkalinity; (c) pH; (d) sulfate; (e) sulfide; (f) calcium; (g) magnesium; and (h) sodium. I did not observe any significant change in the control samples (shown in Appendix C).

5.3.2 Results from Abiotic Experiment

Unlike the biotic experiments, the six abiotic experiments did not show a significant variation with respect to pH and alkalinity (Figure 5.2). The change in pH is the greatest when 6 mL of 1M NaHCO_3 was added. The increasing trend of pH slows as more NaHCO_3 was added. The changes in alkalinity are more straightforward as the alkalinity increased was directly proportional to the volume of NaHCO_3 added. No obvious difference is noted among the samples with different proportion of carbonate to clay tested.

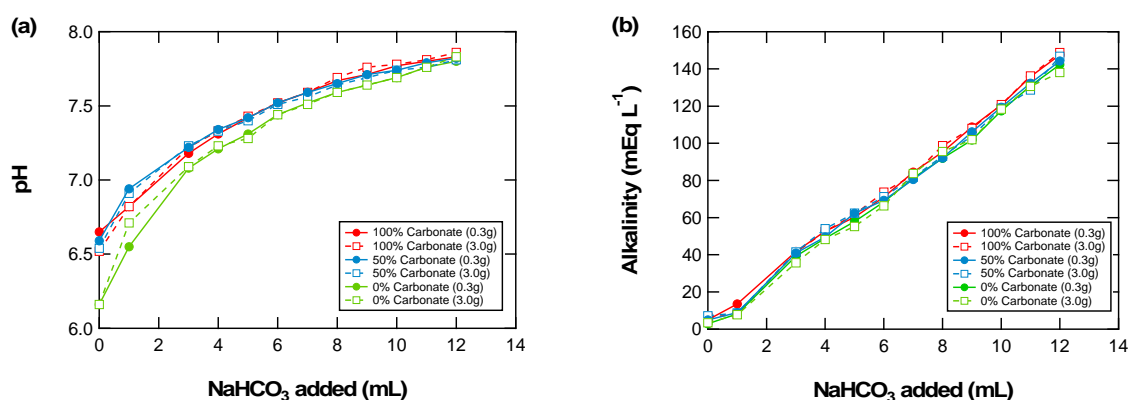


Figure 5.2: Plots showing the results of (a) pH; and (b) alkalinity in abiotic experiments with varying proportion of carbonate to clay and the total volume of mineral seeds.

5.3.3 Nutrient control experiments

Similar to the initial experiments, the bacteria grow rapidly during the first 50 hours of the incubation (Figure 5.3). The OD in the majority of samples increases from 0.07 to 0.25, before experiencing a slight drop at 100 hours and then stabilized over the course of the experiment. The samples incubated with calcite seeds shows an overall lower OD, although changes in pH are similar. The alkalinity, however, differs among the experiments with the different seeding materials. The highest increase in alkalinity is attained by cleaned kaolinite samples from Sigma, where it reaches a maximum alkalinity of 130 mEq L⁻¹ at 300 hours. The rate of alkalinity increase is intermediate in both original and cleaned kaolinite standards. The incubation samples with lowest alkalinity are those with the calcite seeds, similar to the first experiments. The phosphate in all samples drops at least 60% of its original concentration

(700 – 800 μM). A drop in calcium concentration is noted when the alkalinity of the samples reaches 80 mEq L^{-1} in all of the samples. Magnesium drops slightly over the course of the incubation experiment.

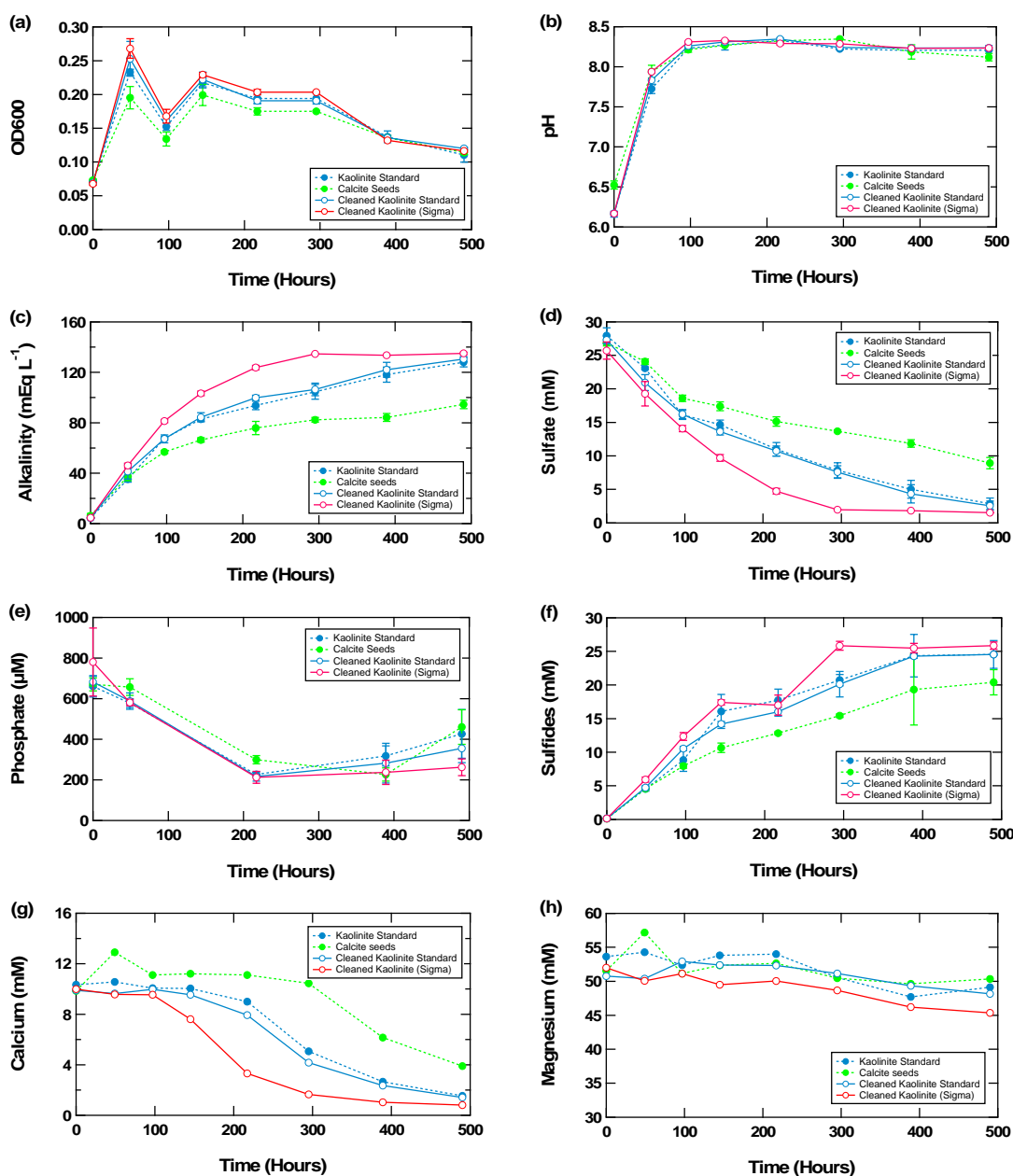


Figure 5.3: Second incubation experiment using different seeding materials to examine the influence on bacterial growth and the evolution of aqueous chemistry (a) OD600; (b) pH; (c) alkalinity; (d) sulfate; (e) phosphate; (f) sulfides; (g) calcium; and (h) magnesium. The results of control samples are given in the Appendix D. The error bars in the figure represents the standard deviation of triplicates. The calcium carbonate minerals formed from the incubation samples are shown in Appendix E.

5.3.4 Results from mineralogical characterization and BET surface area

Characterization of the solid samples using XRD showed that two calcium carbonate polymorphs precipitated from the first incubation experiment: monohydrocalcite (MHC) and calcite (Figure 5.4). My results from X-ray diffraction (XRD) suggest that MHC is the dominant calcium carbonate polymorph formed in the sample with less calcite used as seeding material, whereas the precipitation of Mg-calcite is promoted in samples with higher amounts of calcite as the seeding material (> 80%). The peak shift towards higher 2θ and peak broadening suggest the incorporation of magnesium into the lattice of calcite, decreasing the size of the unit cell and the crystal domains (Lenders et al., 2012, Nielsen et al., 2016; Blue et al., 2017). The BET surface area for calcite, kaolinite standard and cleaned kaolinite (Sigma) were $0.3653 \text{ m}^2/\text{g}$, $14.3121 \text{ m}^2/\text{g}$ and $15.6846 \text{ m}^2/\text{g}$, respectively.

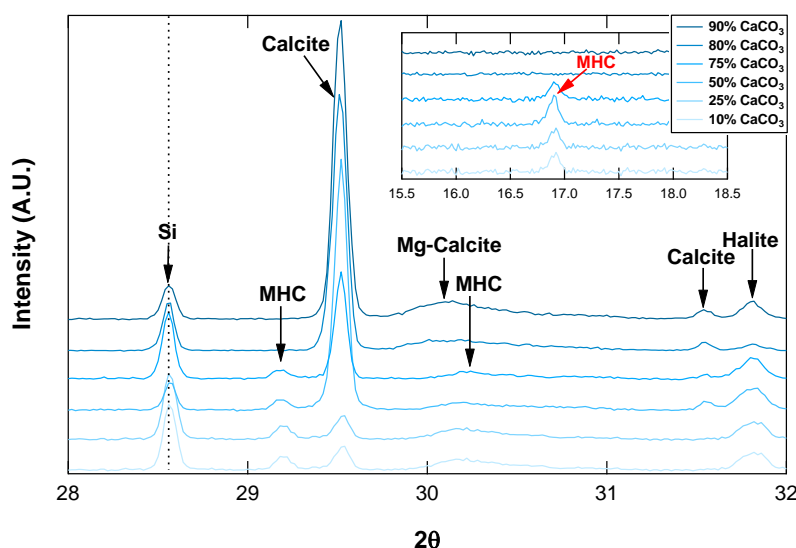


Figure 5.4: XRD patterns collected from selected biotic incubation samples. Monohydrocalcite (MHC) and Mg-calcite are the main calcium carbonate polymorphs that precipitate from the samples. The proportion of MHC increases as the proportion of calcium carbonate in the original seeding material decreases. A small amount of silicon powder is added to the sample as an internal standard to calibrate the peak position (dotted line). Sub-figure shows the presence of MHC in samples with calcite lower than 80% at a low 2θ value (marked in red).

5.3.5 Results from statistical analysis

My statistical analysis shows that the dataset of pore fluid data from ODP cores largely can be explained by three principal components, with a cumulative variance of 80.42%. The first principal component (PC1) has the highest eigenvalue (3.73 - Table 5.2), suggesting a substantial contribution of this component in explaining the major processes that govern the

geochemistry in the sediment cores. The significant positive loadings in the first principal component comprise minimum sulfate concentrations, sulfate concentration at maximum alkalinity, calcium concentration at maximum alkalinity and sediment calcium carbonate percentage, suggesting a good relationship among these variables. PC1 is also negatively loaded with maximum alkalinity and the gradient of alkalinity, meaning that both variables established a significant but inverse relationship with the previous four variables. Principal component 1 can be regarded as the sulfate-reduction factor because of a majority of the positive loadings and both negative loadings. That this factor is positively loaded with sediment calcium carbonate percentage, suggests a relationship between the amount, or degree, of microbial sulfate reduction and the carbonate content in the sediment. The second principal component explained 20.74% of the variance and was mainly associated with the gradient of alkalinity and the depth of maximum alkalinity. This principal component suggests a relationship between sulfate reduction with depth in the core. In this case, the positive loading of depth of maximum alkalinity and negative loading of gradient of alkalinity suggests that sulfate reduction occurs mostly at a shallower depth (inverse relationship). PC3 explained the least variance in the dataset (13.07%) and is positively loaded with sediment carbonate mineral percentage and organic carbon, suggesting organic carbon content increases with carbonate content in the ODP sedimentary database.

Table 5.2: *Principal components of various variables relevant to microbial sulfate reduction in the ODP cores. Note that all data was log-normalized before PCA. The missing data were treated with multiple imputation functions before the analysis. Significant PC loadings greater than 0.4 were given in bold.*

Variables (<i>n</i> = 641)	Principal Components		
	1	2	3
Minimum SO ₄ ²⁻	0.921	-0.073	0.010
SO ₄ ²⁻ at maximum alkalinity	0.921	-0.093	-0.006
Maximum alkalinity	-0.893	-0.060	0.109
Ca ²⁺ at maximum alkalinity	0.720	0.378	-0.001
Gradient of alkalinity	-0.567	-0.772	0.058
Maximum alkalinity depth	-0.264	0.921	0.077
Sediment CaCO ₃	0.433	0.207	0.663
Organic carbon	-0.371	-0.109	0.764
Variance (σ)	46.613	20.741	13.066
C. variance	46.613	67.353	80.420
Eigenvalues	3.729	1.659	1.045

5.4 Discussion

My results indicate that the use of different seeding materials in pure culture influences bacterial growth and this is reflected in changes in aqueous chemistry. My early hypothesis suggested that two factors likely influence the bacterial growth rate – the surface area of the seeding material; and the nutrients associated with the mineral seeds; or a combination of both factors. Another interesting question arises during my study: does a change in seeding mineralogy impact the polymorph of calcium carbonate precipitated? In my previous study (Lin et al., 2018) I used pure seeding material (either calcite or kaolinite) in supersaturated solutions with varying Mg/Ca ratio of the media, which may have masked the role the mineral substrate has on the types of calcium carbonate polymorphs precipitated. In this study, I further investigate the seeding factor by using homogeneous and heterogeneous mineral seeds incubated in seawater.

The discussion is divided into four parts. First, I discuss the role that mineral seeds have on microbial activity. Then, I discuss if the bacterial growth rate is controlled by the surface area or the available nutrients that are associated with the mineral seeds. Then, I explore whether the types of mineral seeds influence the calcium carbonate polymorphs precipitated. Finally, I explore the extrapolation of my findings to the natural environment.

5.4.1 The role of mineral seeds on microbial sulfate-reduction rate

My experimental results show that microbial sulfate reduction is capable of changing the solution chemistry to differing degrees, depending on the proportion of different mineral seeds in the incubation samples. Biotic cultures incubated with different seeding substrates show that a lower calcite-to-kaolinite ratio (less calcite in the medium) enhances bacterial metabolism. A similar result was reported in the 1960s by Stotzky also using pure culture – *Agrobacterium radiobacter* (a common soil bacterium) (Stotzky, 1966a, Stotzky and Rem, 1966). Other studies have confirmed this with a range of microorganisms and fungi (Weaver and Dugan, 1972; Filip et al., 1972; Chaerun and Tazaki, 2003). However, none of these studies have tested this effect in sulfate-reducing bacteria – a species that plays a significant role in sedimentary carbonate formation and whose metabolism is particularly important to understand. Previous studies have also not attempted to look for this in natural settings except Wong et al. (2003). Wong et al. (2003) incubated pure culture of *Desulfovibrio vulgaris* using mixtures of pure bentonite, pure kaolinite and sediment collected from a landfill aquifer and found different results; they observed a lack of sulfate-reduction activity in clay-dominated samples. They suggest that the inhibition of sulfate reduction activity with clay is possibly due

the aluminium toxicity from the clay. I do not see this in my incubation experiments as my medium is at a higher pH range (pH 7 – 8) where aluminium solubility is expected to be low.

So, what is the primary mechanism or influence that mineral seeds have on the rate of bacterial metabolism? Early work suggested several substrate properties influence bacterial respiration and population growth, including pH, inorganic nutrients, cation exchange capacity (CEC) and surface area (Stotzky, 1966a; Stotzky, 1996b; Stotzky and Rem, 1966). These papers argued that the buffering ability of clay minerals creates a suitable environment to stimulate bacterial respiration and sustained growth, and that the favorable pH levels were related to the relative basicity of the exchangeable cations on the clays (Stotzky, 1966a). This early work also reported that among all the clay minerals tested, montmorillonite, in particular, exerted a marked influence on the activity of bacteria in pure culture. This is mainly because montmorillonite has a greater (17 – 20 times) cation exchange capacity compared to kaolinite and other clay minerals, where more basic cations can be exchanged from the expandable 2:1 smectite for H⁺ ions produced during bacterial metabolism.

In contrast to Stotzky's experimental approach which examines a wide range of governing factors on bacterial metabolism, my biotic experiments compare only two different types of mineral seeds in varying proportions, while leaving other variables constant. My results demonstrate a large difference in microbial growth rate (proxied by rate of depletion of sulfate concentrations and rate of OD increase) and alkalinity production between the two end-member seeds, where a higher growth was observed in pure kaolinite samples compared to calcite. Figure 5.5 summarizes the changes of maximum alkalinity and pH as a function of the proportion of calcite seeds in the experiments. I found that similar alkalinity concentrations are generated until there is a high proportion of calcite seeds in the vial, when the maximum alkalinity produced drops dramatically. Such a "drop off" in maximum alkalinity marks the end of the "effective stimulating effect" the mixed substrate containing clay minerals has on microbial metabolism. The changes in maximum pH as a function of the percentage of calcite used as seeding material is less sensitive (Figure 5.6). I observed a two-fold difference in the rate of sulfate consumption rate at a given time point between two end-member samples (100% kaolinite and 100% calcite).

My abiotic experiment shows that this difference in alkalinity is driven by *Desulfovibrio bizertensis* (Figure 5.2). The abiotic experiments suggest that there is no significant difference between the samples with varying calcite-to-kaolinite ratio. This could mean that abiotic reactions including dissolution and re-precipitation of minerals, or ion exchange on mineral surfaces, are not critical in mediating alkalinity and pH in the system. In the biotic experiments,

I find that the offset between the calculated alkalinity and the measured alkalinity (mostly in low calcium carbonate samples) as a function of percent sulfate reduced can be explained by the precipitation of calcium carbonate. Such a claim is supported by the lack of calcium drop in samples with 100% calcium carbonate. Figure 5.5 shows the relationship between the measured alkalinity and sulfate at 400 hours and the calculated microbial metabolic stoichiometry before and after precipitation. The calculated metabolic stoichiometry is based on the following overall equation (Gallagher et al., 2012):



The results show that samples with 100% calcium carbonate did not fall on the calculated stoichiometric lines.

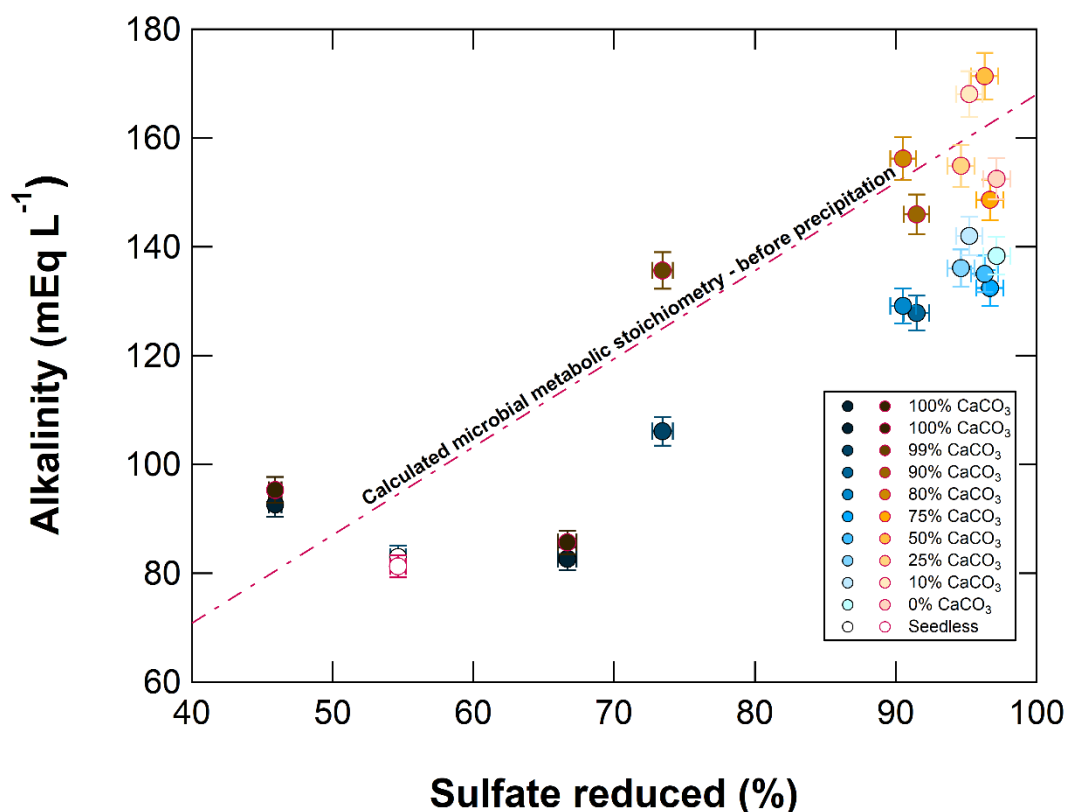


Figure 5.5: The relationship between alkalinity and sulfate reduced in incubation samples at 400 hours shows that after correction for the occurrence of carbonate precipitation a majority of the samples sit close to the calculated microbial metabolic stoichiometry of sulfate reduction coupled to formate oxidation (Gallagher et al., 2012): $4\text{CHO}_2^- + \text{SO}_4^{2-} + \text{H}_2\text{O} \rightarrow 4\text{HCO}_3^- + \text{HS}^- + \text{OH}^-$. The red line indicates the calculated stoichiometry without carbonate precipitation while the takes carbonate precipitation into account. Samples marked in blue indicate the actual measured concentrations at 400 hours, whereas samples in orange are corrected for the alkalinity lost due to carbonate precipitation. The correction was made by adding twice the

difference in both calcium and magnesium concentration between 0 hours and 400 hours (assuming calcium and magnesium were lost due to carbonate precipitation). Error bars in the plot indicate the measurement errors of the method used.

Despite a huge difference in the sulfate reduction rate between end-members substrates, the OD_{600} results do not show as large a variation. In fact, the sample without seeds displays higher OD_{600} than most of the seeded samples, which is odd given the rate of sulfate reduction in seedless samples is substantially lower. This suggests two possibilities: (1) the bacteria preferably grows within the seeds instead of suspended in the medium, so I don't accurately measure the population in the seeded cultures; or (2) the metabolic activity (or cell-specific sulfate reduction rate - csSRR) of the bacteria is different in the sample with and without seeds; or both. I believe that the former is more likely because of the significant difference between the OD_{600} of the seedless sample compared to all the seeded samples, particularly when I compare it to the pure calcite sample which has a similar sulfate reduction rate as the seedless sample.

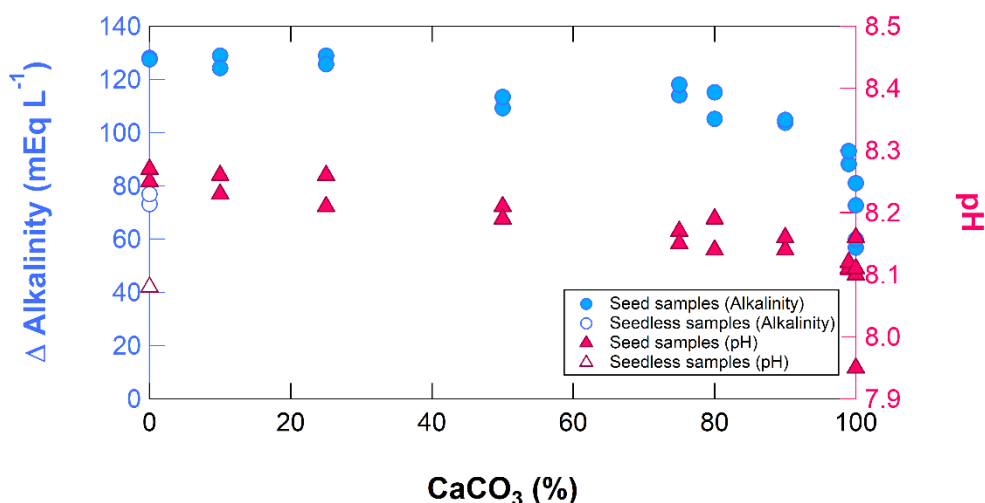


Figure 5.6: Changes in maximum alkalinity and pH as a function of $CaCO_3$ in the incubation experiments. The data plotted displays maximum alkalinity and pH recorded over the course of the experiment.

5.4.2 Surface area or nutrient control?

To answer the question of whether the difference in the rate of bacterial metabolism in the presence of kaolinite is due to surface area or the available nutrients (both organic and inorganic) from the seeding mineral (in this case kaolinite would have more nutrients), I performed a second experiment using cleaned and original (uncleaned) kaolinite. This experiment shows that there is no notable difference in cell growth between the samples with

cleaned and original seeds (Figure 3). The experiment with cleaned kaolinite (from Sigma) had the highest sulfate reduction rate of 1.93 mM day⁻¹. This is followed by the uncleaned kaolinite (1.23 mM day⁻¹), cleaned kaolinite (1.21 mM day⁻¹) and calcite (0.87 mM day⁻¹). I conclude that nutrients associated with the mineral substrate are not influencing bacterial metabolism, or were not removed during the cleaning procedure. However, earlier studies also concluded that clay minerals used microbial culture media do not supply trace elements or favor nutrition of the organisms (Stotzky and Rem, 1966; Vagner and Sroubkova, 1970).

If nutrient content in the kaolinite is not the dominant factor, could surface area be important since both kaolinite and calcite are known to have distinct surface areas? I see a difference in microbial metabolism between the cleaned kaolinite from Sigma and the standard kaolinite despite the fact that both are pure aluminium silicates that shared the same mineralogy – Al₂Si₂O₅(OH)₄. Surprisingly, analysis of XRD shows that the kaolinite from Sigma contains minor illite (Appendix F). I hypothesize such a difference in the microbial metabolism could be attributed to the difference in surface area which can differ widely among clays. The BET analysis shows that the calcite seeds have a very low surface area compared to the clays further confirmed the role of seed's surface area has on the bacterial growth.

Stotzky, (1966b) suggested that surface area could not be established unequivocally, as some methods at that time were questionable. However, unlike his study that only involves clays (where the surface area could be relatively similar), my result suggests the importance of the surface area of the seeding materials. It may be that the cation exchange capacity (CEC) has a more dominant role. I did not examine CEC of the mineral seeds since this variable is very different (between kaolinite and calcite) and closely similar (in my case – among the original and washed kaolinite). All cleaned clays in my experiments should have similar CEC as exchange “standardized” of ions has occurred during the cleaning process that involves soaking of 0.5 M of NaCl. Furthermore, CEC changes with the solution pH, and the pH in my experimental medium evolves over time (Ma and Eggleton, 1999). I, therefore, think that surface area is the dominant factor that governs the bacterial activity in my experiment.

5.4.3 *The influence of substrate mineralogy on calcium carbonate precipitation*

I previously suggested that there is a limited/weak influence of seeding material on the calcium carbonate polymorph that precipitates during microbial sulfate reduction, because of the overwhelming influence from changes in the medium Mg/Ca (Lin et al., 2018). In this study, fixing the medium chemistry while varying the proportion of different mineral seeds allows for a greater constraint on the role of seeding material on the calcium carbonate polymorph that

precipitates. My study shows that MHC precipitates in experiments with a higher proportion of kaolinite, whereas Mg-calcite is the dominant polymorph precipitated in experiments with a higher proportion of calcite. The results suggest that seeding material plays an important role in influencing the type of calcium carbonate polymorph that forms. The evolving medium chemistry also may play a role in the solubility of each calcium carbonate polymorph. After 100 hours, the experimental solutions are supersaturated with respect to various calcium carbonate polymorphs (calcite, aragonite, monohydrocalcite, and vaterite). Monohydrocalcite is likely the dominant polymorph in kaolinite-dominated samples due to the role that solution chemistry plays (high pH, alkalinity, saturation states and phosphate) over the surface nucleation of the mineral seeds. As a result of the higher saturation state, the precipitation kinetics increase and this promotes the formation of spherulitic, less stable polymorphs – like monohydrocalcite (Rodriguez-Blanco et al., 2014; Rodriguez-Blanco et al., 2015). In contrast, the condition is reversed in the calcite-dominated experiments. In the calcite-dominated, a slower carbonate mineral precipitation rate promotes the dehydration process and thus favors the formation of anhydrous and more stable (lower K_{sp}) minerals such as Mg-calcite. In addition, the presence of seeding material with similar mineralogy (calcite in this case) has lowered the energy required for precipitation, allowing Mg-calcite to form instead of the metastable monohydrocalcite. This surface-controlled reaction is possibly seen by the presence of epitaxial growth of Mg-calcite on the original calcite seeds (SEM figure will be included).

5.4.4 Insights of substrate driven metabolism into ODP cores

My results show the important role of seeding mineralogy on microbial sulfate reduction, and it is logical to see if this is reflected in the natural environment. The information extracted from the principal component analysis suggests that microbial sulfate reduction has a close relationship with the percent of calcium carbonate in the sediment (Table 5.2). In the global ocean, lower carbonate mineral content in sediment is associated with higher rates of microbial sulfate reduction, as read by higher overall alkalinity and lower sulfate concentrations in the sediment (Figure 5.7). This could be for several reasons, in addition to the stimulation of microbial activity, in the presence of clay minerals. Sediments that are dominated by clay minerals have lower overall porosity and permeability, and therefore a shallower oxygen penetration depth, and become anoxic more quickly. Furthermore, sediments that are dominated by clay minerals often have organic carbon in the interstices of these minerals which helps support deep biosphere microbial activity.

The anomaly seen in Figure 5.7, where there is a higher average alkalinity in the 90-95% calcium carbonate bin, is due to a series of sites sampled off the shore of the Bahamas and Southern Australia (Figure 5.8). The depth at which the maximum alkalinity was attained in these cores ranges from 77 – 255 cm below the sediment-water interface. Detailed examination of individual cores with maximum alkalinity greater than 20 mEq L⁻¹ suggested that the alkalinity source from the Bahamas (ODP site number 1004, 1005, 1007, 1008 and 1009) are influenced by microbial sulfate reduction. Whereas cores with some exceptionally high alkalinity (> 90 mEq L⁻¹) from the Bahamas (site number 1129, 1131 and 1132) are possibly affected by other processes besides sulfate reduction such as anaerobic methane oxidation. In the ODP data, the “effective stimulating effect” is seen when sedimentary carbonate content dips below 60 – 80%, which is similar to what I observed in pure culture (Figure 5.6). These observations support my laboratory findings.

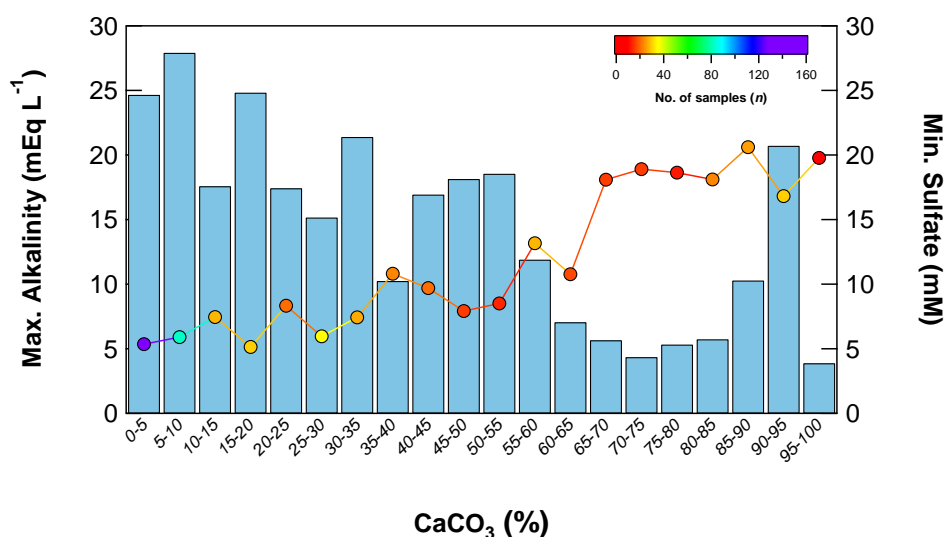


Figure 5.7: Data extracted from ODP database shows that the geochemistry of a majority of sediments are influenced by sulfate reduction. This process is largely influenced by the CaCO₃ content of the substrate. The CaCO₃ (%) is categorized and the data in y-axis were averaged. The bars in the graph represent maximum alkalinity (mEq L⁻¹) while the line with markers indicates the minimum sulfate concentration (mM). The number of samples considered in the analysis is presented in colours.

Which component of sediment mineralogy influences the rates of microbial sulfate reduction can be visualized when the principal component scores are placed on a cross plot of maximum alkalinity versus sediment carbonate content (Figure 5.8). Figure 5.8a demonstrates a pattern of PC1 scores where the samples highly influenced by sulfate reduction are in red while those not influenced by sulfate reduction are in blue. I find that a majority of cores linked to high sulfate reduction are either located next to the coast or places with major ocean upwelling and

high sedimentation rate, as expected (Figure 5.8b). The statistical analysis corroborates my laboratory results in the natural environment.

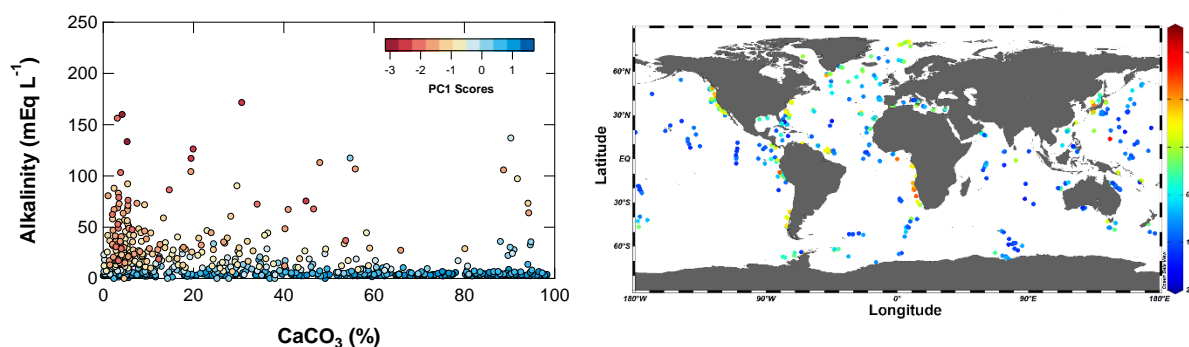


Figure 5.8: (a) Cross plot of alkalinity vs. sediment CaCO₃ (%) with PC1 scores on z-axis; (b) Distribution of ODP cores influenced by PC1.

5.4 Conclusions

In conclusion, my study shows that the degree of microbial sulfate reduction changes as a function of the proportion of clay minerals. Incubation experiments with varying clay and carbonate mineral indicate that the sulfate reduction rate increases with increasing clay content. A substantial drop in maximum alkalinity is particularly noted at above the 80% carbonate 20% clay mixture. I suggest that the preference of the bacteria for clay dominated substrate is due to the higher surface area of the clay. The high surface area of clay minerals correlates with the CEC, which we believe provides nucleation sites for bacterial growth. Further work is needed to further elucidate the mechanism behind this. My findings in the laboratory are also supported by the observation of the same process occurring in natural marine sediments. Using multivariate statistical analysis, I apply principal component analysis on ODP samples. I found that sites with greater CaCO₃ often have lower maximum alkalinity and higher porewater sulfate, suggesting a lower degree of sulfate reduction. Combining results from both laboratory and ODP cores, I conclude that the rate of microbial sulfate reduction is substrate driven.

My experiment also shows that the mineral substrate influences the types of calcium carbonate polymorphs precipitated. The substrate with high carbonate content tends to promote the precipitation of Mg-calcite due to the greater influence of surface nucleation. Precipitation of MHC is favoured in low carbonate substrate because the water chemistry is more important. However, it should be highlighted that both MHC and Mg-calcite can be present in the calcite dominated samples, being that MHC is mainly precipitated from the solution (homogeneous precipitation), while Mg-Calcite takes a longer time to form (at higher

Mg/Ca ratio), shown by a slower drop in the Mg/Na ratio plot. The findings in this study could have wide implications across diverse fields including industrial applications such as iron or metal scavenging processes in contaminated soil, biogeochemistry on carbon balance and budget, paleoenvironmental reconstruction etc.

Chapter 6

The formation of siderite in the laboratory and salt-marsh system

6.1 Introduction

Carbonate minerals are one of the major components of the sedimentary rock record. While the vast majority of carbonate rocks comprise the minerals calcite (CaCO_3), aragonite (CaCO_3), and dolomite ($\text{CaMg}(\text{CO}_3)_2$), other carbonate minerals, such as siderite (FeCO_3) can also be common. Our understanding is that siderite only forms under certain environmental conditions, often linked to changes in pH, changes in $p\text{CO}_2$ or changes in microbial metabolism (Xiouzhu et al., 1996; Van Lith et al., 2003; Dong, 2010; Sanchez-Roman et al., 2014; Sanchez-Roman et al., 2015). Often, the presence of siderite or dolomite is used to flag unique conditions at Earth's surface at various points in Earth history.

The formation of siderite, however, is not straightforward. Siderite, only forms under anoxic conditions due to the need for reduced, ferrous, iron (Fe^{2+}) which is rapidly oxidized in the presence of oxygen; hydrogen sulfide can also not be present because hydrogen sulfide reacts rapidly with ferrous iron to make iron monosulfides and ultimately pyrite. Thus, formation of both siderite and dolomite often involves microbially mediated chemical reactions (such as bacterial iron reduction or microbial sulfate reduction) that induce changes in aqueous geochemistry that may lead to these carbonate minerals becoming the primary carbonate mineral precipitate (Van Lith et al., 2003; Sel et al., 2012; Roberts et al., 2013). With recent advances in analytical geochemistry, the question of what are the surface conditions that drive the formation of less common carbonate minerals is ripe for a new approach. Here I will explore the formation of siderite in a modern marginal marine environment. In the Norfolk salt-marshes, in sediment dominated by bacterial iron reduction, there are often large siderite nodules (up to 20 cm in diameter) found growing in the sediment. In this chapter I will examine the mineralogy and elemental distributions within several of these concretions that I collected from the salt-marsh sediment to better understand the geochemical conditions during their formation and subsequent growth. I also measured the porewater chemistry of sediment cores from two geochemically distinct ponds where siderite concretions are forming, and discuss the change in siderite solubility with depth in these cores. I attempted to map the distribution of the siderite nodules in the salt-marsh using a gradiometer to measure the magnetic susceptibility but this was largely unsuccessful and I will present both the maps and discuss why it was unsuccessful.

I will couple this field-based work to laboratory experiments where I try to understand the microbial conditions under which siderite may precipitate. Studies involving the microbially-induced precipitation of siderite via anoxic incubation of sediment is difficult because if the system turns to microbial sulfate reduction, the ferrous iron will react with aqueous sulfide and will no longer be available to make siderite. Therefore, maintaining incubations at bacterial iron reduction is key for laboratory precipitation of siderite. To the best of my knowledge, microbial precipitation of siderite has only been reported using pure culture of *Geobacter metallireducens*, a bacterial iron reducer, in the laboratory (Mortimer et al., 1997). Zachara et al. (1998) also found that *Shewanella putrefaciens*, CN32, an anaerobic bacterium that can reduce either iron or manganese oxides, was able to reduce iron oxides and lead to the precipitation of vivianite and siderite.

From the previous chapters in this thesis, I know that MHC often serves as a transient metastable phase before transformation into stable calcium carbonate polymorphs. I have shown that the transformation of MHC to other polymorphs depends on the geochemistry of the evolving fluid. In the final project presented in this chapter, I will use MHC to seed siderite formation. One goal is to explore the transformation of MHC to siderite. Understanding this mechanism may provide insights as to how changes in fluid chemistry affect the formation of various carbonate polymorphs in an iron dominated system. Is it energetically more favourable for carbonate minerals to form via MHC compared to classical nucleation?

6.2 Materials and Methods

6.2.1 Field sampling

Two geochemically distinct sediment cores, one with sulfidic sediment and one with ferrous iron from ponds of Norfolk salt-marshes and their pore-fluid was analysed. The iron-rich core was sampled at the Warham salt-marsh while the sulfidic core from the Blakeney salt-marsh. The sampling sites are 5 km apart (Figure 6.1). The sediment was collected using 50 cm polycarbonate push cores, tightly sealed in the field before being transported back to the laboratory for chemical analysis. These cores were sampled at high resolution with every 2 cm down core to a depth of 40 – 45 cm. Fresh samples of siderite concretions were also collected from sediment in the creek nearby. Some of the concretions were found 30 cm below iron-rich ponds. Concretions were wrapped with mud in the field and properly sealed with polyethylene bags to minimize chemical alteration. In the laboratory, fresh concretions

were cut into half, one is used for analysis and the other half was refrigerated and kept in a dark environment until further analysis.

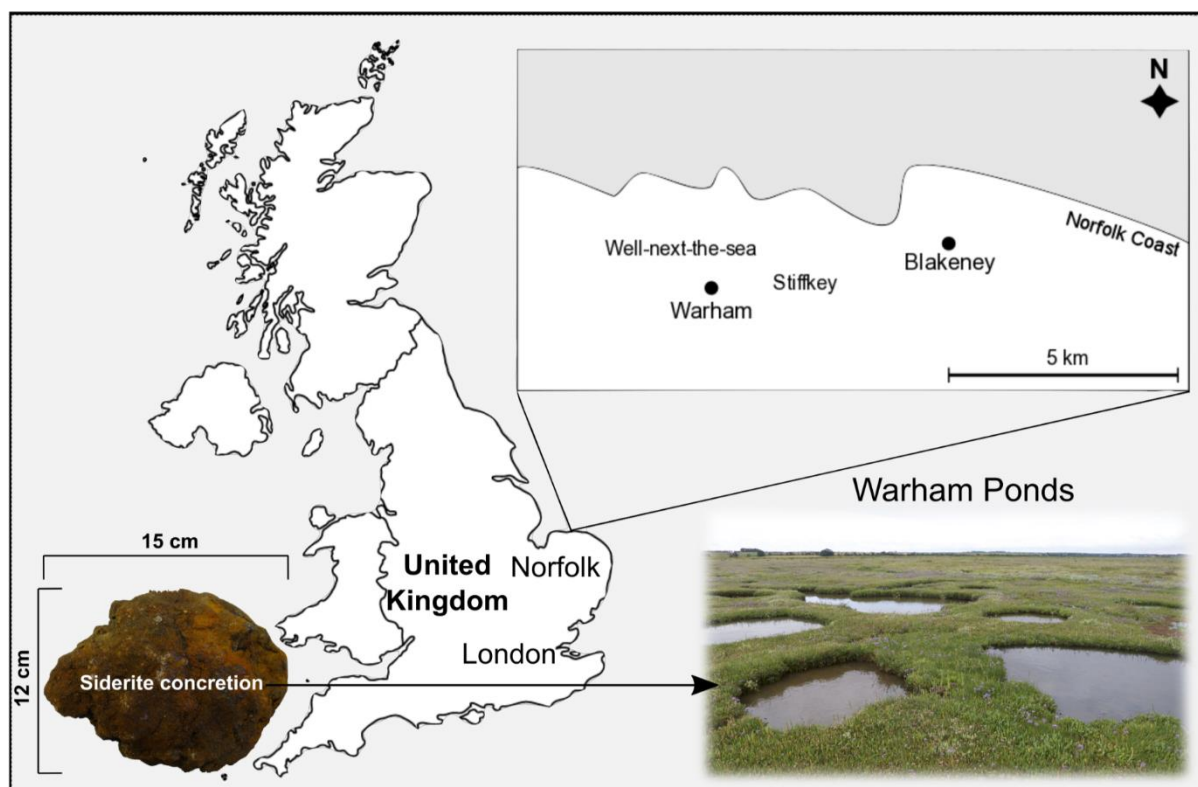


Figure 6.1: The salt-marshes in North Norfolk is an ideal natural laboratory where siderite concretions are actively forming. The geochemical nature of the ponds can be easily distinguished in the field by examining the presence of sulfides.

6.2.2 Analysis of concretions

For mineralogical analysis of the solid samples, fresh concretions were cut into half using a rock cutting machine, crushed, homogenised and powdered using agate mortar and pestle before X-Ray diffraction (XRD) and X-Ray Fluorescence (XRF) using a Avaatech X-ray fluorescence (XRF) core scanner to obtain semi-quantitative elemental data (Figure 6.2). All mineralogical data for XRD were collected in Bragg-Brentano geometry on a D8 Bruker diffractometer equipped with primary Gobbel mirrors for parallels Cu K α X-rays and a Vantec position sensitive linear detector. Collections conditions were: 15-70° in 2θ , 0.02 step size, 450 seconds/step, divergence slits 0.6 mm. Rietveld refinements were performed with software Topas 4.1 (Coelho, 2007). Bulk samples for $\delta^{13}\text{C}_{\text{carbonate}}$ and $\delta^{18}\text{O}_{\text{carbonate}}$ were drilled across from the center to the edge of the concretion. Approximately 50-200 micrograms of dried homogenised sample were transferred into exetainer vials and sealed with silicone rubber septa using a screw cap. The samples were flushed with CP grade helium then acidified with 104% orthophosphoric acid, left to react for 1 hour at 70 °C and then analysed

using a Thermo Gasbench attached to a Thermo Delta V Advantage mass spectrometer in continuous flow mode. Each run of samples was accompanied by 10 reference carbonates (Carrara Z) and 2 control samples (Fletton Clay). Carrara Z has been calibrated to VPDB using the international standard NBS19. The results are reported with reference to the international standard VPDB and the analytical precision is better than ± 0.08 per mil for $^{12}\text{C}/^{13}\text{C}$ and ± 0.10 per mil for $^{16}\text{O}/^{18}\text{O}$ (James Rolfe, personal communication).

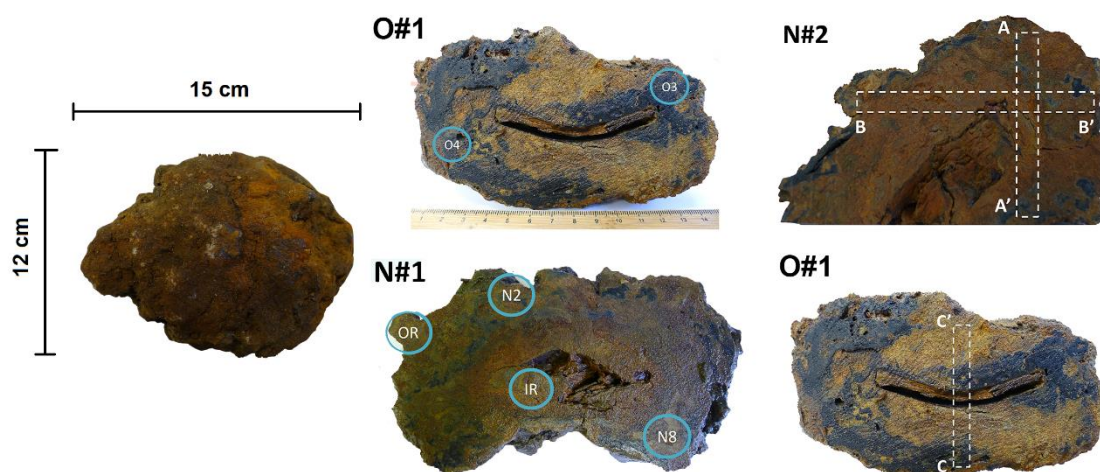


Figure 6.2: Two carbonate/siderite concretions (O and N) with diameter ~15 cm were cut into parallel slices for mineralogical and geochemical analysis. For mineralogical analysis, different parts of the concretion (blue circle) were carefully excavated and pulverized prior to analysing by a D8 Bruker X-Ray Diffractometer (XRD). To examine the bulk geochemical composition across the concretions (12mm dotted line box of A-A', B-B' and C-C'), freshly cut samples were scanned by an Avaatech XRF core scanner.

6.2.3 Pore-fluid analysis

Pore-fluid samples were extracted in the laboratory using rhizons and filtered through a 0.2 μm syringe filter. pH was measured immediately using a Thermo Scientific Orion 4-Star Plus pH meter. Filtered samples were subsequently analysed for alkalinity, dissolved ferrous iron and sulfide, major ions and trace metal concentrations. Unless detailed here, all methods have been discussed previously in the thesis. Alkalinity was determined using the inflection point method by titrating filtered samples with 0.0166N analytical grade hydrochloric acid (HCl). The concentration of various dissolved inorganic carbon species, $p\text{CO}_2$, and total dissolved inorganic carbon were calculated (at $T = 25\text{ }^\circ\text{C}$) using the computer software CO2Calc developed by Robbins et al., (2010). Ferrous iron in the samples was fixed by ferrozine solution ($\text{C}_{20}\text{H}_{13}\text{N}_4\text{NaO}_6\text{S}_2\text{H}_2\text{O}_{(s)}$, MW = 510.48 g/mol) prior to quantification using an Aqua-mate Plus UV-Vis Spectrophotometer at $\lambda = 562\text{ nm}$ (Stokey, 1970). For cores

containing aqueous sulfide, the pore-fluid samples were fixed with zinc acetate (20% ZnOAc) and measured using the methylene blue method (Cline, 1969). Quantification of aqueous sulfide was carried out using a UV-Vis Spectrometer at $\lambda = 670$ nm. Chloride and sulfate concentration were measured by High-Performance Ion-Chromatography Dionex ICS-5000+ SP. The anions were passed through an anion column IonPac AG18 with 31mM of potassium hydroxide (KOH) as eluent. For dissolved metal analysis, filtered pore-fluid samples were acidified to $\text{pH} < 2$ and concentrations determined using an Inductively-Coupled Plasma Optical Emission Spectrometer (Vista). I also computed the mineral saturation states for calcite, aragonite, dolomite, and siderite in the pore-fluid to better understand which mineral is thermodynamically favored to precipitate in the salt-marsh environment. Electrical balance, DIC, and saturation index were computed by PHREEQC using *Wateq4f* database for stability constants. The Davies equation was used for activity coefficients of ion complexes for high ionic strength samples.

Sulfur isotope measurement of the pore fluid sulfate was performed by adding 1mL of saturated BaCl_2 (300 mM) to filtered pore fluid samples to precipitate aqueous sulfate as barite (barium sulfate). For determination of $\delta^{34}\text{S}_{\text{H}_2\text{S}}$, sulfide (fixed with ZnOAc) was reacted with silver nitrate (AgNO_3) to form Ag_2S . The sulfur isotopic composition of the resultant Ag_2S is measured to yield $\delta^{34}\text{S}_{\text{H}_2\text{S}}$. Sulfur isotopic ratios in sulfate ($\delta^{34}\text{S}_{\text{SO}_4}$) and sulfide ($\delta^{34}\text{S}_{\text{H}_2\text{S}}$) were analysed after combustion on a Flash Element Analyser (Thermo Scientific) using a Thermo Finnigan Delta-V-Plus IRMS. The sulfur isotopic composition was corrected based on standards (NBS 127 for sulfate – 20.3 ‰ and SO-6 for sulfide – 6.1 ‰) and reported in standard delta notation as per mil (‰) deviation from Vienna Canyon Diablo Troilite (VCDT).

6.2.4 Incubation experiment with pure Norfolk salt-marsh sediment

Two sets of incubation experiments were conducted using fresh sediment samples from Blakeney and Warham. Both incubation experiments were set up to explore the evolution of aqueous chemistry and the precipitation of carbonate minerals in an environment that mimics the salt-marsh subsurface sediment. In the first incubation experiment, microbial sulfate reduction was retarded using molybdate whereas microbial sulfate reduction was not restricted in the second incubation experiment (Table 6.1).

In the first set of incubation experiments, two 10 cm^{-3} Blakeney sediments were incubated in 50 mL sealed reaction vessels. Approximately 100 mM of formate and acetate were used as sole electron donor in each of the incubation samples. The medium was made of pond water collected from the salt-marsh and 2.5 mL of yeast extract (0.5% w/v). The samples were

degassed with a 90% N₂/10% CO₂ mixed gas for 20 minutes. One millimolar of sodium molybdate was added to both samples to inhibit microbial sulfate reduction. The medium chemistry was monitored over 42 days and the mineralogy of the sediment was analysed at the end using XRD. No control experiment was run.

In the second incubation experiment, 10 cm⁻³ of the Warham sediment was also used. Four samples were set up which includes two replicates and two controls. Diluted seawater (50% seawater strength) was used as the medium to mimic the aqueous solution in the salt-marsh core. Sodium acetate was added to the medium to make up a concentration of approximately 10 mM; this is both the electron and carbon donor. Two steel balls (5 mm in diameter) and 0.4 – 0.5 g of wood were included in the incubated samples to serve as a source of iron and as a nucleus for carbonate mineral precipitation. The steel balls and wood were buried in the sediments in both replicates and one of the controls. The other control sample contained only the medium and a steel ball to examine how much iron is abiotically released into the solution from the steel ball. Then, the reaction vessels were sealed and degassed with 90% N₂/10% CO₂ mixed gas for 5 minutes. All control samples were autoclaved twice to eliminate biological activities.

Table 6.1: Summary of the materials and setup in the first and second incubation experiments.

Incubation samples	Sediment source	Medium	Electron donors	Gas	Nucleation materials	Note
First Incubation Experiment						
Formate	Blakeney	Pond water	Formate	90% N ₂ /10% CO ₂	None	Na ₂ MoO ₄ added
Acetate	Blakeney	Pond water	Acetate	90% N ₂ /10% CO ₂	None	Na ₂ MoO ₄ added
Second Incubation Experiment						
Replicate 1	Warham	Diluted seawater	Acetate	90% N ₂ /10% CO ₂	Two steel balls, wood	50% strength seawater
Replicate 2	Warham	Diluted seawater	Acetate	90% N ₂ /10% CO ₂	Two steel balls, wood	50% strength seawater
Killed control (without sediment)	None	Diluted seawater	Acetate	90% N ₂ /10% CO ₂	One steel ball	50% strength seawater
Killed control (with sediment)	Warham	Diluted seawater	Acetate	90% N ₂ /10% CO ₂	Two steel balls, wood	50% strength seawater

6.2.5 Magnetic susceptibility in the salt-marsh

To map the magnetic susceptibility in the salt-marsh in an attempt to map the location of the siderite concretions, I used a single axis gradiometer (Grad601-1) which was on loan from

Bartington Instruments Ltd. The gradiometer I used contains two magnetometers (one at the top and one facing the surveyed ground) that measure magnetic susceptibility. In particular, the bottom-facing magnetometer serves as the main sensor to measure small variations in the magnetic field that are caused by hidden anomalies in the subsurface sediment. The depth of penetration of the signal is one meter however this depth depends largely on the soil properties. The sensitivity of the instrument is 0.03 nT m^{-1} and the calibration error is $\pm 2 \%$ (Grad601, 2018). I set up a series of survey grids with lines spaced at 1 m of $10 \times 10 \text{ m}$ (Figure 6.3), using a normal walking pace covering the grid in a zigzag traverse. The field data were recorded in the data-logger and retrieved for post-collection processing. The software Surfer was used to process the data and plot the data into contour map for further interpretation. The raw data were treated using the destripe function to eliminate the stripes (positive and negative values) which arose from the alternate traverse. To destripe the data, I used median values from each traverse and subtract it with the original values and then interpolate the data in a map using the kriging algorithm. The location and details of the surveyed grids are given in Table 6.2.

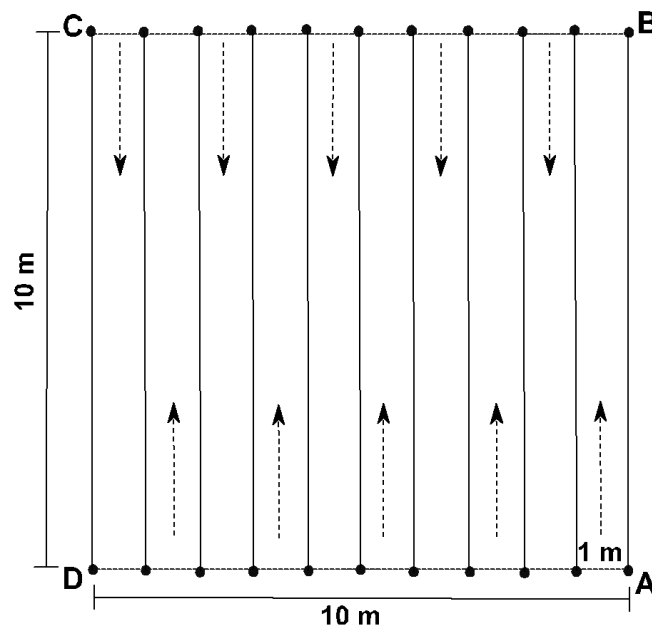


Figure 6.3: Schematic drawing of a grid. The arrows indicate the traverse direction (in zigzag mode).

Table 6.2: Grids surveyed in the salt-marsh, GPS locations and information of the grids.

Grid Number	Marsh/Date of survey	GPS Coordinates	Notes/Gradient range
16	Blakeney (26/12/15)	A = N 52.95615°; E 001.00468° B = N 52.95607°; E 001.00462° C = N 52.95620°; E 001.00455° D = N 52.95610°; E 001.00449°	Concretion buried at middle of Traverse 5 (100 nT m ⁻¹)
19	Warham (27/12/15)	A = N 52.96766°; E 000.89368° B = N 52.96774°; E 000.89370° C = N 52.96775°; E 001.89356° D = N 52.96767°; E 001.89354°	No concretion buried. (100 nT m ⁻¹)
20	Warham (27/12/15)	A = N 52.96766°; E 000.89368° B = N 52.96774°; E 000.89370° C = N 52.96775°; E 001.89356° D = N 52.96767°; E 001.89354°	Concretion buried at middle of Traverse 5 (100 nT m ⁻¹)
21	Warham (27/12/15)	A = N 52.96764°; E 000.89333° B = N 52.96774°; E 000.89335° C = N 52.96775°; E 000.89319° D = N 52.96766°; E 000.89317°	Concretion buried at middle of Traverse 2; huge metal core concretion at Traverse 8 (100 nT m ⁻¹)
23	Stiffkey (28/12/15)	A = N 52.95956°; E 000.93854° B = N 52.95964°; E 000.93858° C = N 52.95966°; E 000.93844° D = N 52.95958°; E 000.93841°	Concretion on surface of Traverse 5 (100 nT m ⁻¹)
25	Stiffkey (28/12/15)	A = N 52.95956°; E 000.93854° B = N 52.95964°; E 000.93858° C = N 52.95966°; E 000.93844° D = N 52.95958°; E 000.93841°	No concretion on this grid (100 nT m ⁻¹)
26	Stiffkey (28/12/15)	A = N 52.95745°; E 000.93516° B = N 52.95756°; E 000.93516° C = N 52.95755°; E 000.93500° D = N 52.95746°; E 000.93502°	Concretion on surface of Traverse 5 (100 nT m ⁻¹)
28	Stiffkey (28/12/15)	A = N 52.95745°; E 000.93516° B = N 52.95756°; E 000.93516° C = N 52.95755°; E 000.93500° D = N 52.95746°; E 000.93502°	No concretion (100 nT m ⁻¹).
29	Blakeney (29/12/15)	A = N 52.95668°; E 001.00379° B = N 52.95676°; E 001.00381° C = N 52.95678°; E 001.00365° D = N 52.95671°; E 001.00364°	Concretion on surface of Traverse 5 (100 nT m ⁻¹)
31	Blakeney (29/12/15)	A = N 52.95668°; E 001.00379° B = N 52.95676°; E 001.00381° C = N 52.95678°; E 001.00365° D = N 52.95671°; E 001.00364°	No concretion (100 nT m ⁻¹).

6.2.6 Transformation experiment

To investigate the transformation and stability of MHC to other, more rare carbonate minerals, I subjected the MHC to elevated temperatures in different aqueous solutions: seawater and other modified media (Table 6.3). Approximately 0.02 g of either or both MHC and calcite seeds were heated under different media in sealed bottles at 100°C for 48 hours (Munemoto

and Fukushi, 2008; Liu et al., 2013). Control samples were set up without seeds included. For samples with ferrous iron incubated under anoxic condition in a 5 ml vial, the media were degassed with N₂ for 10 minutes. The solution was analysed for pH, alkalinity, iron, major cations and anions before and after the transformation experiment. Solid phase samples were collected, dried and analysed for its morphology and mineralogy using SEM and XRD, respectively.

Table 6.3: Summary of the initial media and mineral seeds used in the transformation experiments. Incubation samples with varying iron concentrations were labelled as medium in the initial and followed by the concentration of iron in millimolar. For example, MQ50 indicate the medium is MQ-water with 50 mM of iron. SW denotes seawater as the medium. MQ100 – SW10 were incubated under anoxic condition to make sure ferrous iron is in its dissolved form. Initial CaCO₃ with MHC/Calcite indicates that the initial media is incubated with MHC or calcite (marked with a different colour in the table) and a seedless control in separated vials, therefore, one line on the table, or one type of media may represent three samples.

Samples	pH	Alk (mEq/L)	Ca ²⁺ (mM)	Initial Concentration				Mg/Ca	Medium	Initial CaCO ₃	Initial CaCO ₃ Polymorphs (wt %)					Sdr
				Mg ²⁺ (mM)	Fe ²⁺ (mM)	PO ₄ ³⁻ (μM)	SO ₄ ²⁻ (mM) [§]				C	Mg-C	MHC	A	V	
T05a	8.42	106.225	0.78	53.79	-	429.37	B.D.L	69.28	Medium	MHC	-	-	100	-	-	-
T05b [^]	8.42	106.225	0.78	53.79	-	429.37	B.D.L	69.28	Medium	MHC	-	-	100	-	-	-
T06	7.04	11.012	12.63	24.23	-	137.55	B.D.L	1.92	M.Medium	MHC	-	-	100	-	-	-
T07 [*]	7.99	2.722	10.38	53.02	-	133.83	24.02	5.11	Seawater	MHC	-	-	100	-	-	-
T08	8.64	4.825	8.46	35.36	-	532.54	30.42	4.18	Artificial SW	MHC	-	-	100	-	-	-
T09	8.31	99.791	14.02	47.67	-	429.37	B.D.L	3.40	Medium	MHC	-	-	100	-	-	-
T10	8.65	49.709	0.35	24.02	-	318.78	B.D.L	68.16	Medium+MQ	MHC	-	-	100	-	-	-
T11a	6.57	2.109	10.29	52.72	4.21	-	25.59	5.12	Seawater	MHC	-	-	100	-	-	-
T11b	4.52	6.119	< 0.01	< 0.01	4.84	-	B.D.L	-	M.Medium	MHC	-	-	100	-	-	-
T11c	3.18	5.227	< 0.01	< 0.01	55.63	-	B.D.L	-	M.Medium	MHC	-	-	100	-	-	-
T12	7.42	1.656	< 0.01	101.15	-	125.47	B.D.L	Inf.	M.Medium	MHC	-	-	100	-	-	-
T13	6.85	10.163	10.86	56.02	-	129.18	28.54	5.16	Seawater+F	MHC	-	-	100	-	-	-
MQ50 [*]	3.02	1.780	< 0.01	< 0.01	50.55	-	-	-	M.Medium	MHC/Calcite	100	-	100	-	-	-
SW50 [*]	3.65	1.625	10.80	55.36	53.64	-	-	5.13	M.Medium	MHC/Calcite	100	-	100	-	-	-
MQ100	2.67	2.450	< 0.01	< 0.01	98.57	-	B.D.L	-	M.Medium	MHC/Calcite	100	-	100	-	-	-
MQ50	3.02	8.278	< 0.01	< 0.01	50.63	-	B.D.L	-	M.Medium	MHC/Calcite	100	-	100	-	-	-
MQ25	3.39	7.301	< 0.01	< 0.01	25.78	-	B.D.L	-	M.Medium	MHC/Calcite	100	-	100	-	-	-
MQ10	7.20	13.283	< 0.01	< 0.01	11.03	-	B.D.L	-	M.Medium	MHC/Calcite	100	-	100	-	-	-
SW100	2.97	3.979	10.41	53.12	105.04	-	22.07	5.10	M.Medium	MHC/Calcite	100	-	100	-	-	-
SW50	4.33	5.158	10.53	53.98	48.74	-	17.68	5.12	M.Medium	MHC/Calcite	100	-	100	-	-	-
SW25	5.20	6.503	10.49	52.91	23.67	-	23.68	5.04	M.Medium	MHC/Calcite	100	-	100	-	-	-
SW10	6.78	12.948	10.83	54.75	9.74	-	-	5.05	M.Medium	MHC/Calcite	100	-	100	-	-	-

^{*}Samples incubated under oxic condition.

MHC/Calcite indicate that the initial CaCO₃ for transformation is MHC and calcite. Both MHC and calcite were incubated in separate vials.

B.D.L. indicates below detection limit

6.3 Results and discussion

I present the results from this study as follows. I will present and discuss the results of each part, individually, starting with the mineralogy and geochemistry of the concretions, then the pore water chemistry, then the magnetic susceptibility mapping, then the incubations with the Norfolk sediment, and finally the transformation experiments. I will finish with a summary tying all the presented results together to discuss the formation of siderite samples in the Norfolk salt-marshes.

6.3.1 Concretion mineralogy and geochemistry

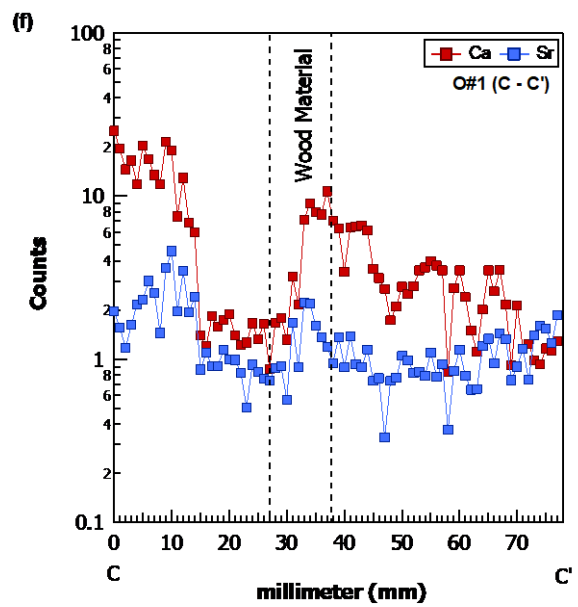
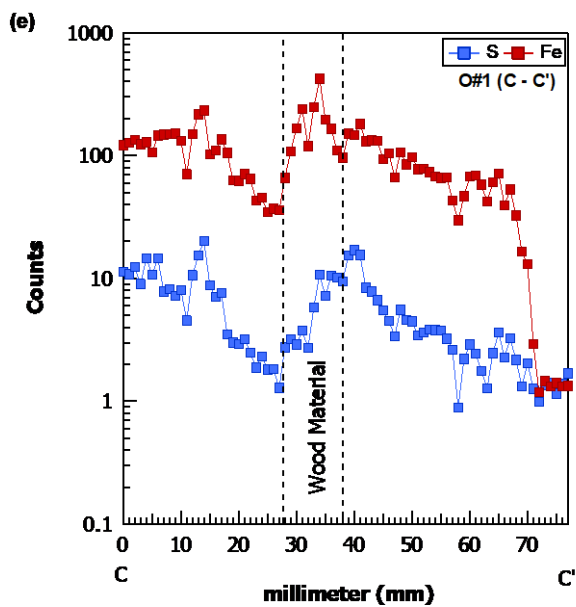
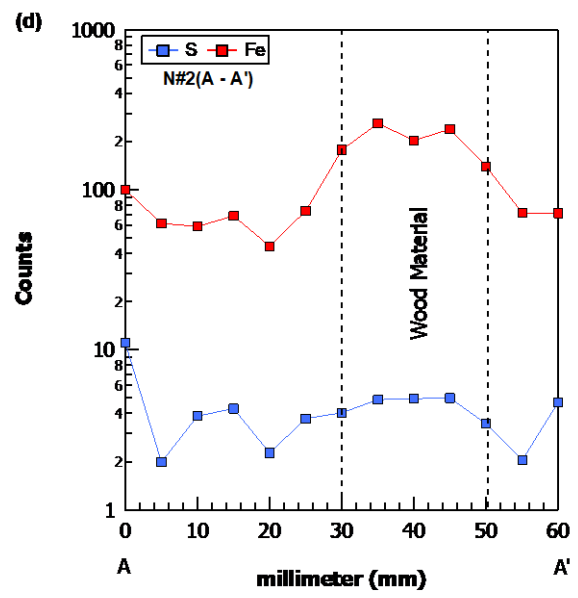
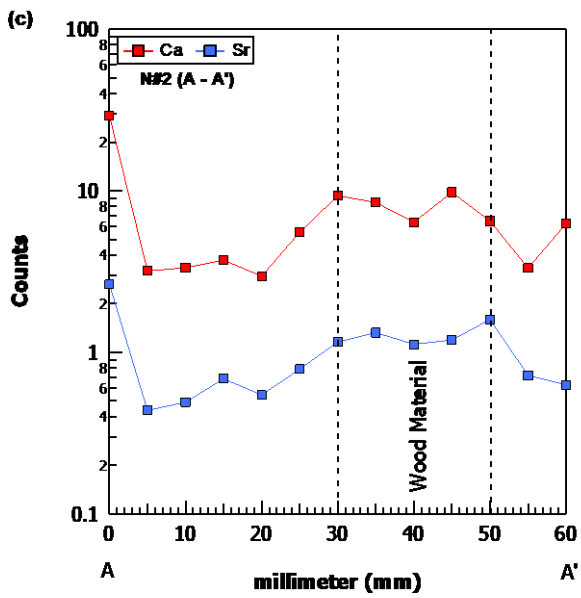
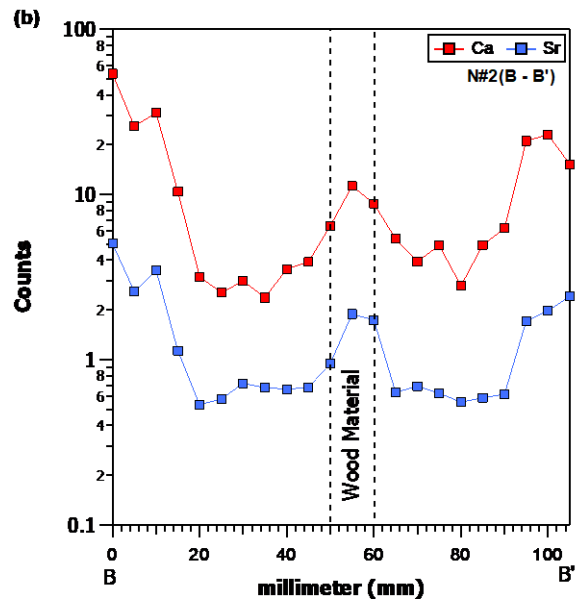
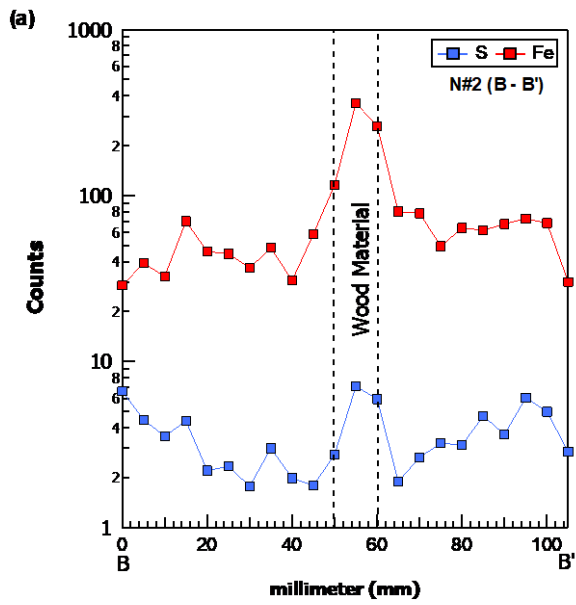
The concretions in the Warham salt-marsh typically nucleate around wood ($n = 4$). I opened up four concretions but only two have been analysed for its geochemistry. No clear inner core or outer core (or laminations) can be seen in either of the concretions that I analysed geochemically. Laminations only become clear at the edge of sample N#2. The texture of both concretions are different, where O#1 comprises sand-size grains while N#1 is mainly composed of very fine sand. Biological signatures such as roots and burrows are present in sample O#1, suggesting that this concretion may have formed at relatively shallow sediment depth in the marsh. A black/dark coloured region is visible towards the edge of the concretion whereas the brown/reddish region often surrounds the nucleus. XRD on bulk samples indicates the concretions are largely comprised of siderite, quartz, high magnesium calcite, orthoclase, albite and small amount of pyrite (Table 6.4). Gypsum, greigite, and dolomite were also observed in parts of the concretions in much smaller quantities. Quartz is the predominant mineral (> 50%); the remainder is mostly carbonate minerals such as siderite (6 – 27%) and high magnesium calcite (5 – 47%). These carbonate minerals likely play a substantial role in the cementation processes of the quartz sands. The dark-colored regions of the concretions are enriched with carbonate minerals, while the brown coloured samples are dominated by quartz and silicate minerals. No ankerite was detected in the samples.

Table 6.4: Weight percentages of phases for concretion samples with relative e.s.d. (in parenthesis). Additional samples collected from the concretions (not shown in Figure 6.2) were homogenized, and analysed in bulk. Abbreviation of the samples are given in the Table's footnote. Sample O#1 is shaded in grey.

Sample	Quartz	Siderite	Mg-Calc	Greigite	Orthoclase	Albite	Gypsum	Pyrite	Dolomite	R_{wp}	χ^2
IR (N#1)	86.7 (±1.6)%	-	-	-	-	-	13.3 (±1.6)%	-	-	40.06	1.57
N2 (N#1) B	40.8 (±1.3)%	-	47.2 (±1.6)%	-	8.2 (±2.5)%	-	-	-	3.8 (±0.9)%	9.30	1.81
N8 (N#1) Br	60.5 (±2.5)%	14.0 (±1.4)%	5.4 (±1.5)%	6.1 (±1.4)%	14.0 (±2.6)%	-	-	<0.1 (±0.8)%	-	4.33	1.35
O3 (O#1) B	72.6 (±1.1)%	27.4 (±1.1)%	-	-	-	-	-	-	-	5.02	1.52
O4 (O#1) Br	78.7 (±3.8)%	-	-	-	12.9 (±3.3)%	5.9 (±2.5)%	-	2.5 (±1.5)%	-	6.30	2.08
OR (N#1)	32.0 (±0.9)%	6.6 (±0.8)%	36.1 (±1.2)%	2.7 (±0.7)%	3.2 (±1.5)%	13.1 (±1.2)%	6.4 (±0.8)%	-	-	6.21	1.59
N#SB (OB)	43.9 (±1.0)%	-	49.8 (±1.2)%	-	-	6.3 (±1.5)%	-	-	-	9.49	2.77
N#SB	53.0 (±1.3)%	-	47.0 (±1.3)%	-	-	-	-	-	-	10.50	3.35
O#SB	59.1 (±0.9)%	-	40.9 (±0.9)	-	-	-	-	-	-	8.19	2.60
PWood (N#1)	40.5 (±2.7)	56.8 (±3.4)%	2.7* (±5.1)%	-	-	-	-	-	-	2.42	1.24
N#MBr	35.3 (±1.2)%	7.2 (±0.8)%	25.6 (±1.3)%	-	9.1 (±1.9)%	18.8 (±1.6)%	4.0 (±0.7)%	-	-	5.39	1.96
N#SB1	46.6 (±2.9)%	9.7 (±1.6)%	10.0 (±2.4)%	-	11.2 (±3.6)%	21.8 (±2.7)%	0.7 (±1.4)%	-	-	6.47	3.08
N#SBr1	46.5 (±2.0)%	10.5 (±1.2)%	-	-	5.0 (±2.5)%	32.3 (±1.9)%	5.4 (±1.0)%	-	-	4.90	2.39
O6 (Bulk)	46.0 (±1.7)%	26.4 (±1.2)%	10.3 (±1.4)%	-	5.6 (±1.9)%	9.4 (±2.1)%	2.3 (±0.9)%	-	-	4.58	2.06
O7 (Bulk)	45.8 (±2.5)%	17.8 (±1.4)%	5.6 (±2.1)%	-	12.8 (±3.0)%	15.5 (±2.3)%	-	-	2.5 (±1.7)%	7.72	3.31

* Vaterite

Abbreviation of samples: O = sample O#1; N = sample N#1; M = Inner core of the concretion; S = Edge of the concretions; B = Black colour region; Br = Brownish/reddish coloured region; Pwood = region next to wood material in N#1; O6 and O7 = bulk samples collected at random place of the sample O#1.



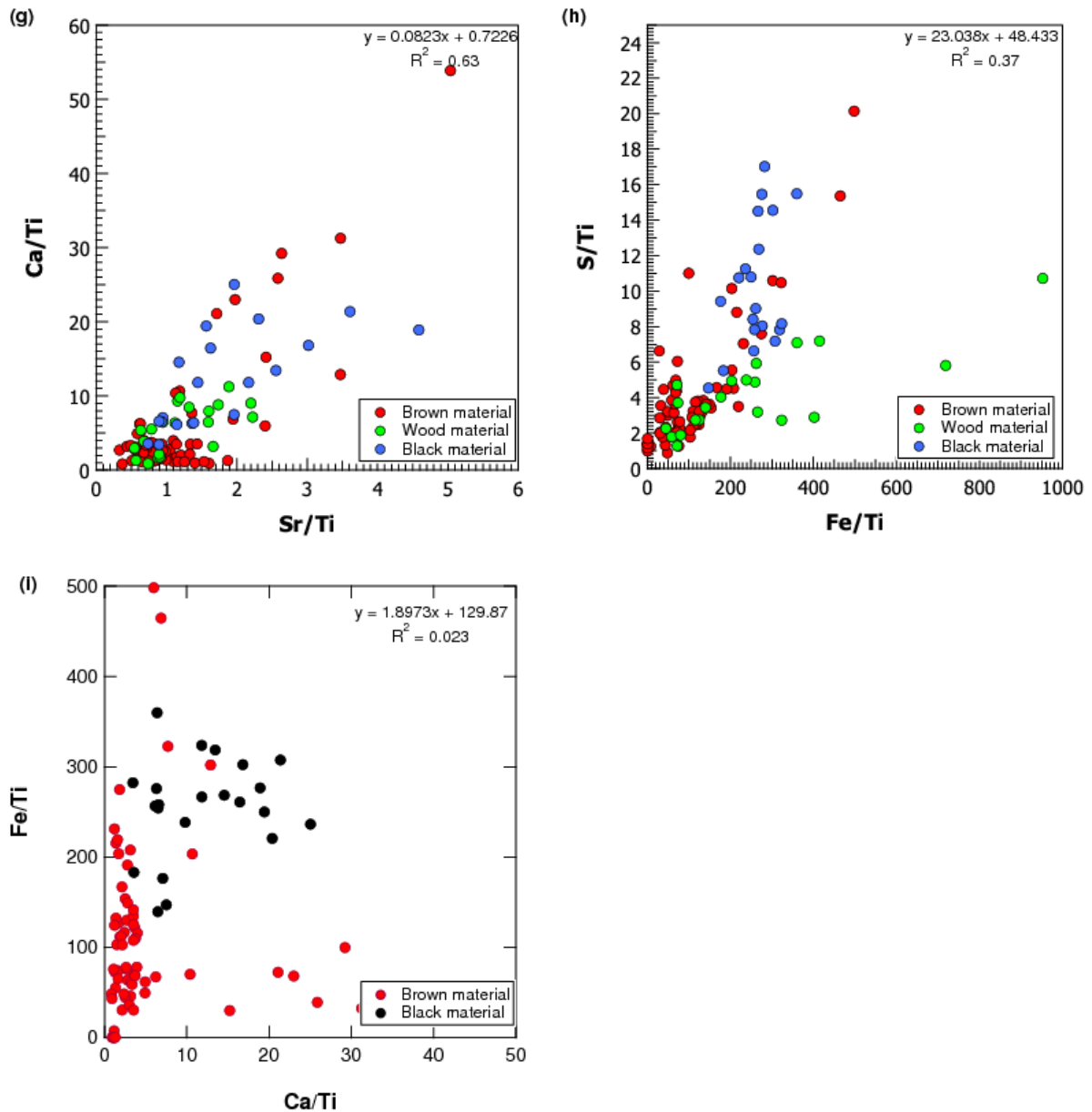


Figure 6.4: Elemental distribution along the cross-section of the concretions (a – f), x-axis in centimeters; and cross-plots with titanium normalized (g, h and i) of the studied elements. Note that higher resolution of scanning is done across transect C of concretion O#1.

The XRF results indicate that the concentration of iron in the concretions is around an order of magnitude higher than the concentration of calcium or sulfur and two orders of magnitude higher than the concentration of strontium (Figure 6.4a, d). Iron and sulfur content are highly enriched in the middle of the concretion but decreases towards the edge of the concretion, while the concentrations of calcium, and strontium are lowest at the center and increase towards the edge. This is shown particularly clearly in sample O#1 (transect C – C') where the abundance of calcium drops significantly between 70 – 85 cm region correspond to the reddish/brownish (sideritic) region of the concretion, whereas high calcium abundance is seen


in places where the black (calcite) region is (Figure 6.4f). The cross plot shows a moderate correlation between calcium and strontium ($R^2 = 0.63$) (Figure 6.4g). Iron and sulfur demonstrate good correlation ($R^2 = 0.76$) among different nodules without taking the wood material into account, this strong correlation is likely due to the presence of iron sulfide minerals within the concretions. The correlation between iron and sulfur, however, drops dramatically ($R^2 = 0.37$) when the wood materials are included. As expected, a weak correlation was found between iron and calcium ($R^2 = 0.023$) (Figure 6.4i). The cross plot shows that the brown material is relatively enriched in iron but low in calcium. Whereas the black material is both high in iron and calcium, suggesting that calcium carbonate was the main mineral and precipitated with iron confined to iron sulfides – yielding the dark color.

The innermost part of the concretion is mainly composed of siderite which likely forms in an environment rich in ferrous iron. The precipitation of siderite in the inner layer depletes the concentration of ferrous iron, which may create a gradient of decreasing iron concentrations away from the center of the nodule. This causes the Fe/Ca to decrease and ultimately towards the edge, the precipitation of calcium carbonate is favoured over iron carbonate. This explains the relatively greater abundance of Mg-Calcite at the outer layer of the concretion.

In general, in carbon isotopes two isotopically distinct layers were observed across the concretion, the isotopically higher inner layer (mean $\delta^{13}\text{C}_{\text{carbonate}} = -4.8\text{‰}$) and the isotopically lower outer layer (mean $\delta^{13}\text{C}_{\text{carbonate}} = -11.8\text{‰}$) (Table 6.5). The $\delta^{18}\text{O}_{\text{carbonate}}$ does not show clear patterns across the nodule and reflects both the isotope composition of the water and the temperature of carbonate mineral formation, neither of which seems to change over the growth of the concretion in any systematic way.

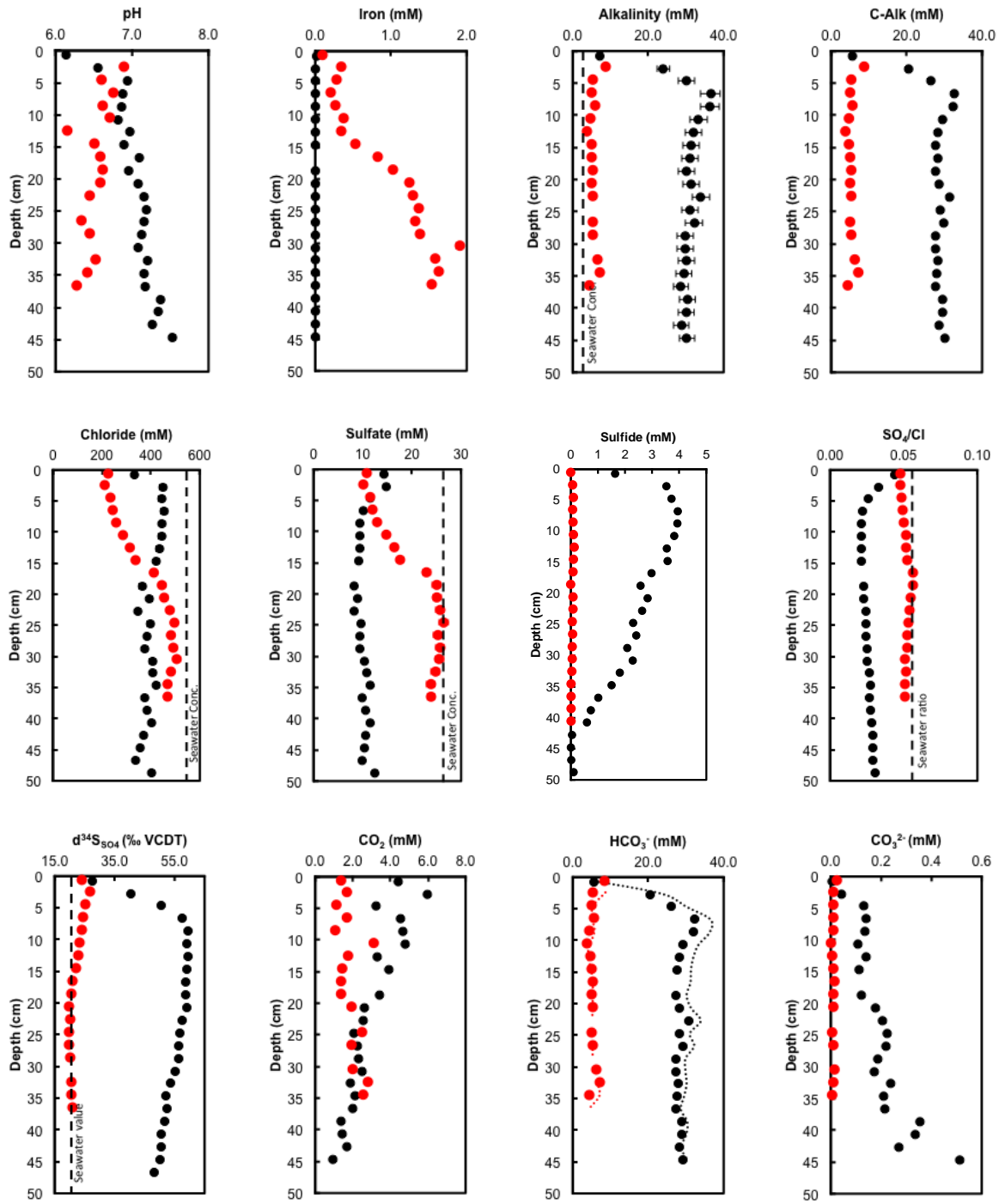
The change in the $\delta^{13}\text{C}_{\text{carbonate}}$ reflects a change in the $\delta^{13}\text{C}$ of the dissolved inorganic carbon (DIC) pool from which the concretion is growing. Assuming that the carbon isotope fractionation from DIC into siderite is similar as it is into high-magnesium calcite, the DIC pool decreases by close to 7‰ over the growth of the concretion. The $\delta^{13}\text{C}$ of the DIC will decrease due to the oxidation of organic carbon, which adds ^{12}C -rich carbon to the pore fluids; a typical pore fluid profile of $\delta^{13}\text{C}$ of DIC in the absence of methanogenesis decreases from 0‰ near the surface to -10 to -12‰ at depth. This change in the $\delta^{13}\text{C}$ of the concretion could reflect the depth of growth, where the concretion nucleates closer to the surface where the $\delta^{13}\text{C}$ of the DIC is more similar to the overlying pond water ($\delta^{13}\text{C}_{\text{DIC}}=0\text{‰}$), and then later grows deeper, where the $\delta^{13}\text{C}$ of the DIC has evolved to a lower overall carbon isotope composition. Alternatively, if the depth of concretion growth hasn't changed, then it could reflect the amount of respired organic carbon or the intensity of local microbial activity.

Table 6.5: Selected locations (C1 – C8) of concretion N#2 with interval approximately 1-2 mm were drilled across from the center to the edge of the concretion. The drilled materials were examined for carbon and oxygen isotopic composition in the Godwin Laboratory. W1 is wood materials located at the center of the concretion; C9 was sampled near to the edge of the concretion where the dark and extremely rigid material is.

	Sampling point	$\delta^{13}\text{C}_{\text{carb}}$ ‰ PDB	$\delta^{18}\text{O}_{\text{carb}}$ ‰ PDB
	W1	-6.45	0.66
	C1	-1.04	-0.51
	C2	-5.54	0.05
	C3	-7.86	0.75
	C4	-12.21	1.69
	C5	-11.14	-0.36
	C6	-11.58	-0.49
	C7	-12.43	0.28
	C8	-11.12	-0.35
	C9	-12.31	0.04

6.3.2 Pore fluid geochemistry

The results of pore-fluid chemistry for the two salt-marsh ponds are shown in Figure 6.5. The data in red are results from the iron-rich pond and the one in black represent the sulfidic pond. The ponds exhibit distinct pore fluid geochemistry. The iron-rich pond has a slightly lower pH, higher dissolved iron concentration and an absence of aqueous sulfide. On the other hand, the sulfidic pond is characterized by higher alkalinity, high concentration of aqueous sulfide and an absence of dissolved iron. The porewater chemistry changes with depth, suggesting different geochemical processes are occurring in the upper and lower sediment layer. Bacterial sulfate reduction is a major process in the sulfidic pond reflected by the higher $\delta^{34}\text{S}_{\text{SO}_4}$ relative to seawater (20 ‰), high alkalinity and the low SO_4/Cl ratio (seawater ratio is about 0.05). The formation of siderite minerals is unlikely in this sulfidic pond due to the lack of ferrous iron. In the iron-rich pond, the concentration of dissolved ferrous iron increases to close to 2 mM at a depth of 30 cm whilst sulfide concentration was almost non-detectable.



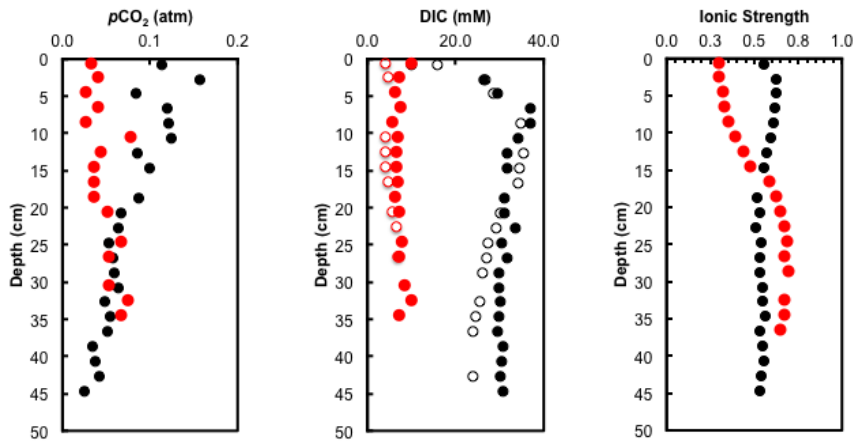


Figure 6.5: Geochemical data of pore-fluid in the salt-marsh. Note that the red color dots represent iron-rich core while black colored data belongs to sulfidic core. CO_2 , HCO_3^- , CO_3^{2-} , $p\text{CO}_2$, DIC were calculated using CO2Calc. Dissolved iron data for sulfidic core were obtained from ICP-OES. C-Alk (carbonate alkalinity) was calculated by subtracting the sulfide concentration from alkalinity data. Ionic strength was manually calculated with a concentration of Ca^{2+} , Mg^{2+} , Na^+ , K^+ and SO_4^{2-} , Cl^- measured in the pore-fluid using the equation $I = \frac{1}{2} \sum m_i \cdot z_i^2$. Dotted lines plotted along the bicarbonate are the alkalinity. The open circle is the measured DIC concentration of different sediment cores from the salt-marsh while the filled circle is my calculation (Warham – Red; and Blakeney - Black). The DIC measurement (open circle) was previously done by Gilad Antler.

6.3.3 Mineral saturation state in the sedimentary pore fluids

The electrical imbalance of the pore fluid is likely due to the lack of negatively charged ions such as F^- , Br^- , NO_3^- and H_2PO_4^- in the analysis (Figure 6.6). Due to missing data and/or analytical errors, chemical analyses of natural waters is rarely electrically charge balanced (Plummer et al., 1991). Both DIC calculated by CO2Calc and PHREEQC show good agreement (Figure 6.6). The calculation of mineral saturation state shows that the pore-fluid in Warham (the iron-rich core) is in equilibrium with respect to siderite and undersaturated with calcite, aragonite, and dolomite. This suggests that siderite is the more favourable carbonate mineral to precipitate in the iron-rich Warham salt-marsh sediment relative to other carbonate minerals. Also, the formation of siderite limits DIC concentration to values where $\Omega < 1$ for calcium carbonates. In the sulfidic core, the porewater is slightly undersaturated with respect to calcite, aragonite, and siderite, although dolomite is slightly oversaturated. I note that siderite does not exceed saturation based on the concentration of DIC and ferrous iron in the North Norfolk salt-marsh sediments. This suggests that the concretions nucleate when the

concentration of ferrous iron in the porewater is even higher than has been measured, and then grow when the Ω_{siderite} is close to unity.

One interesting result was that pyrite is notably absent when I did an XRD of the sediment in the salt-marsh in my first year – in the sulfide-rich core the iron-sulfide minerals are largely iron monosulfide, and not pyrite (Appendix G). This contradicts the results from Mills et al., (2016) who was able to extract pyrite using a chromium reduction solution from the same salt-marsh sediments. Pyrite does precipitate in circum-neutral salt-marshes (Luther et al., 1982; Marnette et al., 1993) and highly reduced soils (Brennan and Lindsay, 1996) and its formation is controlled by the presence of sulfide and iron, as well as the overall pH and Eh (Howarth, 1978; Todorova et al., 2005). The formation of pyrite is seen in incubation samples of the sediments in anoxic condition which will be discussed in the following section.

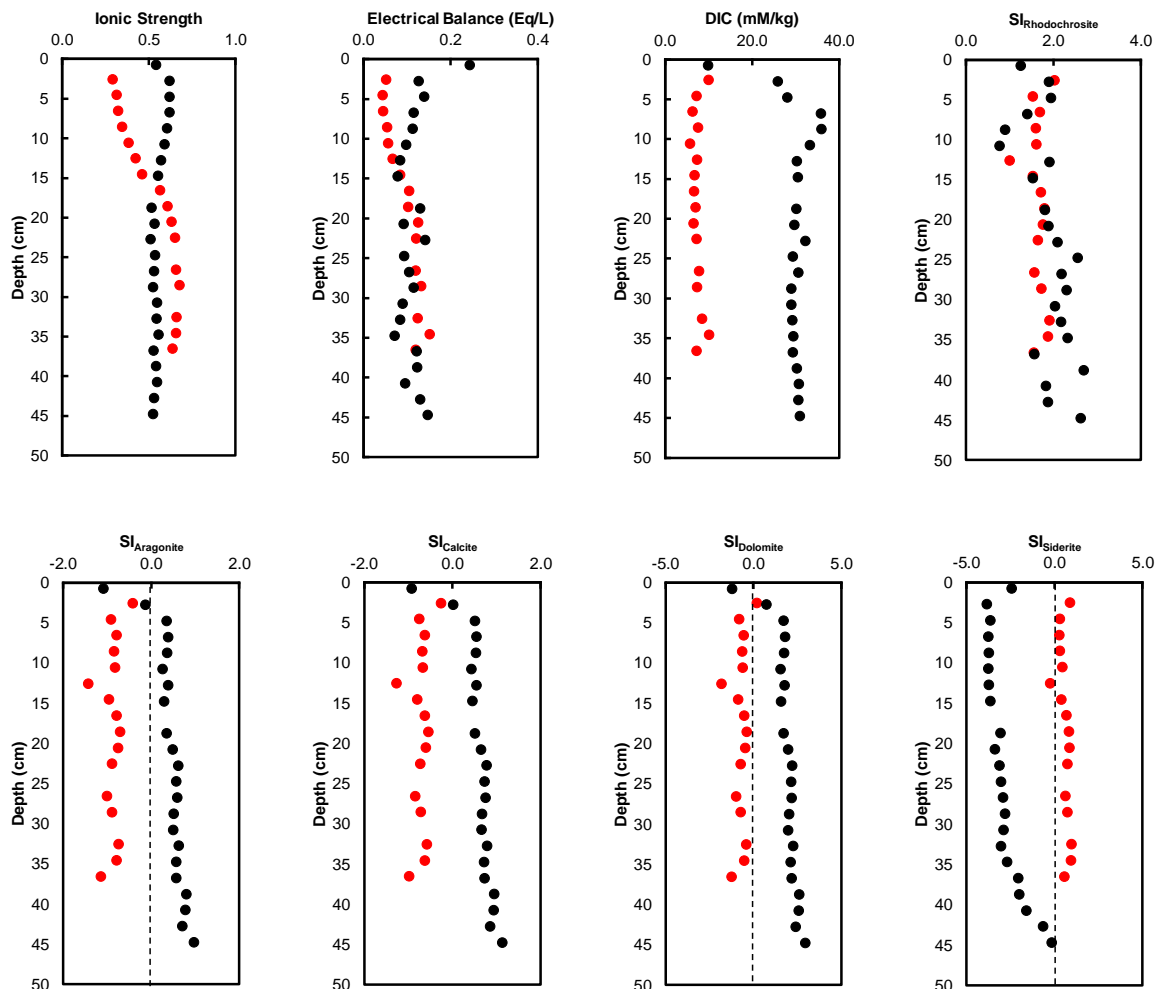
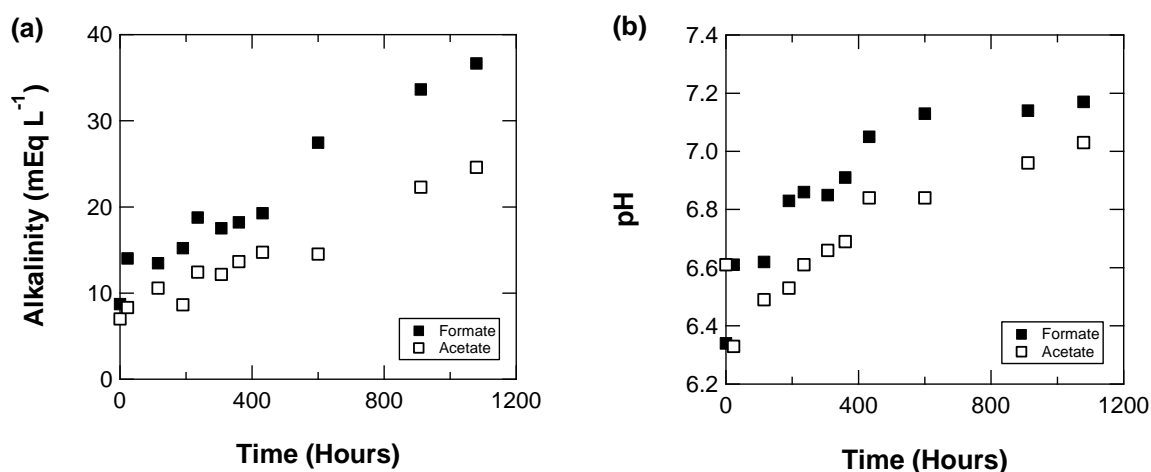


Figure 6.6: Saturation states (Ω) of various minerals in the salt-marsh. If $SI < -0.2$, the porefluid is undersaturated with respect to that particular mineral. While $SI = -0.2 \leq 0 \leq 0.2$, it means

that the pore-fluid is in equilibrium with that mineral. If $SI > 0.2$, this indicates that the pore-fluid is oversaturated with respect to that mineral.

6.3.4 Incubation experiments with Norfolk sediment

The first incubation experiment shows a gradual increase in pH and alkalinity in both samples with added formate and acetate, in spite of the presence of molybdate, which stops the activity of the sulfate-reducing bacteria (Figure 6.7). The alkalinity and pH in the sample with added formate increase to greater values than in the incubation with added acetate, supporting the idea that the types of electron donors influence the pH and the activity of iron-reducing bacteria (Gallagher et al., 2012). A marked increase in alkalinity and pH, coupled with a decrease in iron concentration at 600 hours suggest the occurrence of microbial sulfate reduction. It is possible that the relatively low concentration of sodium molybdate (Na_2MoO_4) used to delay microbial sulfate reduction lost its effectiveness after 600 hours of incubation allowing the dormant sulfate-reducing bacteria to revive and metabolize. As expected, when microbial sulfate reduction begins, I see a decrease in iron concentration due to the removal of iron to form iron monosulfide. Another interesting observation is that the ferrous iron concentration reaches a higher concentration in the sample with acetate compared to the sample with formate. This could be explained by two possibilities: (1) the lower pH attained in the sample with acetate allows greater iron solubility (a higher concentration of iron); or (2) iron-reducing bacteria grow better on acetate rather than formate.



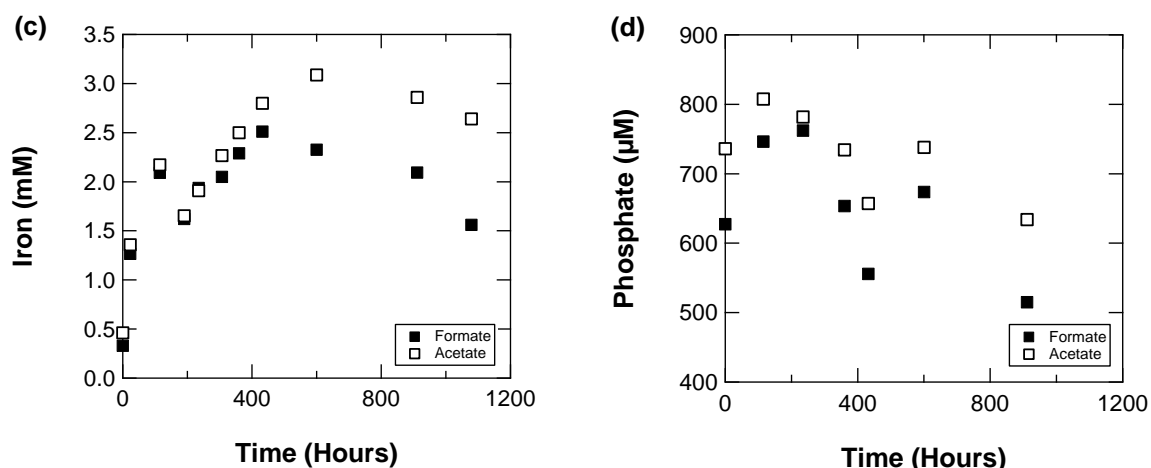


Figure 6.7: Incubation samples using Blakeney sediment samples with formate and acetate as electron donor – (a) alkalinity; (b) pH; (c) iron; and (d) phosphate. Precipitation of siderite is absent in both samples.

In the second experiment, the replicate and control samples experienced a drop in alkalinity in the first 50 hours, which could possibly be explained by the oxidation of sulfide minerals in the sediment. The alkalinity subsequently increases to a maximum of approximately 70 mEq L⁻¹ before it drops gradually or remains constant after 400 hours (Figure 6.8). The increase in alkalinity is microbially controlled as such a change in alkalinity is not observed in the control samples. The pH in the replicates also increases over the course of the incubation experiments from 6.6 to 7.2. A minor increase in pH is seen in the control samples. The iron concentration in the samples increases to 2 mM in the early stage of the incubation as a result of bacterial iron reduction. However, the decrease in iron concentration from 200 – 400 hours is also large, suggesting microbial sulfate reduction starts and hydrogen sulfide is produced which titrates out the ferrous iron in the solution. The iron in the incubation samples subsequently increases gradually to approximately 0.3 mM over the course of the experiment. The slight decrease in iron concentration in the control sample with sediment could be possibly explained by a change in iron mineral solubility as the pH also slightly increases. The increase in iron concentration in the killed control sample with steel ball suggests the release of dissolved iron from the steel ball. The iron concentration decreases after 500 hours can be explained by the precipitation of iron oxides (rust) and iron hydroxides. Ochre and reddish colour precipitates were seen in the incubation vial.

The sulfate concentration in the samples increases at the early stage of the incubation probably due to the oxidation of the sulfide minerals in the sediments. The oxidation of sulfide must be partially abiotic as the control sample (with sediment) also shows similar increase in sulfate concentration. It is unclear what the oxidant might be as the incubations were kept in

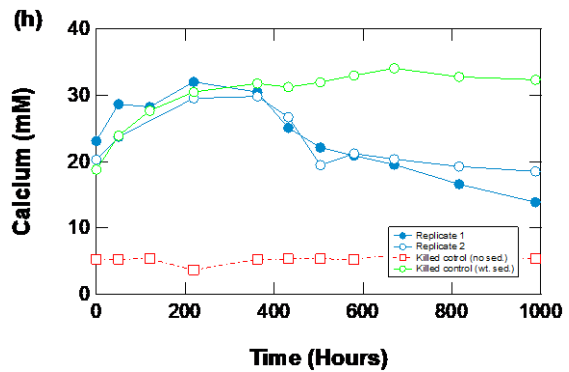
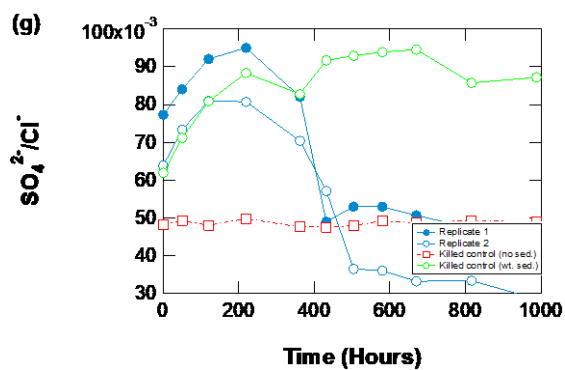
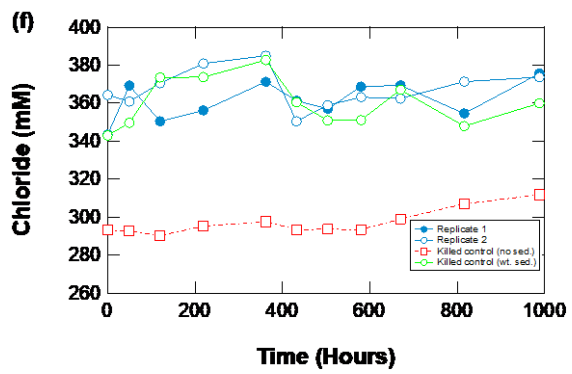
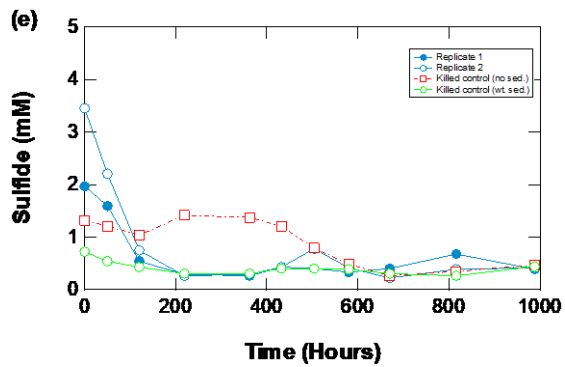
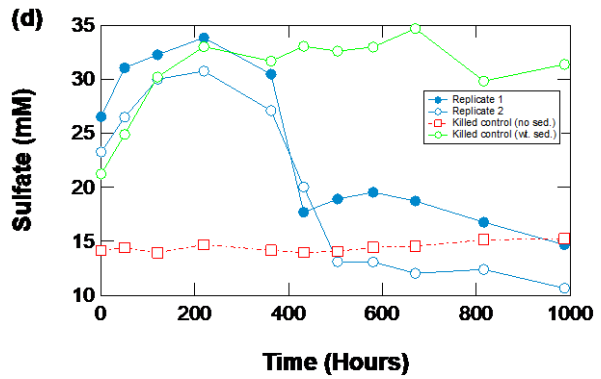
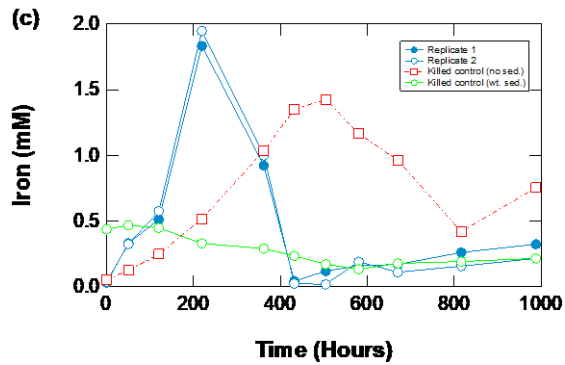
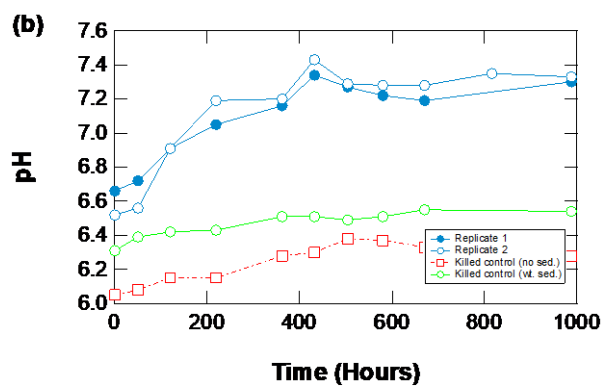
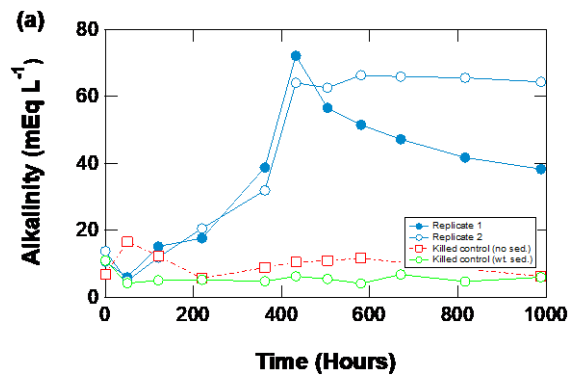
anaerobic conditions. The sulfate concentrations started to drop after 200 hours suggest the onset of microbial sulfate reduction. However, it should be noted that microbial sulfate reduction does not deplete the sulfate in the system, suggesting something limits microbial activity. Sulfide concentrations are relatively low over the course of the incubation except at the beginning of the experiment. The sulfide was removed by the increasing ferrous iron concentrations and drop to extremely low concentration after 200 hours. As expected, chloride and magnesium in all samples remain constant over the course of the incubation experiment. The substantial drops in sulfate-to-chloride ratio (in both replicates) at 400 hours further supports the onset of microbial sulfate reduction. Although the replicates begin and end with slightly different sulfate concentrations, the magnitude of change in sulfate concentration is close. The decrease in sulfate concentration is accompanied by a concurrent decrease in alkalinity and calcium concentration, suggesting the precipitation of calcium carbonate minerals. The solution of both replicates is initially undersaturated with respect to siderite. The dramatic increase in the SI_{siderite} of the replicates corresponds to the increase in the ionic activity product (IAP) of siderite, which is the iron and alkalinity. The SI_{siderite} then drop to near equilibrium when sulfate reduction kicks in before it gradually raises to an SI_{siderite} close to 1.5. It is worth mentioning that the SI_{siderite} for formate and acetate (iron-reducing dominated condition) in the first incubation experiment maintain a high saturation level of 2 – 2.5. The control samples show an SI_{siderite} close to equilibrium.

My laboratory incubation experiments show that microbial iron reduction and sulfate reduction starts as soon as the incubation was initiated. Both bacterially-mediated processes happen simultaneously suggesting the bacterial community in the East Anglian salt-marsh sediments do not follow the conventional redox tower of microbial metabolism, where sulfate reduction only happens when all ferric iron has been reduced. However, at circumneutral pH, similar to the pH in these salt-marshes, the redox tower is more complicated and bacterial iron reduction and microbial sulfate reduction converge on similar free energy yields (Bethke et al., 2011). There is a rapid increase in ferrous iron, reaching 2 mM, with ferrous iron production rate of 0.24 mM day^{-1} in the first 200 hours of incubation. Microbial sulfate reduction also progresses, however, the process was partially masked by the abiotic oxidation of sedimentary sulfide minerals at the same time, as seen in the control samples. The sulfate concentration in the control samples increases by 13 mM, while in the live samples it increases by 7-8mM, suggesting that about 6mM of the sulfide in the live sample may have been consumed microbially or that there is 6mM equivalent of microbial sulfate reduction consuming the oxidized sulfide in the live samples. This discrepancy in sulfate concentration between the live samples and killed control sample suggests a rate of microbial sulfate reduction of 0.6 mM day^{-1} , or about 2.5 times that of bacterial iron reduction. I suggest that abiotic oxidation of

sulfide, and microbial sulfate reduction coupled with active microbial iron reduction result in the following:

- (1) Sulfide minerals are oxidized and thus do not precipitate all the ferrous iron in the system.
- (2) The local microbial sulfate reduction generates alkalinity which helps in increasing the ionic activity product (specifically the concentration of carbonate ions) for siderite.
- (3) Active bacterial iron reduction increases the ferrous iron in the system which also increases the ionic activity product (the concentration of ferrous iron) for siderite precipitation.

These processes result in an increase in the concentration of iron and in the alkalinity without the accumulation of sulfide in the system, thus favoring the formation of siderite. This hypothesis agrees with work done by Pye et al. (1990), where they conclude that the formation of authigenic siderite occurs in the zone of microbial sulfate reduction in the salt-marsh sediment due to a deficiency of sulfide relative to the rate of bacterial iron reduction in the sediment. I suggest this establishes criteria for the prerequisite reactions for the formation of siderite in the salt-marsh. However, the fact that siderite nodules aren't forming everywhere in the marsh or the formation of thick siderite bed/layer suggests that the reactions above are self-limiting, likely by the presence of ferric iron and the presence and availability of a nucleus. In my incubation experiment, I found a thin layer of siderite precipitated around steel balls. I found that the formation of 2 mm of siderite in the incubation requires a month while another field study suggested it takes several months to form 10 – 40 μm siderite aggregates (Allison and Pye, 1994). Although the formation of siderite can be rapid (within weeks), the formation and growth of siderite nodules to a centimeter scale are time consuming (months to years) and the kinetics greatly depend on the degree of siderite saturation. In addition, the materials used to seed siderite is important. My incubation results show that siderite only forms on steel balls and not on wood materials whereas several types of nuclei (calcified arthropod cuticle, non-calcified arthropod cuticle, porous aragonite shell, porous calcite shell, non-porous calcite shell, soft-bodied carcasses, and woody stem material) were used in previous studies (Allison and Pye, 1994). In this study, siderite was found only in the cavities of oyster shells and cuttle-bones (aragonite). Field incubation experiments were also reported in Pye et al. (1990), where they found that 0.1 – 2 mm siderite was formed around phosphor bronze, galvanized steel, aluminium and wood nuclei after six months buried in the Norfolk salt-marsh (Warham) sediment. No siderite was formed on polycarbonate nuclei.



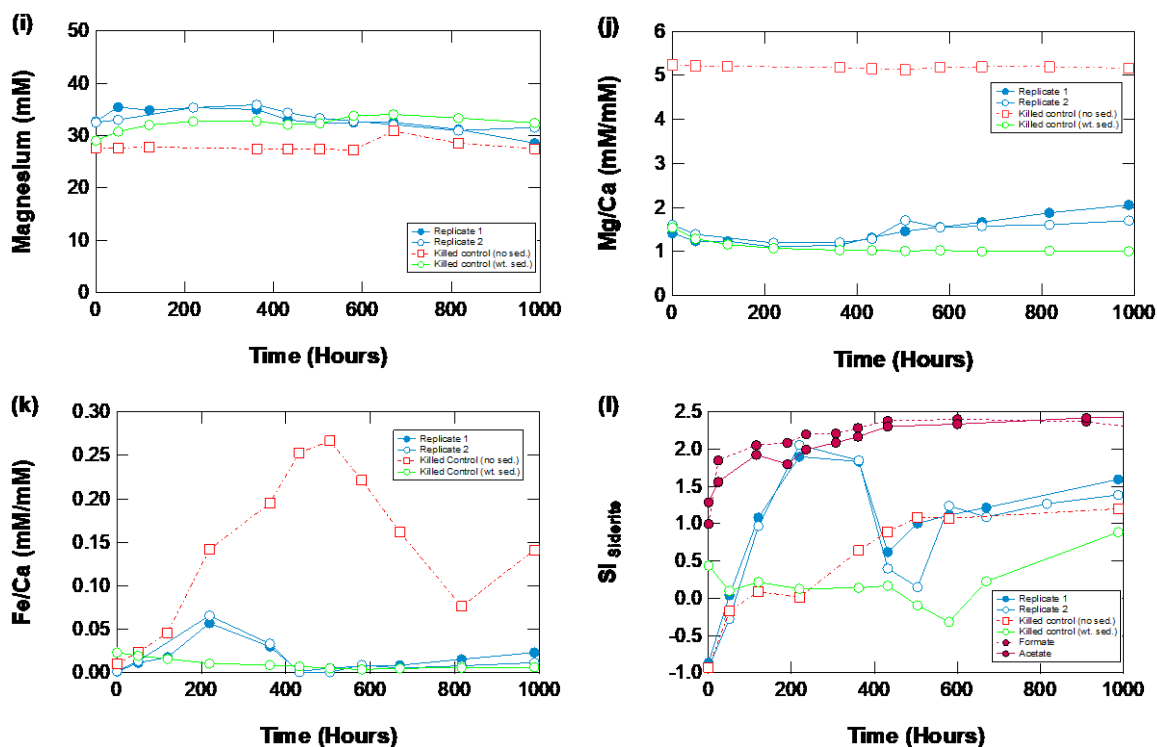


Figure 6.8: The second incubation experiment with plots showing (a) alkalinity; (b) pH; (c) iron; (d) sulfate; (e) sulfide; (f) chloride; (g) SO_4^{2-}/Cl^- ; (h) calcium; (i) magnesium; (j) Mg/Ca; (k) Fe/Ca; and (l) saturation index of siderite.

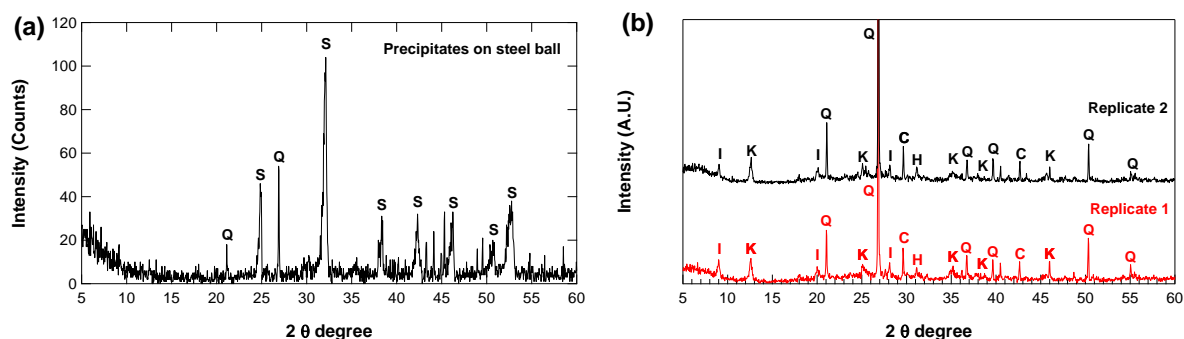


Figure 6.9: Powder X-ray diffraction pattern of the incubation samples (a) outer layer of steel ball; and (b) sediments after the incubation. Q = quartz; S = siderite; K = kaolinite; I = illite; C = calcite.

After the incubation, the solid samples were collected for mineralogical examination. I found a 1 – 2 mm thin layer of black precipitate around the steel ball in the incubated sample. No precipitate was noted in the steel balls of control samples. The black precipitates are comprised of quartz and siderite (Figure 6.9a). The asymmetrical siderite peaks shifted towards lower 2θ suggests the incorporation of calcium into the lattice of the siderite mineral, increasing the size of the unit cell and the crystal domain. In the incubated sediments, calcite/Mg-calcite is the only carbonate mineral precipitated because of the microbial sulfate

reduction, which limits the ferrous iron concentration (Figure 6.9b). Solid samples from the incubation samples examined under the SEM show that 1 – 3 μm rhombohedral siderite was precipitated around the steel balls (Figure 6.10a and b). The siderite is rich in calcium as shown by the EDX analysis (Figure 6.10c and d). The presence of aluminium in the EDX suggests that clay minerals are also associated within the sideritic cements. The abundance of siderite is low in the incubated sediment and is not detected in the XRD. However, SEM examination was able to identify some disseminated siderite crystals as shown in Figure 6.11. The disseminated siderite crystal has a trigonal crystal structure and low in calcium, which is different from the one formed around the steel balls. Despite the absence of a pyrite peak in the XRD pattern of the incubated sediment, this sulfide mineral was present but in low quantity under SEM examination (Figure 6.12). The pyrite has a framboid structure suggests the nucleation and growth from initial iron monosulfide microcrystals (Wilkin and Barnes, 1997).

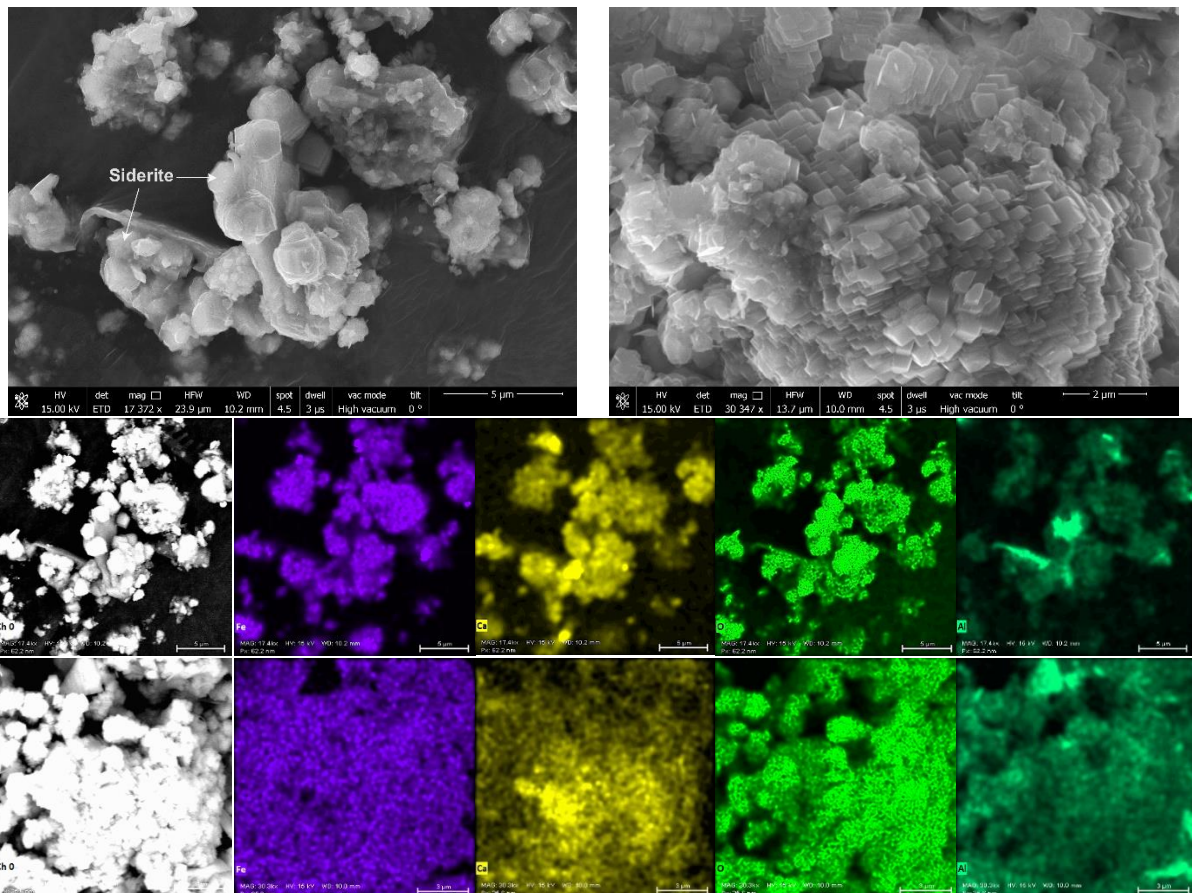


Figure 6.10: Secondary electron images and backscattered electron images of siderite collected from the steel balls. Figures in colour show the elemental distribution for iron, calcium, oxygen, and aluminium from both replicates of the incubation samples.

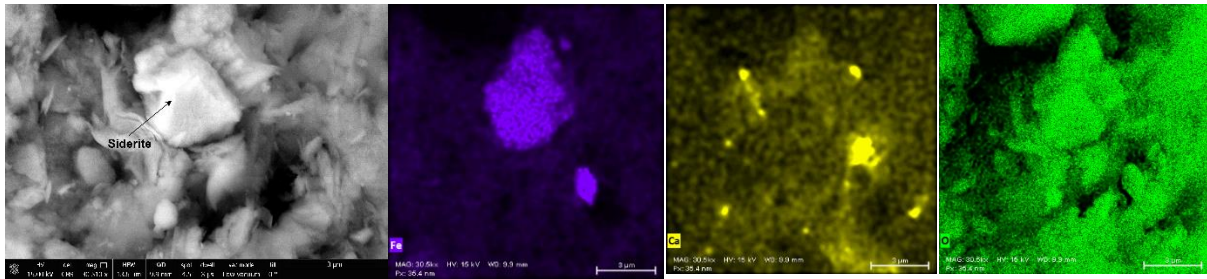


Figure 6.11: Trigonal siderite found in replicate one of the incubated sediment.

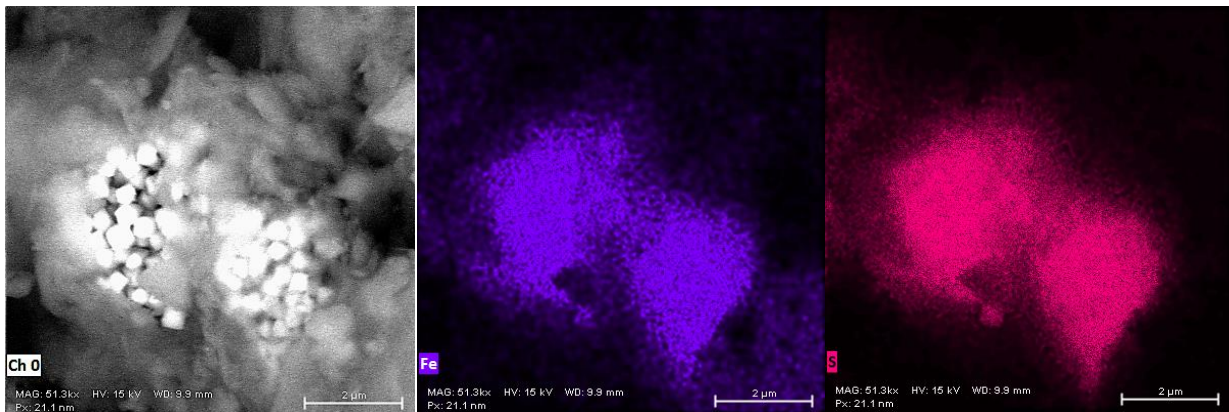


Figure 6.12: SEM images show the presence of framboidal pyrite in the incubation sample (replicate 1).

6.3.5 Magnetic susceptibility mapping in the Norfolk salt-marshes

The contour maps of magnetic susceptibility show that the gradiometer is able to detect siderite nodules (Figure 6.13). However, the tested grids, placing buried and exposed nodules suggest that the signal is only strong or distinguishable when the nodule is buried at a very shallow depth. My experience with the gradiometer is that the depth limit for nodule detection is lesser than 0.5 m depending on the other material in the core of the nodule. If the core material in the nodule is highly magnetic such as metal, then the signal may be detectable at a deeper depth. For example, in Grid 21, a siderite nodule grows around an iron bar was detected at the lower left of the grid. The nodule was buried at a depth approximately 0.3 meters, giving off a strong magnetic signal and was picked up by the gradiometer effectively. However, if the material is paramagnetic or weakly magnetic such as siderite and wood, the signal is weak and detection is problematic. It is worth mentioning that the salt-marsh is rich in some ferrimagnetic minerals such as greigite and magnetite which could contribute to the background noise in the magnetic susceptibility survey (Schinzel, 1993). For example, at times during the survey I received strong signals from the gradiometer but there was nothing when I dug out the upper layer marsh sediment where the strong signal was. This suggests the

presence of magnetic minerals in the marsh that contributed to the noise, thus making determining the location of the siderite nodule more difficult.

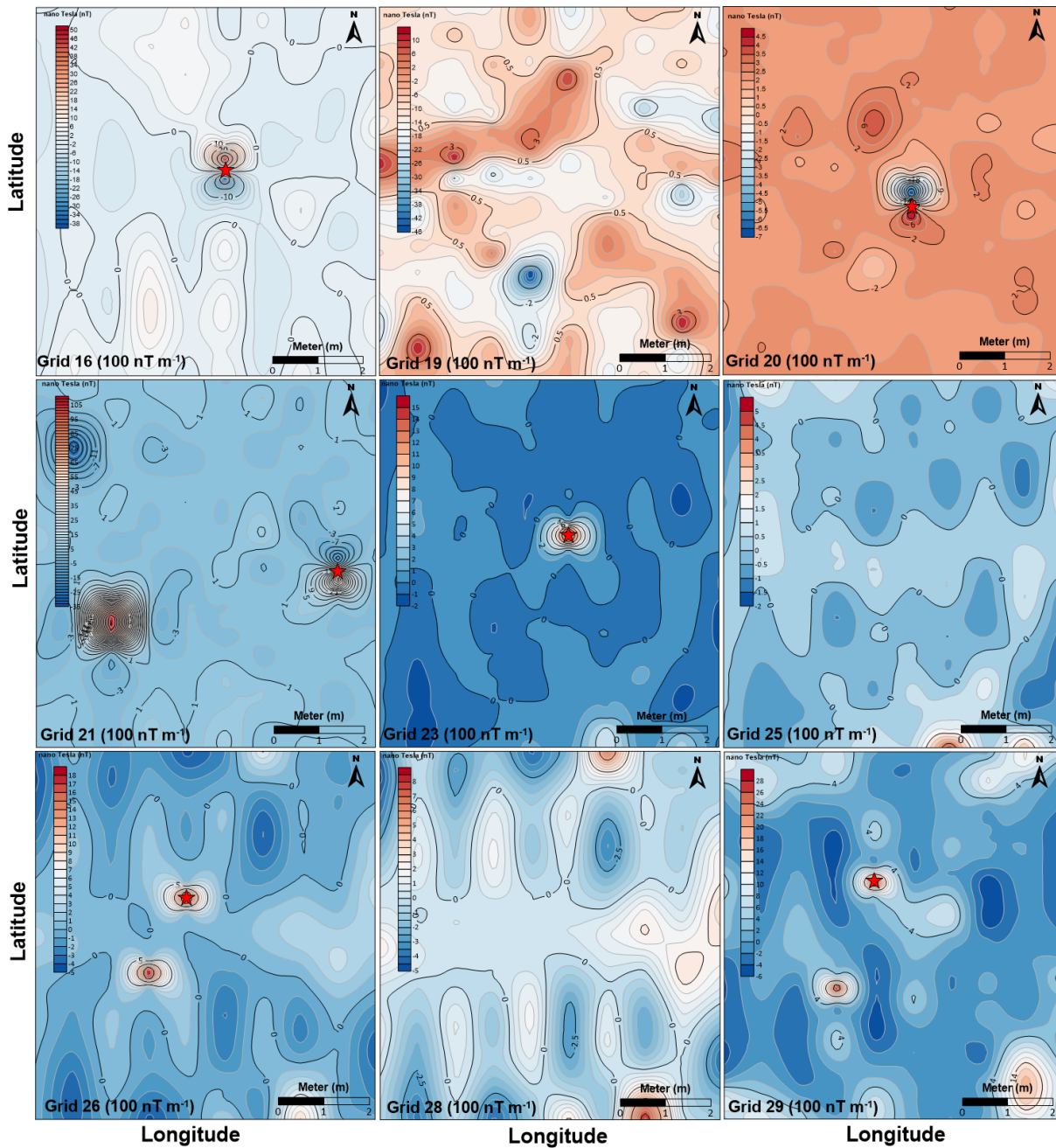


Figure 6.13: Magnetic susceptibility map (unit in nano-Tesla) in Norfolk salt-marshes. Grid 16 and 29 are situated in Blakeney; Grid 19, 20 and 21 in Warham salt-marsh; and Grid 23, 25, 26 and 28 in Stiffkey. Siderite concretion was buried at the middle (marked by a red star) of the plots in both Grid 16 and 20, 21, 23, 26, and 29. Grid 19 is the same plot as Grid 20 and is surveyed without concretion buried. Same goes to Grid 23 and Grid 25; Grid 26 and Grid 28. Grid 25 and 28 are just background without concretion.

6.3.6 Transformation Experiments

The results from the transformation experiments (Table 6.6) confirm previous results that MHC can be transformed into different carbonate minerals depending on the aqueous chemistry of the incubated medium. In sample T05 – T09, which were also presented in Chapter 3, I tested different aqueous Mg/Ca ratio, alkalinity, phosphate and sulfate concentration. I found that Mg/Ca plays a dominant role in controlling the types of carbonate polymorph formed. Water temperature also plays a role, for example, T05a and T05b shared a similar water chemistry but were subjected to different incubation temperature, one at 100 °C and the other at 150 °C. Aragonite was formed in addition to calcite and Mg-calcite in T05b. Other variables such as initial pH, alkalinity, phosphate, and sulfate are less influential in the higher temperature system. In samples with initial Mg/Ca higher than 4, aragonite is the dominant polymorph formed during transformation. Whereas Mg-calcite is the dominant mineral in medium with $4 < \text{Mg/Ca} > 2$. In medium with Mg/Ca less than 2, calcite is the dominant transformed products.

Samples with ferrous iron added show different results. Seawater with 4 mM iron added (T11a) precipitates aragonite as the main transformed product. In this sample, a small amount of MHC remained in the medium suggests that the presence of iron (as an impurity) may aid the stabilisation of MHC. In sample T11b, the same concentration of iron was added but the medium used is MQ-water. The results show that vaterite and calcite are the dominant product transformed. Both vaterite and calcite are known to form in solutions with low Mg/Ca. It is worth noting that MHC transformed to siderite when the iron concentration was increased 10-fold to 40 mM, which is an environmentally unrealistic concentration. I also tested the transformation samples using calcite seeds. Surprisingly, siderite precipitated in all the calcite-seeded samples T40 – T47. The formation of siderite increases as a function of iron concentration in both MQ and seawater medium. A similar observation is also seen in the MHC seeded samples (T48 – T54) although calcite is the dominant mineral after transformation. No carbonate precipitation was found in seedless control samples (T56 – T63) except the formation of some rusts. The formation of siderite in the samples with MHC samples are less than in the calcite-seeded samples, which may suggest a different mechanism of siderite formation. Based on the symmetrical siderite peak in the XRD and the greater removal of ferrous iron in the media, I suspect that siderite was formed via the dissolution of calcite (due to the low initial media pH) and re-precipitation (as siderite) in the calcite-seeded samples. On the other hand, in the MHC seeded samples, the relatively lower drop in the concentration of ferrous iron and lower increase in the concentration of calcium suggests that the siderite in these samples were formed via a solid-state transformation pathway. The transformation pathway of MHC to siderite involves the

incorporation/replacement of iron into the MHC lattice, yielding an asymmetrical siderite peak with peak shifted towards the left in the XRD (Appendix H). A peak shift towards the left in the XRD indicates that the siderite incorporates a substantial proportion of ions larger than iron into the crystal lattice – where in this case, calcium is the most plausible culprit due to the lower aqueous calcium concentration measured (relative to the calcite seeded samples) in the final media. The fact that calcite is the dominant transformed mineral in the MHC seeded samples suggests that a dehydration process (in MHC) is favoured over ionic replacement. The transformation experiments using iron shows that siderite can be formed from both calcite and MHC under a system with low pH, high iron concentration, and elevated temperature. Figure 6.14 shows the morphology of siderite under SEM, where large spherulitic aggregates (200 – 300 μm) of rhombohedral siderite were formed through MHC transformation. Coating of iron oxides is also commonly found on the siderite. Addition of formate does not seem to affect the transformed mineralogy.

Table 6.6: Summary of the aqueous chemistry and the initial and final calcium carbonate polymorphs in the transformation experiment. The experiment was carried out in the oven at 100 °C for 48 hours except stated otherwise. T01 – T04 were presented in Chapter 3. Rows with common shaded colour shared a same initial solution chemistry. T32 and T35 are control samples. Sample T40 – T63 were incubated under anoxic condition. Estimated standard deviation, R_{wp} and χ^2 values for Rietveld quantifications are given in Appendix I.

Samples	pH	Alk (mEq/L)	Initial Concentration					Mg/Ca	Medium	Initial CaCO ₃	Initial CaCO ₃ Polymorphs (wt %)					Sdr
			Ca ²⁺ (mM)	Mg ²⁺ (mM)	Fe ²⁺ (mM)	PO ₄ ³⁻ (μ M)	SO ₄ ²⁻ (mM) ^s				C	Mg-C	MHC	A	V	
T05a	8.42	106.225	0.78	53.79	-	429.37	B.D.L	69.28	Medium	MHC	-	-	100	-	-	-
T05b [^]	8.42	106.225	0.78	53.79	-	429.37	B.D.L	69.28	Medium	MHC	-	-	100	-	-	-
T06	7.04	11.012	12.63	24.23	-	137.55	B.D.L	1.92	M.Medium	MHC	-	-	100	-	-	-
T07 [*]	7.99	2.722	10.38	53.02	-	133.83	24.02	5.11	Seawater	MHC	-	-	100	-	-	-
T08	8.64	4.825	8.46	35.36	-	532.54	30.42	4.18	Artificial SW	MHC	-	-	100	-	-	-
T09	8.31	99.791	14.02	47.67	-	429.37	B.D.L	3.40	Medium	MHC	-	-	100	-	-	-
T10	8.65	49.709	0.35	24.02	-	318.78	B.D.L	68.16	Medium+MQ	MHC	-	-	100	-	-	-
T11a	6.57	2.109	10.29	52.72	4.21	-	25.59	5.12	Seawater	MHC	-	-	100	-	-	-
T11b	4.52	6.119	< 0.01	< 0.01	4.84	-	B.D.L	-	M.Medium	MHC	-	-	100	-	-	-
T11c	3.18	5.227	< 0.01	< 0.01	55.63	-	B.D.L	-	M.Medium	MHC	-	-	100	-	-	-
T12	7.42	1.656	< 0.01	101.15	-	125.47	B.D.L	Inf.	M.Medium	MHC	-	-	100	-	-	-
T13	6.85	10.163	10.86	56.02	-	129.18	28.54	5.16	Seawater+F	MHC	-	-	100	-	-	-
MQ50 [^]	3.02	1.780	< 0.01	< 0.01	50.55	-	-	-	M.Medium	MHC/Calcite	100	-	100	-	-	-
SW50 [^]	3.65	1.625	10.80	55.36	53.64	-	-	5.13	M.Medium	MHC/Calcite	100	-	100	-	-	-
MQ100 ^a	2.67	2.450	< 0.01	< 0.01	98.57	-	B.D.L	-	M.Medium	MHC/Calcite	100	-	100	-	-	-
MQ50 ^b	3.02	8.278	< 0.01	< 0.01	50.63	-	B.D.L	-	M.Medium	MHC/Calcite	100	-	100	-	-	-
MQ25 ^c	3.39	7.301	< 0.01	< 0.01	25.78	-	B.D.L	-	M.Medium	MHC/Calcite	100	-	100	-	-	-
MQ10 ^d	7.20	13.283	< 0.01	< 0.01	11.03	-	B.D.L	-	M.Medium	MHC/Calcite	100	-	100	-	-	-
SW100 ^e	2.97	3.979	10.41	53.12	105.04	-	22.07	5.10	M.Medium	MHC/Calcite	100	-	100	-	-	-
SW50 ^f	4.33	5.158	10.53	53.98	48.74	-	17.68	5.12	M.Medium	MHC/Calcite	100	-	100	-	-	-
SW25 ^g	5.20	6.503	10.49	52.91	23.67	-	23.68	5.04	M.Medium	MHC/Calcite	100	-	100	-	-	-
SW10 ^h	6.78	12.948	10.83	54.75	9.74	-	-	5.05	M.Medium	MHC/Calcite	100	-	100	-	-	-
Samples	pH	Alk (mEq/L)	Final Concentration					Mg/Ca	Medium	Final CaCO ₃	Final CaCO ₃ Polymorphs (wt %)					Sdr
			Ca ²⁺ (mM)	Mg ²⁺ (mM)	Fe ²⁺ (mM)	PO ₄ ³⁻ (μ M)	SO ₄ ²⁻ (mM) ^s				C	Mg-C	MHC	A	V	
T05a ^s	-	-	0.82	16.62	-	-	B.D.L	20.24	Medium	Mg-C, C	?	?	-	-	-	-
T05b ^{^s}	-	-	-	-	-	-	B.D.L	-	Medium	Mg-C, C, A	?	?	-	?	-	-
T06	7.26	5.403	25.11	9.22	-	164.50	B.D.L	0.37	M.Medium	C, A	86.4	-	-	13.6	-	-
T07 [*]	7.51	7.380	25.18	35.71	-	202.61	23.48	1.42	Seawater	A, Mg-C, C	20.9	5.0	-	74.1	-	-
T08	7.87	11.045	18.64	23.64	-	-	27.05	1.27	Artificial SW	A, C, MHC, Mg-C	24.3	2.7	22.7	50.4	-	-
T09	7.10	28.899	8.02	17.67	-	417.29	B.D.L	2.20	Medium	Mg-C, C	39.9	60.1	-	-	-	-
T10	7.32	22.451	5.54	20.69	-	316.92	B.D.L	3.73	Medium+MQ	A, Mg-C, C	23.7	32.4	-	43.9	-	-
T11a ^s	7.55	13.549	25.87	47.58	0.37	-	26.06	1.84	Seawater	A, MHC	-	-	?	?	-	-
T11b ^s	7.71	< 10.0	5.05	< 0.01	0.05	-	B.D.L	-	M.Medium	V, C	?	-	-	-	?	-
T11c	6.44	7.073	63.03	< 0.01	44.55	-	B.D.L	-	M.Medium	Sdr	-	-	-	-	-	100
T12	7.33	11.359	23.03	85.70	-	179.37	B.D.L	3.68	M.Medium	C, A	50.3	-	-	49.7	-	-

T13	7.55	12.727	26.52	45.13	-	201.68	25.82	1.70	Seawater+F	A, C, Mg-C	33.7	-	31.9	34.3	-	-
T20(C)	6.02	8.335	6.02	8.34	54.75	0.98	< 0.01	-	M.Medium	L, Mg-C	-	100	-	-	-	-
T23(C)	6.07	8.578	6.07	8.58	59.65	54.64	< 0.01	-	M.Medium	-	-	-	-	-	-	-
T26(M)	6.08	7.828	6.08	7.83	50.19	1.97	< 0.01	-	M.Medium	L, C	100	-	-	-	-	-
T29(M)	6.42	15.673	6.42	15.67	59.05	53.26	< 0.01	-	M.Medium	C	100	-	-	-	-	-
T32	1.90	5.238	1.90	5.24	0.39	0.94	1.01	-	M.Medium	-	-	-	-	-	-	-
T35	1.55	3.401	1.55	3.40	9.30	48.16	0.66	-	M.Medium	-	-	-	-	-	-	-
T40 ^a	4.33	12.174	80.91	< 0.01	12.42	-	4.33	-	M.Medium	Sdr, C	3.6	-	-	-	-	96.4
T41 ^b	5.77	20.530	48.27	0.43	0.78	-	4.30	0.01	M.Medium	Sdr, C	48.0	-	-	-	-	52.0
T42 ^c	5.98	2.593	24.43	0.39	0.23	-	4.30	0.02	M.Medium	C, Sdr	66.5	-	-	-	-	33.5
T43 ^d	6.30	3.505	10.75	0.40	0.13	-	4.32	0.04	M.Medium	C, Sdr	93.1	-	-	-	-	6.9
T44 ^e	5.82	3.363	99.10	52.93	8.32	-	27.17	0.53	M.Medium	Sdr, C	15.9	-	-	-	-	84.1
T45 ^f	6.10	3.728	58.66	54.12	0.05	-	27.93	0.92	M.Medium	C, Sdr	52.4	-	-	-	-	47.6
T46 ^g	6.37	2.971	34.87	53.31	0.66	-	7.38	1.53	M.Medium	C, Sdr	67.7	1.53	-	-	-	32.3
T47 ^h	6.58	2.807	21.17	54.51	0.05	-	28.00	2.57	M.Medium	C, Sdr	92.6	-	-	-	-	7.4
T48 ^a	5.90	5.664	62.97	1.49	40.99	-	4.32	0.02	M.Medium	Sdr, C	13.0	-	-	-	-	87.0
T49 ^b	6.02	4.344	47.79	1.55	0.76	-	4.34	0.03	M.Medium	Sdr, C	37.2	-	-	-	-	62.8
T50 ^c	6.39	7.009	24.11	1.07	1.64	-	4.32	0.04	M.Medium	C, Sdr	83.8	-	-	-	-	16.2
T51 ^d	6.57	3.685	9.74	0.68	0.43	-	4.33	0.07	M.Medium	C, Sdr	99.4	-	-	-	-	0.6
T52 ^e	6.15	8.567	68.68	54.15	40.69	-	26.25	0.79	M.Medium	C, MHC, Sdr	3.0	-	30.5	-	-	66.5
T53 ^f	6.56	13.436	56.67	52.27	4.69	-	26.82	0.92	M.Medium	-	-	-	-	-	-	-
T54 ^g	6.63	9.833	37.25	48.16	2.42	-	25.71	1.29	M.Medium	C, A	67.0	-	-	33.0	-	-
T55 ^h	6.82	8.918	28.75	44.73	0.87	-	25.18	1.56	M.Medium	C, A	57.1	-	-	42.9	-	-
T56 ^a	2.12	11.904	0.16	< 0.01	101.13	-	4.58	-	M.Medium	-	-	-	-	-	-	-
T57 ^b	2.79	12.253	0.17	0.23	51.83	-	4.53	1.36	M.Medium	-	-	-	-	-	-	-
T58 ^c	3.19	11.086	0.16	< 0.01	26.19	-	4.34	-	M.Medium	-	-	-	-	-	-	-
T59 ^d	3.75	10.977	< 0.01	< 0.01	10.60	-	4.33	-	M.Medium	-	-	-	-	-	-	-
T60 ^e	2.58	-	10.42	54.03	88.34	-	26.20	5.19	M.Medium	-	-	-	-	-	-	-
T61 ^f	2.79	19.363	10.56	55.24	48.14	-	27.51	5.23	M.Medium	-	-	-	-	-	-	-
T62 ^g	3.13	17.392	10.33	54.22	23.37	-	27.23	5.25	M.Medium	-	-	-	-	-	-	-
T63 ^h	3.46	11.189	10.52	55.15	6.67	-	28.53	5.24	M.Medium	-	-	-	-	-	-	-

^aHeated for 1 week. ^bQualitative result. ^cEstimated values. ? = quantification is not done for the sample. M.Medium = Modified Medium (Medium made up of MQ-water) A=Aragonite, C=Calcite, MHC=monohydrocalcite, Mg-C=Magnesium Calcite, L=Lepidocrocite, V=Vaterite, Sdr=Siderite. F=Formate (120 mM). Aqueous samples were measured in duplicates. ^hHeated at 150 °C for 48 hours, dried (complete evaporation) because the grey rubber cap melted.

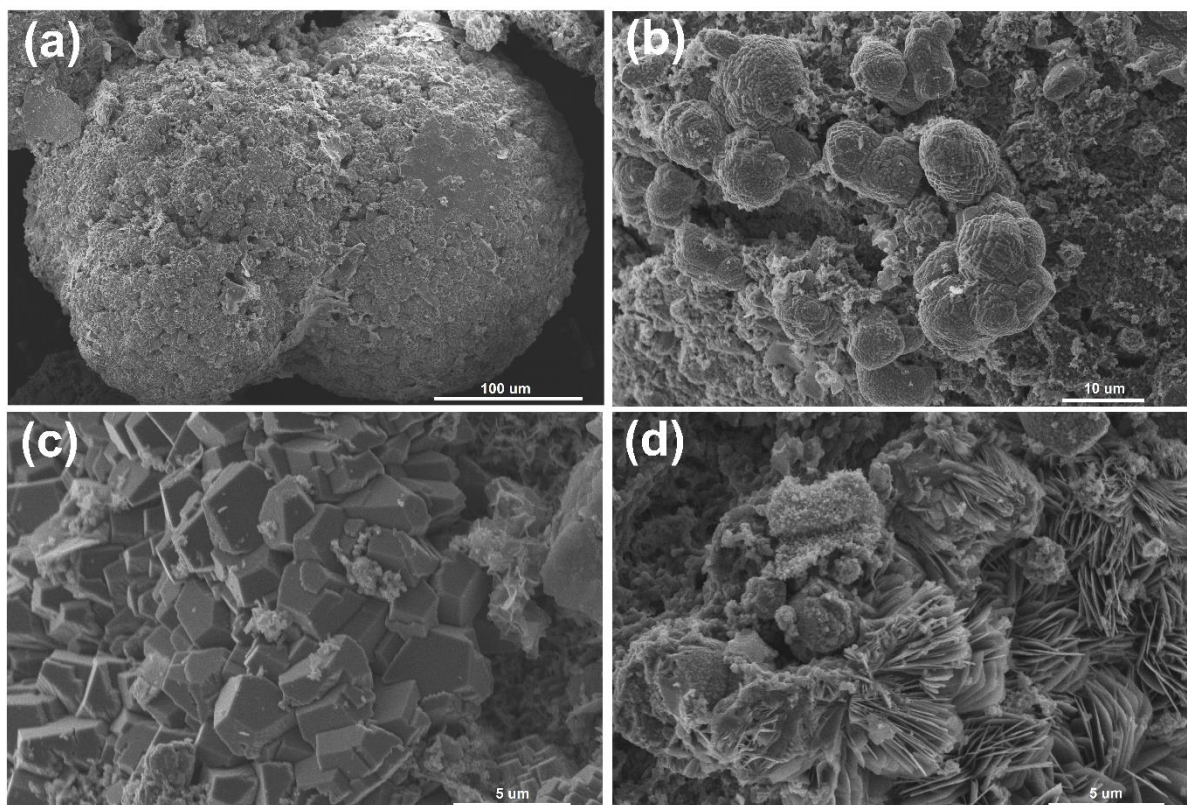


Figure 6.14: Morphology of transformation samples. Spherulitic siderite in sample T11c after heated in modified medium for 48 hours at 100 °C. (a) Aggregates of spherulitic siderite; (b) individual aggregates of spherulitic siderite; (c) rhombohedral siderite; and (d) coating of iron oxide minerals.

6.3.7 Proposed formation of siderite concretion in the marsh

Combining these results from field and laboratory incubation experiments, I suggest that the formation of the concretion in the Norfolk salt-marshes sediment begins in a micro-environment where there is a local source of high ferrous iron and alkalinity. My transformation experiments suggest that the initial precipitate could be calcite which is then exposed to high concentrations of ferrous iron, however it is unclear whether this would transform the calcite to siderite at environmental temperatures, therefore I suggest that the initial precipitate is likely siderite. My results suggest that bacterial iron reduction alone doesn't generate enough alkalinity to drive siderite saturation, and that it is microbial sulfate reduction that is needed to provide enough alkalinity for siderite precipitation however it has to be maintained at a very low level. Also, the level of sulfide has to be low relative to the iron reduction. Abiotic (penetration of oxygen) and biotic (sulfide oxidizing bacteria, e.g. *Beggiotoa*) oxidation of

sulfide could be possible, causing the accumulation of alkalinity and iron in the marsh sediment. In general, the siderite nodule formation process can be divided into two major stages in a geochemically dynamic environment.

- (1) Nucleation stage – rapid precipitation of siderite that envelops the nucleation point.
- (2) Maturation stage – subsequent precipitation of Mg-rich calcite on the siderite core.

During the nucleation stage, my observations suggest that organic matter such as wood may act as a nucleation point (nucleus) when it is buried to a depth below the oxygen penetration depth. Under this oxygen-deprived environment, fermentation breakdown the complex organic matter, producing CO₂ (which lowers pore-fluid pH) and generates more short chain carbon (organic material): an ideal environment for anaerobic bacteria to grow. Bacteria (particularly iron reducing bacteria to generate ferrous iron, and I suggest sulfate reducing bacteria as well) start to colonize and oxidize the available carbon using iron minerals or aqueous pore fluid sulfate as a terminal electron acceptor. As a result of these reactions, bicarbonate is produced, leading to siderite supersaturation. Precipitation of siderite happens when the saturation index of siderite exceeds 2 and requires a pore-fluid pH between 6.0 and 7.2. A pH lower than 6 means precipitation will not happen and if the pore-fluid pH is greater than 7.2, precipitation of calcium carbonate is favoured. However, this depends on the available ferrous iron in the pore-fluid (Gab et al., 2017). This is interesting as bacterial iron reduction tends to push the pH of the pore fluid higher than 7.2 (Soetaert et a., 2007), which means that for siderite to occur, more is needed than simply conditions that favour bacterial iron reduction. It could be that trace amounts of microbial sulfate reduction, producing hydrogen sulfide which lowers pH, can counteract the high pH generated by straight bacterial iron reduction and thus create the 'sweet spot' for siderite precipitation and nodule growth.

My incubation experiments also show that the bacterial sulfate reduction has to be at a much lower rate than bacterial iron reduction to prevent the precipitation of iron-monosulfide. My experiments suggest that carbonate mineralisation can be very rapid (in 2 weeks) and most likely takes place at shallow depth in the marsh (~5 – 20 cm). The preservation of the nucleus (organic matter) in most of the concretions also suggests rapid cementation of siderite minerals among the sediment grains. The influence of meteoric water can be important at this depth, diluting the calcium and sulfate supply from seawater that helps favor iron-reduction and thus siderite formation. Above this, I hypothesize that the water-to-sediment ratio also plays an important role in the formation of siderite concretions in the marsh. A high water to

sediment ratio in the sediment is likely to dilute the release of ferrous iron and alkalinity during microbial iron reduction. As a result, higher bacterial metabolic rate “a sudden flare up of bacterial activity” is needed to create a condition where the pore-fluid is supersaturated with respect to siderite. This nucleation stage often cements the grains surrounding the nucleus (source for carbon or iron), forming the inner core of a concretion. Siderite precipitates in the inner core decrease the IAP for siderite until the pore-fluid is no longer supersaturated with siderite, impacting further growth of the siderite-rich inner core. Rather, the outer core can be more calcite-rich as it is further away from the nucleus. This leads to the maturation stage of the concretion.

During the maturation stage, the siderite concretion is often buried deeper in the marsh sediment. It is possible at these depths that microbial sulfate reduction is favoured, and as a result, higher concentration of sulfide, alkalinity, and pH (pH > 7.5, depicted by deep sulfidic core) produced in the local pore-fluid, favors the precipitation of calcite and Mg-calcite (instead of siderite).

Although I did not measure the $\delta^{13}\text{C}_{\text{DIC}}$ of pore-fluid in this core, I obtained data previously measured by my colleague and the $\delta^{13}\text{C}_{\text{DIC}}$ values were in consistent with the $\delta^{13}\text{C}_{\text{carbonate}}$ in the concretion ($\delta^{13}\text{C}_{\text{DIC}}$ of iron-rich core is -7.0 ‰ PDB; sulfidic core was -13.3 ‰ PDB). Hence, the carbon isotope values in the concretion allow me to provisionally conclude that:

- (1) The inner core of the concretion is caused by rapid cementation of carbonate, mainly siderite, that occurs at an environment where there is a mixture of bacterial iron reduction and bacterial sulfate reduction, but the latter is not intense.
- (2) The outer core of the concretion formed in an environment with a higher mass/assemblage of sulfate-reducing bacteria, where bacterial sulfate reduction is more.

6.4 Conclusions

In conclusion, siderite is one of the rare carbonate minerals that can be found forming in rare modern sedimentary environment. I have made a thin layer of siderite within 3 weeks of incubation experiment in the presence of steel balls. Most of the concretion samples I collected in the field have wood materials in the center and sometimes even lack a nucleus. The next thing to explore how to make siderite precipitate without the use of steel balls. Through a series of exploration using field and laboratory samples, I suggest that the siderite concretion

in the Warham salt-marsh forms under the active bacterial iron-reduction with limited sulfate-reduction. My incubation experiments suggest that bacterial sulfate reduction is needed for the formation of siderite as high alkalinity is required to maintain supersaturation of siderite in the pore-fluid. Without the increased alkalinity, siderite could not precipitate even there are high concentrations of high ferrous iron. The 2 mm thick siderite precipitates around the steel ball in the incubated sediment suggest that alkalinity is the limiting factor for siderite minerals to precipitate during bacterial iron-reduction while iron is the limiting factor when sulfate reduction begins. The formation of siderite and other carbonate minerals via metastable MHC is possible when thermal energy applies, suggesting the potential of MHC as precursor/intermediate for the formation of other carbonate minerals. The lack of pyrite and the presence of disseminated siderite in the incubated sediment suggest the heterogeneity of localized water chemistry within the sediment. This could partly explain the occurrence of siderite concretion only in certain microenvironment of the marsh. The limitation of my incubation experiments is that I added too much carbon source for sulfate reduction to metabolize, creating a system where iron is depleted and hence the formation of siderite is not possible. A Goldilocks point between the degree of iron and sulfate reduction need to be determined in order to make siderite, which is one of the common forming minerals throughout the oxygen-depleted periods of the geological history.

Chapter 7

Conclusions

In this thesis, I have explored the application of geochemical and mineralogical techniques in understanding the formation of a range of calcium carbonate minerals in modified laboratory conditions and in the field. This has allowed me to better constraint the conditions required for the precipitation of various carbonate minerals in the natural environment. By generating a simpler system in the laboratory, I was able to examine individual factors that contribute to the precipitation of different calcium carbonate polymorphs, which can eventually be used to explain the more complex system in the field. In the later part of this thesis, I have explored the occurrence and formation of siderite concretions in the salt-marshes using incubation experiments of sediment collected from the salt-marsh. Transformation experiments of MHC to different calcium carbonate polymorphs, in particular siderite, provides further insights into the unique crystallization pathways of carbonate minerals. The primary contribution of this thesis is the use of microbial populations to induce carbonate mineralisation. Although carbonate mineralisation and stability has been studied for decades, it has nearly entirely been done through abiotic experiments and this thesis has explored how microbial populations may change the mineralisation pathways and polymorphism of various calcium carbonate minerals.

In Chapter 2, a method development chapter, I demonstrated the effect of individual variables that influence the growth of sulfate-reducing bacteria in pure culture. I demonstrated that the type of gas (presence of CO₂), Mg/Ca and yeast extract are the key variables that influence microbial growth in pure culture. Mg/Ca affects overall growth while the presence of CO₂ determines the longevity of bacterial growth. I also noticed that yeast extract is essential to stimulate the bacterial growth rate. This chapter concluded that microbial sulfate reduction is able to induce the precipitation of calcium carbonate via the release of metabolic products that change the solution chemistry. The calcium carbonate polymorph that precipitated from these initial incubation experiments was monohydrocalcite. The monohydrocalcite I created is exceptionally stable. I also made monohydrocalcite in abiotic precipitation experiments. In chapter 3 and 4, I explored the role of Mg/Ca and the types of seeding material in calcium carbonate polymorphism driven by pure cultures of sulfate reducing bacteria. In Chapter 3, I concluded that the calcium carbonate polymorph formed depends on the solution chemistry at the time of precipitation, even though the solution chemistry may then evolve. Mg/Ca is the key variable that strongly influences the types of calcium carbonate precipitated. In a system

where phosphate is high, formation of calcite is the favoured polymorph when the solution Mg/Ca is less than 2, whereas monohydrocalcite is promoted at Mg/Ca greater than 2. The effect of mineral seeds on the calcium carbonate polymorph formed is pronounced when the solution chemistry is identical. Although the saturation index is generally a useful tool to predict calcium carbonate precipitation, kinetic factors should also be considered. In particular, kinetic inhibitors such as magnesium and phosphate often play a key role in calcium carbonate polymorphism.

My incubation experiments with different seeding materials show that the kaolinite promotes the formation of monohydrocalcite while calcite seeds favour the growth of magnesium calcite (Chapter 5). The fact that calcite seeds promote the formation of Mg-calcite was explained by a greater influence on the surface nucleation. My incubation experiments in chapter 5 with varying clay and carbonate mineral suggests that the rate of microbial sulfate reduction increases with increasing clay content. A substantial drop in maximum alkalinity is particularly noted at above the 80% carbonate 20% clay mixture. I suggested that the preference of the bacteria for clay dominated substrate is due to the higher surface area of the clay.

In my final chapter, I demonstrated the formation of siderite (iron carbonate) through the incubation of salt-marsh sediments with steel balls and wood as nucleation point. The formation of siderite on the steel balls but not on wood suggests that iron from the steel ball might be needed for siderite nucleation; this is interesting when contrasted to the natural siderite nodules where wood is often in the centre. I suggest that an iron source is required to tip the balance in the system to make siderite concretions. In addition, my transformation experiments of MHC and calcite to siderite and various calcium carbonate polymorphs suggest that siderite is able to form via a metastable polymorphs (such as MHC) under iron enriched conditions at elevated temperatures.

My studies conclude that the metastability of calcium carbonate minerals depends on the geochemical condition of the surrounding aqueous environment. The metastability of carbonate minerals allows the formation and transformation of various polymorphs and mineral phases, where the stability of calcium carbonate minerals in normal surface conditions (today) increases from amorphous calcium carbonate to monohydrocalcite and then to various calcium carbonate polymorphs such as aragonite, calcite and vaterite. The stability of calcium carbonate minerals greatly depends on the geochemical condition of the surrounding fluid and is driven by thermodynamics (a combination effect of ionic activity and temperature).

Additionally, the presence of kinetic inhibitors affects the stability of a mineral and/or the selection of calcium carbonate polymorphs. In my study, phosphate and magnesium both stabilized monohydrocalcite, while phosphate inhibits the formation of aragonite. My study supports the non-classical mineralization pathway for calcium carbonate formation and concludes that carbonate minerals often formed from the least stable phase and transformed into a more stable phase over time. This is commonly seen in nature, including during both biotically and abiotically induced precipitation. For example, amorphous calcium carbonate is often the transient mineral that forms in calcifying organisms such as planktic foraminifera. Despite the stability of calcite in normal surface conditions, my transformation studies show that calcite can be metastable and readily transformed into other carbonate polymorphs at higher temperature and under a different geochemical condition (high iron concentration). Because of the relatively complex and easily altered nature of calcium carbonate minerals, future works could focus on the impact of transformations on the chemical signal embedded in carbonate minerals and rocks which is often used as a proxy for past surface conditions.

References:

- Aldunate, M., De la Iglesia, R., Bertagnolli, A.D., Ulloa, O., 2018. Oxygen modulates bacteria community composition in the coastal upwelling waters off central Chile. *Deep Sea Research Part II: Topical Studies in Oceanography*. Doi.org/10.1016/j.dsr2.2018.02.001.
- Allison, P.A., Pye, K., 1994. Early diagenetic mineralization and fossil preservation in modern carbonate concretions. *Palaios*. **9** (6), 561 – 575.
- Allmann, R., Hinek, R., 2007. The introduction of structure types into the Inorganic Crystal Structure Database ICSD. *Acta Crystallographica A*. **63**, 412-417.
- Aloisi, G., 2008. The calcium carbonate saturation state in cyanobacterial mats throughout Earth's history. *Geochimica et Cosmochimica Acta*. **72**, 6037 – 6060.
- Aloisi, G., Gloter, A., Kruger, M., Wallman, K., Guyot, F., Zuddas, P., 2006. Nucleation of calcium carbonate on bacterial nanoglobules. *Geology*. **34**, 1017 – 1020.
- Althoff, P.L., 1977. Structural refinements of dolomite and a magnesian calcite and implications for dolomite formation in the marine environment. *American Mineralogists*. **62**, 772 – 783.
- Anbu, P., Kang, C.H., Shin, Y.J., So, J.S., 2016. Formations of calcium carbonate minerals by bacteria and its multiple applications. *SpringerPlus*. **5**, 250.
- Antler, G., Turchyn, A.V., Ono, S., Sivan, O., Bosak, T., 2017. Combined ^{34}S , ^{33}S , and ^{18}O isotope fractionations record different intracellular steps of microbial sulfate reduction. *Geochimica et Cosmochimica Acta*. **203**, 364 – 380.
- APHA, 1999. *Standard methods for examination of water and wastewater*. American Public Health Association, Washington DC.
- Appelo, C.A.J., Postma, D., 2005. *Geochemistry, groundwater and pollution*. 2nd Ed. Balkema, Rotterdam.
- Archer, D., 2010. *The Global Carbon Cycle*. Princeton University Press.
- Arias, D., Cisternas L.A., Rivas, M., 2017. Biomineralization of calcium and magnesium crystals from seawater by halotolerant bacteria isolated from Atacama Salar (Chile). *Desalination*. **405**, 1 – 9.
- Arp, G., Reimer, A., Reitner, J., 2001. Photosynthesis-induced biofilm calcification and calcium concentrations in Phanerozoic oceans. *Science*. **292**, 1701 – 1704.
- Balci, N., Demirel, C. On, S.A. Gultekin, A.H. Kurt, M.A., 2018. Evaluating abiotic and microbial factors on carbonate precipitation in Lake Acigol, a hypersaline lake in Southwestern Turkey. *Quaternary International*. **486**, 116 – 128.

- Balci, N., Menekse, M., Karaguler, N.G., Sonmez, M.S., Meister P., 2016. Reproducing authigenic carbonate precipitation in the hypersaline Lake Acigol (Turkey) with microbial cultures. *Geomicrobiol Journal*. **33**(9), 758 – 773.
- Baumgartner, L.K., Dupraz, C., Buckley, D.H., Spear, J.B., Pace, N.R., Visscher, P.T., 2009. Microbial species richness and metabolic activities in hypersaline microbial mats: Insight into biosignature formation through lithification. *Astrobiology*. **9**(9), 861 – 874.
- Baumgartner, L.K., Reid, R.P., Dupraz, C., Decho, A.W., Buckley, D.H., Spear, J.R., Przekop, K.M., Visscher, P.T., 2006. Sulfate reducing bacteria in microbial mats: changing paradigms, new discoveries. *Sedimentary Geology*. **185**, 131 – 145.
- Ben-Yaakov, S., 1973. pH buffering of pore waters of recent anoxic marine sediments. *Limnology and Oceanography*. **18**, 86 – 94.
- Berner, R.A., 1975. The role of magnesium in the crystal growth of calcite and aragonite from seawater. *Geochimica et Cosmochimica Acta*. **39**, 489 – 504.
- Berner, R.A., Morse, J.W., 1974. Dissolution kinetics of calcium carbonate in seawater. IV. Theory of calcite dissolution. *American Journal of Science*. **274**, 108 – 134.
- Berner, R.A., Scott, M.R., Thomlinson, C., 1970. Carbonate alkalinity in the pore waters of anoxic marine sediments. *Limnology and Oceanography*. **15**(4), 544 – 549.
- Berner, R.A., 2003. The long-term carbon cycle, fossil fuels and atmospheric composition. *Nature*. **426**, 323 – 326.
- Bethke, C.M., Sanford, R.A., Kirk, M.F., Jin, Q., Flynn, T.M., 2011. The thermodynamic ladder in geomicrobiology. *American Journal of Science*. **311**, 183 – 210.
- Bewernitz, M.A., Gabauer, D., Long, J., Colfen, H., Gower, L.B., 2012. A metastable liquid precursor phase of calcium carbonate and its interactions with polyaspartate. *Faraday Discussion*. **159**, 291 – 312.
- Bird, M.I., Chivas, A.R., Radnell, C.J., Burton, H.R., 1991. Sedimentological and stable isotope evolution of lakes in the Vestfold Hills, Antarctica. *Paleogeography, Paleoclimatology, Paleoecology*. **84**, 109 – 130.
- Blank, J.G., Green, S.J., Blake, D., Valley, J.W., Kita, N.T., Treiman, A., Dobson, P.F., 2009. An alkaline spring system within the Del Puerto Ophiolite (California, USA): A Mars analog site. *Planetary and Space Science*. **57**, 533 – 540.
- Blue, C.R., Giuffre, A., Mergelsberg, S., Han, N., De Yoreo, J.J., Dove, P.M., 2017. Chemical and physical controls on the transformation of amorphous calcium carbonate into crystalline CaCO₃ polymorphs. *Geochimica et Cosmochimica Acta*. **196**, 179 – 196.
- Bosak, T., Newman D.K., 2005. Microbial kinetic controls on calcite morphology in supersaturated solutions. *Journal of Sedimentary Research*. **75**(2), 190 – 199.

- Bosak, T., Newman, D.K., 2003. Microbial nucleation of calcium carbonate in the Precambrian. *Geology*. **31**, 577 – 580.
- Bots, P., Benning L.G., Rickaby R.E.M., Shaw S., 2011. The role of SO₄ in the switch from calcite to aragonite seas. *Geology*. **39**, 331 – 334.
- Bots, P., Benning, L.G., Rodriguez-Blanco, J.D., Roncal-Herrero, R.T., Shaw S., 2012. Mechanistic insights into the crystallization of amorphous calcium carbonate (ACC). *Crystal Growth Design*. **12**, 3806 – 3814.
- Bowles, M.W., Mogollon, J.M., Kasten, S., Zabel, M., Hinrichs, K-U., 2014. Global rates of marine sulfate reduction and implications for sub-sea-floor metabolic activities. *Science*. **334** (6186), 889 – 891.
- Braissant, O., Decho, A.W., Dupraz C., Glunk, C., Przekop, K.M., Visscher P.T., 2007. Exopolymeric substances of sulfate reducing bacteria: Interactions with calcium at alkaline pH and implication for formation of carbonate minerals. *Geobiology*. **5**, 401 – 411.
- Brecevic, L., Nielsen, A.E., 1989. Solubility of amorphous calcium carbonate. *Journal of Crystal Growth*. **98**(3), 504 – 510.
- Brønsted, J.N., 1922. Studies on solubility. IV. The principle of the specific interaction of ions. *Journal of American Chemical Society*. **44**, 877 – 898.
- Brooks, R., Clack, L.M., Thurston, E.F., 1950. Calcium carbonate and its hydrates. *Philosophy Transaction of Royal Society A*. **243**, 145 – 167.
- Burdige, D.J., 1991. The kinetics of organic matter mineralization in anoxic marine sediments. *Journal of Marine Research*. **49**, 727 – 761.
- Burton, E.A., 1993. Controls on marine carbonate cement mineralogy: review and reassessment. *Chemical Geology*. **105**, 163 – 179.
- Burton, E.A., Walter, L.M., 1990. The role of pH in phosphate inhibition of calcite and aragonite precipitation rates in seawater. *Geochimica Cosmochimica Acta*. **54**, 797 – 808.
- Burton, J. D., 1996. The ocean: A global chemical system. *Oceanography: an illustrated guide*. in C. P. Summerhayes and S. A. Thorpe. London, Manson: 165-181.
- Busenberg, E., Plummer, N.L., 1985. Kinetics and thermodynamic factors controlling the distribution of SO₄²⁻ and Na⁺ in calcites and selected aragonites. *Geochimica et Cosmochimica Acta*. **49**, 713 – 725.
- Butlin, K.R., Adams, M.E., Thomas, M., 1949. The isolation and cultivation of sulfate-reducing bacteria. *Journal of General Microbiology*. **3**(1), 46 – 59.
- Canfield, D.E., 1991. Sulfate reduction in deep-sea sediments. *American Journal of Science*. **291**, 177 – 188.

- Cao, J-Y., Zhang, G-J., Mao, Z-S, Fang, Z-H, Yang, C., Han, B-L., 2009. Influence of Mg^{2+} on the growth and activity of sulfate reducing bacteria. *Hydrometallurgy*. **95**, 127 – 134.
- Castanier, S., Le Metayer-Levrel, G., Perthuisot, J.P., 2000. Bacterial roles in the precipitation of carbonate minerals. In: Riding, R.E., Awramik, S.M. (Eds) *Microbial Sediments*. Springer, Berlin, Heidelberg, pp 32 – 39.
- Chaerun, S.K., Tazaki, K., 2003. Effect of kaolinite on microbial growth in high concentration of heavy oil. *Clay Science*. **12**, 187 – 196.
- Chafetz, H., Barth, J., Cook, M., Guo X., Zhou J., 2018. Origins of carbonate spherulites: Implications for Brazilian Aptian pre-salt reservoir. *Sediment Geology*. **365**, 21 – 33.
- Chen, L., Shen, Y., Xie, A., Huang, B., Jia, R., Guo, R., Tang, W., 2009. Bacteria-mediated synthesis of metal carbonate minerals with unusual morphologies and structures. *Crystal Growth Design*. **9**(2), 743 – 754.
- Christ, C.L., Hostetle, P.B., 1970. Studies in system $MgO - SiO_2 - CO_2 - H_2O$. (II) Activity-product constant of magnesite. *American Journal of Science*. **268**(5), 439 – 453.
- Cline, J.D., 1969. Spectrophotometric determination of hydrogen sulfide in natural waters. *Limnology and Oceanography*. **14**, 454 – 458.
- Coelho, W.A., 2007. *TOPAS-Academic, Coelho Software*. Brisbane, Australia.
- Coleman, M.L., Hedrick, D.B., Lovley, D.R., White, D.C., Pye K., 1993. Reduction of Fe(III) in sediments by sulfate reducing bacteria. *Nature*. **361**, 436 – 438.
- Curtis Roegner, G., Needoba, J.A., Baptista, A., 2011. Coastal upwelling supplies oxygen-depleted water to the Columbia River Estuary. *PlosOne*. **6**(4), e18672.
- Cury, P., Bakun, A., Crawford, R.J.M., Jarre, A., Quinones, R.A., Shannon, L.J., Verheye, H.M., 2000. Small pelagic in upwelling systems: patterns of interaction and structural changes in “wasp-waist” ecosystems. *ICES Journal of Marine Science*. **57**, 603 – 618.
- Cygan, R.T., Wright, K., Fidler, D.K., Gale, J.D., Slater, B., 2002. Atomistic models of carbonate minerals: Bulk and surface structures, defects, and diffusion. *Molecular Simulation*. **28**, (6-7), 475 – 495.
- D’Hondt, S., Rutherford, S., Spivack, A.J., 2002. Metabolic activity of subsurface life in deep-sea sediments. *Science*. **295**, 2067 – 2070.
- Dahl, K., Buchardt, B., 2006. Monohydrocalcite in the arctic Ikka Fjord, SW Greenland: First reported marine occurrence. *Journal Sedimentary Research*. **76**, 460 – 471.
- Davis, K.J., Dove, P.M., De Yoreo, J.J., 2000. The role of Mg^{2+} as an impurity in calcite growth. *Science*. **290**, 1134 – 1137.
- De Choudens-Sanchez, V., Gonzalez, L.A., 2009. Calcite and aragonite precipitation under controlled instantaneous supersaturation: Elucidating the role of $CaCO_3$ saturation

- state and Mg/Ca ratio on calcium carbonate polymorphism. *Journal of Sedimentary Research*. **79**, 363 – 376.
- De Yoreo, J.J., Filbert, P.U.P.A., Sommerdijk, N.A.J.M., Lee Penn, R., Whitelam, S., Joester, D., Zhang, H., Rimer, J.D., Navrotsky, A., Banfield, J.F., Wallace, A.F., Michel, F.M., Meldrum, F.C., Colfen, H., Dove, P.M., 2015. Crystallization by particle attachment in synthetic, biogenic, and geologic environments. *Science*. **349**(6247). Doi 10.1126/science.aaa6760.
- Dejehet, F., Idrissi, S., Debuyst, R., 1999. Magnesium and occluded water in calcium carbonate monohydrate. *Journal de Chimie Physique*. **96**, 741 – 753.
- Dela Pierre, F., Clari, P., Bernardi, E., Natalicchio, M., Costa, E., Cavagna, S., Lozar, F., Lugli, S., Manzi, V., Roveri, M., Violanti, D., 2012. Messinian carbonate-rich beds of the Tertiary Piedmont Basin (NW Italy): Microbially-mediated products straddling the onset of the salinity crisis. *Palaeogeography, Palaeoclimatology, Palaeoecology*. **344 – 345**, 78 – 93.
- Delaney, M.L., 1998. Phosphorus accumulation in marine sediments and the oceanic phosphorus cycle. *Global Biogeochemical Cycle*. **12**(4), 563 – 572.
- Dickson, J.A.D., 1993. Crystal growth diagrams as an aid to interpreting the fabrics of calcite aggregates. *Journal of Sedimentary Research*. **63**(1), 1 – 17.
- Dickson, A.G., Afghan, J.D., Anderson, G.C., 2003. Reference materials for oceanic CO₂ analysis: a method for the certification of total alkalinity. *Marine Chemistry*. **80** (2-3), 185 – 197.
- Disnar, J.R., Stefanova, M., Breheret, J.G., Macaire, J.J., 2011. Microbial mat development and dolomite formation under pre- evaporitic conditions during the Atlantic in a temperate area: The Sarlieve Lake (French Massif Central). *Organic Geochemistry*. **42**, 1089 – 1098.
- Dobberschutz, S., Nielsen, M.R., Sand, K.K., Civioc, R., Bovet N., Stipp, S.L.S., Andersson, M.P., 2018. The mechanisms of crystal growth inhibition by organic and inorganic inhibitors. *Nature Communication*. **9**, 1578.
- Dong, H., 2010. Mineral-microbe interactions: a review. *Frontiers of Earth Sciences China*. **4** (2), 127 – 147.
- Dong, H., Fredrickson, J.K., Kennedy, D.W., Zachara, J.M., Kukkadapu, R.K., Onstott T.C., 2000. Mineral transformation associated with the microbial reduction of magnetite. *Chemical Geology*. **169**, 299 – 318.

- Donnet, M., Bowen, P., Jongen, N., Lemaitre, J., Hofmann, H., 2005. Use of seeds to control precipitation of calcium carbonate and determination of seed nature. *Langmuir*. **25**, 100 – 108.
- Douglas, S., Beveridge, T.J., 1998. Mineral formation by bacteria in natural microbial communities. *FEMS Microbiology Ecology*. **26**, (2), 79 – 88.
- Dupraz, C., Reid, R.P., Braissant, O., Decho, A.W., Norman, R.S., Visscher, P.T., 2009. Processes of carbonate precipitation in modern microbial mats. *Earth-Science Review*. **96**, 141 – 162.
- Dupraz, C., Visscher, P.T., 2005. Microbial lithification in marine stromatolites and hypersaline mats. *Trends in Microbiology*. **13**, 429 – 438.
- Dupraz, C., Visscher, P.T., Baumgartner, L.K., Reid, R.P., 2004. Microbe-mineral interactions: early carbonate precipitation in a hypersaline lake (Eleuthera Island, Bahamas). *Sedimentology*. **51**, 745 – 765.
- Effenberger, H., 1981. Kristallstruktur und Infrarot-Absorptionsspektrum von synthetischem Monohydrocalcit, $\text{CaCO}_3 \cdot \text{H}_2\text{O}$. *Monatsh. Chem.* **112**, 899 – 909.
- Effenberger, H., Mereiter, K., Zemann, J., 1981. Crystal structure refinements of magnesite, calcite, rhodochrosite, siderite, smithonite, and dolomite, with discussion of some aspects of the stereochemistry of calcite type carbonates. *Zeitschrift für Kristallographie*. **156**, 233 – 243.
- Egger, M., Jilbert, T., Behrends, T., Rivard, C., Slomp, C.P., 2015. Vivianite is a major sink for phosphorus in methanogenic coastal surface sediments. *Geochimica Cosmochimica Acta*. **169**, 217 – 235.
- Egger, M., Riedinger, N., Mogollon, J.M., Jorgensen, B.B., 2018. Global diffusive fluxes of methane in marine sediments. *Nature Geoscience*. **11**, 421 – 425.
- Ehrlich, H.L., 1996. *Geomicrobiology*. New York, NY: Marcel Dekker.
- Elsgaard, L., Isaksen, M.F., Jorgensen, B.B., Alayse, A-M., Jannasch, H.W., 1994. Microbial sulfate reduction in deep-sea sediments at the Guaymas Basin hydrothermal vent area: Influence of temperature and substrates. *Geochimica et Cosmochimica Acta*. **58** (16), 3335 – 3343.
- Elstnerova, P., Friak, M., Fabritius, H.O., Lymperakis L., Hickel, T., Petrov, M., Nikolov, S., Raabe, D., Ziegler, A., Hild, S., Neugebauer, J., 2010. *Acta Biomaterialia*. **6**(10), 4506 – 4512.
- Eswaran, H., Reich, P.F., Kimble, J.M., Beinroth, F.H., Padmanabhan, E., Moncharoen, P., 2000. Global carbon sinks, In: Lal, R., Kimble, J.M., and Stewart, B.A., (Eds.), *Global*

- Climate Change and Pedogenic Carbonates. CRC/Lewis Press, Boca Raton, Florida, pp, 15 – 26.
- Falkowski, P., Scholes, R.J., Boyle, E., Canadell, J., Canfield, D., Elser, J., Gruber, N., Hibbard, K., Hogberg, P., Linder, S., Mackenzie, F.T., Moore III, B., Pederson, T., Rosenthal, Y., Seitzinger, S., Smetacek, V., Steffen, W., 2000. The global carbon cycle: A test of our knowledge of Earth as a system. *Science*. **290**, 291 – 296.
- Faul, K.L., Paytan, A., Delaney, M.L., 2005. Phosphorus distribution in sinking oceanic particulate matter. *Marine Chemistry*. **97**(3 – 4), 307 – 333.
- Feio, M.J., Zinkevich, V., Beech, I.B., Llobet-Brossa, E., Eaton, P., Schmitt, J., Guezennec, J., 2004. *Desulfovibrio alaskensis* sp. nov., a sulphate-reducing bacterium from a soured oil reservoir. *International Journal of Systematic and Evolutionary Microbiology*. **54**, 1747 – 1752.
- Fernandez-Martinez, A., Hu, Y., Lee, B., Jun, Y-S., Waychunas, G.A., 2013. Heterogeneously nucleated CaCO₃ and quartz substrates: Thermodynamics of CO₂ mineral trapping. *Environmental Science and Technology*. **47**, 102 – 109.
- Fernandez-Remolar, D.C., Preston, L.J., Sanchez-Roman, M., Izawa, M.R.M., Huang, L., Southam, G., Banerjee, N.R., Osinski, G.R., Flemming, R., Gomez-Ortiz, D., Ballesteros, O.P., Rodriguez, N., Amils, R., Dyar, M.D., 2012. Carbonate precipitation under bulk acidic conditions as a potential biosignature for searching life on Mars. *Earth and Planetary Science Letters*. 351 – 352, 13 – 26.
- Filip, Z., Haider, K., Martin, J.P., 1972. Influence of clay minerals on growth and metabolic activity of *Epicoccum nigrum* and *Stachybotrys chartarum*. *Soil Biology and Biochemistry*. **4**, 135 – 145.
- Frank, K.L., Rogers, K.L., Rogers, D.R., Johnston, D.T., Girguis, P.R., 2015. Key factors influencing rates of heterotrophic sulfate reduction in active seafloor hydrothermal massive sulphide deposits. *Frontiers in Microbiology*. **6**, 1449.
- Fredrickson, J.K., McKinley, J.P., Bjornstad, B.N., Long, P., Ringelberg, D.B., White, D.C., Krumholz, L.R., Suflita, J.M., Colwell, F.S., Lehman, R.M., Phelps, T.J., 1997. Pore-size constraints on the activity and survival of subsurface bacteria in a late Cretaceous shale-sandstone sequence, Northwestern New Mexico. *Geomicrobiology Journal*. **14**, 183 – 202.
- Fukushi, K., Munemoto, T., Sakai, M., Yagi, S., 2011. Monohydrocalcite: a promising remediation material for hazardous anions. *Science and Technology of Advance Materials*. **12**, 64702 – 64714.

- Fukushi, K., Suzuki, Y., Kawano, J., Ohno, T., Ogawa, M., Yaji, T., Takahashi, Y., 2017. Speciation of magnesium in monohydrocalcite: XANES, *ab initio* and geochemical modelling. *Geochimica et Cosmochimica Acta*. **213**, 457 – 474.
- Gab, F., Ballhaus, C., Siemens, J., Heuser, A., Lissner, M., Geisler, T., Garbe-Schonberg, D., 2017. Siderite cannot be used as CO₂ sensor for Achaean atmospheres. *Geochimica et Cosmochimica Acta*. **214**, 209 – 225.
- Gallagher, K.L., Braissant, O., Kading, T.J., Dupraz, C., Visscher, P.T., 2013. Phosphate-related artifacts in carbonate mineralization experiments. *Journal of Sedimentary Research*. **83**, 37 – 49.
- Gallagher, K.L., Dupraz, C., Visscher, P.T., 2014. Two opposing effect of sulfate reduction on carbonate precipitation in normal marine, hypersaline, and alkaline environments *Geology: Comment*. E313 – 314.
- Gallagher, K.L., Kading, T.J., Braissant, O., Dupraz, C., Visscher, P.T., 2012. Inside the alkalinity engine: the role of electron donors in the organomineralization potential of sulfate-reducing bacteria. *Geobiology*. **10** (6), 518 – 530.
- Grad601, 2018. Magnetic Gradiometer System (Instrument brochure). Bartington Instruments. http://www.bartington.com/Literaturepdf/Datasheets/Grad-601_DS1800.pdf.
- Granasy, L., Pusztai, T., Tegze, G., Warren, J.A., Douglas, J.F., 2005. Growth and form of spherulites. *Physical Review Letters*. **72**, 011605.
- Grant, C.L., Pramer, D., 1962. Minor element composition of yeast extract. *Journal of Bacteriology*. **84**, 869 – 870.
- Grases, F., March, J.G., 1990. Determination of phosphate based on inhibition of crystal growth of calcite. *Analytica Chimica Acta*. **229**, 249 – 254.
- Grenthe, Ingmar, Plyasunov, A.V., Kastriot, S., 1997. Estimate of medium effects on thermodynamic data, in Grenthe, Ingmar, and Puigdomenech, Ignasi, eds., *Modelling in aquatic chemistry*, chap. IX: Paris, OECD Nuclear Energy Agency, p 325 – 426.
- Grim, R.E., 1953. *Clay mineralogy*. McGraw Hill, N.Y.
- Guggenheim, E.A., Turgeon, J.C., 1955. Specific interaction of ions. *Transaction of. Faraday Society*. **51**, 747 – 761.
- Han, M., Zhao, Y., Zhao, H., Han, Z., Yan, H., Sun, B., Meng, R., Zhuang, D., Li, D., Liu, B., 2017a. A comparison of amorphous calcium carbonate crystallization in aqueous solutions of MgCl₂ and MgSO₄: implications for paleo-ocean chemistry. *Mineralogy and Petrology*. DOI 10.1007/s00710-017-0528-9. pp 1 – 16.

- Han, Z., Li, D., Zhao, H., Yan Li, P., 2017 Precipitation of carbonate minerals induced by the halophilic *Chromohalobacter israelensis* under high salt concentrations: Implications for natural environments. *Minerals*. **7**(6), 95; doi:103390/min7060095.
- Han, X., Schultz, L., Zhang, W., Zhu, J., Meng, F., Geesey, G.G., 2016. Mineral formation during bacterial sulfate reduction in the presence of different electron donors and carbon sources. *Chemical Geology*. **435**, 49 – 59.
- Haouari, O., Fardeau, M.L., Casalot, L., Tholozan, J.L., Hamdi, M., Ollivier, B., 2006. Isolation of sulfate-reducing bacteria from Tunisian marine sediments and description of *Desulfovibrio bizertensis* sp. nov. *International Journal of System Evolution Microbiology*. **56**, 2909 – 2913.
- Harrison, C.S., Hales, B., Siedlecki, S., Samelson, R.M., 2016. Potential and timescales for oxygen depletion in coastal upwelling systems: A box-model analysis. *Journal of Geophysical Research: Oceans*. **121**(5), 3202 – 3227.
- Heberling, C., Lowell, R.P., Liu, L., Fisk, M.R., 2010. Extent of the microbial biosphere in the oceanic crust. *Geochemistry, Geophysics, Geosystem*. **11**, Q08003.
- Henzler, H.J., Schedel, M., 1991. Suitability of the shaking flask for oxygen supply to microbiological cultures. *Bioprocess Engineering*. **7**, 123 – 131.
- Higgins, J.A., Fischer, W.W., Schrag, D.P., 2009. Oxygenation of the ocean and sediments: Consequences for the seafloor carbonate factory. *Earth and Planetary Science Letters*. **284**, 25 – 33.
- Hood, A.V.S., Wallace, M.W., Drysdale, R.N., 2011. Neoproterozoic aragonite-dolomite seas? Widespread marine dolomite precipitation in Cryogenian reef complexes. *Geology*. **9**, 871 – 874.
- Hopkinson, L., Kristova, P., Rutt, K., Cressey, G., 2012. Phase transitions in the system MgO-CO₂-H₂O during CO₂ degassing of Mg-bearing solutions. *Geochimica et Cosmochimica Acta*. **76**, 1 – 13.
- Howarth, R.W., 1974. The role of sulfur in salt-marsh metabolism. PhD. thesis. Pp.82.
- Howarth, R.W., 1978. Pyrite: Its rapid formation in a salt-marsh and its importance in ecosystem metabolism. *Science*, **203** (5), 49 – 50.
- Hull, H., Turnbull, A.G., 1973. A thermodynamic study of monohydrocalcite. *Geochimica et Cosmochimica Acta*. **37**, 685 – 694.
- Hurst, C.J., 2016. *Their World: A diversity of microbial environments*. *Advances in Environmental Microbiology* 1. Springer.

- Hyacinthe, C., Van Cappellen, 2004. An authigenic iron phosphate phase in estuarine sediments: composition, formation and chemical reactivity. *Marine Chemistry*. **91**, 227 – 251.
- Ihli, J., Wong, W.C., Noel, E.H., Kim, Y.Y., Kulak, A.N., Christenson, H.K., Duer, M.J., Meldrum, F.C., 2014. Dehydration and crystallization of amorphous calcium carbonate in solution and in air. *Nature Communication*. **5**(3169), 1 – 10.
- Irwin, H., Curtis, C., Coleman, M., 1977. Isotopic evidence for source of diagenetic carbonates formed during burial of organic-rich sediments. *Nature*. **269**, 209 – 213.
- Ito, T., 1993. The occurrence of monohydrocalcite from calcareous sinter of cold spring of Shiowakka, Asyoro, Hokkaido. *Journal of Mineral Petrology and Economic Geology*. **88**, 485 – 491.
- Jorgensen, B.B., 1984. Mineralization of organic matter in the sea bed – the role of sulfate reduction. *Nature*. **296**, 643 – 645.
- Jorgensen, B.B., Revsbech, N.P., Cohen, Y., 1983. Photosynthesis and structure of benthic microbial mats: microelectrodes and SEM studies of four cyanobacteria communities. *Limnology and Oceanography*. **28**, 1075 – 1093.
- Kaleli, H.A., Islam, M.R., 1997. Effect of temperature on the growth of wastewater bacteria. *Toxicological and Environmental Chemistry*. **59**(1 – 4), 111 – 123.
- Kamiya, K., Sakka, S., Terada, K., 1977. Aragonite formation through precipitation of calcium carbonate monohydrate. *Materials Research Bulletin*. **12**(11), 1095 – 1102.
- Katz, A., 1973. The interaction of magnesium with calcite during crystal growth at 25 – 90°C and one atmosphere. *Geochimica et Cosmochimica Acta*. **37**, 1563 – 1586.
- Kawaguchi, T., Decho, A.W., 2002. A laboratory investigation of cyanobacterial extracellular polymeric secretions (EPS) in influencing CaCO₃ polymorphism. *Journal of Crystal Growth*. **240**, 230 – 235.
- Kawano, M., Miyashita, M., 2017. Effect of phosphate and sulfate on the precipitation rate and polymorphism of calcium carbonate minerals in solutions with Mg²⁺ ions. *Clay Science*. **21**, 71 – 78.
- Killam, R.L., Barenfanger, J., Cox, M., 2003. Influence of lack CO₂ on anaerobic bacteria: A quick method to verify the absence of CO₂. *Journal of Clinical Microbiology*. **41**(5), 2201 – 2202.
- Kimura, T., Koga, N., 2011. Monohydrocalcite in comparison with hydrated amorphous calcium carbonate: Precipitation condition and thermal behaviour. *Crystal Growth and Design*. **11**, 3877 – 3884.

- Kipp, M.A., Stueken, E.E., 2017. Biomass recycling and Earth's early phosphorus cycle. *Science Advances*. **3**, eaao4795, 1 – 6.
- Kitson, R.E., Mellon, M.G., 1944. Colorimetric determination of phosphorus as molybdivanadophosphoric acid. *Industrial Engineering Chemical Research*. **16**, 379.
- Kolesar, M., Curlik, J., 2015. Origin, distribution and transformation of authigenic carbonates in loessic soils. *Eurasian Journal of Soil Science*. **4**, 38 – 43.
- Kraal, P., Slomp, C.P., Reed, D.C., Reichart, G.J., Poulton, S.W., 2012. Sedimentary phosphorus and iron cycling in and below the oxygen minimum zone of the northern Arabian Sea. *Biogeosciences*. **9**, 2603 – 2624.
- Lenders, J.J., Dey, A., Bomans, P.H.H., Spielmann, J., Hendrix, M.M.R.M., de With, G., Meldrum, F.C., Harder, D., Sommerdijk, N.A.J.M., 2012. High-magnesian calcite mesocrystals: A coordination chemistry approach. *Journal of American Society*. **134**, 1367 – 1373.
- Lian, B., Hu, Q., Chen, J., Ji, J., Teng, H.H., 2006. Carbonate biomineralization by soil bacterium *Bacillus megaterium*. *Geochimica et Cosmochimica Acta*. **70**, 5522 – 5535.
- Lin, C.J., Yang, S.Y., Huang, S.J., Chan, J.C.C., 2015. Structural characterization of Mg-stabilized amorphous calcium carbonate by Mg-25 solid-state NMR spectroscopy. *Journal of Physical Chemistry C*. **119**, 7225 – 7233.
- Lin, Y.P., Singer, P.C., 2005. Inhibition of calcite crystal growth by polyphosphates. *Water Research*. **39**(19). 4835 – 4843.
- Lin, C.Y., Turchyn, A.V., Steiner, Z., Bots, P., Lampronti, G.I., Tosca, N.J., 2018. The role of microbial sulfate reduction in calcium carbonate polymorph selection. *Geochimica et Cosmochimica Acta*. **237**, 184 – 204.
- Lioliou, M.G., Paraskeva, C.A., Koutsoukos, P.G., Payatakes, A.C., 2007. Heterogeneous nucleation and growth of calcium carbonate on calcite and quartz. *Journal of Colloid Interface Science*. **208**, 421 – 428.
- Lippmann, F., 1973. *Sedimentary Carbonate Minerals*. Springer Verlag, Berlin Heidelberg.
- Liu, R., Liu, F.L., Zhao, S.Q., Su, Y.L., Wang, D.J., Shen, Q., 2013. Crystallization and oriented attachment of monohydrocalcite and its crystalline phase transformation. *Crystal Engineering Communication*. **15**, 509 – 515.
- Loste, E., Wilson, R.M., Seshadri, R., Meldrum, F.C., 2003. The role of magnesium in stabilizing amorphous calcium carbonate and controlling calcite morphologies. *Journal of Crystal Growth*. **254**, 206 – 218.

- Luther III, G.W., Shellenbarger, P.A., Brendel, P.J., 1996. Dissolved organic Fe(III) and Fe(II) complexes in salt-marsh porewaters. *Geochimica et Cosmochimica Acta*. **60**, 951 – 960.
- Ma, C., Eggleton, R.A., 1999. Cation exchange capacity of kaolinite. *Clays and Clay Minerals*. **47** (2), 174 – 180.
- Madsen, I.C., Scarlett, N.V.Y., 2008. Quantitative Phase Analysis. In *Powder Diffraction: Theory and Practice*, edited by Dinnabier, R.E., Royal Society of Chemistry.
- Magnabosco, C., Lin, L-H., Dong, H., Bomberg, M., Ghiorse, W., Stan-Lotter, H., Pedersen, K., Kieft, T.L., van Heerden, E., Onstott, T.C., 2018. The biomass and biodiversity of the continental subsurface. *Nature Geoscience*. **11**, 707 – 717.
- Marnette, E.C.L., Van Breeman, N., Hordijk, K.A., Cappenberg, T.E., 1993. Pyrite formation in two freshwater systems in the Netherlands. *Geochimica et Cosmochimica Acta*. **57**, 4165 – 4177.
- Marschner, H., 1969. Hydrocalcite ($\text{CaCO}_3 \cdot \text{H}_2\text{O}$) and Nesquehonite ($\text{MgCO}_3 \cdot 3\text{H}_2\text{O}$) in carbonate scales. *Science*. **165**, 1119 – 1121.
- McCartney, D.M., Oleszkiewicz, J.A., 1991. Sulfide inhibition of anaerobic degradation of lactate and acetate. *Water Research*. **25**(2), 203 – 209.
- McCusker, L.B., Von Dreele, R.B., Cox, D.E., Louer, D., Scardi, P., 1999. Reitveld refinement guidelines. *Journal Applied Crystallography*. **32**(1), 36 – 50.
- McDaniel, L.E., Bailey, E.G., 1969. Effect of shaking speed and type of closure on shake flask cultures. *Applied Microbiology*. **17**(2), 286 – 290.
- Mechalas, B.J., Rittenberg, S.C., 1960. Energy coupling in *Desulfovibrio Desulfuricans*. *Journal of Bacteriology*. **80**, 501 – 507.
- Meic, I.B., Kontec, J., Jurasin, D.D., Dzakula, B.N., Stajner, L., Lyons, D.M., Sikiric, M.D., Kralj, D., 2017. Comparative study of calcium carbonates and calcium phosphates precipitation in model systems mimicking the inorganic environment for biomineralization. *Crystal Growth Design*. **17**(3), 1103 – 1117.
- Meier, J., Piva, A., Fortin, D., 2012. Enrichment of sulfate-reducing bacteria and resulting mineral formation in media mimicking pore-water metal ion concentrations and pH conditions of acidic pit lakes. *FEMS Microbiology Ecology*. **79**(1), 69 – 84.
- Meister, P., 2013. Two opposing effects of sulfate reduction on carbonate precipitation in normal marine, hypersaline, and alkaline environments. *Geology*. **41**, 499 – 502.
- Meister, P., 2014. Two opposing effects of sulfate reduction on carbonate precipitation in normal marine, hypersaline, and alkaline environments. *Geology: Reply*. E315.

- Meister, P., McKenzie, J.A., Vasconcelos, C., Bernasconi, S., Frank, M., Gutjahr, M., Schrag, D., 2007. Dolomite formation in the dynamic deep biosphere: results from the Peru Margin. *Sedimentology*. **54**, 1007 – 1031.
- Millero, F.J., 1982. The effect of pressure on the solubility of minerals in water and seawater. *Geochimica et Cosmochimica Acta*. **46**, 11 – 22.
- Mills, J., Antler, G., Turchyn, A.V., 2016. Geochemical evidence for cryptic sulfur cycling in salt-marsh sediments. *Earth and Planetary Science Letter*. **453**, 23 – 32.
- Mitchell, A.C., Ferris, F.G., 2006. The influence of *Bacillus pasteurii* on the nucleation and growth of calcium carbonate. *Geomicrobiology Journal*. **108**, 4332 – 4432.
- Morse, J.M., He, S., 1993. Influences of T, S and P_{CO2} on the pseudo-homogeneous precipitation of CaCO₃ from seawater: implications for whiting formation. *Marine Chemistry*. **41**, 291 – 297.
- Morse, J.W., Arvidson, R.S., Luttge, A., 2007. Calcium carbonate formation and dissolution. *Chemical Review*. **107**, 342 – 381.
- Morse, J.W., Casey, W.H., 1988. Ostwald processes and mineral paragenesis in sediments. *American Journal of Science*. **288**, 537 – 560.
- Morse, J.W., Wang, Q., Tsio, M.Y., 1997. Influence of temperature and Mg:Ca ratio on CaCO₃ precipitates from seawater. *Geology*. **25**(1), 85 – 87.
- Mortimer, R.J.G., Coleman, M.L., Rae, J.E., 1997. Effect of bacteria on the elemental composition of early diagenetic siderite: implications for paleoenvironmental interpretations. *Sedimentology*. **44**, 759 – 765.
- Mozley, P.S., Burns, S.J., 1993. Oxygen and carbon isotopic composition of marine carbonate concretions: an overview. *Journal of Sedimentary Petrology*. **63**, 73 – 83.
- Mueller, B., 2015. Experimental interaction between clay minerals and bacteria: A Review. *Pedosphere*. **25** (6), 799 – 810.
- Muller, G., Irion, G., Forstner, U., 1972. Formation and diagenesis of inorganic Ca-Mg carbonates in the lacustrine environment. *Naturwissenschaften*. **59**, 158 – 164.
- Munemoto, T., Fukushi, K., 2008. Transformation kinetics of monohydrocalcite to aragonite in aqueous solutions. *Journal of Mineralogical and Petrological Science*. **103**, 345 – 349.
- Munemoto, T., Fukushi, K., Kanzaki, Y., Murakami, T., 2014. Redistribution of Pb during transformation of monohydrocalcite to aragonite. *Chemical Geology*. **387**, 133 – 143.
- Nielsen, M.R., Sand, K.K., Rodriguez-Blanco, J.D., Bovet, N., Generosi, J., Dalby, K.K., Stipp, S.L.S., 2016. Inhibition of calcite growth: Combined effects of Mg²⁺ and SO₄²⁻. *Journal Crystal Growth*. **16**, 6199 – 6207.

- Nishiyama, R., Munemoto, T., Fukushi, K., 2013. Formation condition of monohydrocalcite from $\text{CaCl}_2\text{-MgCl}_2\text{-Na}_2\text{CO}_3$ solutions. *Geochimica et Cosmochimica Acta*. **100**, 217 – 231.
- Nyiro-Kosa, I., Rostasi, A., Bereczk-Tompa, E., Cora, I., Koblar, M., Kovacs, A., Posfai, M., 2018. Nucleation and growth of Mg-bearing calcite in a shallow, calcareous lake. *Earth Planetary Science Letters*. **496**, 20 – 28.
- Obst, M., Dynes, J.J., Lawrence, J.R., Swerhone, G.D.W., Benzerara, K., Karunakaran, C., Kaznatcheev, K., Tyliczszak, T., Hitchcock, A.P., 2009. Precipitation of amorphous CaCO_3 (aragonite-like) by cyanobacteria: A STXM study of the influence of EPS on the nucleation process. *Geochimica et Cosmochimica Acta*. **73**, 4180 – 4198.
- Okabe, S., Nielsen, P.H., Jones, W.L., Characklis, W.G., 1995. Sulfide product inhibition of *Desulfovibrio desulfuricans* in batch and continuous cultures. *Water Research*. **29**(2), 571 – 578.
- Omoike, A., Chorover, J., 2006. Adsorption to goethite of extracellular polymeric substances from *Bacillus subtilis*. *Geochimica et Cosmochimica Acta*. **70**, 827 – 838.
- Oomori, T., Kyan, A., Kitano, Y., 1988. Magnesium calcite synthesis from calcium bicarbonate solution containing magnesium ions in the presence of fluoride and phosphate ions. *Geochemical Journal*. **22**, 275 – 283.
- Ozery, G., 2014. Kinetics vs Thermodynamics. University of California Davis. [https://chem.libretexts.org/Bookshelves/Physical_and_Theoretical_Chemistry_Textbook_Maps/Supplemental_Modules_\(Physical_and_Theoretical_Chemistry\)/Equilibria/Chemical_Equilibria/Principles_of_Chemical_Equilibria/Kinetically_vs_Thermodynamically_Stable](https://chem.libretexts.org/Bookshelves/Physical_and_Theoretical_Chemistry_Textbook_Maps/Supplemental_Modules_(Physical_and_Theoretical_Chemistry)/Equilibria/Chemical_Equilibria/Principles_of_Chemical_Equilibria/Kinetically_vs_Thermodynamically_Stable)
- Pallud, C., Van Cappellen, P., 2006. Kinetics of microbial sulfate reduction in estuarine sediments. *Geochimica et Cosmochimica Acta*. **70** (5), 1148 – 1162.
- Parkhurst, D., Appelo, C.A.J., 1999. User's guide to PhreeqC (Version 2) – a computer program for speciation, batch-reaction, one-dimensional transport, and inverse geochemical calculations. Water-resources Investigations Report 99-4259, U.S. Department of the interior, Denver, Colorado.
- Parkhurst, D.L., Appelo, C.A.L., 2013. Description of input and examples for PHREEQC version 3 – A computer program for speciation, batch-reaction, one-dimensional transport, and inverse geochemical calculations: U.S., Geological Survey Techniques and Methods, book 6, chap. A43, 497 p., available only at <http://pubs.usgs.gov/tm/06/a43>.

- Picard, A., Gartman, A., Clarke, D.R., Girguis, P.R., 2018. Sulfate-reducing bacteria influence the nucleation and growth of mackinawite and greigite. *Geochimica et Cosmochimica Acta*. **220**, 367 – 384.
- Picard, A., Gartman, A., Girguis, P.R., 2016. What do we really know about the role of microorganisms in iron sulfide mineral formation? *Frontiers in Earth Sciences*. **4**, 68.
- Plummer, L.N., Busenberg, E., 1982. The solubilities of calcite, aragonite and vaterite in CO₂ – H₂O solutions between 0 and 90°C, and an evaluation of the aqueous model for the system CaCO₃-CO₂-H₂O. *Geochimica et Cosmochimica Acta*. **46**(6), 1011 – 1040.
- Politi, Y., Arad, T., Klein, E., Weiner, S., Addadi, L., 2004. Sea urchin spine calcite forms via a transient amorphous calcium carbonate phase. *Science*. **306**, 1161 – 1164.
- Postgate, J.R., 1965. Recent advances in the study of the sulfate-reducing bacteria. *Bacteriological Review*. **29**(4), 425 – 441.
- Potman, R.P., Wesdorp, J., 1994. Method for preparation of a yeast extract, said yeast extract, its use as a food flavor, and a food composition comprising the yeast extract. United State Patent.
- Purgstaller, B., Konrad, F., Dietzel, M., Immenhauser, A., Mavromatis, V., 2017. Control of Mg²⁺/Ca²⁺ activity ratio on the formation of crystalline carbonate minerals via an amorphous precursor. *Crystal Growth Design*. **17**, 1069 – 1078.
- Pye, K., Dickinson, A.D., Schiavon, N., Coleman, M.L., Cox, M., 1990. Formation of siderite-Mg-calcite iron sulphide concretions in intertidal marsh and sandflat sediments, north Norfolk, England. *Sedimentology*. **37**, 325 – 343.
- Qiu, X., Yao, Y., Wang, H., Duan, Y., 2017. Live microbial cells adsorb Mg²⁺ more effectively than lifeless organic matter. *Frontiers Earth Science*. DOI 10.1007/s11707-017-0626-3.
- Raiswell, R., Fisher, Q.J., 2004. Rates of carbonate cementation associated with sulfate reduction in DSDP/ODP sediments: Implications for the formation of concretions. *Chemical Geology*. **211**, 71 – 85.
- Reddy, M.M., Nancollas, G.H., 1971. The crystallization of calcium carbonate. I. Isotopic exchange and kinetics. *Journal of Colloid and Interface Science*. **36**(2), 166 – 172.
- Reid, R.P., Visscher, P.T., Decho, A.W., Stolz, J.F., Bebout, B.M., Dupraz, C., Macintyre, L.G., Paerl, H.W., Pinckney, J.L., Prufert-Bebout, L., Steppe, T.F., DesMarais, D.J., 2000. The role of microbes in accretion, lamination and early lithification of modern marine stromatolites. *Nature*. **406**, 989 – 992.
- Reilly, S., 1980. The carbon dioxide requirements of anaerobic bacteria. *Journal of Medical Microbiology*. **13**, 573 – 579.

- Reis, J.B., Anderson, M.A., Hill, R.T., 2008. Seawater Mg/Ca controls polymorph mineralogy of microbial CaCO₃: A potential proxy for calcite-aragonite seas in Precambrian time. *Geobiology*. **6**, 106 – 119.
- Rivadeneira, M.A., Delgado, G., Ramos-Cormenzana, A., Delgado, R., 1998. Biomineralization of carbonates by *Halomonas eurihalina* in solid and liquid media with different salinities: crystal formation sequence. *Research in Microbiology*. **149**(4), 227 – 287.
- Rivadeneira, M.A., Martin-Algarra, A., Sanchez-Roman, M., Sanchez-Navas, A., Martin-Ramos, J.D., 2010. Amorphous Ca-phosphate precursors for Ca-carbonate biominerals mediated by *Chromohalobacter marismortui*. *ISME Journal*. **4**, 922 – 932.
- Roberts, J.A., Kenward, P.A., Fowle, D.A., Goldstein, R.H., Gonzalez, L.A., Moore, D.S., 2013. Surface chemistry allows for abiotic precipitation of dolomite at low temperature. *PNAS*. **110**, 14540 – 14545.
- Robbins, L.L., Hansen, M.E., Kleypas, J.A., Meylan, S.C., 2010. CO₂calc – A user friendly seawater carbon calculator for Windows, Mac OS X, and IOS (iPhone): U.S. Geological Survey Open-File Report 2010 – 1280, 17 p.
- Rockwell, G.E., 1923. The influence of carbon dioxide on the growth of bacteria. *The Journal of Infectious Diseases*. **32**(1), 98 – 104.
- Rodriguez-Blanco, J.D., Shaw, S., Bots, P., Roncal-Herrero, T., Benning, L.G., 2014. The role of Mg in the crystallization of monohydrocalcite. *Geochimica et Cosmochimica Acta*. **127**, 204 – 220.
- Rodriguez, I.R., Amrhein, C., Anderson, M.A., 2008. Laboratory studies on the coprecipitation of phosphate with calcium carbonate in the Salton Sea, California. *Hydrobiologia*. **604**, 45 – 55.
- Rodriguez-Blanco, J.D., Sand, K.K., Benning, L.G., 2017. ACC and vaterite as intermediates in the solution-based crystallization of CaCO₃. In A.E.S. Van Driessche et al. (eds.), *New Perspectives on Mineral Nucleation and Growth*. DOI10.1007/978-3-319-45669-0_5.
- Rodriguez-Blanco, J.D., Shaw, S., Benning, L.G., 2015. A route for the direct crystallization of dolomite. *American Mineralogist*. **100**, 1172 – 1181.
- Rodriguez-Navarro, C., Jroundi, F., Schiro, M., Ruiz-Agdo, E., Gonzalez-Munoz, M.T., 2012. Influence of substrate mineralogy on bacterial mineralization of calcium carbonate: Implications for stone conservation. *Applied Environmental Microbiology*. **78** (11), 4017 – 4029.

- Rosen, M.R., Miser, D.E., Starcher, M.A., Warren, J.K., 1989. Formation of dolomite in the Coorang region, South Australia. *Geochemica et Cosmochimica Acta*. **53**, 661 – 669.
- Sagemann, J., Jorgensen, B.B., Greeff, O., 1998. Temperature dependence and rates of sulfate reduction in cold sediments of Svalbard, Arctic Ocean. *Geomicrobiology Journal*. **15** (2), 85 – 100.
- Sanchez-Navas, A., Martin-Algarra, A., Rivadeneyra, M.A., Melchor, S., Martin-Ramos, J.D., 2009. Crystal-growth behaviour in Ca-Mg carbonate bacterial spherulites. *Crystal Growth Design*. **9**(6), 2690 – 2699.
- Sanchez-Navas, A., Martin-Algarra, A., Sanchez-Roman, M., Jimenez-Lopez, C., Nieto, F., Ruiz-Bustos, A., 2013. Crystal Growth of Inorganic and Biomediated Carbonates and Phosphates. *Advanced Topics on Crystal Growth Sukarno Ferreira*, IntechOpen. DOI:10.5772/52062.
- Sanchez-Roman, M., Fernandez-Remolar, D., Amils, R., Sanchez-Navas, A., Schmid, T., Martin-Uriz, P.S., Rodriguez, N., McKenzie, J.A., Vasconcelos, C., 2014. Microbial mediated formation of Fe-carbonate minerals under extreme acidic conditions. *Scientific Reports*. **4**, 4767. DOI: 10.1038/srep04767.
- Sanchez-Roman, M., McKenzie, J.A., Wagener, A.L.R., Rivadeneyra, M.A., Vasconcelos, C., 2009. Presence of sulfate does not inhibit low-temperature dolomite precipitation. *Earth and Planetary Science Letters*. **285**, 131 – 139.
- Sanchez-Roman, M., Puente-Sanchez, F., Parro, V., Amils, R., 2015. Nucleation of Fe-rich phosphates and carbonates on microbial cells and exopolymeric substances. *Frontiers in Microbiology*. **6**, 1024. DOI: 10.3389/fmicb.2015.01024.
- Sanchez-Roman, M., Rivadeneyra, M.A., Vasconcelos, C., McKenzie, J.A., 2007. Biomineralization of carbonate and phosphate by moderately halophilic bacteria. *FEMS Microbiology and Ecology*. **61**, 273 – 284.
- Sasaki, K., Noriki, S., Tsunogai, S., 2001. Vertical distributions of interstitial phosphate and fluoride in anoxic sediment: Insight into the formation of an authigenic fluorophosphorus compound. *Geochemical Journal*. **35**, 295 – 306.
- Schinzl, U., 1993. Laboratory experiments on early diagenetic reactions of iron (III) oxyhydroxides in marine sediment (in German). *Berichte*, 36, Fachbereich Geowissenschaften, Universitat Bremen, 189 pp.
- Schrag, D.P., Higgins, J.A., Macdonald, F.A., Johnston, D.T., 2013. Authigenic carbonate and the history of the global carbon cycle. *Science*. **339**, 540 – 543.
- Sekkal., W., Zaoui, A., 2013. Nanoscale analysis of the morphology and surface stability of calcium carbonate polymorphs. *Scientific Reports*. **3**, 1587.

- Sel, O., Radha, A.V., Dideriksen, K., Navrotsky, A., 2012. Amorphous iron (II) carbonate: Crystallization energetics and comparison to other carbonate minerals related to CO₂ sequestration. *Geochimica et Cosmochimica Acta*. **87**, 61 – 68.
- Silver, M.M.W., 2018. An investigation into the suitability of sulfate-reducing bacteria as models for Martian forward contamination. Thesis and Dissertation. 2828.
- Sim, M.S., Ono, S., Donovan, K., Templer, S.P., Bosak, T., 2011. Effect of electron donors on the fractionation of sulfur isotopes by a marine *Desulfovibrio* sp. *Geochimica et Cosmochimica Acta*. **75**, 4244 – 4259.
- Sinkko, H., Lukkari, K., Sihvonen, L.M., Sivonen, K., Leivuori, M., Rantanen, M., Paulin, L., Lyra, C., 2013. Bacteria contribute to sediment nutrient release and reflect progressed eutrophication driven hypoxia in an organic-rich continental sea. *PLoS ONE*. **8**(6), e67061. Doi:10.1371/journal.pone.0067061.
- Smeets, P.J.M., Cho, K.R., Kempen, R.G.E., Sommerdijk, N.A.J.M., De Yoreo, J.J., 2015. Calcium carbonate nucleation driven by ion binding in a biomimetic matrix revealed by *in situ* electron microscopy. *Nature Materials*. **14**, 394 – 399.
- Soetaert, K., Hofmann, A., Middleberg, J., Meysman, F., Greenwood, J., 2007. The effect of biogeochemical processes on pH: *Marine Chemistry*. **105**, 30 – 51.
- Sorokin, Y.I., 1966. Role of carbon dioxide and acetate in biosynthesis by sulphate-reducing bacteria. *Nature*. **210**(5035), 551 – 552.
- Stanley, S.M., Hardie, L.A., 1999. Hypercalcification: paleontology links plate tectonics and geochemistry to sedimentology. *GSA Today*. **9**, 1 – 7.
- Steiner, Z., Rapaport, H., Oren, Y., Kasher, R., 2010. Effect of surface-exposed chemical groups on calcium-phosphate mineralization in water treatment system. *Environmental Science and Technology*. **44**, 7937 – 7943.
- Stockmann, G., Tollefsen, E., Skelton, A., Bruchert, V., Balic-Zunic, T., Langhof, J., Skogby, H., Karlsson, A., 2018. Control of a calcite inhibitor (phosphate) and temperature on ikaite precipitation in Ikka Fjord, southwest Greenland. *Applied Geochemistry*. **89**, 11 – 22.
- Stoffers, P., Fischbeck, R., 1974. Monohydrocalcite in the sediments of Lake Kivu (East Africa). *Sedimentology*. **21**, 163 – 170.
- Stookey, L.L., 1970. Ferrozine – a new spectrophotometric reagent for iron. *Analytical Chemistry*. **42**, 779 – 781.
- Stotzky, G., Rem, L.T., 1966. Influence of clay minerals on microorganisms. I Montmorillonite and kaolinite on bacteria. *Canadian Journal of Microbiology*. **12**, 547 – 563.

- Stotzky, G., 1966a. Influence of clay minerals on microorganisms II. Effect of various clay species monoionic clays, and other particles on bacteria. *Canadian Journal of Microbiology*. **12**, 831 – 848.
- Stotzky, G., 1966b. Influence of clay minerals on microorganisms. III. Effect of particle size, cation exchange capacity, and surface area on bacteria. *Canadian Journal of Microbiology*. **12**, 1235 – 1246.
- Stumm, W., Morgan, J.J., 1996. *Aquatic Chemistry*. John Wiley & Sons, New York. 1022 pp.
- Sun, W., Jayaraman, S., Chen, W., Persson, K.A., Ceder, G., 2015. Nucleation of metastable aragonite CaCO₃ in seawater. *Proceeding of National Academy of Science*. **112**(11), 3199 – 3204.
- Sun, X., Turchyn, A.V., 2014. Significant contribution of authigenic carbonate to marine carbon burial. *Nature Geoscience*. **7**, 201 – 204.
- Suzuki, M., Nagasawa, H., Kogure, T., 2006. Synthesis and structure of hollow calcite particles. *Crystal Growth Design*. **6**(9), 2004 – 2006.
- Tadier, S., Rokidi, S., Rey, C., Combes, C., Koutsoukos, P.G., 2017. Crystal growth of aragonite in the presence of phosphate. *Journal Crystal Growth*. **458**, 44 – 52.
- Takahashi, T., Nakata, H., Hirano, K., Matsuoka, K., Iwataki, M., Yamaguchi, H., 2009. Upwelling of oxygen-depleted water (Sumushio) in Omura Bay, Japan. *Journal of Oceanography*. **65**(1), 113 – 120.
- Taylor, G.F., 1975. The occurrence of monohydrocalcite in two small lakes in the South-East of South Australia. *American Mineralogists*. **60**, 690 – 697.
- Teller, J.T., Last, W.M., 1990. Paleohydrological indicators in playas and salt lakes, with examples from Canada, Australia, and Africa. *Paleogeography, Paleoclimatology, Paleoecology*. **76**, 215 – 240.
- Thompson, J.B., Ferris, F.G., 1990. Cyanobacterial precipitation of gypsum, calcite, and magnesite from natural alkaline water. *Geology*, **18**, 995 – 998.
- Toby, B.H., 2006. R factors in Rietveld analysis: How good is good enough? *Powder Diffraction*. **21**(1), 67 – 70.
- Tommaso, D.D., de Leeuw, N.H., 2010. Structure and dynamics of the hydrated magnesium ion and of the solvated magnesium carbonates: insights from first principles simulations. *Physical Chemistry Chemical Physics*. **12**, 894 – 901.
- Tourney, J., Ngwenya, B.T., 2009. Bacterial extracellular polymeric substances (EPS) mediate CaCO₃ morphology and polymorphism. *Chemical Geology*. **262**, 138 – 146.
- Tracy, S.L., Williams, D.A., Jennings, H.M., 1998. The growth of calcite spherulites from solution II. Kinetics of formation. *Journal of Crystal Growth*. **193**, 382 – 388.

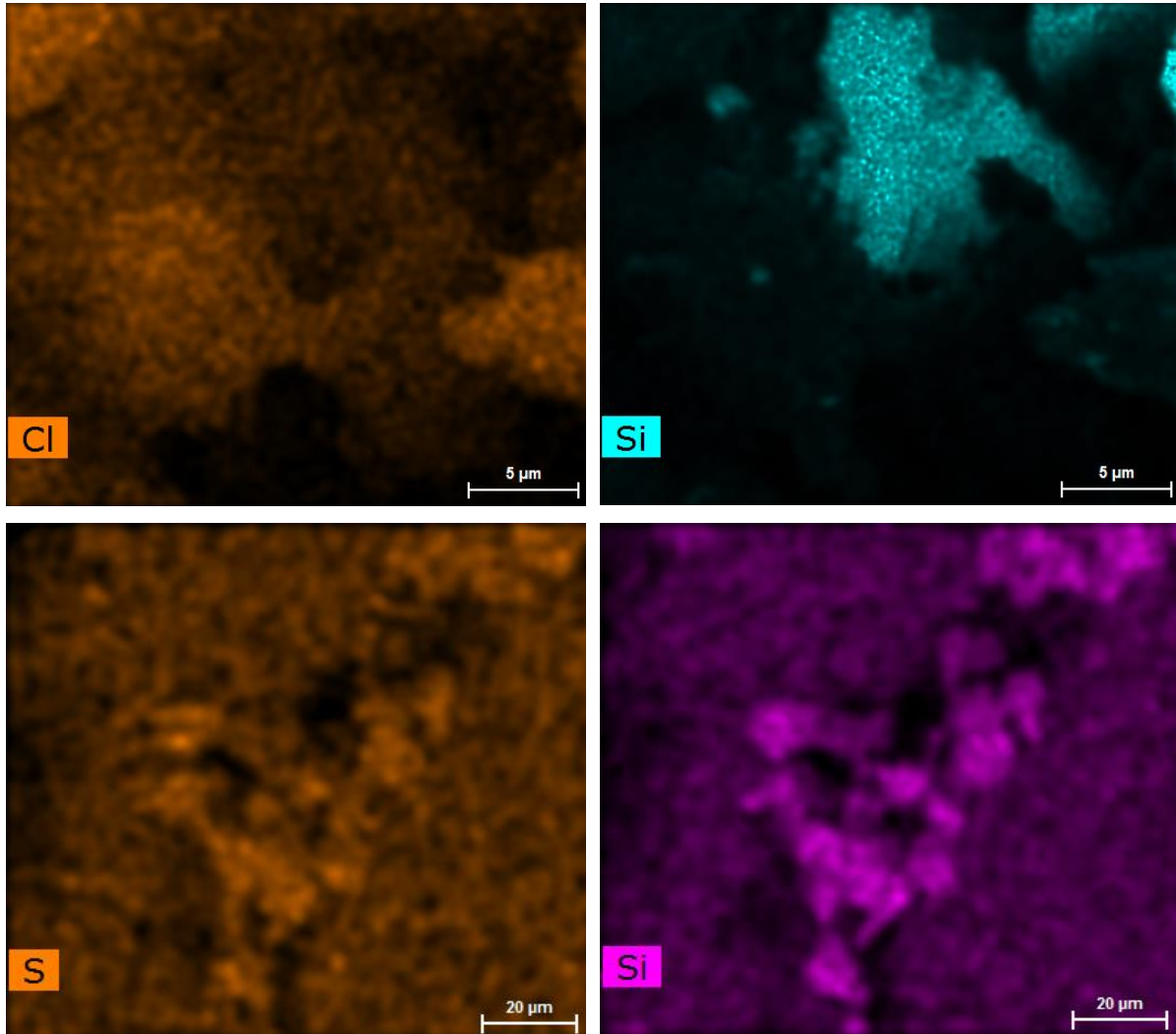
- Trask, P.D., 1936. Relation of salinity to the calcium carbonate content of marine sediments: Shorter contribution to general geology. USGS, Professional Paper 186 – N.
- Tucker, M.E., Wright, V.P., 1990. Carbonate Sedimentology. Blackwell Science. Oxford, UK.
- Ulrich, G.A., Martino, D., Burger, K., Routh, J., Grossman, E.L., Ammerman, J.W., Suflita, J.M., 1998. Sulfur cycling in the terrestrial subsurface: commensal interactions, spatial scales, and microbial heterogeneity. *Microbial Ecology*. **36**, 141 – 151.
- Vagner, M., Sroubkova, E. 1970. About the stimulation effect of bentonite. 8th Ann. Meeting Czech. Microbiol. Soc., Folia Microbiology. (Prague). **15**, 218.
- van Lith, Y., 2001. *The role of sulfate reducing bacteria in dolomite formation. Study of a recent environment, bacterial cultures, and dolomite concretions*. PhD thesis.
- van Lith, Y., Warthmann, R., Vasconcelos, C., McKenzie, J.A., 2003. Sulfate-reducing bacteria induce low-temperature Ca-dolomite and high Mg-calcite formation. *Geobiology*. **1**, 71 – 79.
- Visscher, P.T., Stolz, J.F., 2005. Microbial mats as bioreactors: Populations, processes, and products. *Paleogeography, Paleoclimatology Paleoeology*. **219**, 87 – 100.
- Visscher, P.T., Reid, R.P., Bebout, B.M., 2000. Microscale observations of sulfate reduction: Correlation of microbial activity with lithified micritic laminae in modern marine stromatolites. *Geology*. **28**(10), 919 – 922.
- Visscher, P.T., Reid, R.P., Bebout, B.M., Hoeffts, S.E., Macintyre, I.G., Thompson, J.A., 1998. Formation of lithified micritic laminae in modern marine stromatolites (Bahamas): The role of sulfur cycling: *The American Mineralogist*. **83**, 1482 – 1493.
- Visscher, P.T., Stolz, J.F., 2005. Microbial mats as bioreactors: Polulations, processes, and products. *Paleogeography, Paleoclimatology, Paleoeology*. **219**, 87 – 100.
- Wacey, D., Wright, D.T., Boyce, A.J., 2007. A stable isotope study of microbial dolomite formation in the Coorong Region, South Australia. *Chemical Geology*. **244**, 155 – 174.
- Walter, L.K., Burton, E.A., 1986. The effect of orthophosphate on carbonate mineral dissolution rates in seawater. *Chemical Geology*. **56**, 313 – 323.
- Walter, L.M., 1986. Relative efficiency of carbonate dissolution and precipitation during diagenesis: a progress report on the role of solution chemistry. In Gautier, D.L., ed., *Roles of organic matter in sediment diagenesis*: Soc. Econ. Pal. Min. Sp. Pub. 38, p. 1 – 11.
- Warthmann, R., van Lith, Y., Vasconcelos, C., McKenzie, J.A., Karpoff, A.M., 2000. Bacterially induced dolomite precipitation in anoxic culture experiments. *Geology*. **28**(12), 1091 – 1094.

- Weaver, T.L., Dugan, P.R., 1972. Enhancement of bacterial methane oxidation by clay minerals. *Nature*. **237**, 9172.
- Westrich, J.T., Berner, R., 1984. The role of sedimentary organic matter in bacterial sulfate reduction: The G model tested. *Limnology and Oceanography*. **29** (2), 236 – 249.
- Westrich, J.T., Berner, R., 1988. The effect of temperature on rates of sulfate reduction in marine sediments. *Geomicrobiology Journal*. **6** (2), 99 – 117.
- Whitman, W.B., Coleman, D.C., Wiebe, W.J., 1998. Prokaryotes: the unseen majority. *Proceeding of National Academy of Science*. **95**, 6578 – 6583.
- Wilkin, R.T., Barnes, H.L., 1997. Formation processes of framboidal pyrite. *Geochimica et Cosmochimica Acta*. **61** (2), 323 – 339.
- Wolf, S.L., Jahme, K., Gebauer, D., 2015. Synergy of Mg²⁺ and poly(aspartic acid) in additive-controlled calcium carbonate precipitation. *Crystal Engineering Communication*. **17**, 6857 – 6862.
- Wong, D., Suflita, J.M., McKinley, J.P., Krumholz, L.R., 2003. Impact of clay minerals on sulfate-reducing activity in aquifers. *Microbial Ecology*. **47**(1), 80 – 86.
- Wright, D.T., 1999. The role of sulfate reducing bacteria and cyanobacteria in dolomite formation in distal ephemeral lakes of the Coorong region, South Australia. *Sedimentary Geology*. **126**, 147 – 157.
- Xiouzhu, Z., Unfei, W., Huaiyan, L., 1996. Authigenic mineralogy, depositional environments and evolution of fault-bounded lakes of the Yunnan Plateau, south-western China. *Sedimentology*. **43**, 367 – 380.
- Xu, J., Yan, C., Zhang, F., Konishi, H., Xu, H., Teng, H.H., 2013. Testing the cation-hydration effect on the crystallization of Ca-Mg-CO₃ systems. *Proceeding of National Academy of Science*. **110**(44), 17750 – 17755
- Yagi, S., Fukushi, K., 2011. Phosphate sorption on monohydrocalcite. *Journal of Mineralogy and Petrology Science*. **106**, 109 – 113.
- Yang, X., Xie, B., Wang, L., Qin, Y., Henneman, Z.J., Nancollas, G.H., 2011. Influence of magnesium ions and amino acids on the nucleation and growth of hydroxyapatite. *Crystal Engineering Communications*. **13**, 1153 – 1158.
- Zaarur, S., Wang, D.T., Ono, S., Bosak, T., 2017. Influence of phosphorus and cell geometry on the fractionation of sulfur isotopes by several species of *Desulfovibrio* during microbial sulfate reduction. *Frontiers in Microbiology*. **8**, 890. Doi: 10.3389/fmicb.2017.00890.

- Zachara, J.M., Fredrickson, J.K., Li, S-M., Kennedy, D.W., Smith, S., Gassman, P.L., 1998. Bacterial reduction of crystalline Fe³⁺ oxides in single phase suspensions and subsurface materials. *American Mineralogist*. **83**, 1426 – 1443.
- Zeebe, R.E., Wolf-Gladrow, D., 2001. CO₂ in seawater: Equilibrium, kinetics and isotopes. Elsevier, New York. 346pp.
- Zhao, M.Y., Zheng, Y.F., Zhao, Y.Y., 2016. Seeking a geochemical identifier for authigenic carbonate. *Nature Communications*. **7**(10885), 1 – 7.
- Zhu, T., Dittrich, M., 2016. Carbonate precipitation through microbial activities in natural environment, and their potential in biotechnology: A review. *Frontiers of Bioengineering and Biotechnology*. **4**(4), 1 – 21.

Appendices

Appendix A



Appendix A: The top two figures are linked to Figure 4.10a and the two figures below are additional figures from Figure 4.10b. Comparing Figures in 4.10 with Appendix A, it seems to suggest a stronger signal is attained for phosphorus (with less background noise) compared to minor elements such as chlorine, sulfur and silicon.

Appendix B

Site No.	Lat.	Long.	Max Alk	Max Alk depth	Average CaCO ₃	Average Org CaCO ₃	Gradient of Alk	Ca ²⁺ at max Alk	SO ₄ ²⁻ Conc @ Max Alk	Min. SO ₄
626	25.6	-79.55	4.21	167.4	95.091	NaN	0.010215	14.25	32.63	30.13
627	27.633	-78.3	4.08	22.9	80.553	NaN	0.068996	11.74	32.26	27.19
628	27.533	-78.317	5.22	38.5	87.741	NaN	0.070649	12.84	27.45	25.1
630	27.45	-78.333	5.07	224.8	82.517	NaN	0.011432	17.07	29.74	0
631	23.583	-75.75	13.77	149.3	94.053	NaN	0.075486	15.25	32.41	28.28
632	23.833	-75.433	5.44	99.8	97.231	NaN	0.029459	11.77	33.68	0
633	23.683	-75.617	22.44	149.1	89.667	NaN	0.13374	9.39	19.63	19.63
634	25.383	-77.317	3.56	5.9	92.625	NaN	0.17966	10.51	26.85	26.68
635	25.417	-77.333	3.44	4.1	89.333	NaN	0.22927	10.7	0	0
637	42.083	-12.867	8.92	47.8	27.674	0.30486	0.13431	6.3	17.19	12.8
638	42.15	-12.2	4.99	443.8	46.306	0.50379	0.005611	15.93	25.72	0
639	42.15	-12.25	4.21	7.4	58.347	0.20219	0.23108	9.08	0	0
640	42.017	-12.467	2.4	167.6	48.15	0.99917	-0.0006	15.22	0	0
641	42.15	-12.183	5.07	169.4	21.534	2.137	0.015171	15.52	23.06	22.04
642	67.217	2.9333	10.12	53.3	7.7493	0.82789	0.14296	0	11.7	0
643	67.717	1.0333	7.95	174.15	3.3342	0.57974	0.031295	15	19	0
644	66.683	4.5833	25.32	250.7	5.9975	0.711	0.091025	12	4	0
645	70.45	-64.65	16.48	343.3	9.2212	0.91575	0.040722	7.88	1.39	0
646	58.217	-48.367	5.84	4.35	8.7409	0.34585	0.76782	9.79	22.49	0
647	53.333	-45.267	4.82	215.2	24.682	0.21831	0.010781	22.37	22.4	13.24
650	39.35	13.9	10.74	40.2	18.184	0.24527	0.20498	6.91	1.02	0.73
651	40.15	12.75	6.34	23.33	28.819	0.73636	0.16459	18.25	13.64	0
652	40.35	12.15	3.16	1.4	29.318	1.1943	0.47143	15.4	30.12	21.82
653	40.267	11.45	3.73	13.5	50.09	1.002	0.091111	14.98	25.34	23.96
654	40.583	10.7	3.56	44.7	41.906	1.0071	0.023714	55.65	26.38	15.11
655	40.183	12.467	3.12	57	35.079	1.8459	0.010877	0	0	0
657	21.333	-20.95	5.7	49.65	58.015	0.73025	0.064451	14.9	18.63	16.09
658	20.75	-18.583	44.32	179.33	36.438	1.6403	0.2332	0	5.2	0
659	18.083	-21.033	3.98	92.5	62.805	0.13333	0.016	0	7.81	1.54
660	10.017	-19.25	5.07	13.75	14.726	0.44978	0.18691	0	23.34	20.78
661	9.45	-19.383	7.1	234	31.557	0.14	0.019658	0	10.93	10.93
662	-1.3833	-11.733	7.27	143.6	82.171	0.32687	0.033217	0	17.37	16.96
663	-1.2	-11.883	6.53	97.6	83.478	0.33889	0.041291	8.2	21.31	21.31
664	0.1	-23.233	4.55	197.4	87.889	0.17846	0.010385	10.23	16.51	16.51
665	2.95	-19.667	4.25	48.3	36.449	0.22071	0.036232	12.96	16.9	16.9
666	3.5	-20.167	4.31	108.9	71.147	0.32077	0.016621	10.53	22.92	22.92
667	4.5667	-21.917	5.71	149.7	75.092	0.10324	0.021443	23.43	21.51	16.81
668	4.7667	-20.933	3.34	1.45	66.72	0.154	0.57931	11.41	27.85	27.85
671	15.533	-58.733	4.1	14.85	19.607	0.285	0.10774	12.8	0	0
672	15.533	-58.633	6.52	490.25	17.298	NaN	0.0082	79.2	11.8	0
673	15.533	-58.817	3.62	138.5	7.4593	0.10067	0.008087	30.1	4.2	0
674	15.533	-58.85	3.51	4.45	6.0028	NaN	0.22697	11.5	24.3	0
676	15.533	-58.7	4.71	4.45	14.601	NaN	0.49663	12	25.5	15
677	1.2	-83.733	5.93	76.9	51.631	1.0955	0.044603	10.59	24.12	0
678	1.2167	-83.717	2.72	1.45	44.308	1.0044	0.15172	13.9	0	0
679	-11.067	-78.267	16.61	319.47	9.654	3.232	0.044167	7.63	0.75	0
680	-11.067	-78.083	19.73	19.45	5.7406	6.846	0.88586	8.36	10.95	5.96
681	-10.983	-77.95	22.28	1.45	8.8567	1.9717	13.641	9.58	15.51	0
682	-11.267	-79.067	48.41	248.36	7.8331	3.7092	0.18485	10.77	0.5	0.5
683	-9.0333	-80.4	92.32	127.1	5.3951	3.93	0.70669	8.91	2.08	0
684	-8.9833	-79.95	23.85	35.8	10.903	5.781	0.59637	10.93	0.78	0
685	-9.1167	-80.583	156.37	132.3	3.1111	2.652	1.163	5.51	0	0
686	-13.483	-76.883	63.58	165.71	4.4186	2.2579	0.3686	7.49	0	0
687	-12.867	-76.983	16.25	20.6	6.575	3.0112	0.66748	6.36	6.77	0
688	-11.533	-78.95	265.68	192.88	5.2434	3.044	1.3645	7.4	0	0
689	-64.517	3.1	3.2	20.5	55.742	0.071538	0.034146	11.92	28.02	25.66
690	-65.167	1.2	4.04	143.5	65.487	0.47571	0.010732	13.01	23.46	8.92
693	-70.833	-14.567	3.9	8.45	2.6789	1.1206	0.16568	10.65	28.6	16
694	-66.85	-33.45	3.62	345.95	0.34138	0.48154	0.003238	24.4	16.2	15.4
695	-62.383	-43.45	12.37	335.8	0.18511	0.3865	0.029392	12.81	1.2	1.2
696	-61.85	-42.933	4.39	65.7	1.5512	0.4069	0.028767	19.28	12	1.7
697	-61.817	-40.3	18.35	132.75	0.27241	0.36929	0.1194	14.01	6.5	5
698	-51.467	-33.1	2.91	6.95	90.578	NaN	0.058993	11.37	28.6	26.3
699	-51.55	-30.683	5.6	273	30.92	0.1004	0.011355	26.67	23.9	0
700	-51.533	-30.283	5.12	157.3	75.884	0.019512	0.016656	22.96	23.98	22.82

701	-51.983	-23.217	6.67	211.7	5.1234	0.28836	0.019698	14.18	23.65	23
702	-50.95	-26.367	3.02	45.75	73.275	0.18833	0.011366	13.12	27.3	25.15
703	-47.05	7.9	3.17	231.85	85.089	0.0165	0.00289	13.65	27.91	27.05
704	-46.883	7.4167	4.7	305.1	60.419	0.12308	0.007211	20.26	18.57	13.48
705	-13.167	61.383	3.03	12.95	91.9	0.225	0.040927	11.44	29.35	27.71
706	-13.117	61.367	2.44	18.15	75.293	0.17923	-0.00331	10.9	29.51	23.6
707	-7.55	59.017	3.41	209.9	92.928	0.1029	0.004335	17.96	28.07	28.07
708	-5.45	59.95	4.96	222.75	74.124	0.13676	0.011044	14.24	28.36	23.64
709	-3.9167	60.55	4.59	259.65	89.369	0.062273	0.008049	13.02	27.02	21.12
710	-4.3167	60.983	4.15	112.7	80.968	0.031739	0.014641	14.92	0	0
711	-2.75	61.167	4.12	197.6	57.84	0.06037	0.008198	12.63	0	0
712	-4.2167	73.4	3.05	23.4	91.39	0.092308	0.023504	11.1	28.11	28.11
713	-4.2	73.4	3.07	7.55	69.65	0.025	0.075497	11.74	28.51	26.19
714	5.0667	73.783	4.44	37.65	84.639	0.20718	0.051527	10.81	27.17	26.29
715	5.0833	73.833	4.4	43.05	77.217	0.53182	0.044135	10.49	26.7	26.37
716	4.9333	73.283	6.05	254	94.609	0.37545	0.013976	17.97	26.4	25.7
717	-0.93333	81.383	16.81	823.1	7.0462	0.89371	0.017385	22.46	3.2	0.6
718	-1.0167	81.4	13.21	31.25	7.9286	0.39724	0.34272	9.45	14.05	1.27
719	-0.96667	81.4	15.95	152.6	5.6	0.84	0.088139	5.7	1.08	0
720	16.133	60.75	6.73	23.45	25.274	0.5066	0.18038	4.73	8.5	0
721	16.683	59.867	11.56	85.75	62.778	0.72356	0.10566	6.1	2.01	0
722	16.617	59.8	9.11	82.75	56.985	1.1358	0.079879	6.18	3.5	0
723	18.05	57.617	106.8	332.04	55.821	3.1813	0.31412	2.74	1.64	0
724	18.467	57.783	28.75	234.65	49.253	2.0332	0.11187	4.8	1.8	0.7
725	18.483	57.7	33.93	160.65	53.377	1.7237	0.19564	5.39	0.8	0.8
726	17.817	57.367	5.63	76.15	60.945	1.8473	0.041103	17	22.59	22.59
727	17.767	57.583	44.56	167.45	58.309	2.4143	0.25118	6	2.4	0
728	17.683	57.833	17.49	83.25	54.249	2.4538	0.18006	6.6	0	0
729	17.65	57.95	3.74	2.95	65.425	0.95875	0.42034	10.02	24.6	24.3
730	17.733	57.7	6.75	139.15	56.949	0.96143	0.030543	12.98	3.7	0
731	16.467	59.7	9.06	82.65	40.464	0.47143	0.079371	6.68	918	78
736	-49.4	71.667	4.9	40.95	2.3645	0.41047	0.058608	10.46	24.45	16.03
737	-50.233	73.033	2.74	2.95	26.831	0.20143	0.081356	11.5	27.42	11.78
738	-62.717	82.783	2.96	2.95	82.773	0.058889	0.15593	11.1	25.79	22.85
739	-67.283	75.083	4.12	235.8	1.4958	0.7771	0.00687	14	0	0
740	-68.767	76.683	23.19	1.45	0.13385	0.311	14.269	8.9	12.8	0
741	-68.383	76.383	3	2.95	1.4273	6.8677	0.16949	0	26.5	18.7
742	-67.55	75.417	4.74	2.95	2.3714	0.60119	0.75932	10.7	28.9	6.8
743	-66.917	74.683	3.12	0.94	0.49231	0.332	0.65957	10.56	30.5	22.5
744	-61.583	80.6	3.03	2.95	64.798	NaN	0.17966	10.9	27.6	25.5
745	-59.6	85.85	6.77	105.95	0.13542	0.21	0.040302	16	23.2	19.4
746	-59.567	85.867	4.86	170.75	0.3625	0.12	0.013821	19.9	21.2	17.2
747	-54.817	76.8	3.22	7.45	87.249	0.086	0.096644	10.96	28.09	25.2
748	-58.433	79	2.58	17.05	55.245	0.21758	0.004692	14.88	27.18	21.46
749	-58.717	76.4	2.84	4.45	93.181	NaN	0.076404	10.99	28.66	27.74
750	-57.6	81.233	2.46	331.25	81.689	0.573	-0.00012	16.96	25.25	24.62
751	-57.733	79.817	3.52	162.65	65.267	0.15286	0.006271	15.15	25.12	25.06
752	-30.883	93.583	2.7	23.5	76.985	0.16035	0.008511	11.8	29.9	0
753	-30.833	93.583	2.71	5.95	93.6	NaN	0.035294	11.1	29.5	29.5
754	-30.933	93.567	2.73	4.45	69.391	0.08234	0.051685	11.4	29.6	27.4
755	-31.033	93.55	2.71	5.95	18.01	0.19636	0.035294	11.5	29.1	29.1
756	-27.35	87.6	2.72	135.75	74.93	0.029	0.001621	12.3	31.2	0
757	-17.017	88.183	2.67	2.73	52.228	0.061613	0.062271	12.3	27.3	0
758	5.3833	90.367	3.93	24.55	60.621	0.13027	0.058248	12.3	27.2	0
759	-16.95	115.57	4.34	51.4	26.181	NaN	0.035798	12.4	27.95	15.84
760	-16.917	115.53	3.11	5.95	26.885	NaN	0.10252	11.3	28.46	5.23
761	-16.733	115.53	3.87	21.15	73.53	NaN	0.064775	11.23	29.18	26.12
762	-19.883	112.25	9.64	403.9	71.765	NaN	0.017678	18.3	10.21	1.6
763	-20.583	112.22	8.55	319.4	43.787	NaN	0.018942	0	1.41	0.78
764	-16.567	115.45	3.64	5.95	83.553	NaN	0.1916	10.9	28.54	28.54
765	-15.983	117.58	9.13	71.55	32.895	0.29808	0.092662	7.1	15.6	6
766	-19.933	110.45	3.36	1.47	35.273	0.099474	0.58503	10.5	27.6	18.7
767	4.7833	123.5	8.73	77.45	11.397	NaN	0.080439	11.07	23.1	0
768	8	121.22	6.69	274.9	11.178	NaN	0.015242	11.95	0	0
769	8.7833	121.3	4	12.85	29.223	NaN	0.11673	11.07	29.36	21.71
770	5.15	123.67	3.36	370.3	7.8193	NaN	0.002322	42.57	17.74	17.74
771	8.6833	120.68	0.94	101.4	NaN	NaN	-0.01539	0	27.06	21
778	19.5	146.67	1.34	83.7	3.3968	0.11111	-0.01386	23.9	16.83	12.15
779	19.517	146.7	15.1	246.2	6.6851	0.215	0.051178	3.29	24.9	17.47
780	19.55	146.65	45.83	33.48	4.9457	0.25667	1.2942	0.47	43.52	26.93
781	19.633	146.55	3.27	2.23	2.8484	0.74	0.34529	10.34	26.6	25.77
782	30.867	141.32	3.29	15.75	33.836	0.24236	0.050159	9.62	26.6	24.71
783	30.967	141.78	3.78	1.45	3.5225	0.30923	0.88276	10.51	27.31	6.06

784	30.9	141.73	4.42	45.4	0.39122	0.36324	0.042291	13.5	25.07	7
785	30.817	140.92	2.96	1.45	6.6818	0.33	0.31724	10.1	25.81	25.81
786	31.867	141.23	2.92	5.95	20.468	0.20846	0.070588	14.08	27.02	23.81
787	32.383	140.75	1.52	71.15	11.602	0.13409	-0.01377	23.4	28.4	23.9
788	30.917	140	2.59	145.1	2.6391	0.025	0.00062	11.5	27.9	27.9
790	30.917	139.85	9.4	227.2	15.243	0.39587	0.03037	5.7	18.2	15.1
791	30.917	139.87	4.66	166.9	18.701	0.43415	0.012942	10.8	26.9	24.2
792	32.4	140.38	4.27	26.5	9.3618	0.25326	0.066792	7.9	25.5	15.1
793	31.1	140.88	3.36	76.8	6.3982	0.082075	0.011198	9.8	29.1	11.9
794	40.183	138.23	12.04	50.7	2.3571	0.78436	0.18817	10.2	17.3	0
795	43.983	138.97	25.8	86.75	0.88553	0.8944	0.26859	0	0	0
796	42.85	139.42	15.15	2.05	2.5472	0.81052	6.1707	8.6	9.8	0
797	38.617	134.53	19.27	78.35	3.1188	1.5277	0.21404	7.9	7.6	0
798	37.033	134.8	76.34	108.81	5.4949	1.9641	0.67861	5.48	0.13	0
799	39.217	133.87	42.13	72.75	6.7289	1.6888	0.54474	4.23	0	0
800	21.917	152.32	2.28	21.95	9.675	0.077429	-0.01002	10.5	25.81	11.14
801	18.65	156.37	0.75	44.4	5.5846	0.1028	-0.03941	42.97	36.45	16.62
802	12.1	153.22	1.36	25.7	15.314	0.11	-0.04436	16.22	26.84	0.4
803	2.4333	160.53	3.88	166.05	88.931	0.092667	0.008311	20	23.55	22.53
804	0.93333	161.65	4.55	10.65	86.35	NaN	0.19249	11.15	27.35	24.77
805	1.2333	160.53	5.36	80.25	91.454	NaN	0.035639	17.7	23.56	21.54
806	0.31667	159.37	6.43	164.45	92.479	0.1484	0.023898	15.24	19.23	14.3
807	3.6	156.63	6.32	335.3	91.084	0.19246	0.011393	16.83	21.58	0
808	32.35	134.95	55.14	59.6	3.5127	0.41859	0.88322	5	0	0
810	32.417	157.85	3.33	8.9	76.732	0.84556	0.093258	10.9	25.8	25.8
811	-16.517	148.15	3.22	261.75	96.047	0.24483	0.002751	16.79	0	0
812	-17.817	149.6	3.21	12.35	100.45	0.074737	0.05749	10.43	29.32	27.61
813	-17.833	149.5	3.2	51.15	97.809	0.21826	0.013685	11.09	29.04	28.51
814	-17.833	149.52	3.9	4.45	98.283	0.12696	0.31461	10.35	29.08	26.97
815	-19.15	150	4.69	118.7	69.743	0.24187	0.01845	10.45	5.76	1.52
816	-19.2	150.02	3.38	4.45	82.511	0.33286	0.19775	10.73	26.65	26.13
817	-18.15	149.77	8.1	41.65	94.935	0.30581	0.13445	8.17	26.44	24.81
818	-18.067	150.05	6.68	82.3	96.453	0.14545	0.05079	11.24	26.66	26.42
819	-16.617	146.32	12.42	205.5	52.77	0.40308	0.048273	4.42	1.27	0
820	-16.633	146.3	7.9	62.1	62.318	0.25667	0.086957	4.62	0.8	0
821	-16.65	146.28	9.04	116.35	63.743	0.24929	0.05621	2.91	4.04	0
822	-16.417	146.22	13.83	17.8	46.413	0.36644	0.63652	4.27	0	0
823	-16.617	146.78	12.55	55.8	58.752	0.13898	0.18011	4.1	0	0
824	-16.45	147.77	3.65	2.95	97.378	0.1019	0.38983	10.3	29.19	28.97
825	-16.517	148.15	2.95	250.4	98.203	0.18857	0.001797	16.54	30.38	29.22
827	-15.3	166.35	23.63	50.85	15.254	0.43465	0.41554	7	0	0
828	-15.283	166.28	12.65	18.35	40.175	0.42909	0.55313	10.4	26.3	26.3
829	-15.317	166.35	14.3	104.9	37.707	0.16884	0.11249	4.6	1.6	1.6
830	-15.95	166.78	3.7	4.45	9.6691	0.27279	0.26966	8.4	22.8	0
831	-16.017	166.67	2.98	2.95	67.715	0.054	0.16271	10.7	0	0
832	-14.8	167.57	30.04	76.93	13.656	0.14855	0.35799	2.17	0.8	0.6
833	-14.883	167.88	19.94	23.45	12.405	0.15213	0.74371	2.55	0	0
834	-18.567	-177.87	3.04	5.9	42.616	0.17083	0.091525	9.75	27.63	27.31
835	-18.5	-177.3	3.11	5.9	58.422	0.19704	0.10339	10.5	27.92	26.44
836	-20.133	-176.5	3.09	7.1	36.778	0.2325	0.083099	10.8	27.8	27.8
837	-20.217	-176.82	3.38	4.4	36.152	0.095	0.2	10.3	28.89	28.89
838	-20.833	-176.88	3.08	66.6	37.4	0.042	0.008709	15	28.96	27.92
839	-20.7	-176.77	3.18	2.9	26.974	0.072	0.23448	10.5	27.54	27.26
840	-22.217	-175.75	2.39	144.78	19.438	0.14073	-0.00076	26.4	27.19	26.94
841	-23.35	-175.3	3.43	14.4	3.6364	0.11567	0.064583	13	28.4	10.5
842	19.333	-159.08	2.49	1.45	NaN	NaN	-0.0069	10.2	27.73	26.54
843	19.35	-159.1	2.38	1.45	NaN	NaN	-0.08276	10.46	28.9	28.9
844	7.9167	-90.483	3.13	133.95	43.41	0.36712	0.004703	10.75	27.71	26.72
845	9.5833	-94.583	4.39	21.47	35.206	0.68459	0.08803	10.6	27.96	26.46
846	-3.1	-90.817	7.06	107.95	55.008	0.54727	0.042242	7.81	21.36	20.01
847	0.2	-95.317	5.22	164.35	63.569	0.30038	0.01655	12.81	26.93	26.2
848	-3	-110.48	2.94	1.45	69.772	0.14	0.30345	10.66	28.13	27.62
849	0.18333	-110.52	5.75	225.24	70.995	0.11125	0.014429	10.05	23.25	22.89
850	1.3	-110.52	5.41	145.34	68.224	0.13165	0.020022	9.13	23.8	21.97
851	2.7667	-110.57	3.84	165.75	70.909	0.11	0.008085	10.6	26.39	25.77
852	5.3	-110.08	3.05	27.35	76.354	0.041818	0.02011	11.26	28.55	27.82
853	7.2167	-109.75	2.8	1.45	72.93	0.06125	0.2069	10.41	28.02	27.34
854	11.217	-109.6	2.93	2.95	24.035	NaN	0.14576	10.44	28.23	28.23
855	48.45	-128.63	10.36	16.1	4.0321	0.4566	0.4882	9.88	22.06	0
856	48.433	-128.68	4.99	38.98	11.083	0.2029	0.063879	11.33	28.16	27.84
857	48.433	-128.72	13.02	37.3	3.2157	0.34756	0.28204	10.44	21.24	3.07
858	48.45	-128.72	9.08	207.3	2.7	0.28886	0.031741	44.89	5.08	0
859	-45.9	-75.85	13.22	5.6	1.4712	0.39158	1.9143	2.78	0.2	0

860	-45.883	-75.75	46.98	46.8	2.1613	0.54956	0.95043	3.83	0.9	0.4
861	-45.85	-75.7	62.41	64.4	2.0405	0.55889	0.93028	2.76	0.3	0.2
862	-46.517	-75.833	3.14	9.85	0.94444	NaN	0.064975	10.45	28.7	28.6
863	-46.233	-75.767	20.79	68.4	2.238	0.28712	0.2674	2.15	0.4	0
865	18.433	-179.55	3.35	27.15	92.088	0.89544	0.031308	10.68	28.52	0
866	21.333	174.32	2.8	0.72	96.945	0.35169	0.41667	0	28.18	0
869	11	164.75	3.44	119.95	28.16	0.16377	0.007837	11.3	25.56	12.55
871	5.55	172.35	4.67	68.92	87.981	0.98478	0.031486	11.04	29.2	27.3
872	10.1	162.87	2.74	118.93	96.43	NaN	0.002018	11.66	28.89	27.52
873	11.9	164.92	2.72	39.56	91.887	0.36343	0.005561	11.14	28	29
874	12	164.93	2.95	164.2	65.038	0.90698	0.002741	13.49	29.1	29.1
877	12.017	164.92	2.81	186.67	61.444	3.3762	0.001661	11.36	29.4	29.4
878	27.317	151.88	2.84	2.49	74.903	0.25893	0.13655	10.95	26.2	11.9
879	34.167	144.32	2.51	185.14	62.267	0.49462	5.40E-05	0	0	0
880	34.217	144.32	3.04	7.42	NaN	NaN	0.072776	0	0	0
881	47.1	161.48	8.03	123.75	1.4598	0.23195	0.044687	13.72	24.37	0
882	50.367	167.6	6.94	105.35	4.2979	0.25126	0.042145	6.57	20.32	20.18
883	51.2	167.77	5.99	1.45	22.67	0.1578	2.4069	9.2	23.8	22
884	51.45	168.33	8.67	83.65	5.5965	0.22139	0.07376	11	22.9	20.8
886	44.683	-168.23	2.74	17.25	0	0.10462	0.013913	10.7	28.4	27.1
887	54.367	-148.45	6	19.15	8.635	0.17847	0.18277	10.8	26.6	25.1
888	48.167	-126.67	33.24	103.37	2.1311	0.332	0.29738	7.31	0	0
889	48.7	-126.87	40.83	36.95	3.9833	0.90021	1.0373	3.06	0	0
890	48.667	-126.88	30.94	25.74	2.825	0.39125	1.1049	1.87	0	0
891	44.65	-125.33	28.85	296.11	5.3412	0.37286	0.088987	5.58	0	0
892	44.667	-125.12	20.48	3.79	3.6526	1.4526	4.7441	3.27	0.62	0
897	40.833	-12.467	16.17	149.77	29.175	0.38649	0.091273	7.07	1.82	0
898	40.683	-12.117	18.97	43.66	29.242	0.27912	0.37723	4.73	3.2	0
899	40.767	-12.267	9.38	227.3	23.444	0.25864	0.030268	24.95	19.13	15.5
900	40.683	-11.6	11.94	289.84	29.649	0.24688	0.03257	31.47	15.1	0
902	38.933	-72.767	44.45	75.45	10.519	1.6937	0.556	3.83	1.6	0
903	38.933	-72.817	38.56	485.7	9.5611	1.0449	0.074243	11.81	0.17	0
904	38.867	-72.767	33.85	216.95	24.427	0.69458	0.1445	11.61	0	0
905	38.617	-72.283	46.3	591.8	9.1763	0.96375	0.074011	10.38	0.27	0
906	38.967	-72.767	36.2	134.55	8.465	1.5842	0.25046	10.74	1.87	0.61
907	69.25	-12.7	3.26	4.45	3.3435	0.4298	0.17079	11.04	29	22.1
908	78.383	1.3667	17.42	262	1.357	0.92229	0.056947	11.4	0.3	0.1
909	78.583	3.0667	14.09	33.95	4.0116	1.0121	0.34138	3.6	0	0
910	80.267	6.5833	17.54	18.83	2.9744	0.95594	0.79873	3.74	0.32	0
911	80.467	8.2333	17.14	35.95	2.7278	0.97767	0.40723	3.19	1.3	0.1
912	79.967	5.45	13.53	83.95	2.8185	0.86056	0.13139	3.5	0	0
913	75.483	-6.95	2.65	2.95	1.5363	0.41425	0.050847	10.9	31.3	6
914	63.467	-39.717	2.57	7.51	3.1841	0.26059	0.009321	13.9	29.2	21.8
915	63.467	-39.783	3.57	1.45	4.0067	0.434	0.73793	11.4	29.4	20.8
918	63.1	-38.633	14.79	167.7	6.6999	0.24731	0.073286	5.65	0	0
919	62.667	-37.467	19.52	94.45	3.8208	0.17915	0.1802	3.79	0	0
925	4.2	-43.483	10.58	424.1	66.435	0.1242	0.019052	31.26	12.9	0
926	3.7167	-42.9	10.34	388.5	61.897	0.13773	0.02018	33.5	15.42	9.78
927	5.4667	-44.483	7.94	250.45	57.972	0.080833	0.021721	21.94	18.3	17.32
928	5.45	-43.75	9.37	312.1	57.493	0.16507	0.022012	29.35	17.09	10.58
929	5.9833	-43.733	9.4	218.8	49.563	0.099	0.031536	25.32	20.87	0
930	5.0167	-47.6	18.55	13.15	3.4776	0.80175	1.2205	5.33	0.85	0
931	5.15	-46.633	27.05	5.55	4.4938	0.75436	4.4234	7.3	1.75	0
932	5.2167	-47.033	15.32	13.45	4.8042	0.78062	0.95316	5.7	0.13	0.01
933	5.1	-46.817	17.42	13.36	3.3617	0.78213	1.1168	5.6	0.02	0
934	5.4833	-47.683	16.99	11.75	4.6591	0.85545	1.2332	5.1	0	0
935	5.4333	-47.567	15.93	176.3	3.7929	0.87514	0.076177	5.3	0.4	0
936	5.6333	-47.733	15.9	149.2	3.7746	0.82549	0.089812	6.4	2.2	0
937	4.6	-47.2	14.02	157.1	4.3974	0.86462	0.073329	4.5	0	0
938	4.6667	-47.317	15.37	275	3.6593	0.86	0.0468	4.8	0.4	0
939	4.7167	-47.5	33.29	11.45	2.0514	0.85636	2.6891	7.81	0.1	0.1
940	5.15	-47.533	32.82	29.25	2.9527	0.81273	1.0366	5.6	0.2	0.2
941	5.3667	-48.033	14.51	2.95	6.2677	0.65839	4.0712	6.4	11.3	0.3
942	5.75	-49.083	30.31	143.4	3.5222	0.75593	0.19393	7	1.6	0.1
943	5.95	-47.783	23.8	5.75	6.8333	0.656	3.7043	7	0.1	0.1
944	5.9333	-47.75	22.23	4.4	5.6696	0.6907	4.4841	6.5	0.2	0
945	6.95	-47.933	15.08	16.45	NaN	NaN	0.76474	5.4	0.4	0.2
946	6.95	-47.917	26.28	131.67	8.1	0.8132	0.1806	5.5	0.2	0.2
948	15.533	-58.733	3.62	5.93	8.083	0.26408	0.18887	12.5	27.8	0
949	15.533	-58.717	2.99	1.43	3.0877	0.081388	0.34266	11.18	28.2	0
950	31.15	-25.6	6.2	44.85	40.363	1.0297	0.082497	8.61	20.1	5.53
951	32.033	-24.867	12.24	309.1	40.185	1.0316	0.031511	15.68	0.02	0.01
952	30.783	-24.517	11.24	335.1	36.148	1.1151	0.026082	18.3	1.02	0

953	28.65	-15.15	5.45	13.55	41.696	0.18068	0.21771	5.78	24.2	16.5
954	28.433	-15.533	117.48	179.54	54.684	0.097727	0.64041	18.3	25.4	24.7
955	27.333	-15.233	10.8	52.05	43.162	0.65686	0.15946	4.8	3.57	0.07
956	27.617	-16.167	4.98	50	53.282	0.6796	0.0496	0	0	0
957	26.133	-44.833	2.53	28.8	56.324	NaN	0.001042	17.7	42.5	30.8
959	3.6333	-2.7333	18.89	318.5	24.344	0.92033	0.05146	16.27	1	0
960	3.5833	-2.7333	7.71	115.15	39.077	0.71925	0.045245	16.3	12.36	0.94
961	3.45	-3.0667	3.28	16.05	11.55	0.3175	0.048598	10.48	25.4	5.9
962	3.25	-3.1833	4.7	78.45	29.315	0.89294	0.028043	12.5	19.5	19.5
963	37.033	13.183	7.01	154.4	26.594	0.59817	0.02921	5.14	0.35	0.25
964	36.267	17.75	3.32	52.25	45.094	6.7437	0.015694	17.1	28.91	26.32
965	33.917	32.717	0	6.75	49.144	1.8525	-0.37037	11.9	30.7	30.2
966	33.8	32.7	3.85	22.75	55.66	3.4746	0.059341	12.4	29.4	28.9
967	34.067	32.733	4.87	5.95	37.815	4.9373	0.39832	12	30	29.4
968	34.333	32.75	3.76	5.95	31.207	2.3315	0.21176	12	0.29	0.22
969	33.833	24.883	3.28	5.95	53.676	8.5406	0.13109	16.5	29.3	29.3
970	33.733	24.8	72.45	30.71	34.092	4.9322	2.2778	0	0.1	0.1
971	33.717	24.7	90.38	12.4	29.613	4.6658	7.0871	0	28.09	0.74
972	35.783	18.733	3.67	5.95	33.711	3.9669	0.19664	18.9	32.3	17.2
973	35.783	18.95	17.39	142.83	40.278	7.0415	0.10425	15	37.8	19.8
974	40.35	12.15	3.18	10.95	36.316	0.8262	0.0621	13.7	32.16	23.14
975	38.9	4.5167	4.71	65.55	47.569	0.42196	0.033715	10.63	21.9	0
976	36.2	-4.3167	26.57	15.4	29.835	0.58699	1.563	3.37	1.85	0
977	36.033	-1.95	15.09	17.95	38.715	0.54544	0.70139	4.38	10.66	0
978	36.233	-2.05	3.51	269.5	38.077	0.33161	0.003748	15.2	0.24	0
979	35.717	-3.2	16.81	24.95	32.087	0.68965	0.57355	3.49	0.5	0
980	55.483	-14.7	11.37	54.85	46.018	0.31933	0.16171	3.9	10.2	9.6
981	55.483	-14.65	10.94	277.65	60.481	0.31462	0.030398	11	6.09	0
982	57.517	-15.867	6.72	284.1	86.474	0.13647	0.014854	16.2	14.3	12.6
983	60.4	-23.633	13.29	108.35	16.591	0.28033	0.099585	3.1	1	0
984	61.433	-24.083	14.18	77.55	8.0141	0.20926	0.15061	3.36	3.51	0
985	66.933	-6.45	3.51	51.65	5.1139	0.53575	0.019555	16.7	21.2	10.8
986	77.333	9.0833	33.81	741.15	4.8234	0.80062	0.042245	13.3	2.9	0
987	70.5	-17.933	15.35	33.45	4.29	0.5421	0.38416	2.9	0	0
991	32.983	-75.933	26.88	35.55	33.182	1.325	0.68579	5	0.88	0.09
992	32.983	-75.917	20.18	49.75	27.523	1.8286	0.35538	5.76	5.84	5.84
993	32.967	-75.9	28.69	35.55	17.473	1.75	0.73671	6.72	2.85	1.41
994	31.783	-75.55	104.25	351.98	19.404	1.195	0.28908	2.23	0.76	0
995	31.8	-75.517	117.14	312.08	19.448	1.193	0.36734	2.38	0	0
996	32.5	-76.183	42.21	1.66	35.737	0.44	23.922	3.43	1.87	0
997	31.85	-75.467	126.26	315.35	19.908	1.2382	0.39245	2.46	0	0
998	19.483	-82.933	5.78	220.35	78.041	0.022727	0.014885	22.48	24.12	20.97
999	12.75	-78.733	5.15	78.55	58.757	0.11397	0.033736	7.69	17.94	12.09
1000	16.55	-79.867	12.13	245.25	80.704	0.25196	0.039266	11	4.11	0.77
1001	15.75	-74.917	2.76	26.75	67.982	0.03	0.00972	12.6	25.8	18.9
1002	10.7	-65.167	29.43	107.62	NaN	NaN	0.25023	4.06	0.57	0
1003	24.55	-79.267	30.4	181.45	90.12	0.94324	0.15376	13.72	15.46	0
1004	24.55	-79.25	73.41	92.72	94.078	1.1586	0.76478	6.7	1.2	0.3
1005	24.567	-79.233	63.97	253.65	94.227	1.1018	0.24234	6	0.3	0.3
1006	24.4	-79.467	8.17	76.5	NaN	NaN	0.074118	7.7	12.7	0
1007	24.5	-79.317	24.46	136.9	90.632	0.49803	0.16041	11.39	22.06	0.71
1008	23.617	-79.083	32.78	120.5	94.584	0.29833	0.25129	8.01	13.18	13.18
1009	23.617	-79.05	35.74	222.55	94.726	0.50636	0.14936	10.44	11.9	11.9
1010	29.967	-118.1	4.44	47.98	22.069	0.22328	0.040434	13.2	28.2	0
1011	31.283	-117.62	22.63	79.35	20.946	1.5873	0.25369	5.93	1	1
1012	32.283	-118.38	67.34	161.65	40.952	2.5751	0.40111	4.74	0.7	0
1013	32.8	-118.9	60.66	101.05	28.237	3.8765	0.57556	5.11	1	1
1014	32.833	-119.98	113.08	164.85	47.975	4.9622	0.67079	6.79	0	0
1015	33.717	-118.82	38.53	4.45	4.8419	1.1058	8.0966	5.96	0	0
1016	34.533	-122.28	17.33	50.05	16.083	0.93092	0.2963	5.55	4.9	0
1017	34.533	-121.1	44.59	28.75	8.35	1.661	1.464	2.37	1	1
1018	36.983	-123.28	56.34	37.85	5.3173	1.3097	1.4225	4.32	1	1
1019	41.683	-124.93	103.3	108.15	3.8562	1.0442	0.93204	2.16	0.5	0.5
1020	41.017	-126.43	21.91	135.75	8.612	0.74957	0.14298	7.88	0.2	0.2
1021	39.083	-127.78	9.39	135.95	9.4252	0.34142	0.05068	9.61	19	18.4
1022	40.083	-125.35	17.6	246.55	12.924	0.94862	0.061245	0	0	0
1023	47.917	-128.8	29.74	54.7	3.902	0.55364	0.49799	4.36	0.28	0
1024	47.9	-128.75	22.71	72	4.7147	0.48667	0.28069	5.48	1.13	0.15
1025	47.883	-128.65	16.42	10.9	6.0072	0.703	1.2771	8.76	12.94	8.52
1026	47.767	-127.75	33.76	41.3	3.8743	0.34964	0.7569	6.49	0.88	0.11
1027	47.75	-127.73	30.21	166.2	4.5985	0.57055	0.16673	6.19	1.77	0.03
1028	47.85	-128.5	22.78	16.1	6.4651	0.51444	1.2596	7.61	5.46	2.61
1029	47.833	-128.38	22.15	30.9	3.9683	0.434	0.63592	5.88	1.71	0

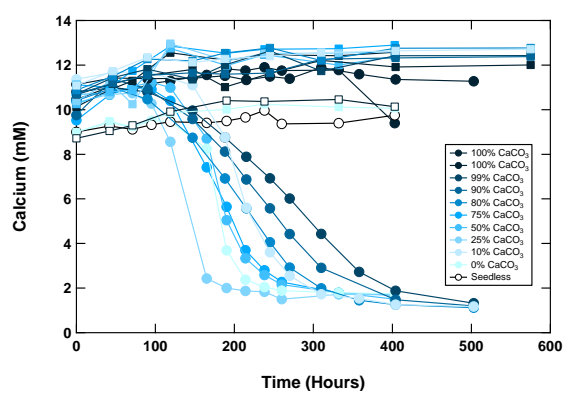
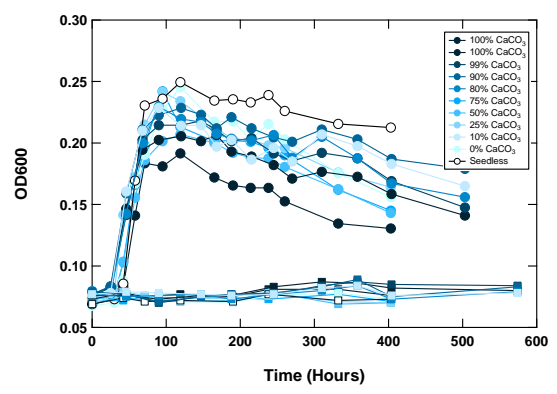
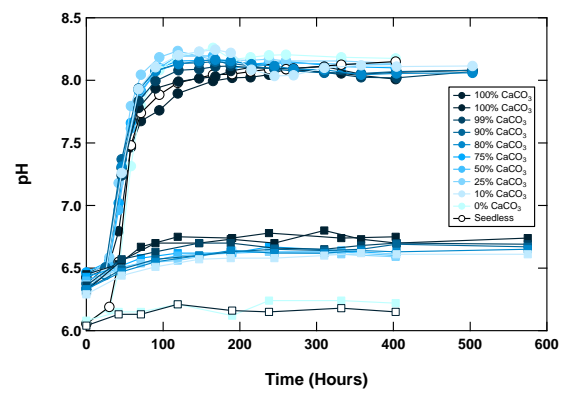
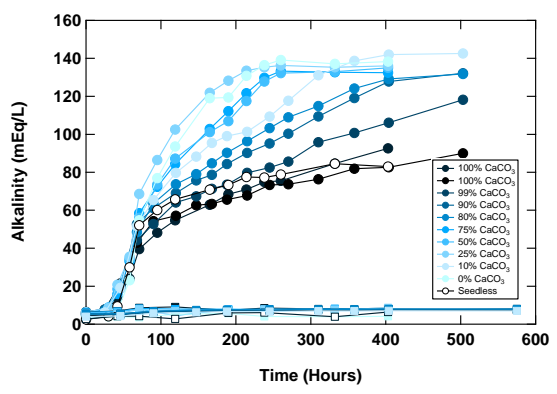
1030	47.9	-128.57	3.34	2.9	9.8424	NaN	0.28966	34.54	23.09	20.51
1031	47.883	-128.57	2.59	1.4	11.286	0.346	0.064286	39.34	24.66	23.72
1032	47.783	-128.12	3.36	195.4	NaN	NaN	0.004401	20.13	1.76	0.54
1035	48.433	-128.68	9.19	90.7	17.896	0.30175	0.07376	30.7	18.6	0
1036	48.45	-128.72	11.38	30.6	4.3479	0.29702	0.2902	45.9	4.1	1.7
1037	40.95	-127.52	42.51	77.5	5.8381	0.36167	0.51626	6.8	2.3	0
1038	41	-127.5	56.83	402.3	4.7168	0.27325	0.13505	19.7	0.9	0
1039	9.6333	-86.2	20.98	18.68	34.693	0.81576	0.98929	8.15	13.3	13.2
1040	9.6667	-86.183	39.33	381.8	21.157	0.92598	0.096464	4.1	0	0
1041	9.7333	-86.117	31.32	15.65	4.1798	1.3762	1.8415	5.23	0	0
1042	9.65	-86.117	8.28	220.9	16.275	1.4214	0.026166	26.1	0	0
1043	9.65	-86.183	24.35	150.55	4.392	1.0837	0.14513	6.5	4.8	0
1049	30.15	-76.117	2.84	66.35	57.97	0.55453	0.005124	12.32	28.5	26
1050	30.1	-76.233	7.32	240.6	60.722	0.10392	0.020033	25.71	22.6	20.7
1051	30.05	-76.35	8.05	403.9	63.505	0.06299	0.013741	29.65	22.1	16
1052	29.95	-76.633	4.35	112.65	59.35	0.27234	0.016423	16.1	26.1	6.02
1053	30	-76.517	6.78	137.45	75.124	0.10633	0.031139	19.19	24.6	24.6
1054	33	-76.283	67.77	195.7	46.58	1.1811	0.33352	4.18	0.15	0
1055	32.783	-76.283	48.47	126.43	40.251	0.79842	0.3636	3.55	0.17	0
1056	32.483	-76.333	36.26	153.89	31.903	0.5735	0.21938	3.28	0	0
1057	32.033	-76.083	35.64	127.65	26.672	0.57833	0.25962	1.68	0.4	0
1058	31.683	-75.433	44.63	148.66	23.907	0.61565	0.2834	1.79	0	0
1059	31.667	-75.417	32.54	20.75	21.709	0.58176	1.4477	2.52	0.46	0
1060	30.767	-74.467	28.64	17.95	18.185	0.74688	1.4563	3.5	0.65	0
1061	29.983	-73.6	28.16	18.22	12.091	0.5835	1.4083	4.14	0.45	0
1062	28.25	-74.417	21.19	41.6	19.202	0.62043	0.44928	4.95	4.21	0
1063	33.683	-57.617	24.12	19.2	17.519	0.87559	1.126	4.21	4.48	0
1064	32.55	-57.083	12.94	12.4	11.957	0.65556	0.84194	8.04	16.27	10.35
1065	40.717	-11.3	0	252.45	37.999	0.3856	-0.0099	24.5	6.9	6.2
1067	40.683	-11.6	0	729.55	25.175	0.091684	-0.00343	39.7	2.9	2.9
1068	40.683	-11.617	0	717.2	36.874	0.065897	-0.00349	40.2	2.3	2.3
1069	40.733	-11.783	0	729.18	27.8	0.078889	-0.00343	35.9	8.7	0.75
1070	40.8	-12.717	0	600.4	2.36	0.1625	-0.00416	30	13.3	12.1
1071	39.25	-72.817	27.84	362.3	6.614	1.0815	0.069942	6.8	1.07	1.07
1072	39.333	-72.733	19.84	230.5	5.8606	0.44778	0.075228	6.45	1.33	0.18
1073	39.25	-72.317	23.86	543.15	8.7114	0.41621	0.039326	8.49	0.29	0
1074	22.783	-46.117	2.91	7.9	NaN	NaN	0.051899	10.63	28.63	27.17
1075	-4.7833	10.083	41.52	72.44	2.6619	2.6	0.53865	5.73	0	0
1076	-5.0667	11.1	36.19	47.2	3.7372	2.5533	0.71377	4.41	0	0
1077	-5.1833	10.433	36.62	75.9	2.8008	2.3007	0.44954	5.11	0.65	0
1078	-11.917	13.4	86.48	150.3	14.625	2.5277	0.55875	4.29	0.39	0
1079	-11.933	13.317	59.01	112.7	13.337	3.0219	0.50142	3.82	1.28	0
1080	-16.567	10.817	47.7	49.64	6.3925	2.4037	0.91056	2.39	0.55	0
1081	-19.617	11.317	30.38	207.2	17.771	4.5037	0.13456	5.23	0.11	0
1082	-21.1	11.817	75.59	160.1	44.897	3.7982	0.45653	4.86	0.02	0
1083	-20.9	11.217	37.04	63.1	53.689	2.6921	0.54739	3.19	0.04	0
1084	-25.517	13.033	171.67	93.07	30.674	6.2716	1.8177	2.86	0	0
1085	-29.367	13.983	27.47	46.1	65.881	0.80655	0.54165	2.79	0.22	0
1086	-31.55	15.667	17.36	125.1	78.581	1.1153	0.11878	6.46	3.91	0
1087	-31.467	15.317	31.23	79.1	79.1	NaN	0.36321	4.42	0.58	0
1088	-41.133	13.567	3.89	4.45	91.363	NaN	0.31236	11.72	28.37	20.44
1089	-40.933	9.9	46.73	89.2	22.986	0.435	0.49585	2.73	0	0
1090	-42.917	8.9	4.12	29.15	39.604	0.19419	0.055575	12.17	25.89	17.64
1091	-47.1	5.9167	9.91	145.8	5.7056	0.59839	0.050823	7.92	23.78	21.48
1092	-46.417	7.0833	3.99	137.4	80.18	0.161	0.010844	14.19	25.58	24.91
1093	-49.983	5.8667	6.88	175.95	9.2321	0.77326	0.024893	9.51	26.93	0
1094	-53.183	5.1333	5.67	20.05	6.5902	0.83438	0.1581	8.95	28.79	26.84
1095	-66.983	-78.483	7.27	106.52	0.82747	0.18542	0.04478	12	5.4	0
1096	-67.567	-76.967	11.2	275.05	2.173	0.28552	0.031631	14.1	0	0
1097	-66.4	-70.75	7.4	287.4	0.67217	0.30667	0.017049	8.4	2.2	1.8
1098	-64.867	-64.2	42.06	41.7	1.0167	0.78767	0.94868	3.5	0	0
1099	-64.95	-64.317	80.7	92.97	1.0672	0.76306	0.84113	3.5	1.5	0
1100	-63.883	-65.7	3.56	2.95	NaN	NaN	0.35932	12	29.3	29.3
1101	-64.367	-70.267	8.03	212.55	3.9263	0.14791	0.026017	11.8	2.8	1
1108	-9.75	151.63	3.21	0.65	10.263	0.46538	1.0923	9.85	28.2	0
1109	-9.5	151.57	13.48	106.85	29.733	0.99015	0.10276	1.69	0	0
1110	-9.7333	151.58	5.47	2.95	27.632	0.17667	1.0068	10.02	27.63	27.6
1111	-9.7167	151.58	26.91	127.23	44.668	0.43	0.19186	2.63	1.47	1.47
1112	-9.75	151.62	3.63	1.45	30.8	0.35	0.77931	10.31	28.96	28.96
1114	-9.8	151.58	3.12	17.26	7.7787	0.44783	0.035921	9.44	28.6	28.2
1115	-9.1833	151.57	6.71	294.24	28.595	0.34106	0.014308	9.04	0.11	0
1117	-9.7833	151.55	2.21	1.4	9.24	0.07	-0.20714	9.55	30	30
1118	-9.5833	151.57	13.06	257.81	17.639	0.27882	0.04096	2.56	0.49	0

1119	-44.75	172.4	27.73	20.15	15.476	0.34	1.2521	3.49	0	0
1120	-50.067	173.37	5.96	211.5	94.624	0.12	0.016359	14.68	24.7	24.62
1121	-50.9	177	3.37	74.1	22.892	0.16625	0.011741	13.8	26.72	23
1122	-46.583	-177.4	40.49	15.2	16.455	0.2464	2.4993	4.08	0	0
1123	-41.783	-171.5	8.53	107	57.53	0.5814	0.056355	7.93	15.42	11.12
1124	-39.5	-176.53	5.58	21.94	35.645	0.35952	0.14038	10.31	25.11	17.93
1125	-42.55	-178.17	10.51	212.7	0.92	NaN	0.037659	7.94	0	0
1126	-33.517	128.07	5.1	28.4	74.553	0.25658	0.091549	25.74	58.59	27.87
1127	-33.35	128.48	105.9	124.95	88.658	0.39376	0.82753	3.48	0	0
1128	-34.383	127.58	11.73	280.7	31.955	0.042656	0.032882	24.8	8.3	2.9
1129	-33.3	128.48	97.28	228.6	91.731	0.51967	0.41461	3.8	11.4	2.2
1130	-33.417	127.6	36.1	19.4	87.954	NaN	1.732	12.2	33.5	28.1
1131	-33.333	128.48	137.05	136.3	90.282	0.38132	0.98716	2.74	37	14.7
1132	-33.317	127.6	28.05	77.7	90.99	0.44939	0.32883	9.19	28.67	24.03
1133	-33.533	128.9	5.24	25.8	89.3	0.20056	0.1062	10	26.7	26.7
1134	-33.533	127.27	4.21	27.9	85.195	NaN	0.06129	39.81	68.79	29.82
1143	9.3667	113.28	14.26	405.43	34.836	0.25917	0.029006	17.8	6.4	6.3
1144	20.05	117.42	34.94	11.35	13.763	0.77175	2.8581	4.8	0	0
1145	19.583	117.63	21.3	34.35	12.42	0.50682	0.54731	4.9	8.3	5
1146	19.45	116.27	28.82	27.35	36.257	0.27015	0.96234	4.2	6.8	0
1147	18.833	116.55	11.83	19.35	12.834	0.558	0.48217	8.02	19.2	14
1148	18.833	116.57	11.64	14.68	29.372	0.22526	0.62262	8.33	19.1	0
1149	31.333	143.37	3.36	2.9	51.759	NaN	0.29655	10.8	28.15	19.03
1150	39.183	143.33	49.03	23.15	3.3428	0.90527	2.0099	3.9	0	0
1151	38.75	143.33	31.99	44.69	3.3088	0.85447	0.65988	0	0	0
1165	-64.383	67.217	7.4	149.7	3.166	0.41596	0.032732	8.7	2.2	0
1166	-67.7	74.783	4.5	2.7	1.1559	2.4579	0.74074	11.7	29.5	8.2
1167	-66.4	72.283	4.2	354.2	0.93138	0.47778	0.0048	28.7	25	24.1
1168	-42.617	144.42	19.28	865.75	43.485	0.96117	0.019382	5.8	0	0
1169	-47.067	145.23	6.77	193.5	87.452	0.3231	0.022067	12.8	17.9	17.9
1170	-47.15	146.05	5.71	353	54.279	0.52365	0.009094	15.5	18	0
1171	-48.5	149.12	11.59	847.85	34.555	0.40198	0.010721	7.3	0	0
1172	-43.967	149.93	11	474.15	42.661	0.48355	0.017927	28.4	13.6	4.6
1173	32.25	135.03	53.49	60.49	5.3957	0.32345	0.84295	7.25	0	0
1174	32.35	134.95	51.31	6.04	5.5769	0.35667	8.0811	4.02	0	0
1175	32.6	134.65	33.2	22.6	12.57	NaN	1.3584	2.59	0.6	0
1176	32.583	134.67	29.21	22.8	10.211	0.572	1.1715	3.03	0	0
1177	31.65	134.02	20.62	338.48	4.0803	0.49684	0.053533	8.84	0	0
1178	32.733	134.48	21.35	145	5.5395	0.73545	0.13	6.35	0.19	0
1179	41.083	159.97	5.43	100.75	0.772	0.25519	0.029082	12.5	25.3	21.17
1192	-20.567	152.4	3.21	225.8	84.851	0.089941	0.003144	15.57	18.28	14.99
1193	-20.233	151.8	2.99	220.95	82.844	0.29333	0.002218	20.7	28.79	19.71
1194	-20.25	151.98	2.94	29.6	82.134	0.206	0.014865	14.39	26.24	18.65
1195	-20.4	152.67	4.62	362.85	82.279	0.16267	0.005843	26.59	17.8	13.09
1197	-21.083	153.07	3.55	514.25	89.997	0.16103	0.002042	18.78	13.02	10.66
1198	-20.967	152.73	4.55	162.9	81.246	0.18667	0.012584	15.51	26.24	16.42
1200	13.783	146	133.44	10.4	5.2863	0.037551	12.59	0.12	0.23	0.02
1201	19.3	135.1	114.26	508.86	NaN	NaN	0.21963	0	13.83	13.83
1202	24.8	122.5	26.66	10.05	NaN	NaN	2.404	0	0	0
1207	37.783	162.75	4.37	134.25	70.933	2.7639	0.013929	12.18	25.43	24.76
1208	36.133	158.2	8.17	67.65	58.696	NaN	0.083814	7.47	20.38	19.52
1209	32.65	158.5	3.29	33.15	80.91	NaN	0.023831	11.59	26.19	23.54
1210	32.217	158.27	3.36	21.35	88.378	0.09875	0.040281	11.14	26.78	0
1211	32	157.85	3.24	8.75	86.338	NaN	0.084571	11.06	28.44	26.55
1212	32.45	157.72	2.78	10.85	85.804	NaN	0.025806	12.58	25.86	21.65
1215	26.033	-147.93	2.78	24.65	47.564	0.049444	0.011359	10.8	28.6	27.6
1216	21.45	-139.48	2.74	47.65	0.39077	0.02	0.005037	11.4	28.6	27.8
1217	16.867	-138.1	3.4	84.65	6.4981	0.11529	0.010632	10.8	28	28
1218	8.8833	-135.37	3.89	117.15	56.929	0.18346	0.011865	11.9	27.7	26.3
1219	7.8	-142.02	2.59	2.95	43.892	0.071852	0.030508	12.3	30.3	25.6
1220	10.183	-142.77	3.45	173.55	18.091	0.01	0.005474	13.1	28.9	27.6
1221	12.033	-143.7	3.2	80.41	4.8169	0.023	0.008705	10.3	29.2	28.5
1222	13.817	-143.88	3	47.85	5.4424	0.04875	0.010449	9	28.9	28.9
1223	22.967	-155.65	1.98	4.45	NaN	NaN	-0.11685	0	0	0
1225	2.7667	-110.57	3.9	97.15	73.017	0.17763	0.014411	0	0	0
1226	-3.1	-90.817	6.88	59.2	35.875	0.91636	0.073986	0	24	0
1227	-8.9833	-79.95	24.15	41.45	49.1	NaN	0.52232	0	0	0
1228	-11.067	-78.083	19.44	31.25	NaN	NaN	0.54208	0	3.37	0
1229	-10.983	-77.95	22.04	0.97	NaN	NaN	20.144	0	16.47	0
1230	-9.1167	-80.583	159.76	109.65	NaN	NaN	1.4342	0	0	0
1231	-12.017	-81.9	4.09	86.28	NaN	NaN	0.018428	0	0	0
1232	-39.883	-75.9	36.75	70.54	1.462	0.17196	0.48554	6.1	0.73	0.45
1233	-41	-74.45	68.59	28.46	5.4282	0.90634	2.3222	2.32	0	0

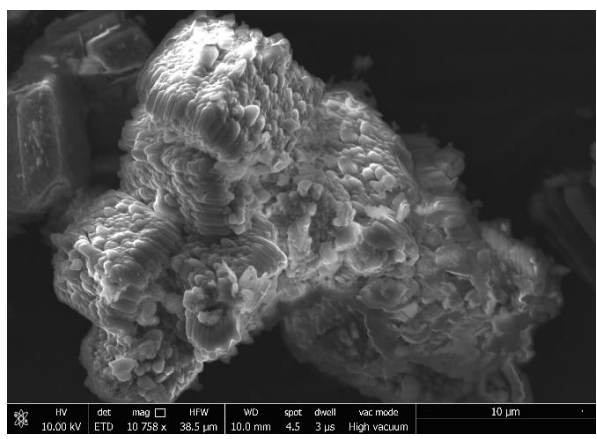
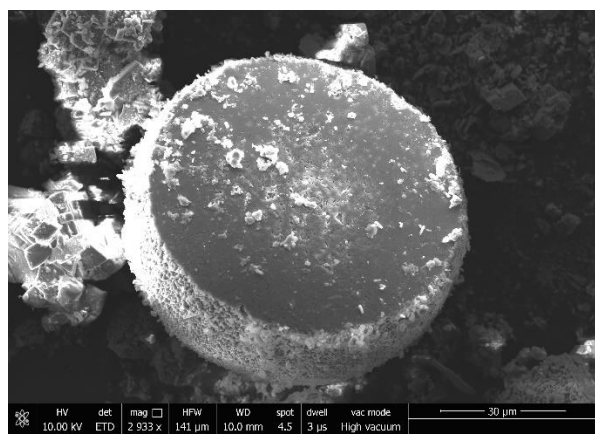
1234	-36.217	-73.683	72.84	27.81	3.5116	1.0471	2.5293	1.75	0	0
1235	-36.167	-73.567	67.27	35.75	2.3913	0.64492	1.8117	1.63	0	0
1236	-21.367	-81.433	2.61	56.53	94.56	0.048261	0.001946	12.4	27	23.6
1237	-16	-76.383	5.3	19.47	76.529	0.38783	0.14381	9.42	25.5	25.1
1238	-1.8667	-82.783	17.5	85.47	60.273	0.89032	0.1755	7.5	8.35	3.21
1239	-0.66667	-82.083	29.56	93.37	59.018	1.5422	0.28981	6	0	0
1240	0.016667	-86.467	18.97	140.95	56.038	0.98286	0.11685	2.95	12.8	12.4
1241	5.85	-86.45	5.88	84.35	67.847	0.37521	0.040071	12.6	27.2	25.2
1242	7.85	-83.6	28.1	68.15	24.391	1.6137	0.37564	4.1	0	0
1244	44.583	-125.12	68.91	59.51	3.203	1.2855	1.1159	3.2	1.5	0
1245	44.583	-125.15	73.31	120.62	7.4658	1.1096	0.58705	3.5	1.1	0
1246	44.583	-125.13	83.14	128.15	3.3625	1.2025	0.62926	5	0.7	0
1247	44.583	-125.15	66.39	130.15	5.3543	1.0933	0.4909	4.1	1	0
1248	44.567	-125.15	71.42	20.6	5.4831	1.1015	3.3456	4	0.7	0
1249	44.567	-125.15	75.29	88.5	NaN	NaN	0.82249	0	0.8	0
1250	44.567	-125.15	78.98	79.81	3.4523	1.3246	0.95828	4.1	0.1	0
1251	44.567	-125.07	160	160.81	4.1863	1.37	0.97942	2.9	0	0
1252	44.583	-125.1	108.24	45.75	NaN	NaN	2.3113	0	0.3	0
1253	9.65	-86.183	2.06	398.9	18.592	0.17437	-0.0011	12.55	28.09	27.21
1254	9.6667	-86.183	0	153.52	4.611	1	-0.01629	7.34	0.42	0
1255	9.65	-86.183	22.65	144.77	3.03	0.57333	0.13919	5.6	7.25	0.22
1256	6.7333	-91.933	4.06	12.02	41.636	0.24469	0.12978	0	26.35	0
1257	9.45	-54.35	6.05	156.16	52.01	2.9362	0.022733	18.1	1.6	0.2
1258	9.4333	-54.733	7.38	170.9	47.958	4.8829	0.028555	20.3	12.3	0
1259	9.3	-54.2	8.86	219.12	63.354	3.4693	0.029025	29.2	17.6	0
1260	9.2667	-54.55	8.71	490.5	56.43	3.5476	0.012661	15.7	0.5	0.3
1261	9.05	-54.317	5.03	545.95	46.337	4.4871	0.004634	28.9	0	0
1262	-27.183	1.5833	2.88	45.45	71.074	0.077674	0.008361	11.68	23.25	21.19
1263	-28.533	2.7833	5.93	47.7	85.502	0.091379	0.071908	12.89	26.41	23.32
1264	-28.533	2.85	3.33	7.4	93.806	0.15571	0.11216	11.05	28.5	0
1265	-28.833	2.6333	3.48	26.4	89.283	NaN	0.037121	13.86	25.5	22.8
1266	-28.55	2.35	4.84	130	84.044	NaN	0.018	17.1	24.37	19.13
1267	-28.1	1.7167	3.34	7.45	75.639	NaN	0.11275	10.1	25	0
1276	45.4	-44.783	0	801.3	14.228	0.81434	-0.00312	0	5.14	3.22
1301	47.75	-127.77	31.62	31.4	5.3043	0.333	0.92739	7.14	3.2	0
1302	50.167	-45.633	9.73	20.55	25.375	0.51185	0.35182	6.04	13.9	5.76
1303	50.2	-45.683	10.56	49.3	29.323	0.462	0.16349	4.55	10.53	9.32
1304	53.05	-33.533	19.27	134.45	36.011	0.4278	0.12473	2.88	5.18	2.81
1305	57.483	-48.533	18.85	57.85	12.292	0.34914	0.28263	2.58	0.07	0
1306	58.233	-45.65	18.7	85.75	3.1861	0.34702	0.18892	3.72	0.66	0.04
1307	58.5	-46.4	10.08	79.15	5.5171	0.12742	0.095768	5.27	1.58	0.56
1308	49.883	-24.233	6.57	285.55	70.443	0.32737	0.014253	14.9	9.9	9
1312	42.833	-23.083	4.77	81.95	90.414	0.12328	0.0277	9.64	25.54	6.07
1313	41	-32.95	6.07	106.15	80.506	0.094648	0.033632	8.86	24.17	24.17
1314	56.367	-27.883	7.46	74.35	34.125	0.2229	0.066711	5.23	6.84	1.12
1316	51.383	-11.733	13.69	78.7	30.996	NaN	0.14219	11.59	11.25	0
1317	51.383	-11.717	18.98	158.75	45.622	NaN	0.10381	8.48	2.94	0
1318	51.433	-11.55	13.6	236.35	25.868	NaN	0.046964	22.13	11.29	10.36
1319	27.267	-94.4	19.45	13.45	16.363	0.7336	1.2602	4	0.5	0.3
1320	27.3	-94.383	15.99	15.45	12.173	0.53465	0.87314	6.7	6.1	0
1322	28.1	-89.033	6.25	193.32	14.535	0.82896	0.019398	8.4	0	0
1324	28.083	-89.133	11.35	584	15.688	0.72635	0.015154	9.6	0	0
1325	48.65	-126.98	52.9	26.67	3.2295	0.54455	1.8898	2.3	0	0
1326	48.633	-127.05	23.1	2.85	4.069	0.44117	7.2281	4.4	0	0
1327	48.7	-126.87	27.4	21.5	2.8304	0.61605	1.1581	2.3	0	0
1328	48.667	-126.85	48.8	140.5	5.672	0.45102	0.32954	4.9	0.3	0
1329	48.783	-126.68	29.1	112.4	3.9788	0.79647	0.23665	4.3	0.1	0

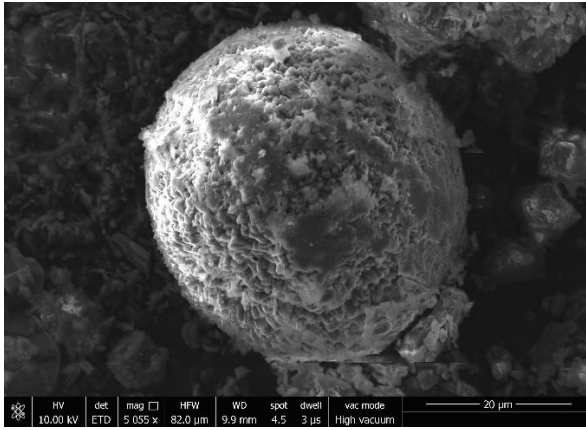
Appendix B: Details of the ODP/IODP data used in the statistical analysis. NaN = data not available/Not a Number.

Appendix C

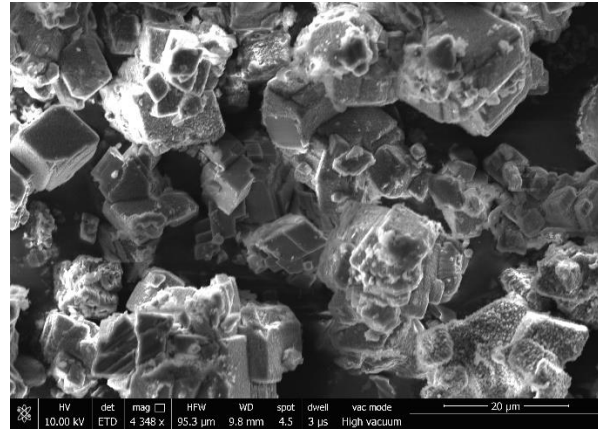


Appendix C: Control samples are shown in square.





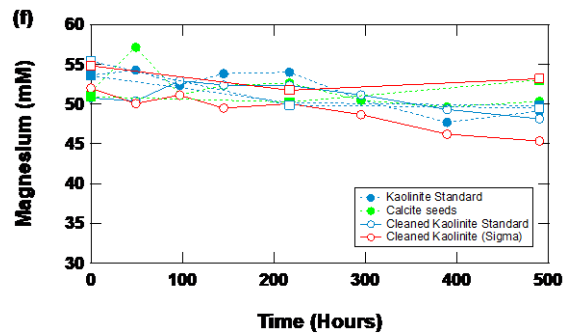
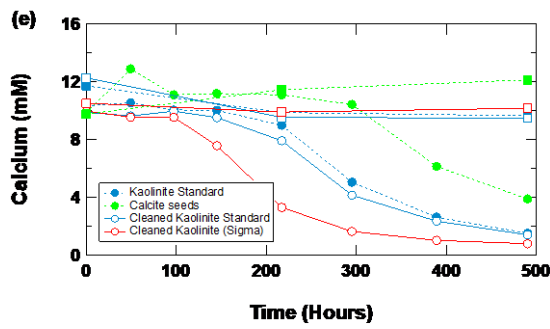
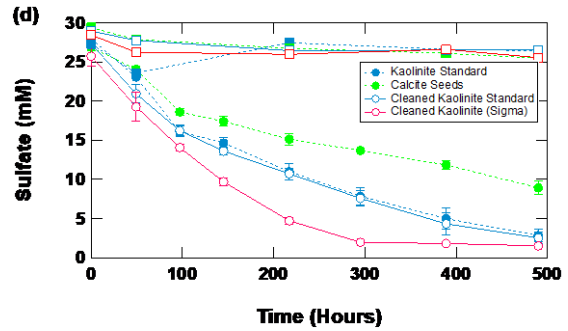
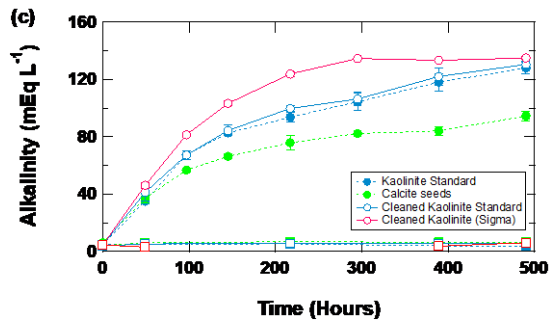
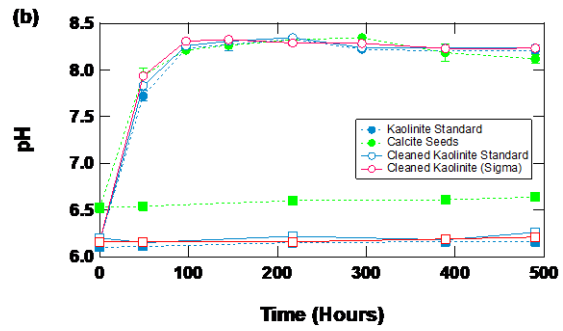
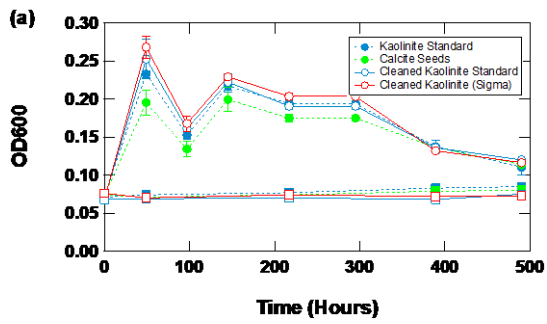
25% CaCO₃



80% CaCO₃

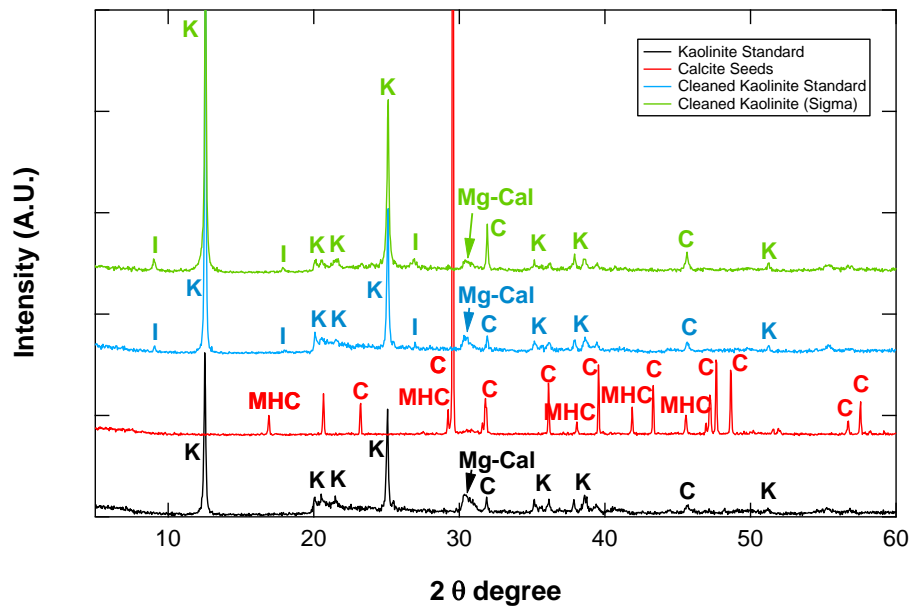
Appendix C: Carbonate precipitates in samples with different proportion of CaCO₃. Precipitates of MHC comprised a spherulitic structure and the epitaxial growth of Mg-calcite on calcite seeds.

APPENDIX D



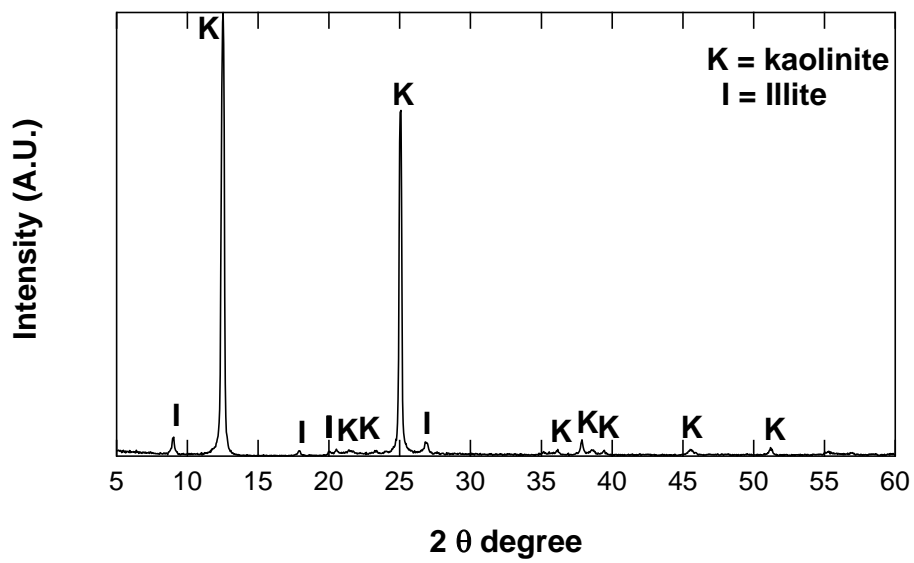
Appendix D: Control samples are shown in square.

Appendix E



Appendix E: Calcium carbonate minerals that formed in the incubation samples.

Appendix F

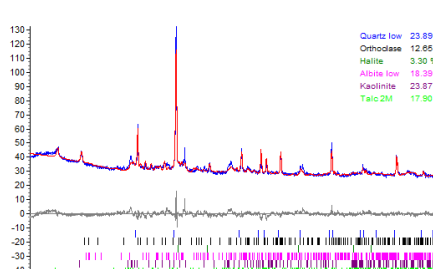
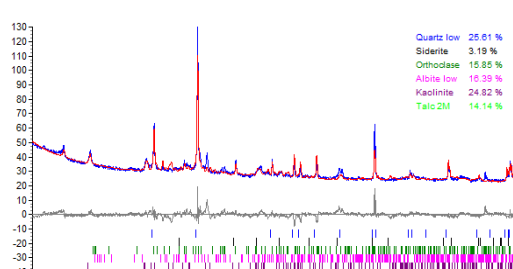
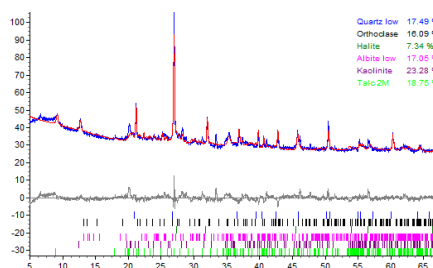
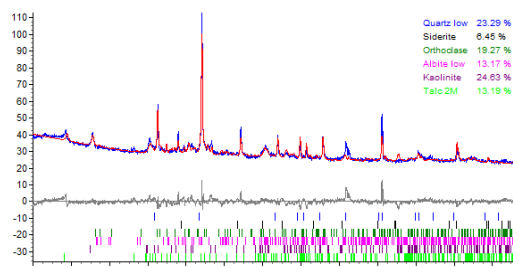
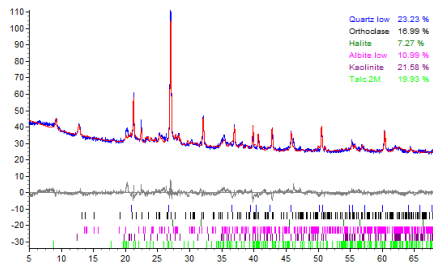
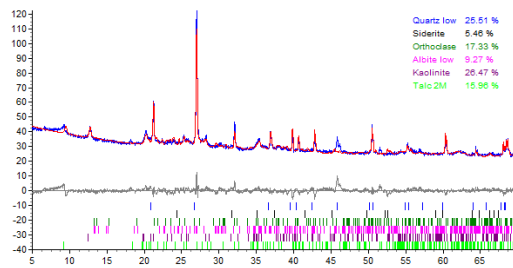
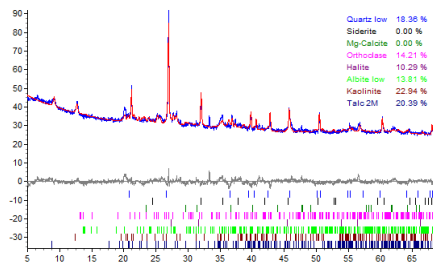
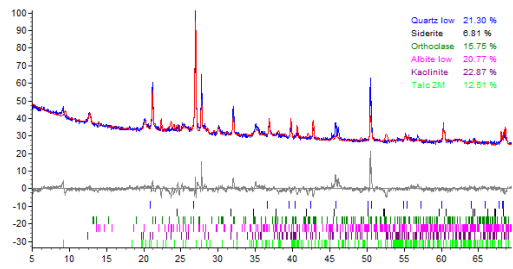
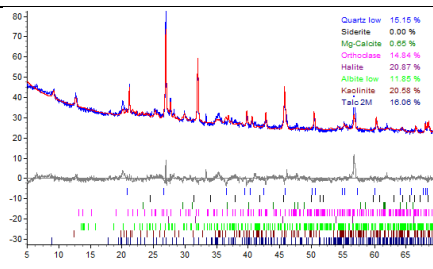
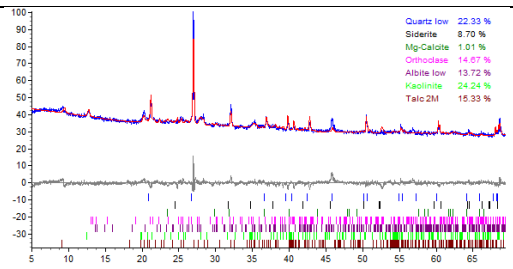


Appendix F: Analysis of XRD shows that the kaolinite from Sigma contains minor illite.

Appendix G

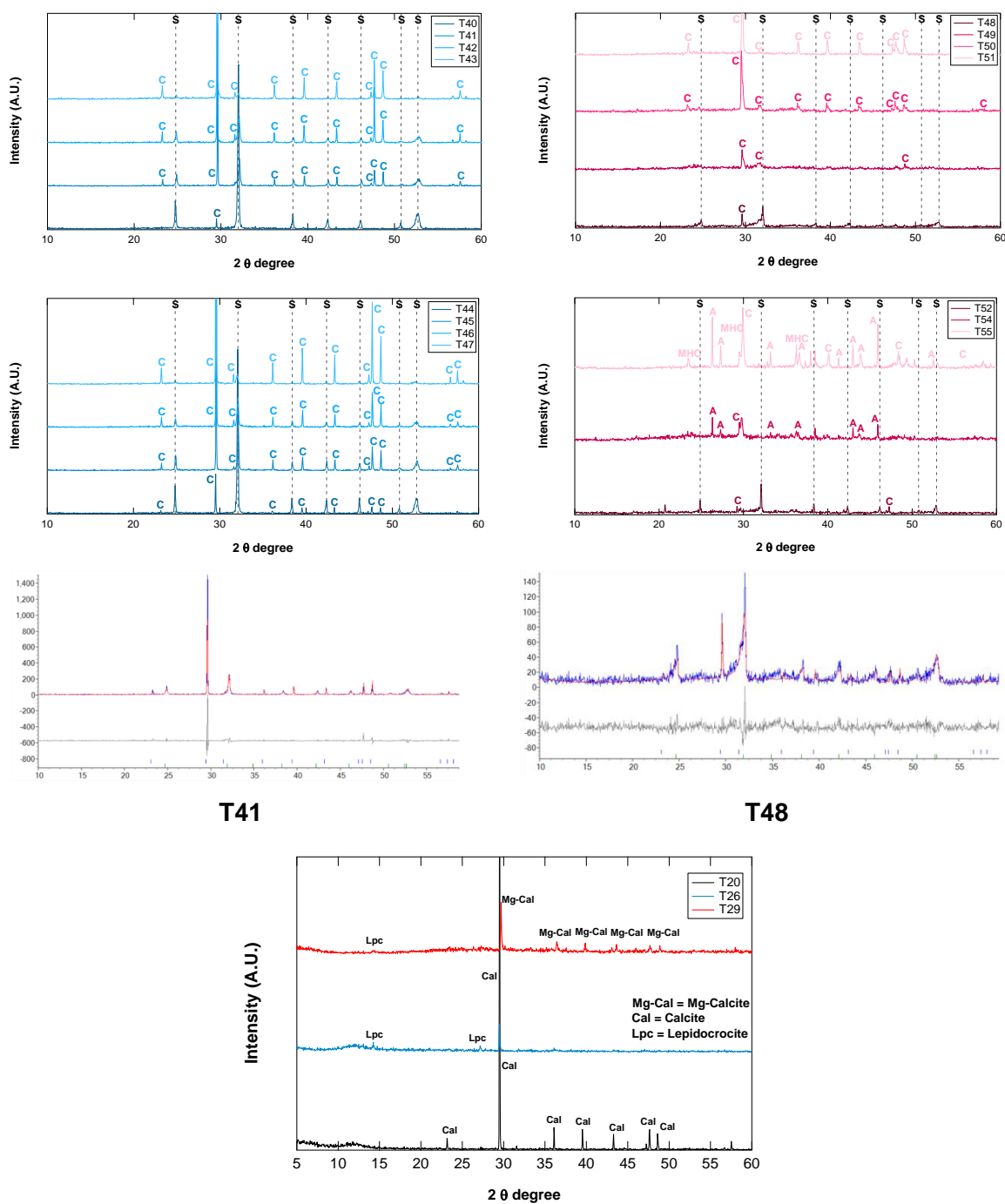
Iron rich core (with depth)

Sulfidic core (with depth)



Appendix G: XRD results of two sediment cores (iron-rich and sulfidic core), where the mineral phase was quantified by Rietveld refinement. y axis (intensity) is in arbitrary units, while the x axis is degrees of 2θ .

Appendix H



Appendix H: The carbonate minerals that precipitate in the transformation experiments. Rietveld refinement experimental (blue), calculated (red) and difference (grey) curves for sample T41 and T48. Peak position marks are shown for calcite (blue) and siderite (green). The pattern was collected on instrument nr.2. Details about the Rietveld fitting procedure are reported in Chapter 2. For sample T48 the asymmetrical peak shape of siderite was modelled using a composite peak with two Lorentzian functions for the right and left sides.

Appendix I

Sample	Minerals	C	Mg-C	MHC	A	V	Sdr	R_{wp}	χ^2	Instrument
T06	C, A	±2.8	-	-	±2.8	-	-	59.04	0.93	Nr 2
T07	C, A, Mg-C	±2.3	±1.9	-	±2.7	-	-	57.81	0.91	Nr 2
T08	A, C, MHC, Mg-C	±2.4	±2.0	±2.0	±1.5	-	-	57.80	0.93	Nr 2
T09	C, Mg-C	±2.1	±2.1	-	-	-	-	56.17	0.88	Nr 2
T10	C, Mg-C	±3.4	±3.8	-	±3.3	-	-	57.56	0.95	Nr 2
T12	C, A	±3.7	-	-	±3.7	-	-	57.43	1.00	Nr 2
T13	A, C, MHC	±2.2	-	±2.0	±2.2	-	-	57.31	0.94	Nr 2
T40	Sdr, C	±0.5	-	-	-	-	±0.5	29.39	1.38	Nr 2
T41	Sdr, C	±1.2	-	-	-	-	±1.2	38.85	1.47	Nr 2
T42	C, Sdr	±1.1	-	-	-	-	±1.1	39.47	1.73	Nr 2
T43	C, Sdr	±1.0	-	-	-	-	±1.0	30.34	1.51	Nr 2
T44	Sdr, C	±0.8	-	-	-	-	±0.8	33.63	1.47	Nr 2
T45	C, Sdr	±1.1	-	-	-	-	±1.1	38.13	1.57	Nr 2
T46	C, Sdr	±1.2	-	-	-	-	±1.2	34.57	1.58	Nr 2
T47	C, Sdr	±0.8	-	-	-	-	±0.8	36.19	1.84	Nr 2
T48	Sdr, C	±1.5	-	-	-	-	±1.5	32.60	1.21	Nr 2
T49	Sdr, C	±3.3	-	-	-	-	±3.3	26.99	1.16	Nr 2
T50	C, Sdr	±1.9	-	-	-	-	±1.9	24.80	1.20	Nr 2
T51	C, Sdr	±1.0	-	-	-	-	±1.0	28.62	1.34	Nr 2
T52	C, MHC, Sdr	±1.5	-	±2.2	-	-	±2.3	29.66	1.14	Nr 2
T54	C, A, Sdr	±1.6	-	-	±1.6	-	-	22.75	1.18	Nr 2
T55	C, A, Sdr	±0.9	-	-	±8.2	-	±0.9	26.36	1.29	Nr 2

Appendix I: Estimated standard deviation, R_{wp} and χ^2 values for Rietveld quantifications of the transformation experiment.